# The role of substrate hydrogeology and surface hydrology in the construction of phreatomagmatic volcanoes on an active monogenetic field (Auckland, New Zealand)

*A thesis presented in partial fulfillment of the requirements for the degree of* ***Doctor of Philosophy in Earth Science***

At Massey University, Palmerston North, New Zealand

MASSEY UNIVERSITY
TE KUNENGA KI PŪREHUROA

Javier Agustín Flores

2015

## Abstract

Phreatomagmatic activity is pervasive in the Auckland Volcanic Field (AVF) with more than two thirds of the erupted volcanoes showing this type of activity at different degrees, dominantly at the onset of their eruptive histories. In general, the volcanoes built in the northern AVF rest on Late Miocene Waitemata Group rocks (turbiditic siltstone and sandstone succession), whereas in the southern AVF the Waitemata rocks are overlain by tens of metres of Plio-Pleistocene, water-saturated sediments (Tauranga Group and Kaawa Formation). Identifying the control exerted by the type of substrate in the eruption dynamics of the phreatomagmatic phases of three volcanoes in the AVF is the objective of this study. The stratigraphic, sedimentary, and pyroclast characteristics of the phreatomagmatic sequences of Maungataketake, Motukorea, and North Head volcanoes, together with supplementary information on the geology and hydrogeology of the area, were investigated to solve the problem. Three phreatomagmatic eruptive scenarios were outlined. Scenario 1 (Maungataketake eruption) and Scenario 2 (Motukorea eruption) depict the formation of maar-diatreme volcanoes in the southern and northern AVF, respectively. The dominant presence of lithics from the upper part of the substrate in their tephra rings suggests the construction of their tephra rings from shallow-seated explosions. Due to the water-saturated sediments filling the diatreme in Scenario 1, the eruption appears to have remained relatively wet throughout. Conversely, the drier Waitemata rocks involved in Scenario 2 promoted a progressive drying of the eruption. Scenario 3 (North Head eruption) represents a Surtseyan eruption scenario in which the rising magma erupted to the shallow sea floor (a few metres-water depth), promoting rapid chilling and explosive fragmentation. This study shows that the characterization of lithics within the tephra ring and the geological and hydrogeological information provide valuable clues to envisage the degree of influence of the substrate in the phreatomagmatic eruption dynamics. Other studies in the AVF appear to confirm this view. It is proposed that any future phreatomagmatic eruption in the AVF will be strongly influenced by the substrate hydrogeology and geology, as well as the surface hydrological conditions.

## Acknowledgements

I am grateful to all people working for the departments of Massey University that in one way or another have contributed to the achievement of this thesis. A special recognition goes to my main supervisor, Karoly Németh, for his patience, priceless guidance, support, and encouragement from the beginning to the end. I am very thankful for the continuous and highly valuable support of supervisors Shane Cronin and Jan Lindsay (The University of Auckland). Many thanks to Kate Arentsen for her great support regarding organizational and administrative matters. I acknowledge the people from the Volcanic Risk Solution department (Eric Bread, Gaby Gómez, Gert Lube, Manuela Toast, Maggi Damashke, Marco Brenna, Rafael Torres, Jonathan Procter, Mark Bebbington, Georg Zellmer, Adam Neather) and especially to my friend and colleague Gábor Kereszturi for his willingness and apt help in the field and with academic matters. I acknowledge the motivation and encouragement of my first mentor of volcanology, Claus Siebe (Instituto de Geofísica, UNAM, México), to continue my studies on volcanoes.

This research was supported by the Massey University-led FRST-IIOF project "Facing the challenge of Auckland's volcanism" (funded by the New Zealand Ministry of Business, Innovation and Employment), the New Zealand Natural Hazards Research Platform project "Living with Volcanic Risks", and the DEVORA (Determining Volcanic Risk in Auckland) project, co-funded by the NZ Earthquake Commission (EQC) and the Auckland Council, GNS Science, The University of Auckland and Massey University. I was provided a scholarship (university fees, insurance and stipend) by the FRST-IIOF project from Dec 2010 to Dec 2013. CONACYT (Mexican National Council of Science and Technology) awarded a stipend during 2014 (I am grateful to Cindy Agustin-Flores and Oscar Alvarado-Flores for paperwork regarding the application in Mexico). I am very thankful to my friends José Rivera, Marc Adamson, Donald Hsieh, and Andrés Arcila for providing with accommodation in Auckland during field work. I am very grateful to the Instituto de Geofísica at UNAM (México) through Claus Siebe, Carles Canet, Dolors Ferres, Ligia Pérez-Cruz, and Lilia Arana for the valuable support in the latest stage of completion of this thesis.

A special acknowledgment goes for Anja Möebis for her valuable technical support at the laboratory. Also many thanks to Doug Hopcroft with Scanning Electron Microscope work, Ritchie Sims for the microprobe analysis at the University of Auckland, and Elizabeth Rangel for the preparation of thin sections. I appreciate the support from the University of Auckland and the Institute of Earth Sciences and Engineering during my staying for one month during 2011 in Auckland. Regarding the published papers (Chapters 5, 6, and 7); I highly appreciate the time and effort of journal reviewers Rafaello Cioni, Claus Siebe, Volker Lorenz, Alexander Belousov, Pierre-Simon Ross, James White, and Gerardo Carrasco for their recommendations to improve the manuscripts.

A highly special recognition goes to the thesis reviewers and examiners Robert Stewart (Massey University, New Zealand), Adrian Pittari (Waikato University, New Zealand), and Pierre-S., Ross (Institute National de la Recherche Scientific, Canada) for their useful and valuable suggestions and observations.

From my heart I thank Natalia Pardo for being there when I needed help, without her unconditional support the process of adapting to an “exciting” Palmy would have been very difficult. There are many people who made my staying in Palmy a lifetime experience, which made me feel motivated during my studies, through their always great company: Alvaro Wehrle, Agustin Oberti, Ana Mar, Adimar Lujan, Angela Denes, Gábor Kereszturi, Gaby Gómez, Jimena Rodiguez, Jimena Yapura, Junior Perawiti, Luca Panizzi, Majela González, Cote Solovera, Marcela Almirón, Manuela San Roman, Patricia Rubio, Rafael Torres, Roberto Calvelo, Soledad Navarrete,Thiago Alves, and many others. Thanks a lot for your love.

The continuous encouragement and financial support at the beginning and the end of my PhD studies from my parents (Yolanda Flores and Javier Agustín) are priceless and unconditional, an effort for which I am very grateful. Thanks a lot for your love.

# Table of contents

Page

## List of Figures

**Page**

# List of Tables

**Page**

# Chapter 1. Introduction

## Contents

Page



## 1.1 Introduction

Monogenetic volcanism is a term that generally refers to “one-off”, short-lived volcanic eruptions that occur in new locations, rather than from a repeatedly active volcanic edifice or vent (Németh, 2010). The specific feature of monogenetic volcanoes (also known as volcanic field or distributed volcanoes) is that each new vent area has unique combinations of geologic, hydrologic and topographic conditions that may strongly influence the eruption style (Kereszturi and Németh, 2012). Particularly for small-scale basaltic field volcanism, it is the combination of these environmental factors that controls whether an eruption will be magmatic explosive, effusive or involves explosive water-magma interaction – known as phreatomagmatism (White 1991a). This type of volcanism has been the subject of increasing research interest, due to both the common location of cities and infrastructure on volcanic fields around the world, as well as the poor understanding of the controls on monogenetic eruptions (e.g. in the Auckland Volcanic Field, AVF, Allen and Smith, 1994; Allen et al., 1996; Smith et al., 2008; Cassidy and Locke, 2010; Kereszturi et al., 2013; Agustín-Flores et al., 2014, 2015; in Jeju Island, Sohn, 1996, and references therein). Typically the most violent eruptions from basaltic monogenetic volcanoes involve explosive phreatomagmatic fragmentation, which results from interaction of magma with groundwater and/or surface water. These eruptions also generate distinctive typical landforms in many fields, including *maars* and *tuff rings* that have low rims and broad craters (White and Ross, 2011). Maars are underlain by a diatreme, a cone-shaped body of pyroclastic deposits containing a mixture of disrupted substrate materials (lithic fragments) and fragmented magma (juvenile fragments). The characteristics of the substrate into which these eruptions form may be complex, including soft, liquefiable muds, through to hard rock, layered multiple lithologies with distinct physical and hydraulic characteristics, and faulted and jointed sequences.

The fundamental factor leading to explosive phreatomagmatic volcanism is optimal contact between magma and external water. The initial and subsequent geometry of this contact zone, the ratio of magma to water, and the physical characteristics of this interaction are variable from site to site, as well as changing during an eruption, depending chiefly on magma effusion rate, water supply, and vent/diatreme stability. However, there is a strong need to identify the key sets of factors that lead to broad differences in

eruption dynamics and their consequent hazard, particularly in order to forecast the types of magma-water interaction and styles of eruptions in areas that could be future sites of eruption.

Much progress has been made in recent years in discerning a number of the host-rock conditions and magmatic factors that control phreatomagmatic eruptions, beginning with the classic evaluation of optimal water to magma ratios that maximise explosive eruption energy (e.g. Wohletz 1983, 1986; Wohletz and McQueen, 1984). To further our understanding beyond laboratory scale experiments and into the complexity of real-world settings, geological studies are needed to integrate volcanic host rock and hydrogeological parameters with the knowledge of eruption processes that can be determined from phreatomagmatic deposits and the pyroclasts characteristics (e.g. White, 1991b; Houghton et al., 1999). Only by combining these factors at past eruption sites, and examining the dynamics and development of observed eruptions can an integrated understanding of phreatomagmatism be gained in these settings (e.g. White 1991b, Lorenz and Haneke, 2004; Németh et al., 2010; Lefebvre et al., 2013; van Oterloo et al., 2013). This work is in its infancy, however, with too few observed eruptions to strongly characterise the depositional evidence, and uncertainty about the impacts of the broad range of possible substrate types, rock strengths, groundwater properties and surface water depths. This PhD research addresses this gap in knowledge using field and theoretical approaches to improve the understanding of the role of substrate geological and hydrogeological properties on the dynamics and stability of explosive phreatomagmatic eruptions. The study site selected for this work is the AVF, New Zealand. In this ~360 $km^2$ basaltic volcanic field, over 50 volcanoes occur, with >35 of these showing phreatomagmatic phases (Allen et al., 1996; Houghton et al., 1999; Cassidy et al., 2007; Cassidy and Locke, 2010; Hayward et al., 2011; Németh et al., 2012; Kereszturi et al., 2013). The phreatomagmatic volcanoes include maars, tuff rings, and a tuff cone, with phreatomagmatism ranging from a short-lived phase associated with vent opening to being the dominant eruption style throughout the entire eruption (Allen and Smith, 1994; Bebbington and Cronin, 2011; Hayward et al., 2011; Kereszturi et al., 2013). Furthermore, the area is known to host a range of substrate rock types, topographic contrasts and other features including faults and surface water of varying depths (Crowcroft and Bowden, 2002; Edbrooke et al., 2003; Irwin, 2009; Kenny et al., 2012). The eruptions from this small field have occurred since 250 ka under a range of paleoclimatic conditions, which may have also strongly influenced the observed range of eruption styles (e.g. Nemeth et al., 2012). The AVF is almost entirely densely populated as the site of the city of Auckland (pop. ~1.4 million), which is New Zealand's largest city and greatest focus of economic activity. For this reason, it is a matter of acute importance to understand the potential hazard from explosive phreatomagmatic volcanism in this area, and various attempts to understand the timing, frequency and type of volcanism have been made in recent years (e.g. Bebbington and Cronin, 2011; Lindsay et al., 2012; Nemeth et al., 2012).

## 1.2 Study site, motivations, and objectives

As stated above, phreatomagmatism is pervasive in the AVF .The AVF is hosted on a mixture of soft rock and poorly consolidated and unconsolidated substrates, through to moderately firm, jointed and poorly permeable rock sequences. The northern part of the AVF was primarily erupted through the consolidated Miocene-aged Waitemata Group rock sequences, with poorly permeable rocks, but generally characterized by joint-controlled aquifers. By contrast, the southern part of the field (the Manukau Lowlands) erupted through tens of meters of water-saturated, soft unconsolidated sediments (Tauranga Group) overlying a few meters of highly permeable poorly consolidated lithologies (Kaawa Formation), which in turn overlie the Waitemata Group rocks.

Therefore two important questions arise: is there any relationship between the eruption dynamics of phreatomagmatic volcanoes and the substrate type in the AVF? To what extent the substrate controls such eruptions in comparison to other factors (i.e. magma to water mass ratios)? Three main study sites were investigated during the course of this thesis covering the main hydro-geological and surface topographic differences seen across the field. The three main volcanoes studied here are Motukorea (erupted in the northern AVF), Maungataketake (emplaced in the southern AVF) and North Head (erupted in the northern AVF on the Waitemata Group sediments but in a shallow submarine setting) so that, collectively, a wide span of substrate types and volcanic locations could be compared. This is important for understanding the spatial variation of hazards in the AVF as it is not possible to know where the next eruption will occur. The city of Auckland, the largest city in New Zealand, is built on the AVF, thus examining the influences of substrate properties on eruption style is of vital importance to assess the hazards related to phreatomagmatic eruptions.

This study investigates the role of the substrate on the styles of phreatomagmatism, building on the many studies that have hinted at its importance (e.g. White, 1990, 1991b; Aranda-Gómez and Luhr, 1996; Sohn, 1996, and references therein; Németh et al., 2001, 2008; Lorenz, 2003; Lorenz and Heneke, 2004; Martin and Németh, 2004; Auer et al., 2007; Carrasco-Núñez et al., 2007; Ort and Carrasco-Núñez, 2009). I hypothesise that if the magmatic conditions are similar (i.e., eruption rate, volume and magma composition), then it will be the properties of the substrate that the magma is injected into which controls the phreatomagmatic eruption style. Specifically the properties of rock strength, groundwater availability and general hydrology of the rock units through which magmas erupt will control the contact geometry and thus water to magma ratios and explosivity of the interaction. To test this hypothesis, this study will examine the phreatomagmatic deposits of three volcanoes associated to similar magma type and magma volume within the AVF. By examining the landforms, paleogeographic conditions (at the times of each eruption), deposit characteristics (including lithic fragments), and the surrounding geology, the eruptive histories of phreatomagmatic eruptions under contrasting substrate geological and hydrogeological

conditions were established. The results of this thesis are also placed within a global context to highlight the relevance of the substrate in the progress of phreatomagmatic eruptions.

Other specific objectives of this study included:

1. Reconstruction of the stratigraphic and morphological structure of the Maungataketake, Motukorea, and North Head phreatomagmatic volcanoes, concentrating on interpretation of eruption dynamics and identification of changes in eruptive styles;
2. Interpreting the temporal and spatial relationships between phreatomagmatic fragmentation, water availability, and substrate geometry and disruption;
3. Deducing conditions of paleo-aquifers and their relationship with eruptive styles and dynamics of the three study sites, as well as the role and influence of surface water;
4. Evaluation of the applicability of the AVF eruption dynamics in relation to other phreatomagmatic volcanoes in other monongenetic fields; and
5. Use the current hydrogeological and hydrological conditions in the Auckland area to define the most likely phreatomagmatic eruptive scenarios expected for future eruptions of the AVF.

The remainder of this thesis is subdivided into eight chapters. Chapter 2 reviews the processes involved in phreatomagmatism and the known influences on these, while Chapter 3 provides specific information on the geological and hydrogeological setting of the studied volcanoes. Chapter 4 outlines the methodology developed for this study to test the research hypothesis described above. Chapters 5, 6 and 7 present the eruption reconstruction of volcanoes of Maungataketake, Motukorea, and North Head respectively. These three chapters are part of already published, peer-reviewed articles for international journals. Chapter 8 integrates the findings and conclusions of this study and compares to previous works on the AVF to examine the main controls on phreatomagmatic eruption styles in the AVF. This chapter goes on to consider the present environmental conditions in the AVF area to forecast the types of volcanism expected in any future eruptions from the field. Based on type of substrate setting and the surface hydrological conditions, three general models for phreatomagmatic eruptions in the AVF are proposed. To put this study in a global context and evaluate a wider applicability of these models, they are compared with existing models of phreatomagmatism. Although the proposed models need to be refined and tested, eruptive prhreatomagmatic scenarions in the AVF and worldwide may be predictable where the substrate hydrogeology and geology, as well as the hydrological and magmatic conditions, are similar to the ones studied.

# Chapter 2. The principles of phreatomagmatism

**Contents** Page



## 2.1 Introduction

Maar-diatreme/tuff ring volcanoes are the second-most common terrestrial volcanic landform across varied tectonic settings (e.g. Chough and Sohn, 1990; Sohn and Chough, 1989; White, 1990; White, 1991a,b; Auer et al., 2007; Brand and Clarke, 2009; Németh et al., 2012a,b; Valentine, 2012; Valentine and Van Wyk de Vries, 2014). Some maar-diatreme structures may be formed by energy released from the gas-driven fragmentation of under-saturated, $CO_2$-rich, nephelinitic or melilititic magmas (e.g. Stoppa et al., 1996; Berghuis and Mattsson, 2013) and at least one documented example occurs of a diatreme formed by non-phreatomagmatic, weak explosive activity (Valentine and van Wyk de Vries, 2014); almost all others are formed by phreatomagmatism.

Phreatomagmatic eruptions produce the “wet” equivalents of scoria cones; i.e., maars, tuff rings, and tuff cones (Lorenz, 1986). These volcanoes are commonly found in monogenetic volcanic fields of basaltic composition (Valentine and Gregg, 2008). However, phreatomagmatic eruptions include silica-rich variants, such as the rhyolitic maars from Mexico (Hoya de Estrada, Cano-Cruz and Carrasco-Núñez, 2008; Tepexitl tuff ring, Austin-Erickson et al., 2011), Argentina (tuff ring in the Ramadas volcanic centre, Tait et al., 2009; Los Loros volcano, Németh et al., 2012b), Turkey (Acigöl maar; Druitt et al., 1995) and New Zealand (Puketarata tuff ring, Brooker et al., 1993). The purpose of this chapter is to present an overview of the background knowledge on phreatomagmatism, based on experimental, theoretical and geological studies. The common terminology applied to phreatomagmatism is introduced here, which stems from and was adapted via a range of studies (Sheridan and Wohletz, 1983; Fisher and Schmincke,

1984; Lorenz, 1986; Sohn and Chough, 1989, 1992; White, 1991a,b; Vesperman and Schmincke, 2000; White and Ross, 2011).

## 2.2 Terminology

Phreatomagmatism was originally defined as the explosive interaction of magma with groundwater (Stearns, 1953). Following Fisher and Schmincke (1984), the term was expanded to include explosive magma-water interaction within any environment, such as with surface water. The term Surtseyan volcanism was introduced by Walker and Croasdale (1972) for the event when magma interacts with shallow sea water. Emergent volcanism is a synonym of Surtseyan volcanism (as in Kokelaar, 1986). Phreatomagmatic fragmentation produces juvenile particles primarily derived from the explosive interaction of magma with water, rather than expansion of magmatic gas bubbles within rising magmas (Wohletz, 1983, 1986; Kokelaar, 1986; Zimanowski et al., 1991, 1997).

Pyroclasts are defined by Fisher and Schmincke (1984) as fragments produced by all types of volcanic eruptions. They can be juvenile (freshly erupted magma) or lithic (country-rock fragments). White and Houghton (2006) are more specific classifying pyroclast as clasts deposited from subaerial, subaqueous, or subsurface jets, plumes, or currents. Then all particles transported in a system triggered by magmatic energy and found in pyroclastic deposits are named pyroclasts, irrespective of their origin. The substrate is the host sediment/rock of an eruption, comprising single or multiple lithologies with distinct physical and hydraulic characteristics. The substrate is where the water is sourced for phreatomagmatic eruptions (c.f. Lorenz, 2003). Two broad types of substrates were distinguished: hard substrate and soft substrate (Lorenz, 2003, Sohn and Park, 2005), although a large range in rock strength and hydraulic properties is naturally possible. Hard rock environments contain water normally in fractures or joints, whereas shallow unconsolidated sediments can be saturated with water between grains (Lorenz, 2003). The AVF is primarily nested within the consolidated, Waitemata Group rocks, although in its southern part, especially the Manukau Lowlands, there is up to tens of meters thick of water-saturated unconsolidated sediments of varying properties. In the case of a Surtseyan eruption, surface water (the sea, a lake, a river) interacts with magma and the substrate does not play an important role in the progress of the eruption (Kokelaar 1983, 1986).

Base surges, the primary radially dispersed currents from phreatomagmatic eruptions, are a dilute form of pyroclastic density current, with a range of steam or water content. In maar-diatreme and tuff ring volcanoes, continuously generated base surges leave deposits that build up ejecta rings around a crater, which is an open pit (White and Ross, 2011). If a crater is cut into the pre-eruptive surface and is underlain by a diatreme a maar is formed (White and Ross, 2011) (Fig. 2.1). A diatreme is a relatively steep-sided (typically cone-shaped) and regular structure within enclosing country rock, and is filled with bedded and unbedded pyroclastic deposits (Fig. 2.1). The craters of both tuff rings and tuff cones are above the pre-

eruptive surface and do not usually have a diatreme (*sensu stricto*) (Fig. 2.1), but may be underlain by a shallow diatreme. Some authors describe the deposits around maars, i.e. ejecta rings, as tuff rings (e.g. Bryner and Grant-Mackie, 1993; Allen et al., 1996; Cassidy et al., 2007; McGee et al., 2012; Geshi et al., 2011), therefore using "tuff ring" (*sensu lato*) referred to such deposits is possible. If ejecta ring craters are filled with lava flows, spatter, and/or scoria and no information of a possible diatreme is known, it is difficult to identify a phreatomagmatic structure as a maar-diatreme or a tuff ring volcano. In this thesis the term tuff ring (*sensu lato*) will be used unless specifically is pointed out that the volcanic structure is a maar-diatreme volcano according to the evidences, otherwise ejecta ring will be used to indicate the tephra ring at the surface.

All types of phreatomagmatic volcanoes are characterized by a vent (or vents), which is an open mouth of a conduit through which material is emitted from the ground during an eruption or phase of eruption (Fig. 2.1). In the next sections the general morphological, stratigraphic, and sedimentary characteristics of phreatomagmatic volcanoes will be presented.

## 2.3 Monogenetic volcanism

Monogenetic volcanoes are formed by single episodes of volcanic activity (Walker, 1993). Around 95% of single scoria cone eruptions last less than 1 year (Wood, 1980), but the lifespan of monogenetic volcanic fields may comprise tens of thousands to millions of years (Walker, 1993). Each magma batch follows a new pathway, because the path used by previous one is frozen (Walker, 1993). Monogenetic eruptions are associated with magma volumes within the range of 0.001 to 0.1 $km^3$ (dense rock equivalent, DRE) that forms lava fields, spatter cones, scoria cones, tuff cones, tuff rings, and maars (Wood, 1980; Walker, 1993; Németh and Martin, 2007; Valentine and Gregg, 2008). Monogenetic volcanoes are typically formed as the consequence of rapid magma ascent (0.5-1.0 m/s for Strombolian eruptions, or faster for fire fountaining activity; Wilson and Head, 1981), with little fractionation or interaction with the crust (e.g. Brenna et al., 2010). They may display changes in eruptive activity in terms of volume or composition (Valentine and Perry, 2006; Martin and Németh, 2004).

The construction of a monogenetic volcano is the consequence of the interaction of several factors, which may include emplacement of magma batches of different compositions (e.g. Smith et al., 2008; Brenna et al., 2010; McGee et al., 2012); abrupt changes in eruptive styles (Houghton et al., 1999; Auer et al., 2007); lateral vent migration (e.g. Auer et al., 2007, Sohn et al., 2012; Valentine, 2012); and long-lived eruptions with changes in magma composition (e.g. Paricutin volcano in Mexico – around 10 years; Luhr and Simkin, 1993; Erlund et al., 2010). Monogenetic volcanoes must be considered in relation to mechanisms of magma production, regional and local tectonics, substrate geology and hydrogeology, climate and weather conditions, and their relationship to neighbouring polygenetic volcanism. In many locations volcanic edifices related to Pleistocene to Holocene phreatomagmatic volcanism are located in coastal

areas [e.g. Jeju island, South Korea (Sohn, 1996); Marion and Prince Edward islands (Verwoerd and Chevallier, 1989); Ambrym Island, Vanuatu (Németh and Cronin, 2011); Hanauma Bay,O'ahu, Hawai'i (Rottas and Houghton; 2012)], contrasting with scoria cones that are formed by magmatic activity farther inland.

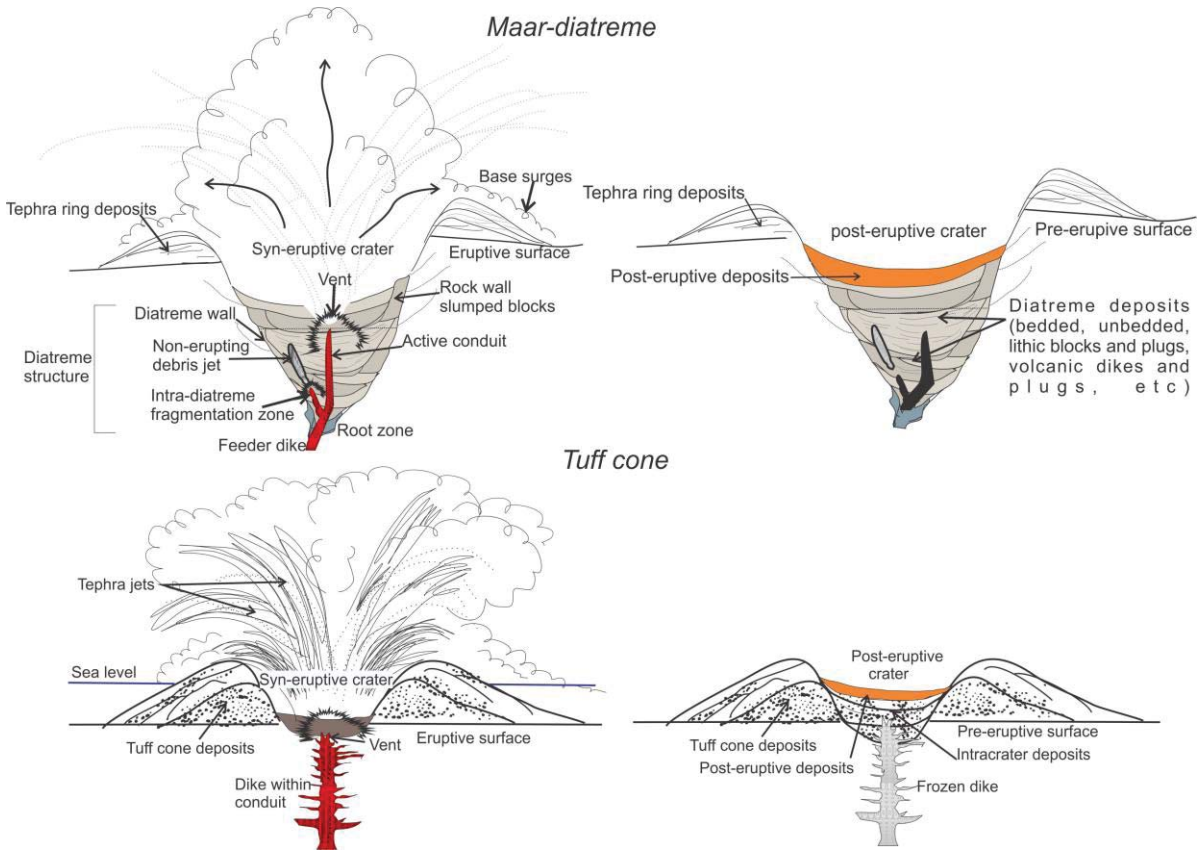


**Fig. 2.1** Schematic cross-section of erupting maar-diatreme and tuff cone volcanoes (left, top and bottom), and of the volcanoes after eruption right when the craters have been partially filled with sediments (modified from White and Ross, 2011). The labels are related to the general terminology used in phreatomagmatic volcanoes.

## 2.4 Generalities of explosive magma-water interaction

### 2.4.1 Magma fragmentation and resulting juvenile pyroclasts

In maar-diatreme and tuff ring eruptions, fragmentation of magma is mainly a consequence of fuel-coolant interactions (FCI). An explosive FCI rapidly converts thermal energy to mechanical energy with a heat transfer rate greatly in excess of normal boiling by several orders of magnitude (Witte et al., 1970). The mechanisms of FCIs and their role in volcanic eruptions are not fully understood (Zimanowski et al., 1991; White, 1996). In general, the phenomenon is seen as a four-stage process: 1) coarse mixing of magma and water and the formation of insulating vapour films ("Leindenfros effect"); 2) collapse of the insulating vapour films resulting in the direct contact of magma with water and rapid heat transfer, causing intense

fragmentation; 3) explosive expansion of coolant mixed with fragmented magma; and 4) additional melt fragmentation induced by hydrodynamic mixing.

Experimental studies (Wohletz, 1983; Zimanowski et al., 1991) suggest that magma is fragmented into sub-millimetre sized particles in FCI-type explosions. *Interactive particles* (Zimanowski et al., 1991) originate directly from the magma-coolant interface, while distant from this, mechanical effects cause fragmentation of both magma and country rock (Wohletz, 1983; Zimanowski et al., 1997). Juvenile pyroclasts formed as the result of FCIs are blocky, poorly-to-non vesicular, with planar or curviplanar smooth surfaces; they may also have more irregular fluidal surfaces ("fused shapes") or plate-like shapes (Fig. 2.2). The fragments may be coated by powders of smaller particles and aggregates (Büttner et al., 1999; 2002). Pitting, secondary mineral growths, and glass alteration may occur. Some of these characteristics may also be present in particles resulting from other types of magma-water interactions (e.g. Zimanowski et al., 1991), or even in some cases of "pure" magmatic fragmentation (e.g. Cioni et al., 1992).

Juvenile pyroclast size and morphology are influenced by degassing of magma and variations in vesiculation, crystallization and chemical composition during an eruption. In addition, coalescence of particles occurs to form aggregates, and further modification occurs during transport and deposition (Zimanowski et al., 1997). Particles may also experience "re-fragmentation" when falling or sliding back into the eruptive vent and becoming involved in subsequent explosions (Kokelaar, 1983; Houghton and Smith, 1993). Then the final morphology of juvenile pyroclasts is the complex result of many factors, so assuming phreatomagmatic fragmentation solely from the morphological and textural characteristics of the juvenile particles alone should be treated with caution.

Magmatic volatile-driven fragmentation may also take place during phreatomagmatic eruptions as it is the case of multiple vent sites with simultaneous magmatic and phreatomagmatic activity, similar to that seen at Surtsey Island, Iceland (Thórarinsson, 1964); Ukinrek East Maar, Alaska (Kienle et al., 1980; Büchel and Lorenz, 1993); Crater Hill maar/scoria cone volcano, AVF (Houghton et al., 1999); Capelinhos and Capelas tuff cone, Azores (Cole et al. 2001; Solgevik et al. 2007), but this is normally of secondary importance. Other subordinate magma fragmentation mechanisms include non-explosive cooling-contraction granulation, as the outer surface of magma cools and shrinks. Further hydrodynamic mechanical processes in the eruption plume produce fragments via particle collision and shear (Frölich et al., 1993).

For emergent-type volcanism (Surtseyan type), FCI's may not be important, and instead bulk-interaction steam explosivity and turbulent mixing dominates (Kokelaar, 1986; Mastin, 1997; Mastin et al., 2004; Mastin, 2007; Mastin et al., 2009). In this case, the magma is torn apart by explosively expanding steam in tephra jets (Fig. 2.1), and magma and water exchange little heat by mixing. Glassy rinds grow on magmatic pyroclasts and they are fragmented by turbulent mixing. High tephra jets generated during these

eruptions eject debris to up to 500 m, so particles landing on the ground surface or water surface may break on impact. The textural characteristics of Surtseyan-related juvenile pyroclastic consist primarily of low-to-moderately-vesicular, lapilli to medium ash that is blocky with smooth, planar grain boundaries or fracture-controlled surfaces (Heiken, 1974; Sohn and Chough, 1993; Mattson, 2010; Murtagh et al., 2011; Murtagh and White, 2013). In these eruptions, so much tephra returns to the vent that common comminution of clasts results from them undergoing repeated explosions (Kokelaar, 1983).

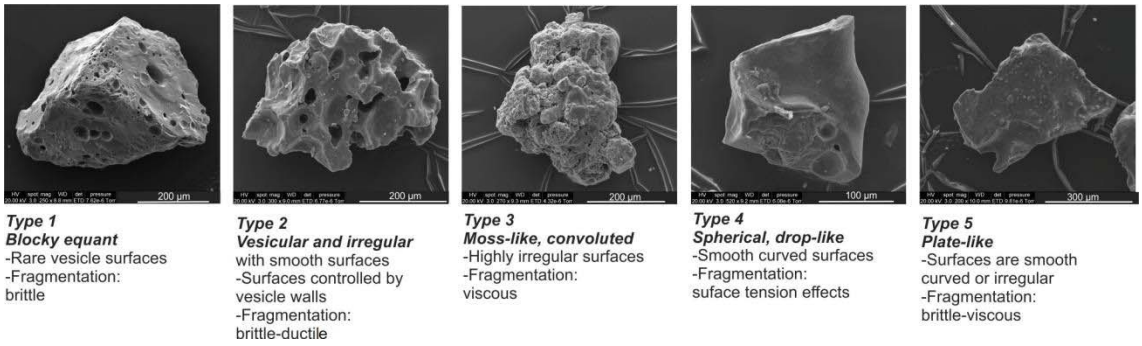


**Fig. 2.2** Main morphological types of juvenile fragments found by experimental results of explosive interaction of magma with water (Wohletz, 1983).

### 2.4.2 Host rock disruption and resulting lithics

From a model developed from experimental and field data, Raue (2004) reports that >60% of the thermal energy of FCI explosions is converted into shock waves, which may disrupt surrounding magma and country rock. Thus the substrate, even if strongly indurated, can easily be fractured and comminuted into blocks or even ash-grade clasts (Raue, 2004; Taddeucci, 2010; Valentine et al., 2011), before being transported and deposited together with juvenile material. Substrates may already be fractured and jointed, or even be composed of unconsolidated sediments, which makes the eruptive fracturing easier (White, 1991b; Lorenz and Haneke, 2004; Agustín-Flores et al., 2014). Furthermore, dike emplacement leading to an eruption may induce hydraulic shearing and fracturing in the host rock (Delaney, 1986). Substrate or host rock can also be disrupted during inward collapses of crater walls (e.g. Sohn and Park, 2005; Auer et al., 2007).The size distribution of lithic particles produced during phreatomagmatic eruptions is broad in tuff rings and maar-diatreme volcanoes and partly reflects the rock properties (Lorenz and Haneke, 2004; White and Ross, 2011). In Surtseyan eruptions the disruption of host rock is negligible, because the eruptions occur in shallow water environments (Kokelaar, 1983), but water-saturated, unconsolidated sediments may be involved (Leat and Thompson, 1988).

### 2.4.3 Transport and deposition of pyroclasts

Phreatomagmatic eruptions produce a range of pyroclast transport processes, including formation of convective tephra plumes, jets (especially Surtseyan eruptions) and explosive blasts, as well as the dominant (in maar-diatreme/tuff ring eruptions but not in Surtseyan eruptions) radially distributed base surges (Lorenz, 2007). Base surges are highly expanded, low particle-concentration flows that are generally vertically stratified, with high particle concentrations and shear acting at the base, and overriding dilute suspensions (Cas and Wright, 1987; Valentine, 1987; Sulpizio et al., 2007) (Fig. 2.3).

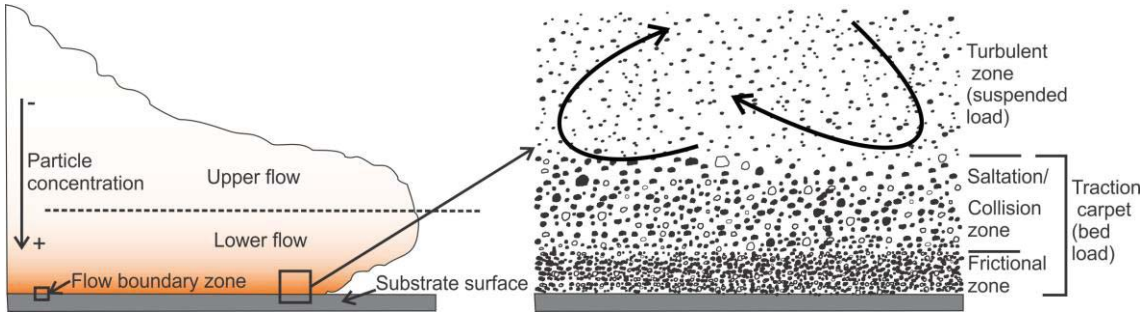


**Fig. 2.3** Generalized schematic cross-section of a dilute pyroclastic density current (base surge). It shows the density stratified nature of the current and the modes of transport of particles within the thickness of the flow. In nature single flows present varied dynamics that are the result of several factors like topography; size, shape, and density of particles; flow inertia, and presence of water.

The sedimentological characteristics of the deposits that make up ejecta rings are often related to the particle concentrations, velocities, and dynamic properties of base surges (e.g. Branney and Kokelaar, 2002; Dellino et al., 2008; Sulpizio et al., 2008; Brand et al., 2014). The processes leading to vertical density stratification of base surges are not well understood (Wohletz and Sheridan, 1979, Valentine, 1987; Sohn, 1997; Branney and Kokelaar, 2002; Sulpizio et al., 2007). Wohletz and Sheridan (1979) attribute the stratification to the variations in the degree of fluidization within a current, Valentine (1987) considers that it reflects the degree of turbulence, while Branney and Kokelaar (2002) infer that at least the basal part of the flow is not fully supported by fluid turbulence, but instead by particle-particle interactions, including frictional forces, rolling, saltation, and suspension (Fig. 2.3). A sharp boundary between turbulent and frictional domains and its relationship with the particle concentration is not clear (Sohn, 1997; Valentine and Fisher, 2000). The basal, denser portion of the current is a *flow-boundary zone* where particles settle from suspension and form a bed load, before particle-particle interaction promotes deposition (Valentine 1987; Dellino et al., 2008; Sulpizio and Dellino, 2008) (Fig. 2.3). Conversely, the upper portion of the current is an expanded gas-rich cloud that contains mainly fine particles held in suspension by turbulent stress (Dellino et al., 2008) (Fig. 2.3).

Hundreds of base surges are normally generated y in eruption sequences. Deposits reflect this by being layered or stacked, each recording deposition from a single current with properties varying depending on the conditions of each explosion (Cas and Wright, 1987). The physical properties of base surges (e.g. density, stratification, and height) and topography are intrinsically interrelated and both define the behaviour of currents (Sulpizio and Dellino, 2008). Particle deposition occurs during steady and unsteady flow of a base surge (Branney and Kokelaar, 2002), which implies that currents have separate transport and depositional systems (Valentine, 1987). Deposition from a base surge may cause it to become more dilute with distance, thus affecting its run-out distance. The rate of deposition depends on the rate of decreasing current velocity and fluid escape from the flow boundary zone. Both factors, in turn, are dependent upon the clast concentration within the flow. Basal particles at flow boundary zone accumulate at the base and aggrade upwards (Fig. 2.3), although Branney and Kokelaar (2002) explain that the final deposit reflects only the conditions of the flow boundary zone during period(s) of deposition, thus the deposit is not representative of the whole depth of the flow that generated such deposit. This contrasts with *en masse* deposition (Sparks, 1976; Wright and Walker, 1981; Carey, 1991) where the flow comes to an abrupt halt over its entire depth. In the case of small-scale PDCs, Sulpizio et al. (2007) proposed a combination of the *en masse* and aggradation models where the sedimentary characteristics of base-surge deposits are formed by halting pulses within density stratified currents on a surface that changes in gradient. Each pulse is characterized by individual flow-boundary zones for their entire thickness. Although this model was developed from small-scale dry pyroclast density currents (e.g. Sulipizio et al., 2007, 2008), the general lithofacies transitions are common to base surge deposits described at tuff rings (e.g. Sohn and Chough, 1989; Chough and Sohn, 1990; Dellino et al., 2004; Vazquez and Ort, 2006).

The role of steam and liquid water in the transport and deposition dynamics of base surges is poorly understood. Based on deposit characteristics, “wet” and “dry” are used as qualitative descriptions of phreatomagmatic eruptive conditions (Brand and Clarke, 2009; Brand et al., 2009). Wet phreatomagmatic conditions occur when external water at the zone of water-magma interaction is not efficiently converted to steam or steam quickly condenses during flow (Sheridan and Wohletz, 1983; Wohletz and McQueen, 1984). In dry base surges, of superheated steam occurs, but it does not condense during flow (Wohletz, 1998). In wet surges in particular, ash particles may accrete together because of cohesion to form various types of clustered particles or coatings on pyroclasts (Valentine and Fisher, 2000; Branney and Kokelaar, 2002). Wet surges are typically identified from deposits by a combination of accretionary lapilli, fine-grained vesiculated tuff, pervasive soft sediment deformation, cross-bedding with stoss-side accretions and evidence for plastering, mud cracks, debris-flow filled erosion channels and lahars (Brand and Clarke, 2009). Some bedforms (for example, antidunes) and highly fragmented ash particles are common to both wet and dry base surges (e.g. Dellino et al., 1990; Brand and Clarke, 2009). Vesiculated tuff is not definitive evidence of water, since vesicles may form in fine-grained eolian soils in arid and semiarid settings by non-volcanic mechanisms (McFadden et al., 1998).

Surtseyan eruptions are characterized intermittent jetting or continuous uprush of tephra, erupted with copious volumes of steam (Kokelaar, 1983; 1986). During the ascent of tephra jets, steam condenses and particles are sorted according to their momentum. Tephra jets deposit most of their load close to vent and rapidly build up cones (Kokelaar, 1986). Additional minor base surges may occur in the form of steam clouds as tephra jets land (e.g. Kokelaar, 1986; Belousov and Belousova, 2001), but most tephra generally falls out. Steep depositional slopes create the conditions for slides and slumps, grain flows, and debris flows as tephra jets land (e.g. Sohn and Chough, 1992; Sohn and Chough, 1993; Sohn et al., 2012). Dry deposition of Surteyan jets leads to grain flows with deposits showing steeply inclined beds of lapillistone and lapilli tuff that are inversely graded, coarsen downslope and have an openwork texture (e.g. Sohn and Chough, 1993). On the other hand, wet tephra jets slump to form debris flow deposits with evidence of gravity-flowage ripples, slump folds, armoured lapilli and plastered tuffs (e.g. Sohn and Chough, 1992).

### 2.4.4 Resulting landforms and deposits

Phreatomagmatic eruptions produce maars, tuff rings, and tuff cones, whose shapes reflect a range of eruptive parameters as well as syn- and post- eruption modification. Complex landforms occur if vent locations shift during an eruption, of if multiple vents are active. Adjacent vents may vary greatly in production rate, and vent configuration or prevailing winds may cause strongly asymmetric deposits (Wohletz and Sheridan, 1983). Similarly, adjacent vents may have different eruption conditions including a combination of wet and dry vents erupting together (e.g. see section 2.4.1).

Maar-diatreme volcanoes are characterized by having craters cut below the pre-eruptive ground surface, surrounded by an ejecta ring, and underlain by a diatreme (White and Ross, 2011) (Fig. 2.1). Maar ejecta rings, as well as tuff rings, usually have low rim heights (from a few meters to tens of meters above the pre-eruptive surface level) and wide craters (a recent thorough review of the literature found that most crater widths range between 200 and 1,500 m; Ross et al., 2011). Diatremes are cut into the pre-eruption substrate, often as an up-turned cone form connected to feeder dikes at depth and capped by a post-eruptive crater fill (lake or other sediment) (Németh et al., 2001; Lorenz, 2003; Németh and White, 2003; Lorenz and Kurszlaukis, 2007; Geshi et al., 2011; White and Ross, 2011) (Fig. 2.1). Tuff rings comprise broad and relatively thin deposits of ejecta similar to that around maar volcanoes, but their craters do not cut below the syn-eruptive ground surface (White and Ross, 2011). Tuff cones are steeper and taller, with smaller craters than tuff rings (Fig. 2.1). Post-eruptive erosion may lower the tephra ring and widening of the crater may occur due to inward collapse (Lorenz, 2007).

Maars and tuff rings exhibit well-stratified deposits, whereas tuff cone deposits are more massive or weakly stratified (White and Ross, 2011). Similar to tuff rings, much of the bedding in maar ejecta rings represents deposits from individual base surges. Typical base surge deposits vary in character with

distance from the vent, beginning with thick, massive and commonly block-rich beds, to well-developed cross-bedding and dune bedforms in medial reaches and thin planar beds in distal reaches (Cas and Wright, 1987; Sohn 1996, and references therein; White and Ross, 2011). A range of complex variations to this typical scheme occur, and many bedforms (ripples, dunes, and antidunes, chute-and-pools, and plane parallel bed) are used to interprete the flow regime and energy of the parent pyroclast density current (Valentine and Fisher, 2000). Long wavelengths and low-angle symmetrical dunes to antidune, climbing-dunes, and chute-and-pool structures in base surges mostly indicate high-energy flow (e.g. Brand et al., 2009). However, factors such as pre-eruption topography and condensed water content affect the flow of currents (Valentine and Fisher, 2000). Douillet et al. (2013) propose that dune bedforms typically indicate high Reynold's Number ($R_e$). Bedforms typically associated with supercritical flow regimes (e.g. chute-and-pool structures) may also form in dominantly sub-critical flow regimes, with local variations within the flow over space or time, probably related in nature to pre-eruptive topography (Sulpizio et al., 2007). Distal planar beds may be related to fall-out processes from highly diluted, low energy, currents (e.g. Sulpizio et al., 2008).

In general, Surtseyan deposits are generally composed of massive or weakly stratified ash beds (e.g. Sohn and Chough 1992, 1993; White 2001; Solgevik et al. 2007). Cross stratification is rare, but crude, planar, or lenticular layers with reverse grading are common (Sohn and Chough, 1992, 1993). Characteristically, the wet-deposited tephra may be yellowish and strongly indurated due to post-eruptive alteration of basaltic glass via palagonitization (Stroncik and Schmincke, 2002). Accretionary and/or armoured lapilli and bedding sags may be present within deposits (Schumacher and Schmincke, 1991; Gilbert and Lane, 1994). Although several models have been proposed for their generation (Scolamacchia et al., 2005), accretionary lapilli are formed as moist aggregates of ash in eruption columns or pyroclast density currents (Fisher and Schmincke, 1984), while armoured lapilli represent ash formed around a solid nucleus (e.g crystals, pumice, and lithic fragments.).

Juvenile particles dominate in tuff cone deposits, but very high contents of lithics may occur in deposits of maars and tuff rings (White and Ross, 2011). The variability in proportions of juvenile to country rock fragments relates to the extent of excavation into the substrate (c.f. Lorenz, 2003). Complex vent conditions with phreatomagmatic explosions at different levels within the crater-diatreme may cause each phreatomagmatic explosion to be characterized by a variable ratio between juvenile and country rock fragments throughout the entire tephra ring (Valentine and White, 2012; Kurszlaukis and Fulop, 2013).

### 2.5 Controls on phreatomagmatic eruptions

The nature of a phreatomagmatic eruption depends upon a range of magma-system properties (eruption rate, composition, gas content, etc.) and environmental factors (substrate geology and hydrology, topography, tectonic structure, and even climate at the time of eruption) (Lorenz, 2003; Auer et al., 2007;

Németh et al., 2008; Kereszturi et al., 2011). In general, a significant amount of water is needed to trigger phreatomagmatic eruptions and there is a wide overlap that may occur between purely magmatic fragmentation and phreatomagmatic eruptions both between eruption events and sites and also during eruptions. Eruptions may include a specific phase or multiple phases of phreatomagmatism, intercalated with magmatic events, with both phreatomagmatic onsets and terminations possible.

Section 2.4.1 mentions that in subaerial maar/tuff ring eruptions magma interacts with ground water and generate highly energetic FCIs. Conditions that influence these eruptions include the geometry of water-magma contact, confinement pressure, the water to magma mass ratio and the temperature difference between magma and water (Sheridan and Wohletz, 1983; Büttner and Zimmanowski, 1998; Zimanowski and Wohletz, 2000). Other factors include, but are not limited to, magma eruption rate and the hydrogeological conditions of the substrate (Zimanowski, 1998; Houghton et al., 1999). The latter comprises the rock strength, saturation state, permeability, and wider water supply, which affects the interaction of magma with groundwater.

Of these many factors, the mixing ratio of water to magma was proposed to be the main factor that contributes to the explosive style of phreatomagmatic eruptions (e.g. Wohletz, 1983; Sheridan and Wohletz, 1983; Wohletz, 1986; Kokelaar, 1986). Experimentally, Wohletz (1983) found a value of 1:3 as the optimum water to magma ratio for maximum efficiency in the conversion of thermal to mechanical energy. However, from quantitative experiments, Zimanowski et al. (1991) obtained lower values, between 1:25 and 1:35, for the water to magma ratios in highly explosive interactions. Magma to water ratios vary both spatially in an eruption site, but may also vary temporally during an eruption due to changes in magma flux (Kokelaar 1983, 1986), exhaustion or exclusion of external water (Brand and White, 2007), turbulence and mixing processes (Büttner and Zimanowski, 1998; Mastin et al., 2004), or variable magmatic volatiles (Houghton and Wilson, 1989; Houghton et al., 1999). On the other hand, White (1996) and Schipper et al. (2011) found during experiments that fine sediment/mud at the site of water-magma interaction strongly enhances hydrodynamic mingling, creating an efficient fuel-coolant mix for energetic FCIs. In natural systems, mixtures of sediments (or volcaniclastic debris) and water are the coolant, changing the dynamics on interacting with magma (White, 1996). Sediment slurries have a starkly different density, viscosity, heat conductivity and heat capacity to pure water and decrease the surface contact of “pure” water and magma, while sediment in the slurry acts a partial heat sink for magma. Consequently, slurries may inhibit an initial explosive interaction, although once started, sediment-laden coolants may promote FCI explosivity by increasing the availability of nucleation sites (White, 1996). In addition, White (1996) noted that other factors should not be overlooked, such as lithological and hydrogeological conditions of aquifers, groundwater/surface water characteristics, confinement pressure, magma properties, and physical properties of the country rock. Sohn (1996) inferred that morphological variations in tephra ring deposits are directly caused by depositional processes irrespective of water to magma mass mixing ratios. Indeed, “wet” characteristics of deposits also most strongly represent conditions at the time

of deposition and only secondarily properties of the FCIs. Water may also be directly ejected from the vent area (White, 1996), or condense from steam during transport (Sheridan and Wohletz, 1983; Wohletz and McQueen, 1984). These observations enhance the importance of the hydrogeological conditions substrate and surface hydrology characteristics as ultimately water is the main control of phreatomagmatic explosions.

Identification of widespread phreatomagmatism in many volcanic fields suggests extensive surface and groundwater availability (e.g. Sohn, 1996). Groundwater involved in phreatomagmatic eruptions is contained in aquifers with diverse lithological and hydrogeological characteristics. Different degrees of rock strength, porosity, permeability, jointing, and folding contribute to strong variations in the ability of a substrate to supply water to a phreatomagmatic vent site. In porous media, groundwater may flow through pores to the vent site, but in some lithologies the only water flow may be via fracture systems. The flow of water to the vent site also depends on the hydraulic head, the rate of porous or fracture flow and the general lateral availability of water. The hydraulic characteristics of aquifers may be enhanced by the creation of new fractures or the enlargement of old fractures by volcanic seismicity, fracturing by dike intrusion (Delaney, 1986), or by shock waves generated in FCIs (Lorenz and Kurszlaukis, 2007; Valentine, 2012). During the course of the eruption, water will permeate a diatreme infill, which becomes a site for magma-water interaction (Valentine and White, 2011) in intra-diatreme fragmentation zones (White and Ross, 2011). Moreover, natural phreatomagmatic vents are complex dynamic environments, disrupted by seismicity, overlain by tons of wet debris, and enclosed by unstable walls (White, 1996). These lead to variations in confining pressure, fluidization, heterogeneity in fill properties and hydrology, all of which affect the explosivity of magma-water mixing The fact that aquifers are usually restricted to the last few hundred meters from the surface and FCI explosions are more effective at depths <1 km, and specially <100 m below the water table (Büttner and Zimanowski, 2003), phreatomagmatic explosions may occur dominantly at these depths. Independently of all the factors that control phreatomagmatic eruptions, the role of the substrate – or the presence of surface water – as the container of water is significant as demonstrated by this thesis (Agustín-Flores et al., 2014; 2015a, 2015b) and other studies (White 1991b, 1996; Lorenz, 2003, Sohn and Park, 2005; Auer et al., 2007; Németh et al., 2010, 2012a; Valentine, 2012).

## 2.6 Overview on kimberlite pipes in the substrate context

The volcanic origin of kimberlite pipes is fully accepted. Although there has been considerable debate about whether explosive kimberlite eruptions were driven by exsolving magma volatiles or by explosive magma – external water interaction, no magma system erupts just one way or the other (Cas et al., 2008). It depends on whether or not rising magma encounters external water. So, just like with any other magma system, some kimberlite explosive eruptions will have been driven by exolving magmatic volatiles, and some may have involved explosive interaction with external water (Cas et al., 2008). Due to the lack of

modern volcanological methodology in the study of kimberlites, the formation of a kimberlite pipe is not well understood (Cas et al., 2008). Regarding the diatreme shape and geometry there are similarities between kimberlite pipes and maar-diatreme volcanoes associated to phreatomagmatic explosions. Stiil there are some differences in some aspects of infill deposit structure. The most remarkable difference between kimberlite pipes and phreatomagmatic-related maar-diatreme volcanoes is the magma composition. As other non-phreatomagmatic-related maar-diatreme volcanoes, kimberlite pipes are associated to the eruption of volatile-rich, ultramafic magmas.

Irrespective of the mode of magma fragmentation in kimberlite pipes, according to Field and Scott Smith (1999), the emplacement mechanism of kimberlite pipes is strongly controlled by nature and strength of local country rock. From the study of kimberlites in Africa and Canada, the authors propose three general modes of emplacements in relation to three different geological settings: competent country rock, poorly consolidated sediment, and basement covered by a veneer of poorly consolidated sediments. Supporting this view, Barnett (2008) found that large scale rock mass behaviour around an excavation, such as a volcanic pipe, is dependent on the rock mass strength, the in-situ rock stress conditions and the excavation geometry. Cas et al. (2008) argue that the three end members view by Field and Scott Smitth (1999) are an oversimplification because the variability of kimberlite pipe morphology and deposit type is also influenced by magma volume and rise rate, volatile content, presence of absent of external water, depth, size, and nature of aquifers, and not only by the competency of the country rock. However, the influence of the substrate in the emplacement of kimberlite pipes, although not fully understood, appears to be attested by other studies. Cas and Wright (1987) document the occurrence of phreatomagmatic craters associated to the emplacement of kimberlite pipes within a cover of aquifer-bearing sediments overlying the basement, in western Victoria (Australia). In places where the cover sediments are absent, scoria cones and lava shield form. Without inferring the mode of magma fragmentation, Pittari et al. (2008) recognize from the facies architecture the relationship between the emplacement processes of kimberlite pipes (Orion Central kimberlite volcanic complex, Canada) and the type of substrate. The identification of phreatomagmatic phases related to the type of substrate encountered in the emplacement of kimberlite pipes is documented in Canada (Field and Scott Smith, 1999; Lefebvre and Kurszlaukis, 2008) and Western Australia (Lewis, 1990). In general, the phreatomagmatic activity in the emplacement of kimberlite pipes in the last examples is related to substrates that contained aquifers and were located in the upper lithologies before magma reached the surface. This is similar to the conditions for a phreatomagmatic explosion to occur in the formation of maar-diatreme volcanoes (see last section).

Regardless the differences in the magma composition that originated kimberlite pipes and most maar-diatreme volcanoes, still the substrate appears to control the eruptions dynamics in the formation of both types of volcanic structures. However, due to the controversies on the emplacement of kimberlite pipes, maar-diatreme, tuff ring, and tuff cone examples associated unambiguously to phreatomagmatism will be used for comparison to the volcanoes studied this thesis.

## 2.7 Conclusions

This review chapter shows that a wide range of factors play a role in phreatomagmatic eruptions. Quantitatively assessing the extent of how each variable in isolation influences these eruptions is very difficult. In general only the major influencing factor can be understood from examining eruption deposits. In some cases, where very small volumes of magma are involved and if substrate conditions are known (e.g. Orakei maar in the Auckland Volcanic Field; Németh et al., 2012a; this study) hydrogeological controls may be elucidated.

Maar-diatremes, tuff rings and tuff cones are the typical forms of monogenetic phreatomagmatic volcanoes generated by explosive interaction of magma with water. The fragmentation of magma is primarily characterized by FCIs in maar-diatreme and tuff rings, and by bulk interaction explosivity in tuff cones. The disruption of the substrate, promoted in part by the energy released by FCIs, may be important in maar-diatreme/tuff ring formation, whereas in tuff cone construction this substrate influence is practically negligible. Base surges are generated primarily during maar-diatreme/tuff ring formation, whereas Surtseyan/emergent volcanism is dominated by tephra jetting and secondary base surges, as these jets collapse onto the ground surface. Although tephra fall is associated with phreatomagmatic eruptions, the eruptive products of phreatomagmatic eruptions are commonly dominated by either repetitive base surge or tephra jetting deposits.

Base surges are composed of a two-phase (solid and gas) and/or a three-phase (solid, liquid, gas) flow and transported as density stratified, low concentration pyroclastic density currents. These have generally a lower frictional regime, dominated by grain-grain interactions overlain by a dominantly turbulent and more dilute regime. Deposition is normally related to the decreasing current velocity and turbulence, and the rate of fluid escape. Water in the liquid state may affect transport and depositional processes. The deposits are commonly stratified with dune and planar bedforms, and depending on the wetness by the time of deposition may contain accretionary lapilli and soft sediment deformation structures. In the case of tuff cones formed by Surtseyan/emergent volcanism, they are formed mainly by the deposition of material from tephra jets, which have shorter run-out distances than base surges. Instead, tephra piles up more steeply on the volcano flanks.

Phreatomagmatic processes occurring from the initial opening of the vent to the termination of eruption comprise several factors that interact in a complex manner. Simple views of magma to water mass ratios as control on phreatomagmatic volcanism were popular in the 1980s, but these are far too simple to explain the variability of eruptive dynamics in these types of events. Consequently, the role of other factors in influencing phreatomagmatic eruption styles must be better investigated. The remainder of this thesis will thus primarily assess the role of the hydrogeological conditions of the substrate in phreatomagmatic eruptions, using maar, tuff ring, and tuff cone examples from the AVF.

# Chapter 3. Geological and hydrogeological setting

**Contents** Page



## 3.1 Introduction

The general approach of this study is to integrate an understanding of the hydrogeological conditions of the range ofsubstrates into the framework of the studied phreatomagmatic eruptions in the AVF (Fig. 3.1). In the northern AVF phreatomagmatic eruptions have occurred through a hard substrate (the Waitemata Group), whereas a combination of hard rock and unconsolidated sediment substrates (the Waitemata Group overlain by the Kaawa Formation and the Tauranga Group) are present in the Manukau Lowlands (southern AVF) (Fig. 3.2).The three sites selected for study were the following volcanoes (Fig. 3.1):

- Maungataketake/Ellett´s Mt. (subaerial volcanism - thick unconsolidated sediment cap over firm Waitemata rocks),
- Motukorea/Browns Island (subaerial volcanism – firm Waitemata rock-substrate over hard rock basement), and,
- North Head/Maungauika (Surtseyan volcanism, shallow water over firm Waitemata Group substrate).

These volcanoes provide good exposure in which to examine major portions of the stratigraphy and sedimentology of their phreatomagmatic deposits. While there have been significant glacio-eustatic sea-level changes over the last 250 k.y. (henceforth *k.y*, thousand of years, implies duration of time, but *ka* indicates an age) period in the Auckland region, the substrate lithology and structural conditions have remained essentially constant and past hydrogeological parameters can be inferred from current parameters.

Maungataketake volcano is located in the Manukau Lowlands, in the southern AVF (Fig. 3.1). The phreatomagmatic phases of this eruption occurred primarily within unconsolidated sediments, which

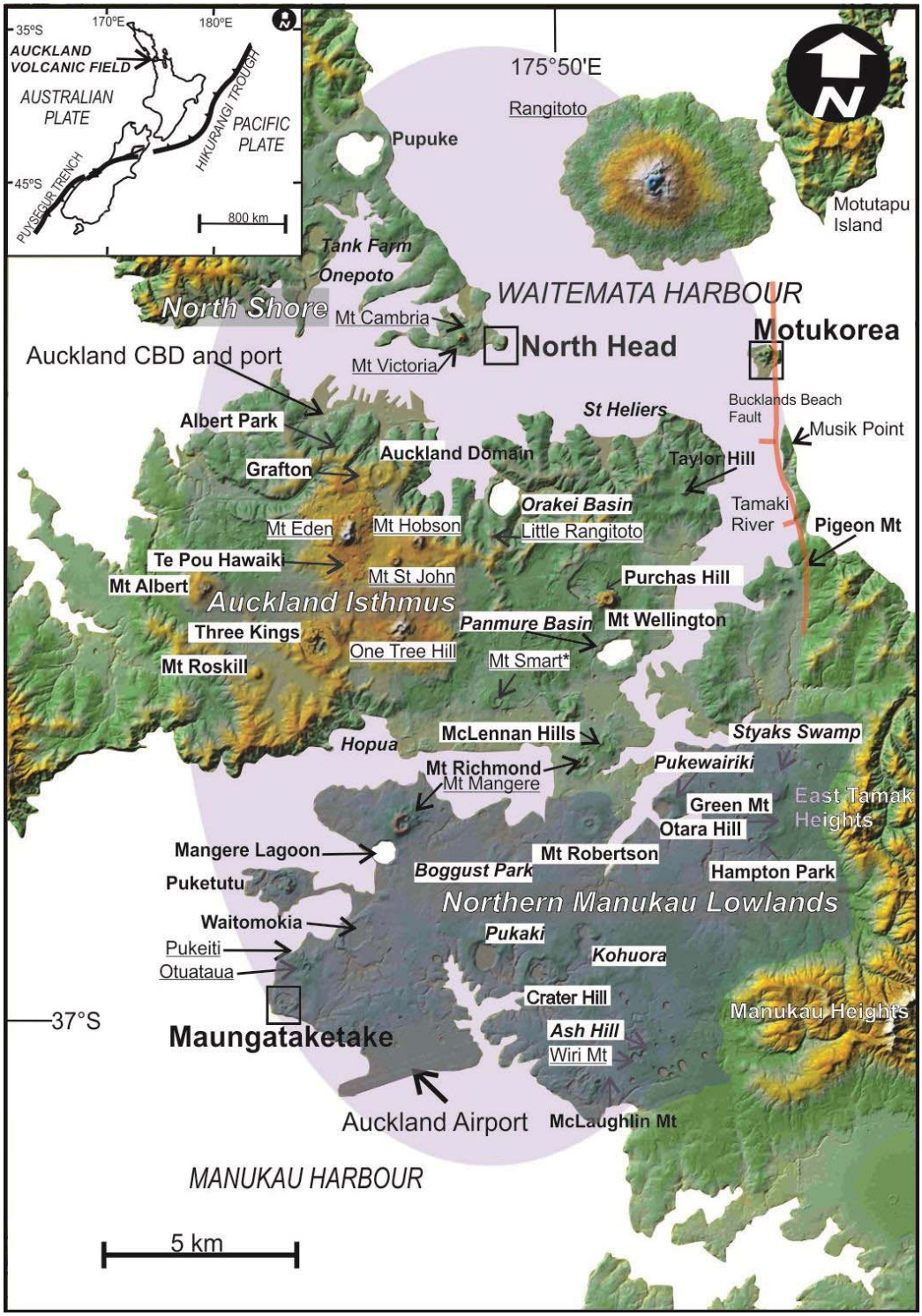


**Fig. 3.1** The AVF with the location of Maungataketake, Motukorea, and North Head volcanoes, along with other volcanoes. Underlined names in regular fonts represent volcanoes that do not have evidence of phreatomagmatic activity (e.g. Mt. Hobson); names in bold fonts include both magmatic and phreatomagmatic activity (e.g. Pupuke); and names in italic bold fonts are those that show phreatomagmatic activity only (e.g. Onepoto). The superposed ellipse corresponds to the boundary of the AVF according to Spörli and Eastwood (1997). The Auckland City urban area covers most of the displayed region (the Auckland central business district, CBD, port, and airport are indicated). The shaded area is the (Northern) Manukau Lowlands. The maximum altitude above sea level in the shown area is 260 m at the summit of Rangitoto volcano. The red line represents the N- trending fault, down-thrown to the west, inferred by Kenny et al. (2012).

include the few m-thick, shallow marine Kawa Formation shelly sands, capped by approximately 60 m of muddy estuarine deposits (Tauranga Group) (Fig. 3.2).The former comprises a good aquifer, whereas the latter is an aquitard. The unconsolidated sediments are underlain by the Waitemata Group rocks. Although the phreatomagmatic crater was covered by magmatic products, magnetic anomalies indicating a subsurface magmatic body lying in the possible phreatomagmatic crater (Cassidy and Locke, 2010) may suggest that a phreatomagmatic crater cut into the pre-eruptive surface. Then a maar-diatreme volcano was formed in the initial stage of the eruption. The age of the Maungataketake volcano is a matter of debate, with age estimates ranging from ~33 ka to 177 ka (Lindsay et al., 2011). Based on morphological, sedimentary, and paleoenvironmental information, an old age is favoured (see chapter 5 for discussion).

Motukorea volcano is located in the north-eastern sector of the AVF (Fig. 3.1). Although the volcano is currently an island, its eruption took place at a lower sea level than the present day and was a subaerial event. The eruption was hosted within the Waitemata Group rock sequence, which is a turbiditic siltstone and sandstone succession (Fig. 3.2). Based on an early Holocene high stand terrace the built over lava flows (Bryner, 1991) the volcano must be older than 7-9 ka. The volcano erupted when sea-level was around 120 m lower than that of the present day, pushing its minimum age back toward 15 ka. This is consistent with a recent Ar-Ar age determination on juvenile material of 14.3 ± 5.5. ka (Leonard Graham, written communication 2014). It is unknown whether the Motukorea phreatomagmatic crater cuts the pre-eruptive surface, but from the lithic contents and ejecta ring size (see chapter 6), it is evident that it formed a maar-diatreme volcano. Most often it is regarded as a tuff ring, but in this study if referred as a tuff ring it will be in the broad sense meaning.

North Head is located in the northern sector of the AVF (Fig. 3.1). This volcano was apparently formed during a period when sea level was higher than the present day and it represents the only known example of Surtseyan volcanism in the AVF. The Waitemata Harbour (Fig. 3.1) was formed by post-glacial rise in sea level, from 14 to 10 ka BP (Searle, 1959). However, the absence of post 14 ka BP tephra layers corresponding to North Head in nearby sediment cores (Molloy et al., 2009; Bebbington and Cronin 2011) suggests a much greater age for this centre. The only time over the last 250 k.y. when sea level was higher than current levels during the last interglacial at 128-116 ka, when sea level was up to ~12 m higher than the present day (Pillans, 1983, Siddall et al. 2006). Recognizing the tectonic stability in the AVF area during the last 125 k.y. (Beavan and Litchfield, 2012), this is the most likely eruption age range for North Head. The eruption formed an initial tuff cone followed by the deposition of spatter, scoria, and a small lava flow.

### 3.2 Geological and tectonic setting of the AVF

Based on measurements from light detection and ranging (LiDAR) data in combination with geological mapping, the minimum DRE volume of the eruption products of the AVF is 1.7 $km^3$ (Kereszturi et al., 2013), a more conservative figure than the 3.42 $km^3$ estimated by Allen and Smith (1994) using simple

geometrical approaches at each volcano. The revised output suggests overall average spatial and temporal magma fluxes of 0.005 $km^3/km^2$ and 0.007 $km^3$/k.y. respectively (Kereszturi et al., 2013). Eruptions were very sporadic over the last 250 k.y., with the majority clustered over the last ~50 k.y. (Allen and Smith, 1994; Molloy et al., 2009, Bebbington and Cronin, 2011). The rocks of the AVF are olivine-phyric moderately primitive basalts, basanites, and nephelinites (Smith et al., 2009).

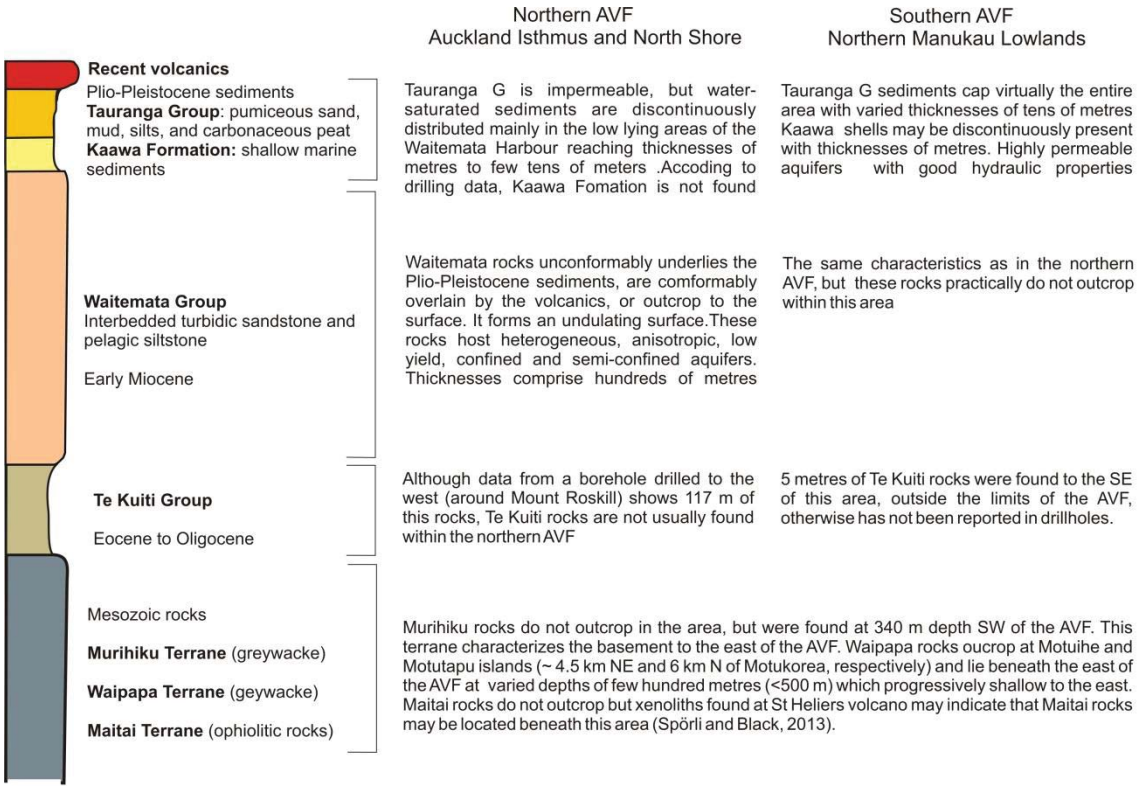


**Fig. 3.2** Generalized regional stratigraphic column of the lithologies found beneath the AVF. General characteristics (e.g. approximate thicknesses) of those lithologies underneath the two specific regions of the AVF are also shown. ***For more detailed information about the distribution and thicknesses of the substrate lithologies beneath the AVF see Appendix A.1.***

The AVF lies on the Australian Plate approximately 400 km from the trench formed at the convergence with the subducting Pacific Plate (Smith, 1989) (insets Figs. 3.1, 3.3). The regional basement of the AVF is composed of Permian to Mesozoic, north-westerly striking terranes formed or accreted along the margin of east Gondwana (Spörli and Black, 2013). They consist of the Murihiku, Maitai and Waipapa Terranes from west to east (Figs. 3.2, 3.3). The Murihiku Terrane is composed of a belt of very low grade metamorphic (up to zeolite facies) Mesozoic volcaniclastic rocks (Briggs et al., 2004) deposited in a deep water fore-arc basin (Spörli 1978). The Maitai Terrane is composed by variably serpentinised ultramafic ophiolitic rocks that cause strong NNW-trending gravity and magnetic anomalies, known collectively as the Junction Magnetic Anomaly (Cassidy and Locke, 2010). The Waipapa terrane dominantly consists of a Late Jurassic terrigenous clastic greywacke sandstone/mudstone sequence (Adams and Maas, 2004). It includes regularly interspersed seams of basic volcanic rocks, red cherts, and red and green argillites (Spörli and Black, 2013).

The basement rocks are overlain on a sharp unconformity by the Oligocene Te Kuiti Group and the Miocene Waitemata Group (Hayward, 1993; Edbrooke et al., 1998; Edbrooke, 2001) (Fig. 3.2). This records the uplift of large islands above sea level on a broad submerged plateau during the Cretaceous to the Early Eocene (Kermode, 1992). The Te Kuiti Group is only exposed south of the AVF and includes basal coal measures overlain by a calcareous unit (Edbrooke, 2001) (Fig. 3.3).

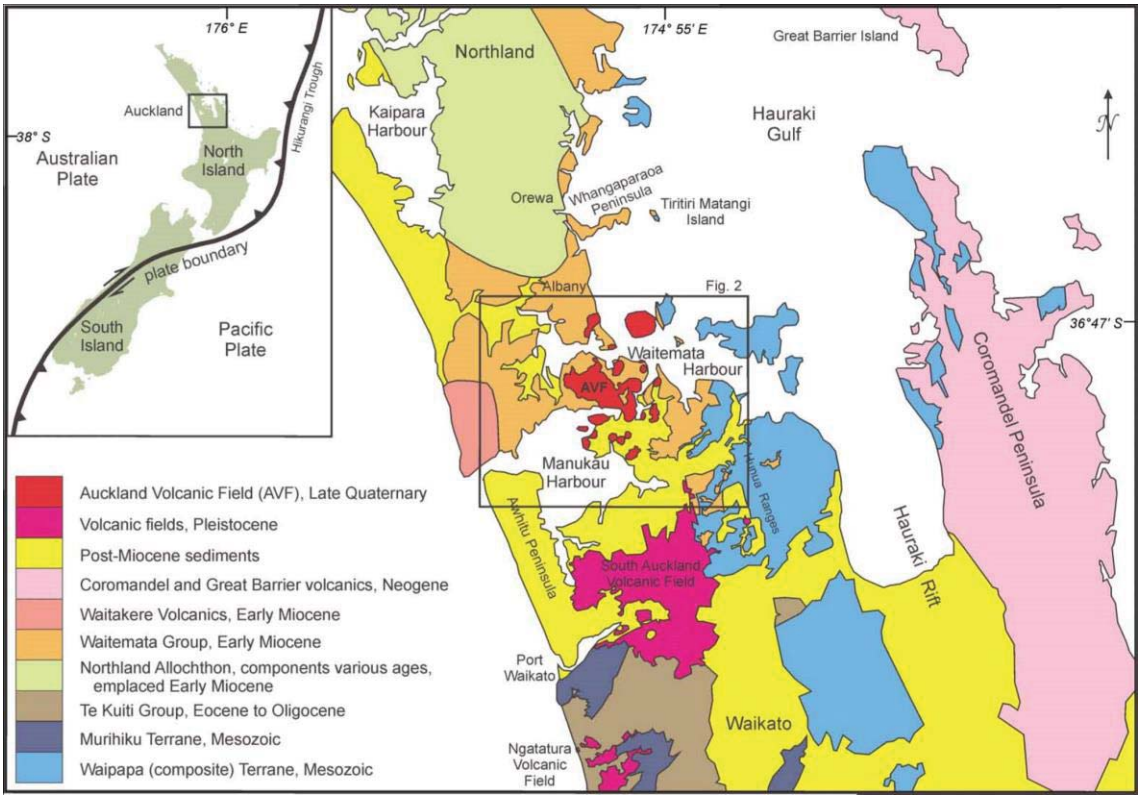


**Fig. 3.3** Simplified geology map from the area surrounding the Auckland region (from Kenny et al., 2012). The inset shows a box representing the enlarged area in Fig. 3.1. The post-Miocene sediments correspond to the Kaawa Formation and Tauranga Group deposits (Fig. 3.2).

It is widely accepted that the Miocene Waitemata Basin is an intra-arc basin developed between two calc-alkaline volcanic arcs (Balance, 1974; Hayward, 1979, 1993). During the Early Miocene (17 to 15 Ma) the Auckland area was characterized by volcanism related to the subduction of the Pacific Plate to the east (Kermode, 1992; Booden et al., 2011). The subduction progressed southward causing the migration of volcanism from Northland to the Auckland area coincident with development of the deep marine Waitemata Basin. The basin was slowly filled with sands and muds primarily sourced from the Northland Allochthon (composed by Upper Cretaceous and Upper Oligecene sediments, and volcanic units) (Fig. 3.3) and the volcanic sediments from the active western volcanic arc (Irwin, 2009). Sedimenation continued within the subsiding Waitemata Basin until at least 17 Ma and large-scale slab block faulting of the infill began about 15 m.y. ago. In the Late Miocene and Pliocene (7-2 Ma) crustal movements raised the greywacke hills to the east (Waipapa Terrane) and also the consolidated sediments of the Waitemata Basin (c.f. Kermode, 1992, Hayward, 2004). Plio-Pleistocene sediments were subsequently deposited in

depressions formed during block faulting, infilling the valleys in the more strongly uplifted Auckland isthmus area (Affleck et al., 2001), while capping the lowlands of the Manukau Harbour and the Hauraki Gulf (Berry, 1986) (Figs. 3.2, 3.3).

From approximately 10 Ma onwards intraplate volcanism developed in Northland (Smith et al., 1993). In the Late Pliocene to Quaternary, small basaltic volcanic fields also developed in the south Auckland area (Briggs and Goles, 1984; Briggs et al., 1990; 1994) (Fig. 3.3). The AVF is the youngest and most northern of four volcanic fields which extend approximately 100 km southwards. A hot spot is not considered the origin of this set of fields; instead it is attributed to the opening of the Hauraki Rift to the East in the Miocene (Hodder, 1984; Hochstein and Balance, 1993), or the fracturing of the lithosphere (Spörli and Eastwood, 1997).

McGee et al. (2013) suggests that there are three specific components in the source region of magma generation beneath the AVF: dominantly fertile peridotite, more depleted peridotite at shallower levels and a small proportion of eclogitic material. Garnet-bearing peridotite is involved in the generation of all magmas in the AVF, implying melting in the asthenospheric mantle (~80-90 km). With larger degrees of melting in the asthenosphere some of the subduction-metasomatized lithospheric shallow mantle (~60-70 km depth) is involved, such as at the largest and youngest volcano in the field, Rangitoto volcano (McGee et al., 2011; 2013). Crustal assimilation does not appear to occur in the AVF and the magma is little modified or unmodified by low pressure fractional crystallization (McGee et al., 2013), thus magmas likely rose rapidly from source to the surface.

The Auckland region is one of New Zealand's most tectonically stable areas and only the Wairoa North Fault in the Hunua Ranges is considered to be active (Kenny et al., 2012). Although the seismic hazard in Auckland is low (Stirling et al., 2002; Sherbun et al., 2007), the presence of low-level seismicity together with numerous faults surrounding the central Auckland area indicate that there could be concealed faults in the Auckland area (Kenny et al., 2012). Using borehole, structural, and geophysical data, Kenny et al. (2012) inferred two of these fossil faults sets beneath the AVF. One set dominantly trends NNW and truncates the other trending approximately ENE. These fit the regional structural pattern and link the position of the Junction Magnetic Anomaly (JMA) with Auckland volcanism. This may imply that the eastern and western boundaries of the JMA form the outer boundaries of the AVF, and the Maitai Terrane rocks (which represents a "suture" structure between the Waipapa and Murihiku Terranes) (Fig. 3.3) may provide a zone of weakness for magma ascent. Cassidy and Locke (2010) and Kenny et al. (2012) suggest that when the rising magma encounters the Waitemata Group sediments it might follow joints or other planes of weakness, fanning outwards to reach the surface near faults but not necessarily along them, explaining the pattern that most vents are located within 500 m of mapped faults. In the Yucca Mountain region, Nevada, Connor et al. (2000) showed that individual vents and short vent alignments occur along and adjacent to faults, particularly at fault intersections, and left-stepping *en echelon* fault

segments. The identification of several new faults in the area covered by the AVF may mean that there is greater structural control on volcanism that was previously thought (Cassidy and Locke, 2010; Kenny et al., 2012). However, the AVF volcanoes show no apparent spatial-temporal eruption pattern, so that although there may be spatial patterns, there is still spatial-temporal independency (Bebbington and Cronin, 2011; Le Corvec et al., 2013).

Spatial and temporal magma flux and eruption recurrence rates for the AVF appear highly variable. From a geochemical approach, McGee et al. (2013) suggest that the size of a volcanic centre is controlled by the degree of partial melting in the deep asthenosphere. Vent location is probably a function of the source melting (Le Corvec et al., 2013) modified by fault and crustal structural control (Kenny et al., 2012). Kereszturi et al. (2013) show that the AVF is neither "volume predictable" (i.e. supply controlled), or "time predictable" (controlled by external forces operating on a regular timescale). The field is young (<250 ka), which suggests that it may be at a very early stage in its evolution (Cassidy and Locke, 2010).

The eruptions of the AVF are characterized by eruptive styles ranging from effusion of lava flows, fire-fountaining and Strombolian events, through to phreatomagmatic explosions, producing a range of lava fields, scoria cones, tuff rings, maars, and tuff cones (Searle and Mayhill, 1981; Allen and Smith, 1994; Kereszturi et al., 2013) (Fig. 3.1). Generally, the phreatomagmatic phases were followed by "dry" magmatic explosive and/or effusive phases. Each volcanic centre, however, displays a complex variation in eruption styles, such as those related to variations in magma-water interactions during phreatomagmatic phases (e.g. Crater Hill volcano; Houghton et al., 1999; Motukorea volcano; McGee et al., 2012; this study).

The phreatomagmatic volcanoes of AVF have craters ranging from ~200 to 1600 m in diameter. These are usually surrounded by tephra rings, comprising pyroclastic surge and fall deposit successions (Allen et al., 1996; Houghton et al., 1999; Németh et al., 2012a). The estimated total bulk volume for ejecta rings in the AVF is 0.38 $km^3$ (Kereszturi et al., 2013). Further, Cassidy and Locke (2010) showed that substantial lava or diatreme-like bodies lie beneath many Auckland maars, the resolution of the applied geophysical methods is however unable to indicate any insights into these proposed diatremes and their structure.

Kereszturi et al. (2013) estimated the duration of a phreatomagmatic phase of an AVF eruption to be 0.1 to 30 days based on eruption volumes and an average magma effusion rate of 10 $m^3/s$. Although the proportion of volume erupted is greatest within magmatic phases, base surges during the phreatomagmatic eruptions are likely the most deadly events, with currents travelling up to 3 km from the vent (c.f., Walker, 1984). In these currents, the combination of high velocities and the solid components result in dynamic pressures >100 kPa (where structural damage is severe between 20-30 kPa) (Valentine, 1998). Brand et al. (2014) suggest that complete destruction of buildings will occur within 1.5 km from the vent, heavy damage to reinforced structures out to 2 km, and severe damage to weaker structures up to 3 km away. Other important syn-eruptive hazards associated to phreatomagmatic eruptions are: syneruptive

earthquakes, eruption clouds, tephra fall, ballistic blocks and bombs, and lahars (Lorenz, 2007).The AVF is almost completely urbanised within the boundaries of Auckland city (population ~1.4 million) and thus hazards associated with phreatomagmatism in the field is not negligible.

## 3.3 The AVF hydrogeology

Substrates are important to characterise because phreatomagmatic explosions in maar-diatreme and tuff ring volcanoes take place below the ground surface, as much as 2 km deep, but mostly within a few hundred metres, where water vapour has a much larger specific volume generating more energetic phreatomagmatic explosions (c.f. Lorenz, 1986). The groundwater content and circulation within a substrate then are important characteristics to investigate in order set the framework in which a phreatomagmatic eruption occurs, and infer the control of such substrate. ***The distribution and thicknesses of the substrate lithologies is described in Appendix A.1 and some of the hydrogeological parametres related mostly to the Waitemata rocks is presented in Appendix A.2.***

### 3.3.1 The Waitemata group

Most of the AVF is underlain by up to 1000 m of early Miocene, Waitemata Group sediments (Fig. 3.2). These consist mainly of inter-bedded turbiditic sandstones and pelagic siltstones with subordinate breccias and conglomerates, and rare limestone and quartztose sandstone (Ballance, 1974; Hayward, 1979; Raza et al., 1999) (Fig. 3.2). These sediments were subjected to a complex combination of non-tectonic and tectonic deformation during and after their deposition (Spörli and Rowland, 2007). The Waitemata rocks units have a ~5 MPa compressive strength, characteristic of a weak but dominantly indurated rock (Spörli and Rowland, 2007). A variety of sandstone bedding thicknesses and types occur in the Waitemata lithologies (Simpson, 1987; Sheridan, 2006; Irwin, 2009, Kenny et al., 2011).The mud content of the units dictates their hydraulic conductivity (Sheridan, 2006), leading to low and very low permeability (average of $2.7x10^{-2}$ m/day) (Viljevac et al., 2002), except where fracturing enhances ipermeability. Aquifers within the Waitemata Group rocks are confined or semi-confined and can supply anything from few $m^3$ to over 1000 $m^3$ of water per day in pump tests (Scoble and Millar, 1995; Crowcroft and Smaill, 2001). The water includes a hard, calcium carbonate-rich, neutral pH, shallow (<200 m) aquifer with high >40 $g/cm^3$ silica content, and a soft, sodium bicarbonate-rich, deeper water with high pH, low total iron and silica content (Crowcroft and Smaill, 2001). ***Appendix A.2 shows a table with data on the hydraulic properties and thicknesses of Waitemata aquifers in the Auckland area***.

### 3.3.2 Basin filling Pliocene sediments: the Kaawa formation

Across the Manukau Lowlands, the Waitemata Group basement is unconformably overlain by poorly consolidated Pliocene shallow marine and estuarine beds of the Kaawa Formation (Edbrooke et al. 2003) (Fig. 3.2). The thickness of these highly permeable, poorly consolidated, shallow marine sediments is not

well documented in the Manukau Lowlands (Viljevac et al., 2002). Searle (1959) reported that the Kaawa Formation was present as discrete lenses at different depths. Using geological and borehole information, Viljevac et al. (2002) inferred that in the southern coast of the Manukau Harbour (~12 km S-SE of the studied Maungataketake volcano) it was anything from a few metres to ~50 m, with a maximum thickness of >250 m attained farther south. Since Kaawa sediments filled paleochannels, the thickness of these sediments is strongly dependant on an irregular paleosurface of the Waitemata basement sediments (e.g. Affleck et al., 2001).

The Kaawa Formation is a good aquifer with a high permeability and hydraulic conductivity in the Manukau lowland, especially its ~0.5-6 m-thick, medium sand shell-beds (Crowcroft, and Smaill, 2001; Crowcroft and Bowden, 2002; Viljevac et al., 2002). Pump tests indicated yield values of 800 – 1200 $m^3$ per day of moderate pH, and moderately carbonated water (Crowcroft and Smaill, 2001). Overlying impermeable Tauranga Group beds provide an aquitard.

### 3.3.3 Pliocene to Holocene basin filling sediments: the Tauranga group

The lowermost sequence of the Quaternary Tauranga Group consists of pumiceous sand, mud, silt, and carbonaceous peat that were deposited in fluvial, lacustrine, and estuarine environments (Kermode, 1992; Edbrooke, 2003). It forms a continuous sedimentary infill of variable thickness in the lowland areas around the Manukau Harbour (tens of meters) and is present intermittently at intervals in the northern AVF around the Waitemata Harbour with thicknesses of meters to few tens of meters (Fig. 3.2). The Tauranga Group sediments unconformably overlie the Pliocene Kaawa Formation or are directly deposited on the basement rocks of the Waitemata Group. The youngest sediments of the Tauranga Group comprise hillslope and coastal alluvium, intertidal and beach ridge lithoral deposits that interfinger with the volcanic units (Kermode, 1992). The sedimentary environment of these units was a broad coastal plain.

## 3.4 Understanding of the hydrogeological conditions at the time of the eruptions

Deposits of phreatomagmatic volcanoes have varied proportions of lithics (from a few vol.% in tuff cones to up to 90 vol.% in some maar-diatremes; White and Ross, 2011). Lithic fragments, along with knowledge of the local substrate geology can help to understand the specific substrate characteristics at the locus of explosions. If there was progressive downward excavation, for example, this should be reflected by a pattern of progressively deeper lithologies being preserved in successively higher deposits within a maar ejecta ring (Lorenz, 1986). The volume and lithologies of disrupted substrates can be used to evaluate depths of explosions and the extent of penetration into the substrate (e.g. Valentine, 2012; Lefebvre et al., 2013).

Hydrogeological characteristics of the substrate are best established via drill-hole information (either direct or interpolated data), and hydrogeological studies in the area. However, modern measurements must be

carefully considered with respect to the climate, sea level and other conditions that prevailed at the time of the eruption. In addition, the hydrogeological conditions of the substrate may vary during the course of the eruption, with dike emplacement inducing hydraulic and/or shearing fracturing in the host rock (Delaney, 1986), and FCI fracturing the surrounding rock/aquifer.

The maar volcanoes studied here (Maungataketake and Motukorea) contain large fractions of lithic material (~30-40 vol.%) in their tephra rings. Geological, physical, and hydrogeological conditions of the substrate are known to different degrees for the AVF area (***see Appendix A.2 for some of hydrogeological data***) and must be extrapolated to the volcano sites. The lack of significant tectonic uplift in the last 1 Ma (Alloway et al., 2004) in the Auckland area (Beavan and Litchfield, 2012, report that there has not been important uplifiting in the Auckland area for the last 125 k.y.), as well as paucity of important active faulting in the past 0.3 Ma (Kenny et al., 2012), suggest that the current geological and physical conditions of the substrate were similar throughout the AVF, considering that the lifespan of the field is 250 k.y. However, during this period major glacio-eustatic sea-level changes occurred, with seas mostly at a lower level (during the Last Glacial Maximum) than the present day (with two exception periods: last and present Interglacials). In addition, levels of precipitation probably also varied considerably. Hence the past hydrological settings may have differed for some of the volcanoes to those of the present day.

## 3.6 Conclusions

Variation in the geological and hydrogeological conditions of the substrate is expected to exert a strong influence on the type and explosivity of phreatomagmatic eruptions. In the AVF, generally, the northern areas (e.g. under the Motukorea Volcano study site) is characterized by the firm aquifer-bearing Waitemata Group rocks, whereas in the southern parts (Manukau Lowlands) the volcanoes (e.g. Maungataketake Volcano) erupted through the Waitemata rocks that were covered by large thicknesses of Plio-Pleistocene, water-saturated, unconsolidated sediments. This implies that at least two substrate types prevail in the AVF: “hard substrate” in the northern AVF and a combination of “hard” and “soft substrate” to the south. For the North Head volcano example, the substrate did not play an important role in the eruption as indicated by the very low content of lithic material in the tephra. Instead, a shallow water-related, Surtseyan-style of volcanism occurred. The three study cases thus provide distinct substrate and phreatomagmatic eruption scenarios spanning the range expected for the AVF. These will be further examined in the following three case studies, presented as chapters 5, 6, and 7.

# Chapter 4. Methodology

**Contents** Page



## 4.1 Introduction

The reconstruction of the eruptive processes at Maungataketake, Motukorea, and North Head volcanoes was based on studying the characteristics of the pyroclastic deposits. Conventional methodology was followed, including field work together with dry sieving, binocular, petrographic, scanning electron microscope (SEM) work, as well as energy-dispersive spectrometry (EDS). In addition, selected juvenile pyroclasts from Maungataketake and North Head were analyzed via electron microprobe and Maungataketake fine-ash was analyzed by X-ray diffraction. Data obtained via these methods was combined with information on AVF paleo-environment, geology, and hydrogeology to reconstruct the eruption dynamics and history of each studied volcano, and to gain insight into the role of the substrate and environment on phreatomagmatic processes.

## 4.2 Field work

The general guidelines for field work carried out in this study were mainly taken from Sohn and Chough (1989; 1992; 1993) and Chough and Sohn (1990). These authors developed a system for describing and grouping the stratigraphical and sedimentary characteristics of ejecta ring deposits of phreatomagmatic volcanoes in Jeju Island, South Korea. There, deposits are well exposed from proximal to distal locations along axes perpendicular to the crater rim. Lateral and vertical changes in sedimentary structures, bedding and lamination characteristics, thicknesses of deposits, grading, sorting, vertical unconformities, grain size and componentry are exhibited throughout. The authors note that any identified variation in these characteristics may provide clues into the changing mode of transport and the sedimentation and deposition rates of pyroclasts within specific pyroclastic units from proximal to distal locations. Through detailed characterization, each unit can be compared with the overlying and underlying units to recognize vertical and lateral variations. In this way, the dynamics in the construction of the volcano can be interpreted, as well as the changes in eruptive styles. Unfortunately, such extensive outcrops are not found in the AVF. However, to a certain extent lateral and vertical variations are shown in Maungataketake in a cliff that is roughly perpendicular to the crater rim (chapter 5). Except for one outcrop exhibited over a short distance (tens of meters), lateral variations from proximal to distal locations are not exposed at Motukorea, rather deposits were examined along a cliff that runs sub-perpendicular to the direct radial

travel path from the crater. At North Head, the exposures are on a line roughly parallel to the cone rim. Therefore in the last two cases only vertical variations were recorded.

The morphological features of the phreatomagmatic edifices were identified in the field and with the aid of aerial photographs, Google Earth satellite images, and a shaded relief model of the LiDAR derived Digital Surface Model.

Layers of <1 cm-thickness are termed laminae, while beds comprise units >1 cm-thick (following Ingram, 1954). Particles were grouped using the pyroclast size terms of Sohn and Chough (1989), which is a subdivided version of the widely accepted classification of pyroclast fragments by Schmid (1981). Unconsolidated volcaniclastic particles are termed ash or lapill, whereas consolidated equivalents are termed *tuff* if composed of ash-size-pyroclasts, or *lapilli-tuff* if composed dominantly of lapilli-sized pyroclasts (after Schmid, 1981). Lapilli-tuff also indicates a consolidated, poorly-sorted mixture of both lapilli and ash-sized grains. Field observations at a macroscopic scale, the significant vertical changes in juvenile grain size and distribution, and the dominant sedimentary structures, allowed the grouping of beds into "units", which are composed of a single or multiple beds (with internal laminae or not). At Maungataketake (chapter 5) and Motukorea (chapter 6), distribution of juvenile clasts played an important role in definition of units, since lithic grain size and distribution was relatively uniform throughout the entire sequences. In these cases most lithics were in the ash grade, apart from the relatively scarce presence of coarse lithics (lapilli to blocks). Therefore the horizons (either laminae or beds) containing juvenile fragments (usually dark, coarse ash to lapilli) were used as indicators of changes in pyroclast distribution and many sedimentary characteristics were able to be characterized on this basis. North Head is mostly composed of juvenile lapilli whose characteristics (size and distribution) allowed the definition of units.

Once these units were identified, key representative locations were selected for detailed description. At each key site the following tasks were carried out: recognition and description of sedimentary structures and bedforms; identification of vertical changes, as well as lateral ones, and distinguishing of boundary types and grading; measurements of units, sedimentary structures, and bedforms; visual estimations of grain size and componentry; identification of juvenile and lithic morphology and their proportions. Sampling of pyroclastic deposits was done where possible. Usually, the samples were collected from spots that appeared to represent the grain size distribution of an entire unit at a specific location. In very poorly sorted tephra ring deposits, where changes in grain size and sedimentary characteristics occur over short vertical and lateral distances (even on a decimeter scale), representative sampling of phreatomagmatic sequences can be difficult to achieve. Since segments of units or the entire unit are usually entirely characterized by either tuff or lapilli-tuff, sampling was done specifically on one of these two types of deposit independently from the presence of minor associations of "anomalous" grain size distributions (e.g. juvenile-lapilli trains or isolated pockets composed of coarser particles). Single lithic or juvenile fragments were also sampled for further observations. The total number of samples (including tuff or lapilli

tuff, lithics, and juvenile fragments) for each volcano is 46 from Maungataketake, 26 from Motukorea and 39 from North Head. Except for Motukorea, which is an island in the Harbour (Fig. 3.1), the access to the other two volcanoes allowed several visits to check and cross-check the information gathered in previous visits.

The term lithofacies was adapted (from Sonh and Chough, 1989) and lithofacies and their associations were recognized when possible. Each ltihofacies and its nomenclature was described on a case by case basis, generally being characterized by a sedimentary bedform(s) or structure(s) that is relatively widespread within a single unit or a number of units. Conversely, the sporadic presence of certain sedimentary structures were not considered as separate lithofacies or taken into account for interpretative aspects. Lithofacies are typically labelled in the figures; their characteristics, descriptions and interpretations are summarised in tables.

The criteria used to define the different key sites, units, subunits and sequences for each volcano is described in each corresponding chapter: Maungataketake (chapter 5), Motukorea (chapter 6), North Head (chapter 7).

### 4.3 Sample preparation and analysis

Unconsolidated lapilli samples were dry sieved directly between -4.0 and 4.0 $\phi$ (16-0.0625 mm) at 0.5 $\phi$ intervals. Less consolidated tuff samples (from Maungataketake and Motukorea) were disaggregated by soaking in water, then dried, lightly crushed and sieved. between 1 and 4.0 $\phi$ (0.5-0.0625 mm), at 0.5 $\phi$ intervals. For Maungataketake samples, particles smaller than 4.0 $\phi$ (0.0625 mm) were analysed using a Horiba Partica LA-950 laser diffraction particle size distribution analyser. With the obtained data, grain size distribution parameters (Inman 1952; Folk and Ward 1957) were calculated using the SFT (Sequential Fragmentation/Transport) program (http://www.ees1.lanl.gov/Wohletz/SFT.htm). The grains representing some fractions (see below) were used for componentry, compositional, and morphological analyses. Additionally, powder X-ray diffraction analyses were carried out for a few of the Maungataketake samples in the <2 $\phi$ fraction. The grain size and componentry data of the consolidated lapilli-tuff samples were obtained from field observations and thin section analyses.

Manual disaggregation of tuff samples adds a considerable error in grain size distribution calculations, so the obtained grain size distribution parameters for these samples are not statistically reliable. However, these samples were useful in the identification of proportions of juvenile to lithic contents and the nature of lithics. For consolidated or semi-consolidated deposits, the approximate grain size distribution and sorting of deposits were best estimatedby field observations, as well as photograph and thin section analyses (using a petrographic microscope and the JMicrovision software). Samples from the 2 and 3 $\phi$ sieved fractions (0.25-0.125 mm) from the three volcanoes were used for componentry and grain morphology analyses. These particles were cleaned with 10% HCl and rinsed with acetone in an ultrasonic bath for 30-

60 s. On the other hand, thin sections from the more consolidated tuff and lapilli tuff, as well as few juvenile and lithic fragments, were prepared for grain size and componentry analyses.

The morphological features, textural characteristics, and componentry of pyroclasts were identified by direct observation of deposits and hand specimens in the field and by viewing loose and thin sectioned small lapilli-to-ash-sized grains under binocular, petrographic and/or scanning electron microscopes (FEI Qanta 200 environmental scanning electron microscope operated at 20 kV, Massey University Microscope Centre). Some juvenile samples were also analysed by energy-dispersive spectrometry (EDS) (Edax 10 $mm^2$ detector with data processed by Edax Genesis 5.21 software) to confirm composition. Counts of 500 grains were performed in the 2 and 3 $\phi$ fraction sizes of samples from different stratigraphic levels for the componentry analyses (15 samples from Maungataketake, 16 samples from Motukorea; 14 samples from North Head). For juvenile clasts, general vesicle volume was calculated based on 500 point counts on thin section images using the JMicrovision software. This was performed on selected images from specific stratigraphic levels (see chapters 5, 6, 7 for detailson each volcano). Since North Head samples were mostly composed of loose lapilli, the vesicularity index of some 2-4 mm-lapilli grains from some North Head juvenile samples was obtained. The density of these grains was calculated using a Micromeritics GeoPyc 1360 envelope density pycnometer.

15 North Head juvenile sideromelane grains were selected for measurement of groundmass glass compositions and were analysed at the University of Auckland with a JEOL JXA-840 electron microprobe microanalyser (EPMA) interfaced with a Princenton Gamma Tech Prism 2000 Si (Li) EDS X-ray detector at an accelerating voltage of 15 kV, a beam current of 800 pA and a total count time of 100 s. 17 Maungataketake juvenile sideromelane grains were analysed by a Jeol JXA-8900R electron microprobe at the Laboratorio Universitario de Petrología (LUPI), Instituto de Geofísica, UNAM, México City. Measuring conditions were a beam current of 10 nA, an accelerating potential of 20 kV, and a beam diameter of 15 µm for glass and 1-5 µm for crystal analyses. During analyses, Na and K were analysed using 10 s counting times, whereas a 40 s-counting-time was used for other elements.

# Chapter 5. Reconstruction of the Maungataketake phreatomagmatic eruption and implications of the substrate

## 5.0 Preface

This chapter comprises the reconstruction of the eruptive history of the phreatomagmatic phase of Maungataketake volcano, situated in the Manukau Lowlands (Fig. 3.1) (soft substrate overlying hard substrate). The study is based on collected stratigraphic, sedimentary, and pyroclast data from the tephra ring deposits in conjunction with supplementary hydrogeological, geological, and paleo-environmental information. The main objective was to get insights into the influence of a soft substrate in phreatomagmatic eruptions in the AVF. The eruption was characterized by shallow-seated explosions within the unconsolidated sediments.

**Contents** Page



**Chapter 5 comprises the published article (*Appendix B*):**

**Phreatomagmatic eruptions through unconsolidated coastal plain sequences, Maungataketake, Auckland Volcanic Field (New Zealand)**

**Authors:** Agustín-Flores J., Németh K., Cronin S., Lindsay J., Kereszturi, G., Brand, B., Smith I.E.M., 2014. **Journal of Volcanology and Geothermal Research**, 180: 203-224. http://dx.doi.org/10.1016/j.jvolgeores.2014.02.021

.

**The contribution of each author is as follows:**

**Javier Agustín-Flores (PhD candidate)**: Organization and completion of the whole field work and most laboratory work, main contributor on writing and editing of manuscript draft, and subsequent correcting and editing for final version.

**Karoly Németh (main supervisor)**: Oversight of research process, assistance in the field and laboratory work, as well as in manuscript revision, editing, discussion, and correcting from the initial draft to the final version.

**Shane J. Cronin (supervisor)**: Discussions during the whole research project and assistance in manuscript revision and discussion from the initial draft to the final version.

**Jan M. Lindsay (supervisor)**: Discussions during the whole research project and assistance in manuscript revision and discussion from the initial draft to the final version.

**Gábor Kereszturi**: Overall field assistance and manuscript revision and discussion.

**Brittany Brand**: Assistance in manuscript revision and discussion from the initial draft to the final version.

**Ian E.M. Smith**: Geochemical data, manuscript editing and discussion.

## 5.1 Introduction

Fragmentation of ascending magma in phreatomagmatic eruptions is primarily due to highly energetic, explosive fuel-coolant interactions (FCI) (Sheridan and Wohletz, 1983; Wohletz, 1983), also called molten fuel-coolant interactions (MFCI) by Zimanowski et al. (1997). Around 60% of the thermal energy of the involved magma (the fuel) when it interacts explosively with water (the coolant) is converted into shock waves that have the potential to disrupt surrounding magma and/or country rock (Raue, 2004). The types of non-juvenile fragments in the phreatomagmatic deposit sequences, as well as the morphology of the diatreme, may be controlled by the degree of excavation into the substrate (White and Ross, 2011). In turn, the extent of excavation and ejecta ring/crater structure are influenced by the composition and strength of this substrate (Lorenz, 2003). Recent studies have also shown that the final architecture of the crater and underlying diatreme are strongly dependent on the energy release of individual explosive eruptions as well as their relative position in reference to the surface (Valentine et al., 2011, Valentine, 2012; Valentine and White, 2012). The hydrogeology and the rheology of the country rocks are still expected to play a major role in the shape, size and facies architecture of the craters and diatremes, although the exact nature of this role is not well constrained.

The importance of the physical and/or hydrogeological properties of the substrate in phreatomagmatic eruptive processes has been addressed by many authors (White 1991a,b, 1996; Lorenz, 2003, Sohn and

Park, 2005; Auer et al., 2007; Németh et al., 2010, 2012a; Valentine, 2012). Some of the features regarded as typical of small basaltic eruptions through soft/unconsolidated substrates include: the common syn-eruptive downward slumping of crater walls; the formation of broad, shallow "champagne glass"-shaped craters; and the formation of a shallow diatreme (Lorenz, 2003). However, it is difficult to link the subsurface hydrogeological/lithological conditions with diatreme and eruptive conditions and processes, largely due to the lack of coupled subsurface and surface deposit exposures.

Coastal erosion beside the Manukau Harbour in the southern AVF (Fig. 3.1) has carved an almost complete cross-section on the SW flank of the Maungataketake ejecta ring (Fig. 5.1). This is one of several south Auckland volcanoes that lie near present-day sea level and are underlain by tens to ~60+ metres of saturated, soft, Pliocene to Recent mud, sands and gravels that rest on a >300 m-thick, poorly consolidated turbiditic sandstone/siltstone sequence (Kermode, 1992). The Auckland area has not experienced active faulting since 0.3 Ma (Kenny et al., 2012) and no significant tectonic uplift since 1 Ma (Alloway et al., 2004). These considerations and the inferences drawn from paleo-environmental studies indicating wetland or near coastal conditions (Marra et al., 2006) suggest that the current hydrogeological conditions correspond to those existing when Maungataketake volcano erupted.

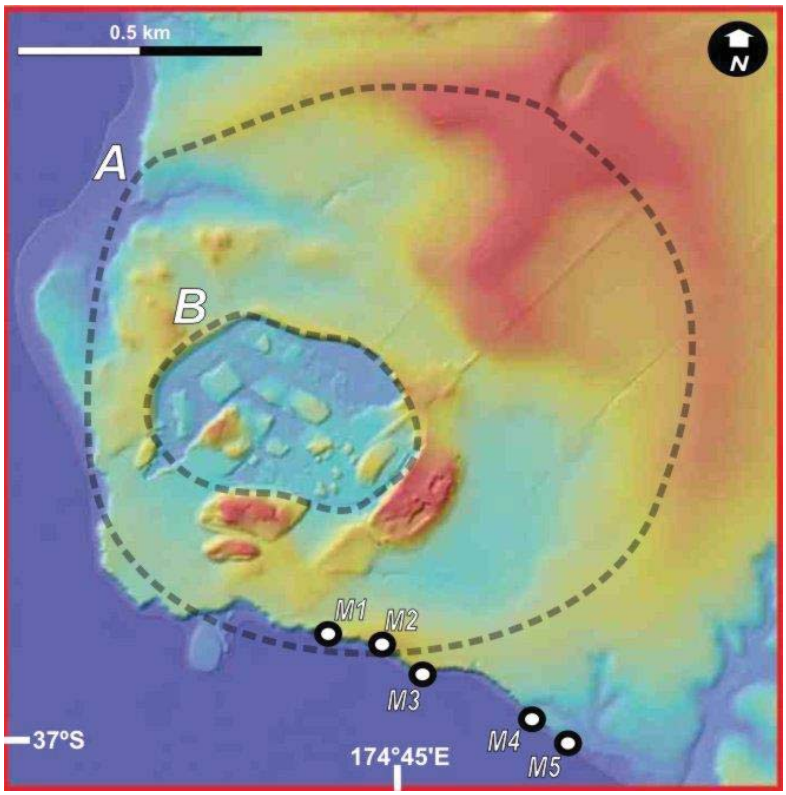


**Fig. 5.1**. Plan view of Maungataketake volcano (modified from Brand et al., 2014) showing five key sites (M1 to M5) located along a NW-SE-direction cliff. Line A indicates the highest edge of the ejecta ring rim (broken-lined bigger contour) and line B the extent of quarry area (broken-lined smaller contour). For the purpose of this study, proximal, medial, and distal deposits are represented by sites M1-M2, M3, and M4-M5 respectively. ***(See Appendix B.1 for information of additional sites, represented by stratigraphic logs, not included in the published manuscript).***

Maungataketake presents a case scenario of an eruption through a highly deformable, fine-grained, water-saturated substrate. Its ejecta ring deposit sequence is presented here, along with information about the geological and hydrogeological setting, and an eruption scenario is constructed. Concise geochemical information is provided in support of the physical eruption scenario and to help infer the conditions during the phreatomagmatic eruption phase. This study improves the understanding of phreatomagmatic eruptions (and related hazards) in the soft-sediment dominated coastal plains of the southern AVF, and it is an example for basaltic volcanism in similar near shore soft-sediment settings.

### 5.1.1 Maungataketake age[(1)]

The ages for Maungataketake are not conclusive, with estimates ranging from ~33 to 177 ka (Lindsay et al., 2011). There are three origins of ages. The first is from radiocarbon determinations on lignite and wood fragments within the ejecta ring deposits and range from ~35 to 47 ka B.P. (McDougall et al., 1969; Polach et al., 1969). Bebbington and Cronin (2011) also estimated an age of 41,390 ± 430 yrs using a probabilistic approach to correlate a possible match with dated tephra deposits in neighbouring maar lakes. The second suite of ages range between ~106 to 177 ka and include K-Ar (McDougall et al., 1969) and Optical-Spin Luminescence (Marra et al., 2006) age determinations. Thirdly, the most recent Ar-Ar age determinations yielded an age of 87.4 ± 2.4 ka (Leonard G., written communication 2013) and 189.7 ka ±13.8 (from a cauliflower bomb from the base of the phreatomagmatic section) (Karoly Németh, personal communication). The K-Ar technique (McDougall et al., 1969) revealed excess Ar and the obtained ages are not reliable (Lindsay and Leonard, 2011). It is very likely that the initial phreatomagmatic phase was followed without a long time break by the magmatic one, so any age obtained from samples throughout the sequence would necessarily be close to one another.

A marine terrace, cutting the ejecta ring, approximately 1 m above the present sea level (Marra et al., 2006) may have been formed during the highest post-glacial sea level transgression at around 6.5 ka or during the highest Last Interglacial sea level transgression at around 125 ka. The occurrence of intensely weathered clay-texture terrace cover beds, irregular secondary iron concretions and cementation in the soil matrix as well as on wave-cut gravels and cobbles faces tend to support and older age for the terrace (Marra et al., 2006). This observation rules out any age younger than 125 ka for at least the formation of the Maungataketake ejecta ring. Still, the ages older than 125 ka are within a broad range. The paleo-environmental reconstruction by Marra et al. (2006) supports the prevalence of interglacial conditions with coastal or wetland flora and fauna. These authors, supported by one OSL age of 177.1 ±23.4 ka (from the lowermost tuff unit), placed the eruption in the late 7 MIS (marine isotope stage) or early 6 MIS age. Also, the Ar-Ar age of 189.7 ±13.8 ka is within the late 7 MIS. Following a sea level curve (Sidall et al., 2006), the sea level would be approximately -70-80 m below current sea level during those ages. Considering that Marra et al. (2006) imply wetland or near coastal conditions at the moment of the eruption, a coastal condition may have not been present at those low sea levels. On the other hand, Marra et al. (2006) also

***[(1)]Section 5.1.1 is not originally included in the published manuscript. It was considered necessary to clarify the information given in the original introduction of the manuscript about the Maungataketake ages and the most likely age for the eruption.***

report an OSL age of 140.3±14.2 ka (from the lowermost tuff unit) that would place the eruption in the early 5 MIS when sea levels where few metres below current sea level, more akin to coastal conditions.

The conclusion that arises at this point is that the age of Maungataketake eruption may be older than 125 ka, between the early 5 MIS and late 7MIS (still a broad range of ages). The sedimentary and lithic characteristics of the ejecta ring deposits point to a sub-aerial eruption and the presence of water-saturated substrate with a water table close to the surface (as it is today). Both coastal and wet scenarios suit the formation Maungataketake phreatomagmatic volcano. More reliable dating is needed. Nevertheless, the true age of Maungataketake probably corresponds to the oldest in the AVF.

## 5.2 Geological and hydrogeological setting

Maungataketake (previously also known as Ellett's Mountain, before quarrying operations destroyed the hillt) is a small basaltic volcano located on the western edge of the northern Manukau Lowlands at the SW edge of the AVF (Fig. 3.1) in the North Island of New Zealand. The AVF comprises about 52 individual eruption centres over a 360 $km^2$ area (Kermode, 1992; Allen and Smith, 1994; Spörli and Eastwood, 1997; Hayward et al., 2011). The minimum DRE volume of the eruption products of the AVF is 1.7 $km^3$, based on measurements from a light detection and ranging (LiDAR) digital durface model in combination with geological mapping (Kereszturi et al., 2013). Eruptions have been sporadic since 250 ka, but primarily since ~50 ka (Allen and Smith, 1994; Molloy et al., 2009, Bebbington and Cronin, 2011).

The AVF is almost completely urbanised with the City of Auckland (population ~1.4 million) built on top of it (Fig. 3.1). The outstanding feature of the AVF is the predominance of phreatomagmatism, with tuff rings and maars and scoria cones preceded by phreatomagmatic activity present throughout the field (approximately 75% of the volcanoes show evidence of phreatomagmatism). Explosive phreatomagmatic eruptions producing violent base surges are considered to be the most hazardous events expected to threaten the city's inhabitants (Allen and Smith, 1994; Németh et al., 2012a).

At least 20 volcanic centres have been identified in the Manukau Lowlands. Based on observations of the preserved pyroclastic successions, 16 of these volcanoes involved variable degrees of phreatomagmatic explosive phases. The northern Manukau area is located within a fault-bounded graben formed within Early Miocene Waitemata Group rocks (Kenny et al., 2012). These rocks comprise >300 m-thick inter-bedded turbiditic sandstones and pelagic siltstones with subordinate breccia and conglomerate units (Ballance, 1974; Hayward, 1979; Hayward, 1993; Raza et al., 1999). The undulating Waitemata paleo-surface was part of an ancient fluvial system that irrigated the Manukau area in the Pleistocene (Searle, 1981; Kermode, 1992).

Waitemata rocks are weakly indurated with a compressive strength of ~5 MPa (Spörli and Rowland, 2007). Jointed siltstone and sandstone beds and conglomerates with a range of thicknesses act as

aquifers (Simpson, 1987; Sheridan, 2006; Irwin, 2009; Kenny et al., 2012), often confined by low-permeability mudstones (Scoble and Millar, 1995; Crowcroft and Smaill, 2001; Sheridan, 2006). They are low yield aquifers that are heterogeneous with anisotropic hydraulic properties. From a combination of pump testing and laboratory values, the average hydraulic conductivities (K) in *x* and *z* directions are $K_x=10^{-6}$ m/s and $K_z=10^{-10}$ m/s for the Waitemata rocks (Crowcroft and Smaill, 2001; Pattle Delamore and Partners LTD, 2003; Sheridan, 2006). Using field observations on jointing and bedding patterns and porosity laboratory studies of Waitemata rocks, Sheridan (2006) concludes that the anisotropic hydraulic conductivity values of Waitemata aquifers reflect the rock jointing and bedding patterns.

Across the Manukau area, the Waitemata Group sediments (especially within the graben) are unconformably overlain in depressions by poorly consolidated Pliocene shallow marine and estuarine beds of the Kaawa Formation (Edbrooke et al., 2003; Viljevac et al., 2002) (Fig. 3.2). This sequence forms confined aquifers with high permeability (average $K=\sim10^{-5}$ m/s, but variable) that are favourable for groundwater storage (Viljevac et al., 2002). Around the Maungataketake area the thickness of Kaawa sediments is not known for certain, but lenses are found in drillings (Searle, 1959)

The overlying low-permeability, water-saturated, recent Tauranga Group sediments confine the Kaawa Formation aquifers in many places (Viljevac et al., 2002) (Fig. 3.2). The lowermost sequences of the Tauranga Group consist of pumiceous sand, mud, silt, and carbonaceous peat deposited in fluvial, lacustrine, and estuarine environments (Kermode, 1992; Edbrooke, 2003). This forms a sedimentary infill of variable thickness, reaching up to tens of metres in the area (Kermode, 1992; Edbrooke, 2003). Extrapolation from borehole data (PETLAB database, G.N.S. Science, New Zealand, http://pet.gns.cri.nz/pet/index.jsp) suggests that the thickness of sediments overlying the Waitemata Group in the Maungataketake area might be 40-60 m (***Appendix A.1***). Tauranga Group sediments interfinger with the volcanic eruptive products of the AVF, showing that the Manukau Lowlands volcanoes, including Maungataketake, erupted on a broad, flat coastal plain. Tauranga Group and Kaawa Formation are generically called Plio-Pleistocene sediments for this study.

***See Appendices A.1 and A.2 for additional information on distribution and thicknesses of the lithologies described above and hydrogeological information of Auckland aquifers.***

### 5.3 General architecture of Maungataketake volcano

The base of the Maungataketake complex comprises an ejecta ring with an irregular rim of approximately 1100 by 1300 m, with a long axis oriented NW-SE (Fig.5.1). The outermost deposits define a 2000 by 1700 m area of $2.8\times10^6$ m$^2$. The total bulk volume of the present tuff ejecta deposit is $\sim20.9\times10^6$ m$^3$, which gives a dense rock equivalent eruptive volume of $7.2\text{x}10^6$ m$^3$ (Kereszturi et al., 2013). The present-day ejecta ring reaches up to ~25 m in maximum height, and its base at M3 (Fig. 5.2) roughly coincides with the maximum high tide levels in the Manukau Harbour.

Following the emplacement of the ejecta ring, there was lava fountaining from closely-spaced vents that built a lava spatter cone up to ~73 m from its base (Searle, 1959). The cone, which has now been removed by quarrying, had two craters oriented NE-SW, with the major crater to the E (Searle, 1959). From the cone remnants, Conybeer (1995) documented stratified to crudely stratified, variably agglutinated, grey to red-grey scoria and spatter. Lava flows were produced by fire fountaining and also emerged at the base of the cone on the western side, covering tuff to the NW and E (Searle, 1959). The lava flows do not extend beyond the limits of tuff deposits and consist of vesicular basalt. Despite the removal of most of the cone by quarrying, strong gravity and magnetic anomalies occur at Maungataketake (Cassidy and Locke, 2010), and are attributed to a large solidified magma body ponded under the former vent area.

Although the phreatomagmatic crater was covered by magmatic products, magnetic anomalies indicating a subsurface magmatic body lying in the possible phreatomagmatic crater (Cassidy and Locke, 2010) may suggest that a phreatomagmatic crater cut into the pre-eruptive surface. This information and Maungataketake ejecta ring size and componentry suggests that the phreatomagmatic edifice at Maungataketake can be considered a maar-diatreme volcano.

## 5.4 Methods and terminology

Ejecta ring deposits were examined from proximal to distal locations along a low coastal cliff oriented roughly perpendicular to the crater rim (Fig. 5.1). A systematic lithological description was carried out at five sites (Fig.5.1). The outcrops on the NW section are discontinuous and were not used in the reconstruction. The uppermost phreatomagmatic sequence is highly weathered and/or eroded at several places along the cliff. The sites are located in the proximal inner wall of the maar ejecta ring (Site M1), the ring crest (Site M2), its outer wall (Site M3), and the distal fan (Sites M4 and M5) (Fig. 5.1).

Pyroclasts are defined by Fisher and Schmincke (1984) as rock fragments '*produced by many processes connected with volcanic eruptions*', without reference to the causes of the eruption or origin. Pyroclasts can be juvenile (fresh erupted magma) or country-rock fragments (non-juvenile), which in this case may also include older volcanic clasts. White and Houghton (2006) are more specific classifying pyroclast as clasts deposited from subaerial, subaqueous, or subsurface jets, plumes, or currents. Then all particles transported in a system triggered by magmatic energy and found in pyroclastic deposits are named pyroclasts, irrespective of their origin. Following this, the poorly to moderately consolidated Maungataketake ejecta ring deposits were classified as tuff and lapilli tuff (after Schmid, 1981) (Table 5.1). Particles were grouped following the subdivision for pyroclast size terms of Sohn and Chough (1989) (see Table 5.1). <1 cm-thick and >1 cm-thick layers are described as laminae and beds respectively (following Ingram, 1954).

Base surge is defined for the text as a low concentration, turbulent, pyroclastic density current (a dilute pyroclastic density current, DPDC) of phreatomagmatic origin and that consists of two phase (solids and gas) or three phase (solids, gas, and water) systems. Although not equivalent, current(s) or flow(s) may be used as a synonym of base surge here.

Most of the deposits are moderately consolidated, and thus not suitable for sieving. Poorly consolidated-tuff samples were disaggregated by soaking in water and lightly crushing. These were mechanically sieved between 1 to 4.0 $\phi$ at 0.5 $\phi$ intervals. Particles smaller than 4.0 $\phi$ were analysed using a Horiba Partica LA-950 Laser Diffraction Particle Size Distribution Analyser. Grain size distribution parameters (Inman 1952; Folk and Ward, 1957) were calculated using the application SFT (Sequential Fragmentation/Transport application) (developed by Ken Wohletz, available at http://www.ees1.lanl.gov/Wohletz/SFT.htm). These parameters may in this case be affected by errors resulting from the manual disaggregation of samples, but most units show comparable distributions to those of other tuff rings (Fig. 5.2). Particles from the 2$\phi$ and 3$\phi$ fractions were cleaned with 10% HCl and rinsed with acetone in an ultrasonic bath for 30-60 s. Morphological and compositional characteristics of fragments were characterized in the lab by viewing samples (loose grains and thin sections) under binocular/stereo and transmitted polarised light microscopy and scanning electron microscopy (FEI Quanta 200 environmental scanning electron microscope operated under 20 kV, Massey University Microscope Centre), as well as by application of energy-dispersive spectrometry (EDS) (Edax 10 $mm^2$ detector. with data processed by Edax Genesis 5.21 software). Counts of 500 grains were performed in the 2 and 3 $\phi$ fraction size for the componentry analyses. Bulk powder X-ray diffraction analyses were carried out, showing quartz and feldspar along with few clay minerals in the <2 $\phi$ fraction. The grain size and componentry data of the consolidated lapilli tuff were obtained from field observations and thin section analyses.

Using optical and scanning electron microscopy on six thin sections (see section 5.5.1 for the definition of units and sample details), the textural and vesicle characteristics of 15 juvenile sideromelane grains were described (Table 5.1, Fig. 5.3). A modal analysis performed for each grain included 800 count points (results are shown in Fig. 5.3a and briefly described in Table 5.1). The samples overall have identical textural and vesicularity characteristics throughout the entire deposit sequence.

***The methods used for whole rock and glass chemistry analyses are presented in Appendix C (section C.1)***. The compositional data are intended for comparison of this eruption with others in the AVF.

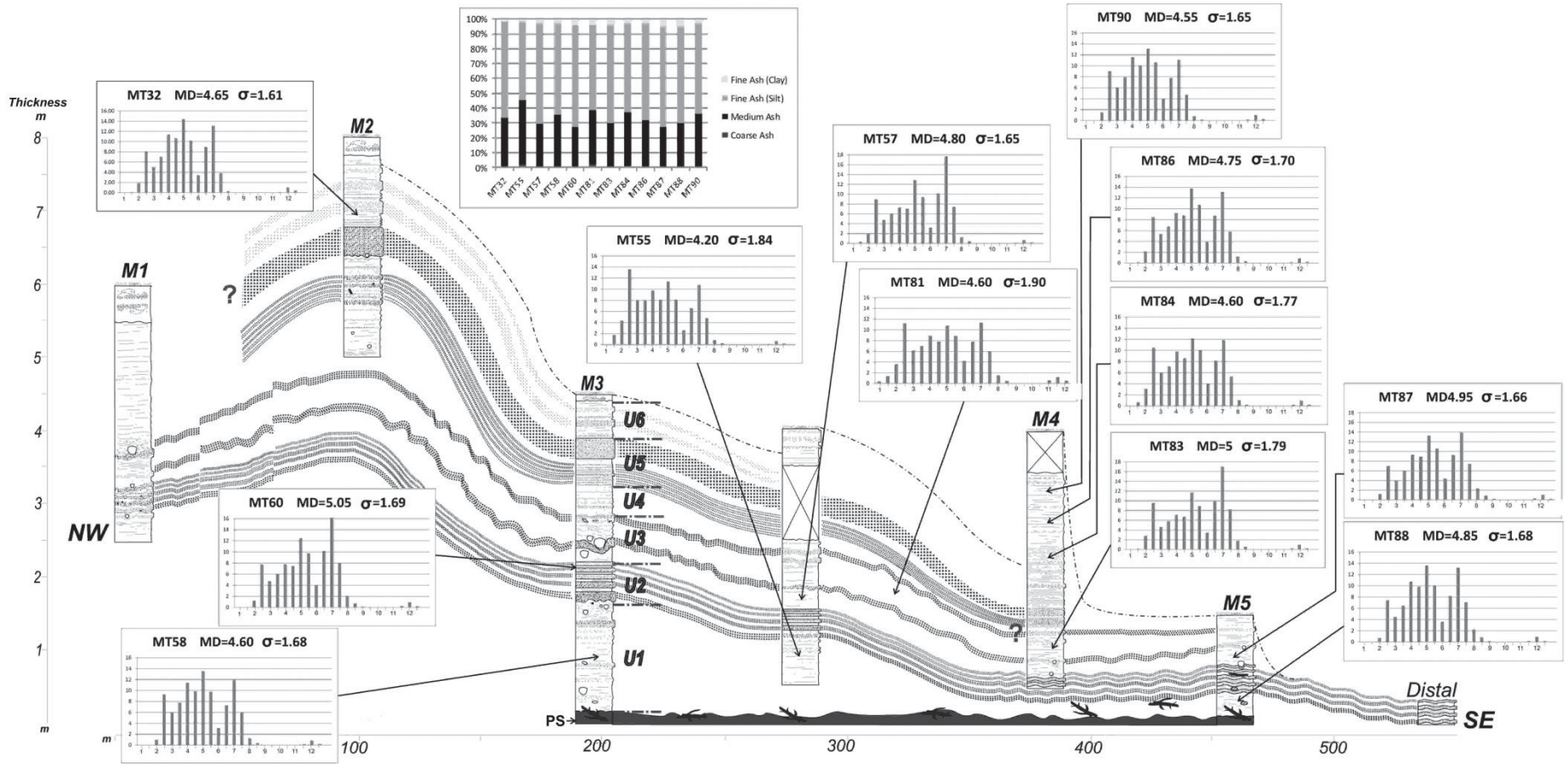


**Fig. 5.2**. Schematic correlation of logs and identified units (U), overlying peaty soils (PS), along cliff exposures. It represents the cross section of the ejecta ring from NW to SE. Vertical exageration is ~30 times. The vertical axis represent the maxium thickness of the exposed sequence. The base of the tuff deposits at site M3 roughly coincides with the back beach level. Site M1 is located in the inner slope of the ejecta ring (see Fig. 5.1 ). Site M2 is located at the crater rim. The other locations correspond to the outer ejecta ring deposits. Frequency histograms of 12 selected samples are displayed indicating the position of samples in the exposures. The percentages of grain size fractions are shown in the uppermost graph.

***Fig. 5.2 as it is presented in the published manuscript is not clear. For this reason, in Appendix B.1 this correlation is presented without the frequency histograms and the graph (Fig, B.1.10). Additionally in the Appendix B.1, the frequency histograms are included together with the stratigraphic logs corresponding to each site (also included are extra stratigraphic logs not included in the published manuscript). Moreover, the graph with the percentage of grain size fractions is shown separately (Fig. B.1.11) and the raw data of the grain size distribution from sieving are also presented in Table B.1.1.***

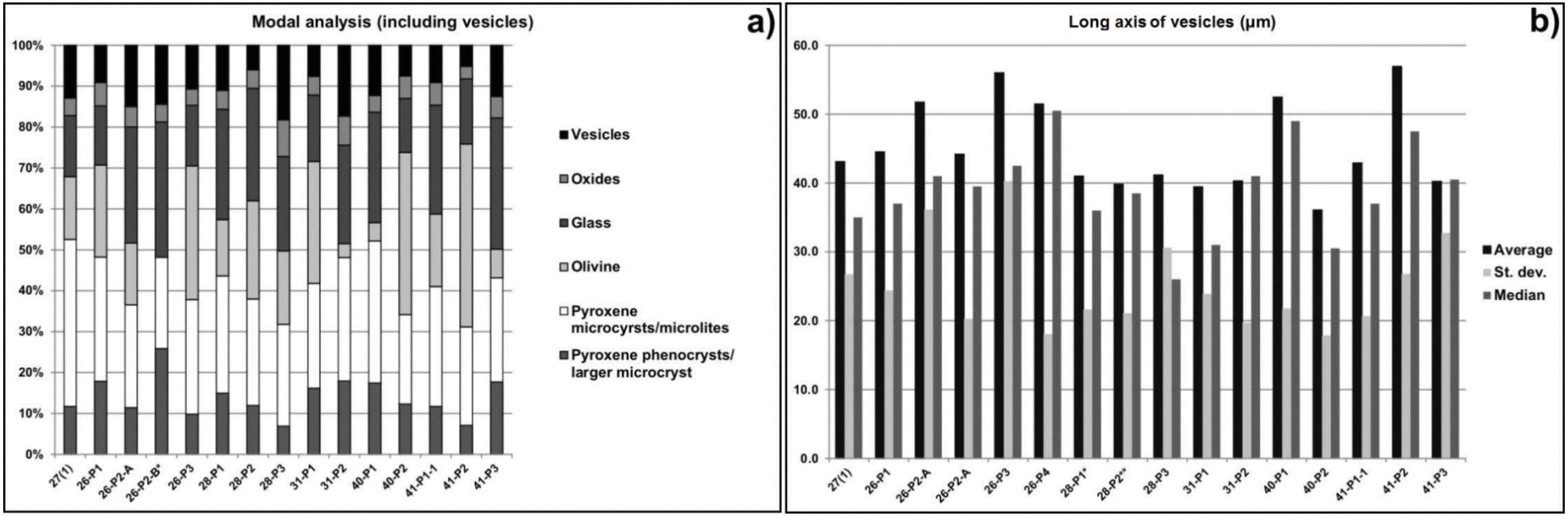


**Fig. 5.3**. a) Graph representing the modal analysis of 15 juvenile fragments (vol.%) (800 point counts exclusively on selected juvenile grains displayed in thin sections). Stratigraphic position of samples increases to the right. Some sample numbers are represented by more than one juvenile grain. Specific sample positions are as follow (see Fig. 5.2 for location of sites and units): sample 27 (from upper U2 at site M1), sample 26 (from middle U3 at site M1), sample 28 (from upper U3 at site M1), sample 31 (from middle U5 at site M2), sample 40 (from lower U6 at site M5), and sample 41 (from upper U6 at site M5); b) graph representing the long axis of of vesicles in the same juvenile fragments described above.

**Table 5.1** Nomenclature of deposit types and grain size. Also the proportions of different sizes and composition of fragments within the deposits are shown, as well as the morphological and some textural characteristics of juvenile and non-juvenile fragments.

| Deposit type | Clast size | ~Vol.% within deposit type | ~Vol.% in total deposit | ~Proportion of accidental to juvenile | Morphology and origin of accidental fragments | Morphology of juvenile fragments | Texture and vesicles of juvenile fragments (0.5 to 2.5 mm) |
|---|---|---|---|---|---|---|---|
| Not layered, scattered fragments | Block/bomb (-6 to -8 ϕ) | 70 | <10 | 9:1 | Subrounded to rounded Waitemata sandstone (*Fig. 5.6a,b*) and poorly-consolidated, sand/silt aggregates of Plio-Pleistocene sediments (*Fig. 5.6a*). Soft aggregates do not show plastic deformation or internal structures. | Dense, subangular to subrounded, poorly vesicular. Few breadcrust-type bombs. | **Modal components***(Fig. 5.3a,b)*:<br>- Ca-Augite, tabular microlites (usually <78x8 µm) :up *to ~46 vol.%*<br>- Ca-Augite, elongated microphenocrysts/phenocrysts: *<20 vol.%*<br>- Euhedral olivine phenocrysts (70-600 µm): *8-47 vol.%*<br>- Oxides: <10 vol.%<br>- Sideromelane matrix: *15-40 vol.%*<br>**Vesicles**: round to subtly elongated, exhibit weak deformation (*Figs. 5.3a,b; 5.4e,f,g,h,i)*<br>- Wall thickness: *<100 µm*<br>- Modal percentage: *5.2-18.2 vol.%*<br>- Vesicle length: *39 µm (median)*<br>- Vesicle eccentricity: *1.7 (median)* |
| | Coarse lapilli (-4 to -6 ϕ) | 30 | | | | | |
| Lapilli tuff | Medium lapilli (-2 to -4 ϕ) | <5 | 20-40 | 2:8 | Fragments of soft rock Waitemata sandstone, sand/silt aggregates of Plio-Pleistocene sediments. | Subangular to subrounded, poorly vesicular. Some clasts are coated by a fine film of accidental ash. Some grains show some degree of palagonitization. | |
| | Fine lapilli (-1 to -2 ϕ) | 10-20 | | | | | |
| | Coarse ash (1 to -1 ϕ) | 60-80 | | | | | |
| Tuff | Medium ash (4 to 1 ϕ) | Up to 40 | 60-80 | 9:1 | Down to 3 ϕ fraction: Blocky, opaque individual grains of quartz and feldspar (>40 vol.%) (*Fig. 5.4a,b,c*).Silica-rich, non-vesicular glass fragments (*Figs. 5.4a,b*).Round aggregates of smaller fragments (*Fig. 5.4a*).<br>Fragments of Plio-Pleistocene sediments dominate.<br>Note the presence of accretionary lapilli (*Fig. 5.4d*) | Down to 3 ϕ fraction. Subangular to subrounded, poorly vesicular fragments (*Fig. 5.4a,c,e,f,g*). Adhering fine ash particles and secondary minerals growths occur on the outer surfaces and inside the cavities of vesicles (*Fig 5.4h,i*). Rare surficial cracks are present. Some degree of palagonitization. | |
| | Fine ash <4 ϕ | Up to 60 | | | | | |

## 5.5 Results

The tuff deposits generally show poorly-sorted, polymodal distributions, and negative skewness (Table 5.1 and Fig.5.2). Variations in grain size distribution and particle componentry (Table 5.1) are used to characterize stratigraphic divisions within the tuff. The characteristics of juvenile fragments provide information about magma fragmentation (Wohletz, 1983; White, 1996; Zimanowski et al., 1997) (Table 5.1; Fig. 5.4), but the properties of non-juvenile fragments supply clues into the involvement of the host rock and related aquifers (e.g. Valentine, 2012, Lefebvre et al., 2013; van Otterloo et al., 2013) (Table 5.1; Fig. 5.4). These properties were used to define lithofacies (Table 5.2) and lithostratigraphic units (Table 5.3), which in turn provide the basis for the reconstruction of the eruptive history of the Maungataketake maar. (***See Appendix B.2 for detailed description of lithofacies and units***).

### 5.5.1 Stratigraphy and sedimentary characteristics of the maar ejecta ring deposits

The exposures studied along the cliff extend from proximal to distal reaches and are thought to be representative of other sectors of the maar ejecta ring which have similar dimensions (Fig. 5.1).

Ten lithofacies were recognized (following Sohn and Chough, 1989) ***(see Appendix B.2 for detailed descriptions of lithofacies)***. Bedforms and other depositional features were described that reflect the main transport mechanisms (c.f., Sohn, 1997; Valentine and Fisher, 2000; Branney and Kokelaar, 2002). Three main modes of transport are considered here (these definitions do not strictly follow the previous authors' definitions): 1) lower traction carpet (from Sohn, 1997), characterized by a non-turbulent regime where friction between fragments is ubiquitous; 2) bed load (Valentine, 1987) (similar to upper traction carpet of Sohn, 1997), where the transport is mainly by saltation and rolling in a non-turbulent to turbulent regime; and 3) suspended load, characterized by turbulent transport of fragments (Valentine, 1987). Bedforms were related to the mode of transport in a first-order manner, recognising that bedforms in some transport regimes will represent the deposition of grains only at the boundary layer of a progressively aggrading current (Branney and Kokelaar, 2002). A general view is that lower traction carpet, bed load, and suspended load modes of transports may promote respectively the formation of planar, inversely graded or massive beds; massive and/or planar to cross-bedded layers with internal trains of coarser fragments; and cross-bedding and/or cross-lamination. However, from the sedimentary characteristics of Maungataketake deposits these relationships are not clear-cut and do not always follow this general scheme (see Table 5.2 and section 5.6). As flow distance increases, and at obstacles or slope-breaks, turbulence patterns decrease or change (Valentine, 1987; Sulpizio and Dellino, 2008), but within a single current, at a single point in any specific time, turbulence increases upwards. Also, grain concentration and grain size will decrease with distance and upwards within flow (Sohn and Chough, 1989). These will be reflected in bedforms and are considered in the interpretation of bedforms of lithofacies in Table 5.2, and in turn in interpretation of the lithostratigraphic units (Table 5.3).

Lithostratigraphic units (U) (henceforth called units) (Table 5.3, Figs. 5.2, 5.5, 5.6) are deposit packages of strata with lower and upper boundaries that represent a more or less distinct change in grain size and componentry (***units are described with detail in Appendix B.2*).** These changes were most easily identified at the proximal sites. A correlation was established with the distal deposits (where some vertical changes are faint) based on distinct stratigraphic markers (Fig.5.2). The units may be characterized by at least one lithofacies with some showing variations grading from proximal to distal locations (Figs. 5.2, 5.5, 5.6). A total of 6 units were identified. Based on stratigraphic and sedimentary characteristics, the phreatomagmatic phase of the Maungataketake eruption is interpreted to have occurred in four sub-phases (PH-1 to PH4). Table 5.3 shows each PH represented by its units, which are described and interpreted. The sedimentary characteristics of the lithofacies contained in each unit are more extensively described in Table 5.2. The information in Tables 5.2 and 5.3 is the basis for the following reconstruction of the Maungataketake eruption.

Macroscopically, the whole deposit displays a massive to plane-parallel, slightly undulating bedding. In detail, however, faint lamination is widespread, along with plane-parallel/slightly undulating bedding with a dominance of low-angle cross-lamination. Distal deposits are mostly plane-parallel bedded and laminated. Accretionary lapilli are present in varying amounts throughout the deposit, but are more abundant in the upper U6 (Table 5.3) and units of the distal deposits.

Fig. 5.5c shows a tree log within the tuff. Tree logs and moulds are present within U1 deposits (there is a standing tree trunk between sites M3 and M4; not shown). Also, there are fallen trees along the low tide beach (not shown). According to Hayward and Hayward (1995) and Marra et al. (2006), the standing trees belonged to a live forest (forest 2, Fig. 5.7) that was disturbed by the eruption, whereas the lower fallen units are part of a fossil forest dominated by different species (forest 1, Fig. 5.7) that was already dead at the time of the eruption. Hayward and Hayward (1995) demonstrated that the main orientation of the fallen logs was random, indicating that they were not knocked down by the base surge blast. During this study we concurred with the view that there were two forests. Therefore, the presence of fallen tree logs will not be discussed here and we will assume that only forest 2 was disturbed by the eruption. Brand et al. (2014) discuss a theoretical approach on the dynamic pressure of the initial base surges generated at Maungataketake eruption and its impact on forest 2.

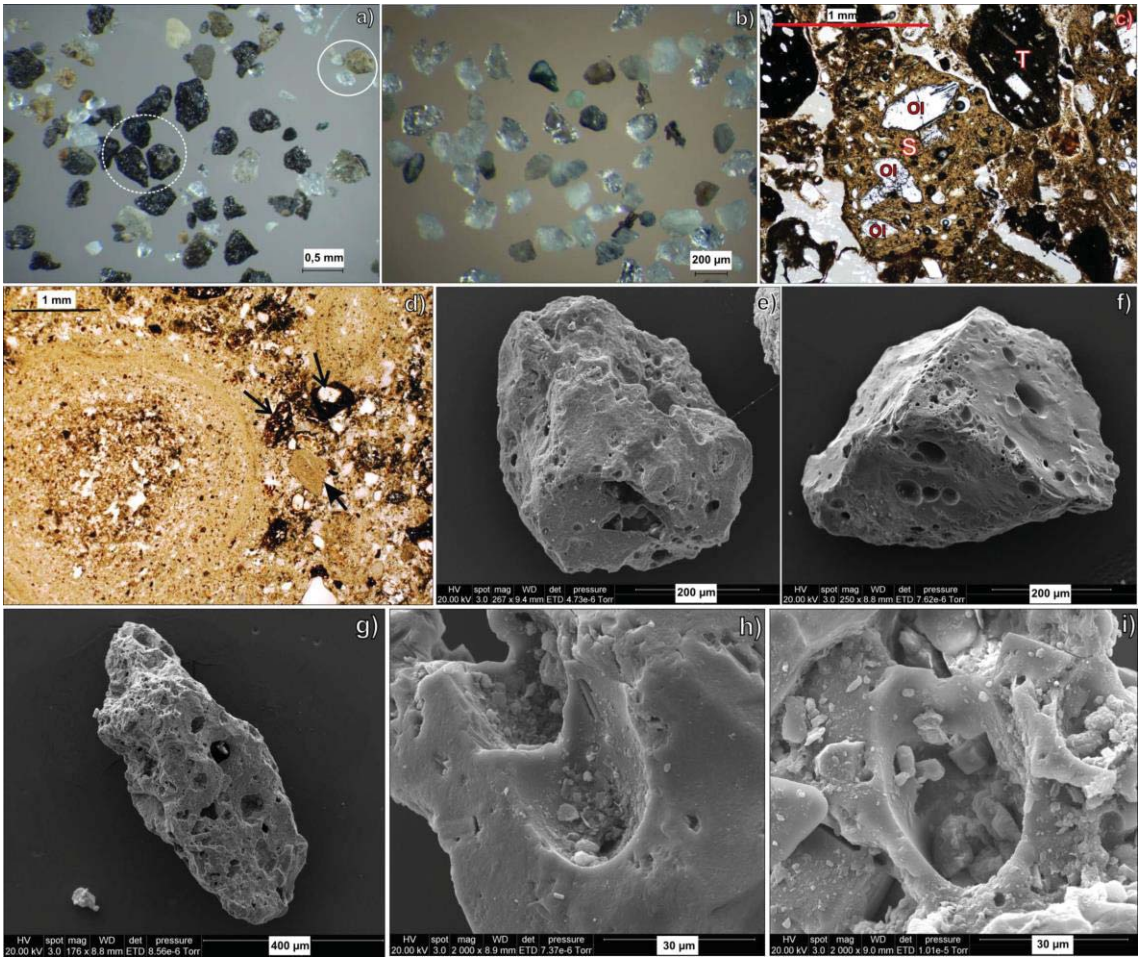


**Fig. 5.4**. a) Stereo light microscope image of 2 ϕ fraction-size fragments from unit 2 (U2) at medial distance from the vent (between sites M3 and M4). Distinct juvenile fragments are within the broken-lined circle. Subangular shapes dominate. The encircled particles within the solid line are: a country-rock lithic, and quartz and feldspar crystals. b) Stereo light microscope image of 3 ϕ fraction-size fragments from U1 at medial distance (same as above). Note the great majority (>90 vol.%) of accidental crystals (mainly quartz or feldspathic grains and mineral aggregates). c) Plane-polarised, transmitted light photomicrograph of juvenile particles from U3 at site M1. The bigger grain (S) corresponds to a subangular-to-sub-spheric sideromelane glass. Tachylite grains (T) are also present. Euhedral and subhedral olivine phenocrysts (Ol) are common in the fragments. d) Plane-polarised, transmitted light photomicrograph of tuff from U6 at location M2 showing rim-type accretionary lapilli. Open arrows point to juvenile fragments and filled arrow indicates an accidental lithic (siltstone). Quartz and feldspar grains (bright irregular shapes) are pervasive. e), f), and g) Scanning electron microscope (SEM) images of typical juvenile grain morphologies. Fragments are from U2 and U3 at medial distance (between sites M3 and M4). They show subangular-to-subrounded edges and low vesicularity. h) and i) SEM images of vesicles of juvenile particles from U1 at the medial distance. The vesicles are sub-spherical and show surface adhering and secondary mineral growths. Thick vesicle walls and smooth inner surfaces are present in most juvenile fragments. For location of sites and units see Fig. 5.2.

**Table 5.2** Nomenclature, characteristics and interpretations of lithofacies assigned for the Maungataketake phreatomagmatic deposits. The definitions (with their references) for the interpretations on transport processes from bedform sedimentary characteristics are explained in section 5.5.1. Photographs related to the depiction of lithofacies are referred in the table and contained in Figs. 5.5 (general view) and 5.6 (closer view). ***Appendix B.2 contains detailed description of lithofacies and their interpretations.***

| **Lithofacies** (Thickness (m) / ***accidental to juvenile ratio (based on vol.%)*** | **Grain size** | **Internal structure** | **Interpretation** |
|---|---|---|---|
| **Accidental-fragment dominated, poorly consolidated, matrix supported tuff (T)** | | | |
| **T1** *(Figs. 5.5c,b,e; 5.6a,b,f)* 0.2 to 0.5 m / ***9:1*** | Fine ash (~ up to 55 vol.%) and medium ash (~ up to 35 vol.%) of accidental origin | Beds with subtle low-angle, discontinuous cross-lamination and occasional dune bedding, containing some accretionary lapilli | Soft deformation, poor sorting and the presence of accretionary lapilli point to deposition of wet base surges. |
| **T2***(Figs. 5.5a,b,c,d,e; 5.6a,b,c,d,e,f)* 0.1 to 0.15 m / ***9:1*** | Fine ash (~ up to 55 vol.%) and medium ash (~ up to 35 vol.%) of accidental origin. | Beds containing subtle cross-lamination, contain rare accretionary lapilli. Subtle trains of juvenile fragments (coarse to medium ash). | Soft deformation, poor sorting, accretionary lapilli, subtle cross-lamination, and thin trains of juvenile fragments suggest the deposition of wet base surges transported as a weak-turbulent, suspended load. |
| **T3***(Figs. 5.5a,c; 5.6a,b,d,g)* 0.2 to 0.5 m / ***9:1*** | Fine ash (~ up to 55 vol.%) and medium ash (up to 40 vol.%) of accidental origin. | Beds with laminations that pinch and swell laterally and are often truncated by overlying laminations. Pervasive soft deformation and accretionary lapilli. | Intense soft deformation, poor sorting, accretionary lapilli, cross-lamination indicate the deposition of wet base surges that were transported in a low-energyt, rapidly decelerating cloud. |
| **T4***(Figs. 5.5c, 5.6c)* 0.5 m / ***8:2*** | Fine ash (~up to 40 vol.%) and medium ash (~ up to 30 vol.%) of accidental origin. | Planar beds with diffuse boundaries. Contain some accretionary lapilli. | The presence of juvenile richer bands, accretionary lapilli, and poorly sorting point to the deposition of density stratified, wet, moderately diluted PDCs that were transported as a combination of suspended loads and traction carpets. |
| **T5***(Figs. 5.5b,c; 5.6c,e)* 0.3 to 0.5 m / ***7:3*** | ~70 vol.% of juvenile clasts with grain sizes ranging from fine lapilli (4 mm) to coarse ash (1 mm to 0.3 mm) | Crudely bedded which contain diffusely distributed juvenile fragments. Beds are not affected by impact structures. Accretionary lapilli are not observed. | Diffuse stratification, poorly sorting, ash-coated juvenile fragments suggest the deposition of moderately concentrated, low-energy, wet base surges that were transported mainly as bed loads/traction carpets. |
| **T6***(Figs 5.5d; 5.6d,h)* 1.0 m / ***6:4*** | Fine-to-medium sized ash of accidental origin (40 vol.%) and medium-to-coarse, juvenile ash. | Planar beds of fine ash with juvenile-rich layers arranged in trains or thin beds of irregular thickness (from few mm to up to 3 cm). Subtle soft deformation and abundant accretionary lapilli. | Accretionary lapilli, parallel bedding, juvenile-rich beds with diffuse boundaries indicate the deposition of density stratified, low-energy, rapidly decelerating, wet base surges. |
| **T7***(Figs. 5.5a,d,h)* 0.5 to 1.5 m / ***9:1*** | Fine-to-medium sized ash of accidental origin (up to 70 vol.%). <30 vol.% juvenile coarse ash (<1 mm). | Planar beds with subtle low-angle, cross-lamination and sub-parallel trains of juvenile coarse ash. Devoid of lapillus and block size fragments. Common accretionary lapilli. | Accretionary lapilli, cross-lamination, juvenile-rich beds with diffuse boundaries indicate the deposition of density stratified, low-energy, rapidly decelerating, wet base surges that were mainly transported as suspended loads and bed loads. |
| **Juvenile-fragment dominated, consolidated, clast supported lapilli tuff (LT)** | | | |
| **LT1***(Figs. 5.5c,d,e; 5.6a,b,d,f)* 0.1 to 0.15 m/ ***2:8*** | >80 vol.% of coarse ash to fine lapilli juvenile fragments. Ash to block size accidental fragments usually comprise less than 10 vol.%. | <15 cm beds that are sub-parallel and/or slightly undulating, laterally continuous. Normal or reverse graded. | The degree of consolidation, poorly sorting, pinch and swell, and variable grading may point to the deposition of a relatively high concentrated, wet PDCs transported dominantly in a traction carpet mode |
| **LT2***(Figs. 5.5a,c; 5.6a,b,d,g)* 0.05 to 0.4 m / ***2:8*** | | Beds are ungraded, normal or reverse graded. Intense soft deformation is evident and beds can be affected by impacts of blocks of accidental origin (up to 40 cm). | Intense soft deformation. The degree of consolidation, poorly sorting, and variable grading may point to the deposition of a relatively high concentrated, wet PDCs transported dominantly in a traction carpet mode and later deformed by impact fragments |
| **LT3** *(Fig. 5.5b,e)* 0.5 m / ***1:9*** | | Ungraded, normal or reverse graded, and may show load structures at the base. Diffuse stratification. | Juvenile clast morphology may suggest the deposition of a high concentrated, wet, non-turbulent PDC probably emplaced more like a Surtseyan tephra jet transported as a grain flow |

**Table 5.3** Nomenclature, characteristics, and interpretation of lithostratigraphic units for the Maungataketake phreatomagmatic deposits. It is recommended to turn to Figs. 5.1, 5.2 and 5.5 in order to get a better understanding of the spatial distribution of sites, lithofacies, and units. ***Appendix B.2 contains a detailed description of units.***

| PHASE | LITHO-STRATIGRAPHIC UNITS | **1.** ASSOCIATED LITHOFACIES<br>**2.** AVERAGE THICKNESS/APPROXIMATE ACCIDENTAL TO JUVENILE RATIO<br>**3.** BOUNDARY CONTACT WITH LOWER UNIT<br>**4.** DOMINANT BEDFORMS | | | INTERPRETATION OF UNITS |
|---|---|---|---|---|---|
| | | PROXIMAL (SITES M1,M2) | MEDIAL (SITE M3) | DISTAL (SITES M4,M5) | |
| PH1 (vent opening/ shallow explosions) | **U1**<br>*(Figs. 5.2; 5.5c,e)* | Not present | **1.T1/LT1**<br>**2.**1.5 m / 9:1<br>**3.** Sharp and irregular, moderately erosional<br>**4.**Generally massive, plane-parallel/cross laminated. Few impact sags | **1.T1**<br>**2.**0.5 m / 9:1<br>**3.**As previous<br>**4.**Generally massive | Vent opening explosions generated fine-grained ash-laden base surges. The flows were wet, either due to condensation of steam and/or original sediment pore water. Ash particles were cohesive, forming accretionary lapilli. |
| | **U2**<br>*(Figs. 5.2; 5.5c,d,e; 5.6a,b,d)* | **1.LT2/T2**<br>**2.**<0.5 m / 5:4<br>**3.**Not visible<br>**4.**General plane-parallel/cross laminated | **1.LT1/T2**<br>**2.**0.5 m / 5:4<br>**3.** Sharp with scour surfaces and/or load structures<br>**4.**General parallel-slightly undulating bedded, plane-parallel/cross laminated tuff | **1.LT1/T2**<br>**2.**0.5 m / 5:4<br>**3.** Sharp to gradational<br>**4.** Undulating bedding | The presence of a "bipartite base surge" with a lower coarser-grained bed (LT1) overlain by a finer-grained layer (T2) suggests that U2 was formed by a series of density stratified base surges. |
| PH2 (deeper excavation) | **U3**<br>*(Figs. 5.2; 5.5a,c,d)* | **1.LT2/T3**<br>**2.**Variable (usually <0.8 m)<br>3. Gradational<br>**4.**Laminated (intense soft deformation). Cross lamination | **1.LT2/T3**<br>**2.** 0.7 m / 7:3<br>**3.**Gradational<br>**4.**Intense soft deformation of laminated beds. Visible and common impact bedding sags | **1.LT1/T6**<br>**2.**0.5-0.7 m / 7:3<br>**3.** Gradational<br>**4.**Parallel-slightly undulating, laminated tuff | This phase starts with lithofacies T3 deposits (sites M1 and M3, Fig. 5.5a,c), indicating base surges with an unsteady and pulsatory behaviour. This was followed by deposition of LT2, which indicates a deepening locus of explosions and/or shifting of vent. |
| PH3 (shallow seated explosions) | **U4**<br>*(Figs. 5.2; 5.5b,c,d; 5.6c,d)* | **1.T3**<br>**2.**~0.5 m / 8:2<br>**3.**Gradational<br>**4.**Laminated (intense soft deformation). Cross lamination | **1. T4**<br>**2.**0.5 m / 8:2<br>**3.**Gradational<br>**4.**Plane-parallel/diffusely bedded. The fine tuff is cross-laminated. Devoid of impact structures | **1.T6/T1**<br>**2.**0.3 m / 6:4<br>**3.**Gradational<br>**4.**Plane-parallel bedded/laminated. Devoid of impact structures | The eruption proceeded without interruption as suggested from the gradational contact from U3 to U4, depositing a rhythmic sequence of base surges (T4). With distance, the currents rapidly deflated, reduced in turbulence and particle load, which are represented in lithofacies T6 (Fig. 5.6a). |
| | **U5**<br>*(Figs. 5.2; 5.5b,c,; 5.6c,d)* | **1.LT3/T2/T4**<br>**2.**1.0 m / 2:8<br>**3.** Sharp slightly erosional with load structures<br>**4.**General crudely bedded. Plane-parallel/cross laminations in T2 | **1.T5/T2**<br>**2.**0.7 m / 3:7<br>**3.**Sharp to gradational<br>**4.**Diffuse bedded/massive. Devoid of impact structures | **1.T6**<br>**2.**<0.5 m / 4:6<br>**3.** Gradational<br>**4.**Plane-parallel bedded, laminated.Devoid of impact structures | LT3 shows that the eruption shifted suddenly to a phase of production of coarser and more common juvenile fragments, either due to a reduction of external water interaction or an increase in magma ascent rate. |
| PH4 (vent stabilization and waning) | **U6**<br>*(Figs.5.2; 5.5a,b,d; 5.6d)* | **1.T7/T5**<br>**2**. up to 1.5 m / 9:1<br>**3.**Sharp<br>**4.**Parallel-undulating bedded, cross-laminated. Devoid of impact bedding sags | **1. T7/T5**<br>**2.**<0.5 m / 9:1<br>**3.**Gradational<br>**4.**Plane-parallel bedded, cross-laminated. . Devoid of impact bedding sags. Abundant accretionary lapilli | **1.T7/T5**<br>**2.**1.5 m / 9:1<br>**3.**Gradational<br>**4.**Plane-parallel bedded, cross-laminated. Devoid of impact bedding sags. Abundant accretionary lapilli | U6 shows a regular pattern of deposition from PDCs. In general, the succession exhibits regular deposition patterns that suggest stabilization of the vent |

## 5.6 Eruption reconstruction

A model for this eruption (Fig. 5.7) integrates all textural, morphologic, lithologic and sedimentary characteristics contained in Tables 5.1, 5.2, and 5.3. Following Table 5.3 the reconstruction of the eruption will be described according to four different phreatomagmatic phases. The lithofacies and units mentioned in the following 4 subsections are described with more detail in Table 5.2 and Table 5.3 respectively.

### 5.6.1 Phase 1. Vent opening and shallow explosions

The Maungataketake vent probably opened when the total vaporization energy exceeded the limit of containment (Sheridan and Wohletz, 1983). Since the sedimentary record of the lower U1 includes the presence of lithofacies T1 (Table 5.2), composed primarily of disaggregated material from the unconsolidated Plio-Pleistocene sediments (Table 5.1, Table 5.2), and the apparent absence of a tuff breccia horizon, it is likely that the vent opening explosions disrupted primarily the ~60 m-thick unconsolidated Plio-Pleistocene sediments (Fig. 5.7a). However, although not evident in the deposit record, deeper disrupted material and early tuff deposits could have been recycled into the diatreme due to slumping into the widening crater (c.f., Valentine, 2012). A series of turbulent to non-turbulent, wet, base surges formed the basal deposits (U1, Table 5.3). These first currents entered a live forest (forest 2) (5.7a,b). Some of the trees were knocked down by the impact of the currents (see Fig. 5.5c) (Brand et al., 2014), or later fell under the weight of tephra. Subsequent explosions were likely also shallow seated (overall presence of T1, see above), within unconsolidated sediments, which also likely continually slumped inwardly from unstable crater walls (c.f., Auer et al., 2007) (Fig. 5.7c). At M3, the boundary between U1 and U2 is sharp with erosive characteristics (Table 5.2, Fig. 5.6c) that suggest a change in the eruption dynamics. However, at M4/M5 sites this boundary is more gradational, which rules out any suggestion of elapsing time between the deposition of U1 and U2.

U2 reflects deposition from distinctively density stratified base surges (lithofacies LT1/T2) (Table 5.2, 5.3) with higher contents of juvenile particles (Table 5.3, Fig. 5.5c,d,e). This could indicate a higher magma effusion rate, or a reduction in external water (c.f., Houghton et al., 1999). Since the juvenile-rich, lower part of the currents (lithofacies LT1 in U2, Table 5.3; Figs. 5.5c, 5.6a,b) show evidence of lower traction carpet transport, the contribution of fallout was probably never dominant (Table 5.2), or was erased or modified by the multiple base surges produced through the eruption. Shallow seated explosions may have been dominant at this stage as indicated by the overall presence of Plio-Pleistocene sediments and lack of deeper Waitemata Group fragments. At distal sites (Figs. 5.5d,e, 5.6d), U2 shows low-amplitude (0.5 m) undulations that may be the result of the paleo-surface topography, but this is not clear.

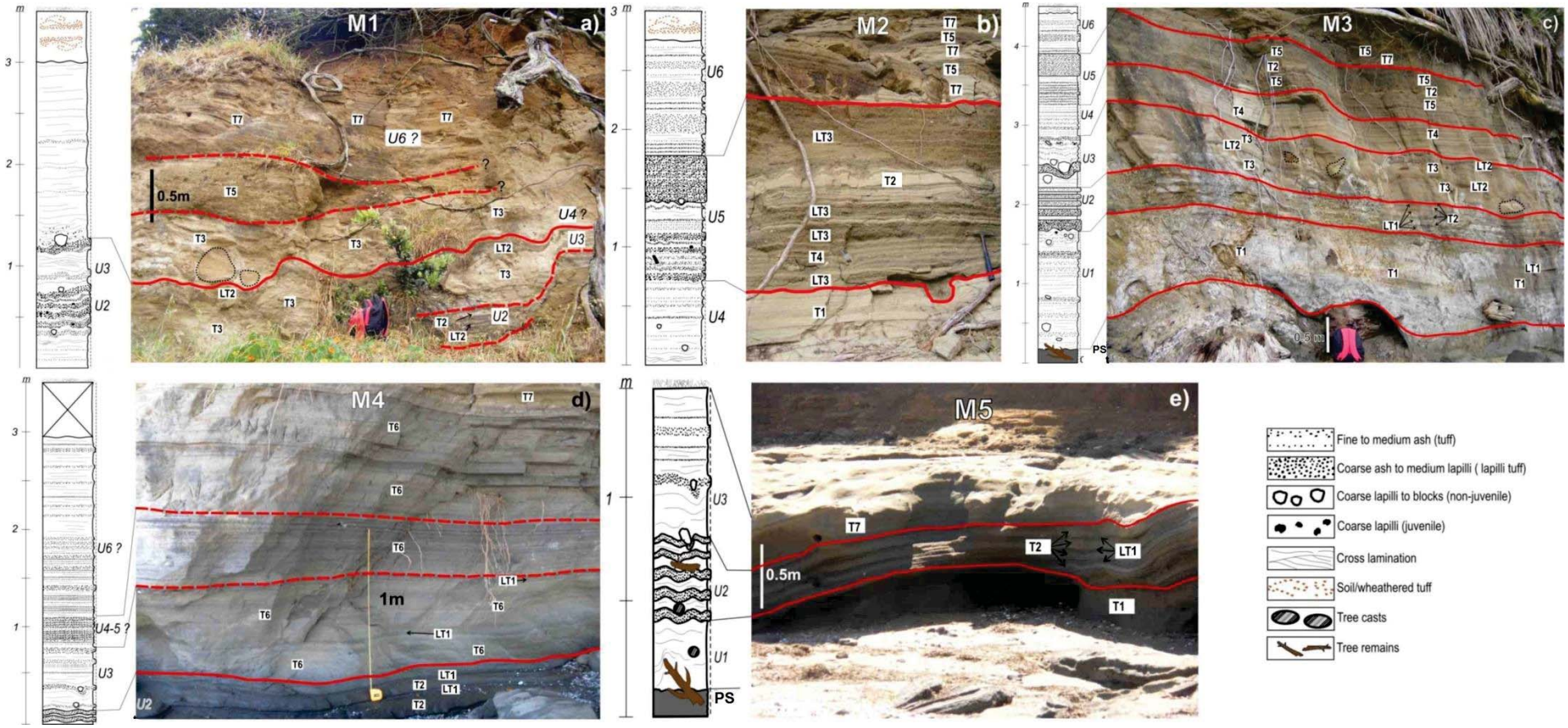


**Fig. 5.5**. Photographs and corresponding logs for key sites M1 to M5 (see Fig. 5.1 for location of sites and Fig. 5.3 for log correlation). Solid red lines indicate the boundary between units (U) (see description and interpretation of units in Table 5.3 and ***Appendix B.2***). Uncertain boundaries are marked by dashed red lines. Some accidental Waitemata blocks are delineated in dotted-fine black lines, as in photographs a) and c). Accretionary lapilli are found in all locations. Lithofacies outlined in photographs are explained in Table 5.2 and ***Appendix B.2***. PS in c) and e) represents the peaty soil underlying the phreatomagmatic deposits. Vertical axis correspond to thickness of deposits. The base of the stratigraphic logs are at approximately back beach level for M3, M4, and M5. M1 and M2 are 3 m and 5 m above back beach level respectively. ***Additional sites (MM1, MM2, MM3) with corresponding logs are presented in Appendix B.1*** .

***Fig. 5.5 is included in the published manuscript. However, Appendix B.1 separately contains the logs (with pictures, descriptions, and available frequency histograms) corresponding to these sites and three additional sites. It is important to note that there is a discrepancy of the level of the base of the logs in the published papers. Now, the base of stratigraphic logs is referred to the back beach level.***

### 5.6.2 Phase 2. Excavation into the Waitemata group rocks

A gradational boundary between U2 and U3 and the absence of juvenile-rich lithofacies (Table 5.3, Figs. 5.5c, 5.6a,b) suggest an uninterrupted activity that in general progressed towards a return (as U1) to the dominance of accidental ash-laden base surges that deposited U3 (composed of lithofacies T3 and T6) (Table 5.3, Figs. 5.5c, 5.6a,b). The prevalence of accidental ash characterized by Plio-Pleistocene sediments and the initial absence of Waitemata rock fragments could indicate that shallow seated explosions prevailed. However, in the mid- section of U3 (Figs. 5.5d, 5.6a,b), there is possible evidence of deeper excavation into the underlying Waitemata Group deposits (Fig. 5.7d), with small blocks and coarse lapilli of this lithology present (Figs. 5.5c, 5.6a,b). These are, however, rounded clasts, and thus likely represent Pleistocene fluvial deposits on top of the Waitemata paleosurface, consistent with other reconstructions of the paleogeography of this area (Searle, 1981; Kermode, 1992). Thus explosions probably did not penetrate deeper into the Waitemata rocks, but excavated the fragments at the boundary between the Waitemata Group and the Plio-Pleistocene sediments at depths of approximately down to 100 m below the eruption paleosurface (Fig.5.7d). Whether these deeper explosions were the result of vent shifting is not clear, but the presence of coarse fragments of Waitemata rocks decreasing towards distal exposures (M4, Fig.5.5d) suggests that the vent probably did not migrate. Regardless of the locus of these explosions, they were accompanied by greater slumping of crater wall material (the water-saturated, unconsolidated Plio-Pleistocene sediments were readily removed) filling the vent with liquefied sediments (e.g. Sohn and Park, 2005) (Fig. 5.7c). This situation prevailed with further shallow seated explosions (Fig. 5.7e) after the event marked by the excavation of the Waitemata rocks.

### 5.6.3 Phase 3. Shallow seated explosions

As indicated by the gradational boundaries between upper U3 and lower U4 (Fig. 5.6a,b), the shallow explosions continued without interruption (Fig. 5.7e),promoting the deposition of U4. The evidence of this can be seen in the sedimentary characteristics of deposits U4 (Table 5.3) showing the absence of Waitemata-pebble fragments and the rhythmic succession of deposits from low-energy base surges (lithofacies T4, Table 5.2; Figs. 5.5c, 5.6c). The change from lithofacies T4 to lithofacies T6 with distance (Table 5.3, Fig. 5.5c,d) suggests decreasing flow energy (changes in the shear stress rate of the flow).

The shallow seated explosions went on and the conditions promoted the generation of a juvenile-rich phase that deposited U5. The presence of massive/crudely bedded, coarser grained lithofacies (LT3 and T5 at M2 and M3 respectively; Fig.5.5b,c) indicate a less energetic phase with shallower explosion locus where the involvement of accidental disaggregated sediments was less important. On the other hand, the lateral sedimentary changes in U5 from proximal to distal sites (coarse-grained, crudely bedded to relatively finer-grained, diffuse bedded) (Table 5.3, Figs. 5.5c,b,d, 5.6c,d) do not represent the deposition

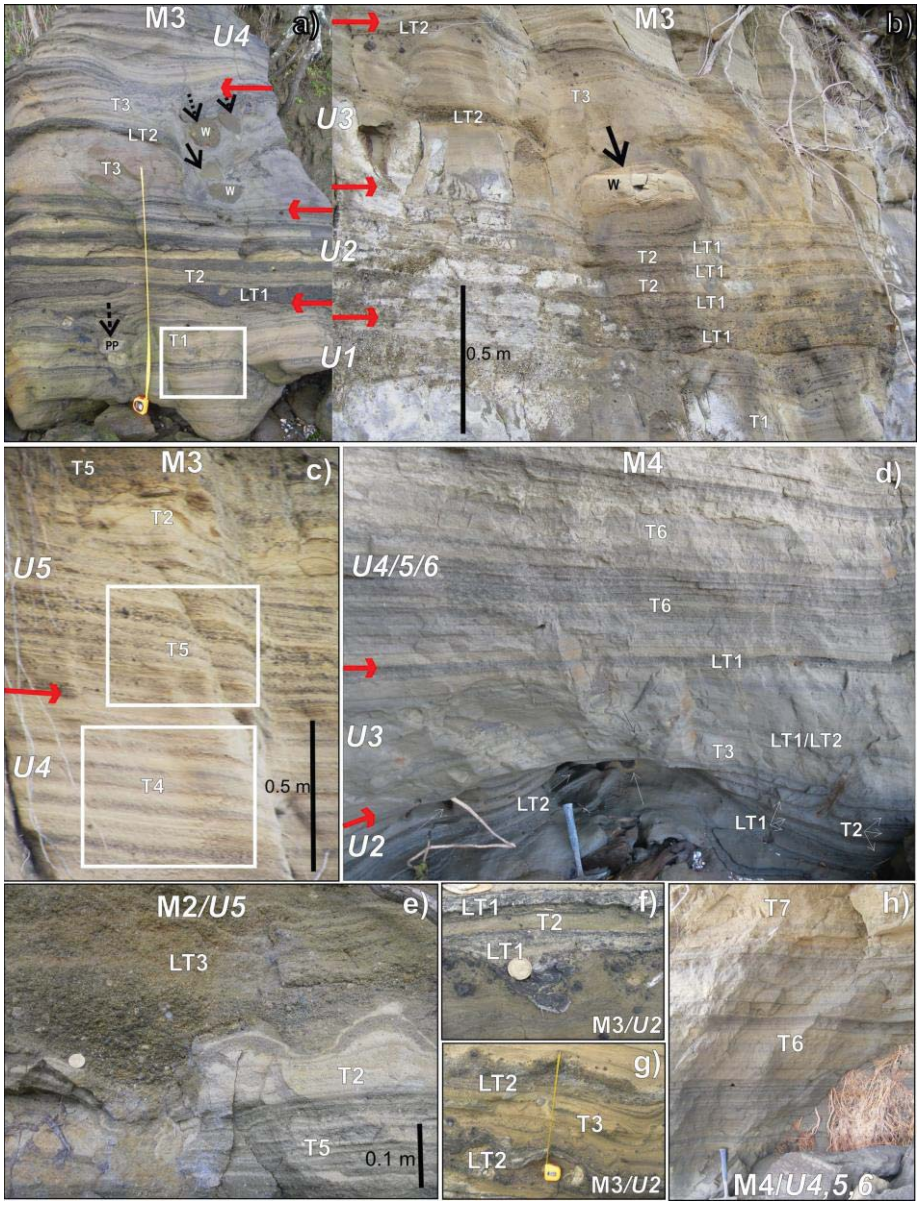


**Fig. 5.6**. Photographs showing the lithofacies (for the descriptions and interpretations see Table 5.2. Lithofacies are also shown in Fig. 5.5) and boundaries between units in more detail. a) Photograph of fallen block displaying part of the stratigraphic sequence exposed as in photograph b). Both photographs represent site M3 and are roughly at the same scale (measuring tape is 1 m). Red arrows indicate the boundaries between units (see Table 5.3 for description and interpretation of units). The uppermost part of unit 1 (U1) shows more concentrated trails of juvenile fragments, sometimes exhibiting impact sags or bedload structures. Note in U2 the upward thinning of beds containing lithofacies LT1; also their grain size diminishes in the same direction. Soft sediment deformation is distinct in the middle section of U3. The white-outlined square within a) highlights lithofacies T1. W and PP indicates blocks of Waitemata rock and block aggregates of Plio-Pleistocene sediments respectively. c) Plane parallel bedding is evident, but juvenile-rich beds (darker layers) form diffuse bedding as the transition to more accidental rich tuff is gradual. This photograph is part of site M3 and the two white-outlined squares highlight lithofacies T4 and T5. d) Photograph of a site located a few meters downflow direction from site M4. Red arrows indicate the boundaries between units. From the middle section of U3 upwards the whole sequence exhibits plane-parellel beds with distinct, but subtle aggradation. e) Detail of lithofacies LT3, T2, and T5 (Table 5.2) within U5 at site M2. Note the load structures at the base of LT3. f) and g) Detail of lithofacies LT1, LT2, T2, and T3 (Table 5.2) within U2 at site M3. Coin in f) is 2.6 cm and measuring tape in g) is 20 cm. h) Detail of lithofacies T6 and T7 (Table 5.2) within U4, U5, and U6 at M4. Location of sites is shown in Fig. 5.1. ***See Appendix B.2 for detailed description of lithofacies.***

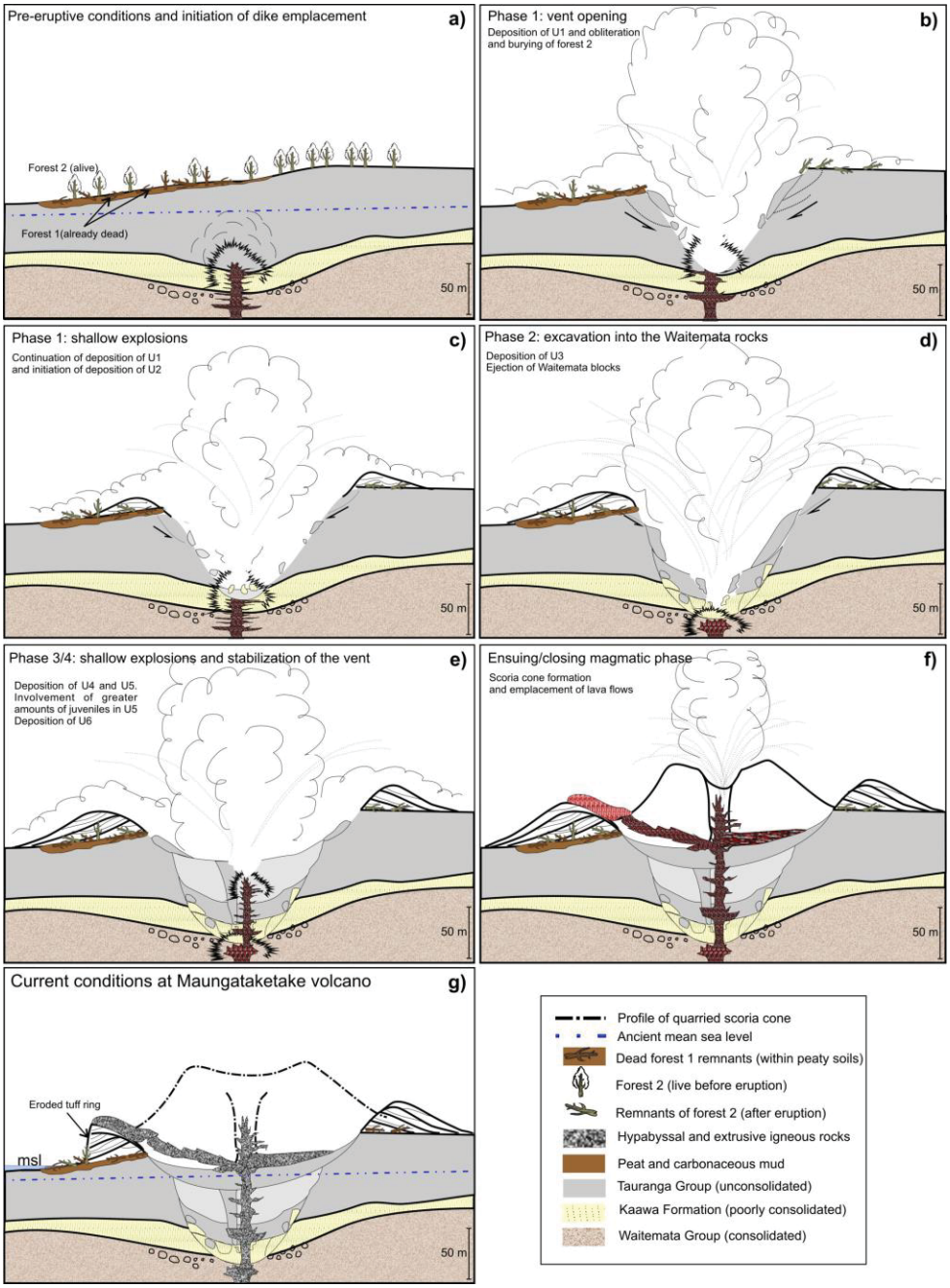


**Fig. 5.7**. Cartoons that represent a simplified model of the Maungataketake eruption history. Not to scale; the vertical scale shown in the cartoons is displayed only for approximate thickness reference of the existing lithologies. The orientation of the section is roughly NNE-SSW intersecting the crater rim at site M2. See section 5.6 in the text for a detail description. a) Conditions previous to the vent opening and initiation of phreatomagmatic explosions at shallow depth as a consequence of dike emplacement. Note that there are two forests on the surface. b) The vent opens (phase 2) and forest 2 is obliterated and buried within the lower deposits of U1. The fallen and buried trees seen on the right section of the vent are speculative as their presence cannot be verified in the field. c) Slumping of crater walls into the vent and promotion of shallow seated explosions (continuation of phase 2 and deposition of U1-U2). d) Excavation into the Waitemata rocks and ejection of blocks. Generation of wet base surges. e) Filling the vent with slumped material from the crater walls (dominantly Plio-Pleistocene sediments). Overall prevalence of shallow seated explosions that characterizes phases 3 and 4. Culmination of the phreatomagmatic activity at Maungataketake with the deposition of U6. f) Shifting to the magmatic phase of the eruption. g) Current conditions at Maungataketake where the scoria cone has been extensively quarried and the western section of the maar ejecta ring has been eroded by the sea.

of a typical base surge, instead U5 deposits at M2 (Fig. 5.5b) may have been related to a concentrated collapsing jet (Ross and White, 2006) that became diluted with distance (see changes of lithofacies within U5 from Fig.5.5b to Fig. 5.5c,d). Although the sharp boundary between U4 and U5 at site M2 (Fig. 5.5b) may indicate a break, the gradational boundaries observed at M4 (Figs. 5.5d, 5.6d) between these same units are the evidence of the lack of pauses during this eruption phase. The same reasoning is applicable for the transition from U5 to U6 (Figs. 5.5b,d, 5.6d). Therefore the whole sequence shows continuous activity with no time breaks (or at least time breaks that were not long enough to exhibit clear evidence of elapsing time as described at other sites by Sohn and Park, 2005).

### 5.6.4 Phase 4. Vent stabilization and waning of eruption

The uppermost unit (U6) is a fine-grained, plane-parallel bedded, regular sequence devoid of impact sags (lithofacies T7, Table 5.2). We infer that the lack of ballistic blocks and the rhythmic sequence of lithofacies T7 indicate a stabilization of the vent (Fig. 5.7e) (c.f., Németh et al., 2012a). The prevalence of fragments from the Plio-Pleistocene sediments suggests that the explosions remained shallow seated where water was abundant, which is attested by the ubiquitous accretionary lapilli and the presence of vesicular tuff beds. The phreatomagmatic phase was followed by construction of a complex scoria cone and short lava flows (Fig.5.7f). At site M1 there is evidence (not shown) of an erosional unconformity between the phreatomagmatic deposits and the scoria deposit that may suggest some time gap between the phreatomagmatic and magmatic phases, but the lack of more contact exposures makes it difficult to infer the time that elapsed between them. Geochemically, however, both eruptive phases seem to belong to a single magma batch with rock compositions that show trends consistent with differentiation (see section 5.7).

## 5.7 Maungataketake whole rock and glass chemistry

The whole rock chemical composition shown by Maungataketake samples (16 from the scoria cone; 5 of the rare coarse lapilli ballistics from the ejecta ring) falls toward the low-silica high alkali end of the spectrum of compositions observed from the AVF (McGee et al., 2011). They are low $SiO_2$ (41-45 wt.% loss free) alkali basalts with intermediate Mg-numbers (62-65) (Fig. 5.8a,b, ***Appendix C, Table C.1***).On variation diagrams (Fig. 5.8a,b), Maungataketake basalts show trends that are consistent with a differentiation process. All major elements except $Al_2O_3$, but including $SiO_2$, show negative trends with MgO (and Mg#) (Fig. 5.8a,b). Similarly mantle compatible trace elements (Ni,Cr) show positive trends with MgO, whereas incompatible trace elements (LILE, HFSE) show a negative trend. Samples from the ejecta ring fall toward the relatively evolved (low MgO, higher $SiO_2$, high alkalis and incompatible trace elements) end of the compositional spectrum, but there is not a clear correlation observed between stratigraphic position as has been observed in other volcanoes of the Auckland Volcanic Field (Crater Hill, Smith et al., 2008; Motukorea, McGee et al., 2012).

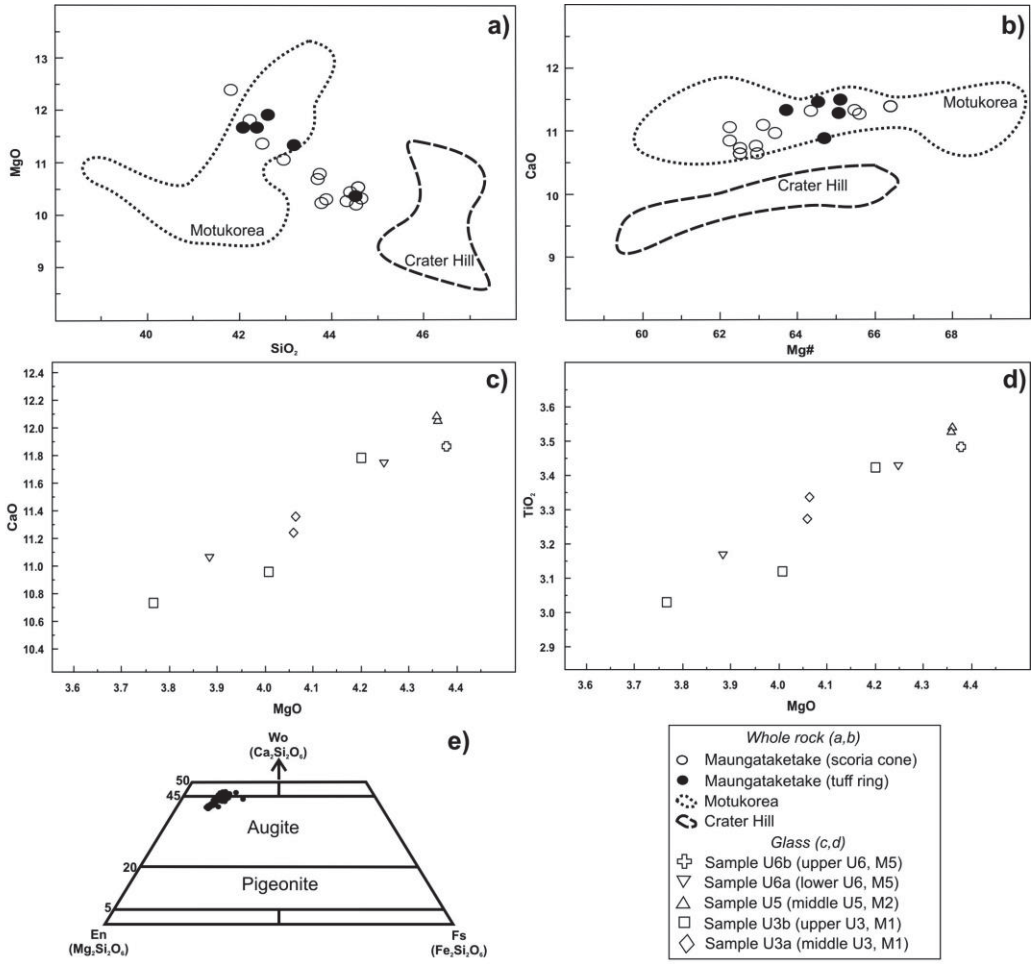


**Fig. 5.8**. a) and b) major element (wt.%) variation diagrams (whole rock) (***Appendix C, Table C.1***). For comparison, the field occupied by sample data from Motukorea (dotted line) (McGee et al., 2012) and Crater Hill (broken line) (Smith et al., 2008) volcanoes is indicated (see Fig. 3.1 for location of volcanoes). c) and d) major element (wt.%) variation diagrams of glass compositions of selected samples (***see Appendix C, Table C.2, for details of samples***) listed in an ascending stratigraphic order (from U3 to U6), and from proximal to distal locations (form site M1 to site M5). e) Pyroxene crystal (microlite/microphenocrysts) compositions. The data include microprobe measurements on inner, central, and outer crystal spots.

Samples used for microprobe analyses (glass and crystal compositions) come from throughout the stratigraphic sequence, but do not correspond directly to the samples representing whole-rock composition (***see Appendix C, Table C.2, for details***). The glass shard compositions tend to be more $SiO_2$-rich than the whole-rock samples; CaO shows a positive trend with MgO (Fig. 5.8c; ***Appendix C, Table C.2***), but shows a wider range than MgO.$TiO_2$ (Fig.5.8d) and FeO describe a positive trend with MgO, indicating late stage crystallization of oxides. A high rate of nucleation (on shifting the liquidus to higher temperatures) is triggered by the exsolution of the last $H_2O$ from the melt in the very shallow conduit (e.g. Schipper et al., 2010). Microlite composition is shown in Fig.5.8e, and indicates Ca-rich pyroxene.

## 5.8 Discussion

### 5.8.1 Magma fragmentation and host rock disruption

Sedimentary features such as accretionary lapilli, soft-sediment deformation, vesiculated tuff, and plastering of fine ash onto obstacles throughout the deposit sequence point to deposition mainly from "wet" base surges. Juvenile pyroclasts show particle coatings or adhering fine particles (e.g. Sheridan and Wohletz, 1983; Cioni et al., 1992) and include sideromelane glass (Fisher and Schmincke, 1984) (Fig. 5.7c,i) (Table 5.1). These all indicate phreatomagmatic fragmentation. Although there is an absence of non-vesicular, equant, blocky juvenile fragments (2-3 $\phi$) regarded (from experimental data) to be representative of interactive particles resulting from FCI fragmentation (c.f., Sheridan and Wohletz, 1983; Wohletz, 1983; Zimanowski et al., 1997), this rationale may not be satisfactorily applicable in natural cases where vesiculated fragments may be also the result of FCI (e.g. Cioni et al., 1992). The majority (>80 vol.%) of juvenile particles throughout the sequence are 0-2 $\phi$ in size and are equant and subangular, microlite-rich and poorly vesicular (Table 5.1; Fig. 5.3a; Fig. 5.4c,e,f,g). These characteristics could indicate general low-energy FCIs with high water to magma mass ratios (c.f., Sheridan and Wohletz, 1983; Wohletz and McQueen, 1984). Also, the juveniles may be the result of "secondary fragmentation" as the result of disruption of surrounding magma by shock waves produced in the MFCIs processes (Zimanowski, 1991; Raue, 2004). Additionally, recycling of juvenile and non-juvenile clasts may have occurred (Houghton and Smith, 1993), contributing to the homogenous morphology.

Raue (2004) reports that >60% of thermal energy of magma in such eruptions is converted into shock waves that may disrupt surrounding magma and/or country rock. At Maungataketake, the morphological, stratigraphic, and sedimentary data suggest the vent opening explosions occurred at shallow depths (around 60-100 m), primarily within Pleistocene-Holocene Tauranga Group and Kaawa Formation sediments. Part of the mechanical energy produced in the FCI was probably expended in the excavation of this soft host material. Due to the unconsolidated nature of the capping sediments, slumping and refilling of the vent area by the saturated and unconsolidated deposits, appears to have been common at Maungataketake, with periodic replenishment of fine sediment and groundwater to the eruption site. The fact that accidental ash (which comprises up to 80 vol.% of the deposit) is principally composed of Plio-Pleistocene sedimentary grains and grainsize distribution of the tuff is constant laterally and vertically (Fig. 5.2) suggests the primary involvement of the unconsolidated Tauranga Group and the Kaawa Formation sediments. Other than the rare coarse, rounded, Waitemata rock fragments in U3 (Table 5.3, Section 6.2), there is no clear evidence of the presence of this lithology in the tuff. However, downward disruption of the Waitemata Group rock units into a diatreme cannot be excluded.

### 5.8.2 Water availability within the host material

The explosive interaction of magma with water is the most common mechanism by which maar-diatreme and tuff ring volcanoes are formed (Chough and Sohn, 1990; White, 1990). In many locations the volcanic edifices related to phreatomagmatic activity are located at coastal margins where shallow sea water or groundwater is present [e.g. Jeju Island, South Korea (Sohn, 1996); Marion and Prince Edward Islands (Verwoerd and Chevallier, 1989); Ambae Island, Vanuatu (Németh and Cronin, 2009)], whereas scoria cones are formed on higher and drier ground inland. In the AVF, phreatomagmatic activity is characteristic of the low-lying, coastal areas such as the Manukau Lowlands. The thicknesses of the Tauranga Group, Kaawa Formation, and Waitemata Group are only inferred by extrapolations from borehole data (***see Appendix A.2***). Kaawa Formation sediments could even be quite thin (<10 m) (Viljevac, 2002), but these are highly controlled by an irregular paleosurface and are far thicker in paleovalleys (Edbrooke et al., 2003). Kaawa Fm sediments have excellent conditions for water storage and good hydraulic properties (average hydraulic conductivity, $K=\sim10^{-5}$). The Tauranga Group sediments (~30-50 m thick) are almost impermeable and host only low-yield bores, although they are water-saturated (Kermode, 1992). The underlying Waitemata sediments have lower hydraulic conductivity, but may still hold water forming a heterogeneous aquifer (for example, a 200-m depth, 90-100 mm-diameter well can yield 30-300 $m^3$/day; Crowcroft and Bowden, 2002). The combined aquifers extend to at least 500 m depth (Crowcroft and Bowden, 2002). As described above, the sea levels and water tables in the area at the time of the eruption were similar to the present ones (currently, groundwater is found ~2-6 m below the surface). Although quantitative data of water availability is lacking, it appears that water from the unconsolidated sediments and the Kaawa aquifers was sufficient to promote the first FCIs during the vent opening. As shallow-seated explosions were dominant in the construction of the maar ejecta ring, this shallow sediment was obviously still able to yield enough water to sustain subsequent FCI explosions. A complex interaction between magma and water-laden sediments (or sediment-laden water) (c.f., White, 1996) thus took place during most of the course of the phreatomagmatic eruption.

### 5.8.3 Unconsolidated water-saturated sediments and FCI

From the study of lithics (componentry data) and substrate distribution, it is likely that soft host sediment was mainly involved throughout the eruption. In such cases, conditions for the explosive mixing of water, unconsolidated sediment and magma are more complex (White, 1996; Schipper et al., 2011). The conventional view (from experimental results) is that a large fine-ash fraction is produced at optimal water to magma mass ratio of ~0.3 (Wohletz 1983, 1986; Sheridan and Wohletz, 1983). Higher or lower water to magma ratios mostly generate overall coarser juvenile fragments (e.g. Dellino et al., 1990; Brand and Clarke, 2009). This is only valid for simple FCI models for volcanic eruptions (White, 1996). White (1996) presents a model where the explosivity of w/m interactions depends strongly on the physical properties of the coolant (which is a mixture of sediment and water) rather than water to magma mass ratios alone.

Using stratigraphic, sedimentary, and hydrogeological data in the reconstruction of four phreatomagmatic volcanoes, Sohn (1996) arrives at a similar conclusion. Intrusion of magma in water-saturated and unconsolidated sediments often generates explosive water-magma interaction, despite initial inhibition. Once started, sediment-laden coolants may promote FCI explosivity by increasing the availability of nucleation sites (White, 1996).

The opening of the vent of the Maungataketake phreatomagmatic eruption probably occurred 60-100 m below the pre-eruptive surface, where magma mixed with pore water and sediment. Slumping and liquefaction of the unconsolidated host materials repeatedly clogged the vent with more water-saturated sediment, which would have also served to maintain a confining hydrostatic pressure. Shallow explosions related to the emplacement of multiple dykes, dyke branches, small sills or arrested jets of magma may have widened the area of magma contact with water saturated sediments (as in the model by White, 1996). A large-sub-volcanic presence of cooled magma indicated by geophysical studies (Cassidy and Locke, 2010) shows that significant sills or lacoliths developed[1]. Deeper explosions may have been promoted by water released from the Kaawa-Waitemata sediments plus also possibly from the Waitemata aquifers enclosing the deeper conduit. The boundary between consolidated (Waitemata Group) and unconsolidated sediments (Plio-Pleistocene sediments) may have caused the least principal stress on a magma dyke to deviate towards a vertical position (e.g, Lorenz and Haneke, 2004), generating possible dyke splays, or temporary ponding in sills. The homogeneity in both the textural characteristics (Table 5.1) and the composition of juvenile fragments may indicate shallow stalling. This is suspected in other similar settings based on exposed dyke and sill complexes in association with preserved diatremes (e.g. Martin and Németh, 2007). As a consequence, further complex geometry of contact between magma and saturated sediment would be generated, causing many areas with differing magma-coolant contact and differing water to magma ratios.

Observations made here point to the fact that water to magma ratios need to be considered with caution. For example, U3 (Table 5.3) (with intense soft deformation) has features that could be interpreted as higher levels of water involved in the phreatomagmatic explosions, compared to those of units 1, 2, 4, and 6 (Table 5.3), when in reality this just reflects the water contained at the moment of deposition. This does not necessarily reflect the water to magma ratios in the FCIs involved, but could be due to water directly ejected from the vent area without being vaporized (c.f., White, 1996) and added to the generated base surges. Water that never took part directly in a FCI could have been transported with the excavated water-saturated substrate during the course of the phreatomagmatic eruption. The wet sedimentary features of the tuffs indicate that base surge temperatures during this eruption were low and often locally below boiling point. The Maungataketake eruption was very stable, with only subtle transitions, mainly related to minor changes in the depth of shallow-seated (mostly <100 m) explosions.

***[1]In the original published manuscript it was suggested that shallow explosions were connected to the late emplacement of magmatic bodies into the water-saturated diatreme fill. The presence of subvolcanic rocks is attested by geophysical studies. However, the geophysical results do not prove that such subvolcanic rocks were emplaced in the late stage of the Maungataketake eruption and these data should be used with caution. But since Maungataketake is a monogenetic eruption, such emplaced bodies might be related to the last stage of the eruption.***

### 5.8.4 Duration and waning of the phreatomagmatic eruption

The broadly uniform mineralogical assemblages and textural characteristics, the absence of evidence for time breaks in the depositional record (section 5.6), and the overall small volume of the maar ejecta ring suggest a brief eruption. The ~1000 m-diameter, low rim, ejecta ring compares well with historic maar forming-eruptions documented, e.g. the Ukinrek maars between 0.5 to <11 days (Kienle et al., 1980); Taal, a few days, (Moore et al., 1966); Ambrym AD1913 eruption, <12-hours growth, with 4 additional days of activity (Németh and Cronin, 2011). Based on the eruptive volumes of the AVF maar-diatreme and tuff ring volcanoes (Kereszturi et al., 2013), the eruption could have lasted a maximum of 16 days, based on an average eruption rate of 5 $m^3/s$. Therefore, Maungataketake volcano was likely formed over only a few days.

The rapid deceleration and loss of turbulence and energy of the base surges is evidenced by the presence of the general plane-parallel bedding in the distal deposits (c.f., Valentine and Fisher, 2000) (Table 5.2). Wet ash particles often aggregate, accelerating their deposition and damping turbulence (Branney and Kokelaar, 2002). Even if the deposit reflects only a wet condition of the flow-boundary zone, the constant eruptions through water-saturated substrate (Tauranga Group and Kaawa Formation) could have always provided water to the flows (a continuous three-phase system).

It is not clear whether the transition to subsequent “dry” activity at Maungataketake was associated with a break in eruptive activity. However, the entire Maungataketake eruption was fed from a single magma batch. In any case, the last phreatomagmatic unit (U6) (Table 5.3) indicates that the vent had become very stable. It seems hardly likely that water supply to the vent area ceased. Thus, the main reason for the waning of the phreatomagmatic eruption was probably due to a rise in magma eruption rate, and/or the isolation of the rising magma conduit from the substrate by a lava moat or similar.

## 5.9 Conclusions

Maungataketake volcano in the southern part of the Auckland Volcanic Field was formed by a distinctive type of phreatomagmatic eruption that occurs in saturated, shallow, deformable and fine-grained sediments. This is characteristic of low gradient alluvial basins, deltas and coastal margins, where the water table is high, and fine-grained porous unconsolidated sediments may be hundreds of metres deep. The Maungataketake phreatomagmatic explosions were dominantly shallow (<100 m depth) and associated with an abundance of water and liquefiable sediment. As the eruption progressed, magma rose into this deformable material, spreading laterally and developing complex contact geometries with the saturated host deposits. Low-energy FCI explosions excavated the wet sediments forming base surges that travelled up to ~1km from the vent with rapidly outwardly decreasing turbulence and velocities. A maar ejecta ring was thus built by the deposition from a series of relatively wet, highly pulsating, density stratified, base surges of moderate energy. Sedimentary and pyroclast features exhibit subtle changes

either laterally or vertically. The homogeneity of the accidental composition (Plio-Pleistocene sediments) and the gradational vertical changes through the sequence appear to indicate excavation and refilling of the vent area with water-saturated sediments via wall collapse and inward flow of liquefied unconsolidated sediment.

The contrast in mechanical and hydrological properties of the host material at the boundary between the consolidated Waitemata Group and the deformable Pleistocene sediments generated conditions for magma to spread from simple dyke geometry and form sill structures and a complex contact between magma and saturated sediments before and after the vent opening. Water was available in excess, and shallow seated explosions occurred at locations differing slightly in depth and location, forming an irregular ejecta ring.

This phase of the Maungataketake eruption was likely brief, lasting only hours to days, and it was followed by a phase of scoria and lava flow production only after the magma eruption rates rose significantly, or water was blocked from the conduit. This example demonstrates one of the lower-hazard variants of explosive phreatomagmatic eruption, contrasting with those occurring with deeper and more focussed FCI explosions, such as those within the Waitemata Group rocks elsewhere in the AVF (e.g. Motukorea volcano, McGee et al., 2012). Thus phreatomagmatic hazard models need to be more closely tailored to the known features of the host geology in an area, e.g. with those occurring in deep, saturated loose sediments, such as low-energy coastal and fluvial settings, having a smaller radius of potential destruction.

MASSEY UNIVERSITY
GRADUATE RESEARCH SCHOOL

## STATEMENT OF CONTRIBUTION
## TO DOCTORAL THESIS CONTAINING PUBLICATIONS

(To appear at the end of each thesis chapter/section/appendix submitted as an article/paper or collected as an appendix at the end of the thesis)

We, the candidate and the candidate's Principal Supervisor, certify that all co-authors have consented to their work being included in the thesis and they have accepted the candidate's contribution as indicated below in the *Statement of Originality*.

**Name of Candidate:** Javier Agustín Flores

**Name/Title of Principal Supervisor:** Karoly Németh

**Name of Published Research Output and full reference:**

Agustín-Flores, J., Németh, K., Cronin, S., Lindsay, J., Kereszturi, G., Brand, B., Smith, I.E.M., 2014. Phreatomagmatic eruptions through unconsolidated coastal plain sequences, Maungataketake, Auckland Volcanic Field (New Zealand). J Volcanol Geotherm Res, 180: 203-224.http://dx.doi.org/10.1016/j.jvolgeores.2014.02.021

**In which Chapter is the Published Work:** Chapter 5

Please indicate either:

- The percentage of the Published Work that was contributed by the candidate:

  and / or

- Describe the contribution that the candidate has made to the Published Work:

  Organization and completion of the whole field work and most laboratory work, main contributor on writing and editing of manuscript draft, and subsequent correcting and editing for final version

Javier Agustin-Flores
Digitally signed by Javier Agustin-Flores
DN: cn=Javier Agustin-Flores, o=Massey University, ou=Institute of Agriculture and Enviroment, email=kiaoranet@yahoo.co.nz, c=NZ
Date: 2015.04.23 14:18:47 -05'00'

Candidate's Signature

08/05/2015
Date

Karoly Nemeth
Digitally signed by Karoly Nemeth
DN: cn=Karoly Nemeth, o=Massey University, ou=Institute of Agriculture and Environment, email=k.nemeth@massey.ac.nz, c=NZ
Date: 2015.05.11 16:33:19 +12'00'

Principal Supervisor's signature

11/05/2015
Date

# Chapter 6. Reconstruction of the Motukorea phreatomagmatic eruption and implication of the substrate

## 6.0 Preface

This chapter comprises the reconstruction of the eruptive history of the phreatomagmatic phase of Motukorea volcano, situated in the northern Auckland Volcanic Field (Fig. 3.1) and erupted through a hard substrate (Waitemata rocks and the underlying Waipapa greywacke rocks). The study is based on collected stratigraphic, sedimentary, and pyroclast data from the tephra ring deposits in conjunction with supplementary hydrogeological and geological information. The main objective was to get insights into the influence of a hard substrate in phreatomagmatic eruptions in the AVF. The eruption was characterized by shallow-seated explosions mostly involving the uppermost 200-300 m-thick Waitemata rocks.

**Contents** Page

**Chapter 6 comprises the published article (*Appendix D*):**

**Shallow-seated explosions in the construction of the Motukorea tuff ring (Auckland, New Zealand): evidence from lithic and sedimentary characteristics**

**Authors**: Agustín-Flores J., Németh K., Cronin S., Lindsay J., Kereszturi, G. **Journal of Volcanology and Geothermal Research**, 304: 272-286. Doi 10.1016/j.jvolgeores.2015.09.013

**The contribution of each author is as follows:**

**Javier Agustín-Flores (PhD candidate)**: Organization and completion of the whole field work and most laboratory work, main contributor on writing and editing of manuscript draft, and subsequent correcting and editing for final version.

**Karoly Németh (main supervisor)**: Oversight of the research process, assistance in the field and laboratory work, as well as in manuscript revision and discussion from the initial draft to the final version.

**Shane J. Cronin (supervisor)**: Discussions during the whole research project and assistance in manuscript revision and discussion from the initial draft to the final version.

**Jan M. Lindsay (supervisor)**: Discussions during the whole research project and assistance in manuscript and discussion from the initial draft to the final version.

**Gábor Kereszturi**: Overall field assistance, manuscript revision and discussion.

## 6.1 Introduction

Many tuff rings and maar-diatreme volcanoes are the result of the explosive interaction of magma with groundwater or a body of water (Valentine and White, 2012). Fragmentation of ascending magma is primarily due to highly energetic, explosive, fuel-coolant interactions (FCI) (Sheridan and Wohletz, 1983; Wohletz, 1983, 1986; Zimanowski et al., 1991, 1997). These can occur under a range of conditions, from magma intruding rapidly into saturated soft sediments (e.g. Houghton et al., 1999; Auer et al., 2007; Ort and Carrasco-Núñez, 2009; Ross et al., 2011; Agustín-Flores et al., 2014), through to interacting with water in cracks within hard/brittle rock sequences (e.g. Sohn and Chough, 1989; Chough and Sohn, 1990; Aranda-Gómez and Luhr, 1996; Auer et al., 2007).

The study of the nature and proportion of lithics within the tephra ring can provide insights into the substrate from where these fragments were sourced (e.g. Auer et al., 2007; Ross et al., 2011; Carrasco-Núñez et al., 2007; Valentine, 2012; Lefebvre et al., 2013). In some cases the proportions of lithic types do not accurately represent the disrupted substrates (e.g. Valentine, 2012; Lefebvre et al., 2013), because not all disrupted host rock is directly deposited in the ejecta ring (Valentine and White, 2012). Deep explosions lift some of the deeper source material to the shallow portion of the diatreme via debris jets (Ross and White, 2006), but the deep lithics may not be ejected directly to the ejecta ring. Predominantly

shallow-seated explosions source the growth of the ejecta ring, with lithic clasts comprising mostly shallow country rock, with rare deeper material.

This study aims to examine how the nature and proportion of lithics in a tuff ring, as well as the sedimentary bedforms and their distribution, can explain the depth and progression of explosion conditions during a phreatomagmatic eruption located in a hard substrate. Detailed field descriptions of the sedimentary characteristics of the Motukorea tuff ring were carried out, along with examination of lithics. This, combined with the sedimentary characteristics of the stratigraphic sequence, sheds light into the explosion and eruption dynamics of phreatomagmatic eruptions through consolidated rocks in the Auckland Volcanic Field (AVF) and enables the depiction of a scenario of future eruptions within the field in similar substrates.

## 6.2 The Auckland Volcanic Field and the Waitemata Group rocks

The AVF comprises at least 52 individual eruption centres over an approximate area of 360 $km^2$ (Kermode, 1992; Allen and Smith, 1994; Spörli and Eastwood, 1997; Hayward et al., 2011) (Fig. 3.1); the magmas involved are mostly olivine-rich alkali basalts and basanites (Smith et al., 2009). At least 1.7 $km^3$ of DRE magma was erupted in sporadic eruptions since250 ka, with the last eruption <600 years ago (Allen and Smith, 1994; Molloy et al., 2009, Bebbington and Cronin, 2011; Kereszturi et al., 2013).

Phreatomagmatism is common in the AVF, with tuff rings and maars, sometimes at the base of scoria cones, found at approximately 80% of the eruption centres. The AVF is also almost completely urbanised and covered by the city of Auckland (population ~1.4 million, 2013 census, Statistics New Zealand) (Fig. 3.1). Explosive phreatomagmatic eruptions producing violent base surges are considered to be the most hazardous events during future eruptions (Allen and Smith, 1994; Németh et al., 2012a; Sandri et al., 2012; Brand et al. 2014).

In contrast to the distinctively low-lying landscape in the southern part of the field covered by Pleistocene-Recent soft sediment (Manukau Lowlands; Fig. 3.1), the 30 small basaltic volcanoes in the northern part of the AVF are built mostly at higher elevation on the consolidated Miocene Waitemata Group rock suite (Fig. 3.2). The >300 m-thick, early-Miocene Waitemata Group consists mainly of inter-bedded turbiditic sandstones and pelagic siltstones, with subordinate breccia and conglomerate, and rare limestone and quartzose sandstone (Ballance, 1974; Hayward, 1979). Waitemata rocks are weakly to moderately indurated, with a typical compressive strength of ~5 MPa (Spörli and Rowland, 2007). A variety of bed thicknesses and types occurs, with differing degrees of folding, faulting, and jointing (Simpson, 1987; Irwin, 2009; Sheridan, 2006; Kenny et al., 2011). From a combination of pump testing and laboratory studies, the average hydraulic conductivities ($K$) in horizontal and vertical directions are respectively $Kx$=$10^{-6}$ m/s and $Kz$=$10^{-10}$ m/s for the Waitemata rocks (Crowcroft and Smaill, 2001; Pattle Delamore and Partners Ltd., 2003; Sheridan, 2006). Siliciclastic and volcaniclastic gravels and conglomerates within the

sequence are more permeable, giving the Waitemata Group a highly variable hydrogeological character, containing both confined and semi-confined aquifers (Scoble and Millar, 1995; Crowcroft and Smaill, 2001). Along fractured zones a few $m^3$ to over 1000 $m^3$ per day of water can be extracted (Crowcroft and Smaill, 2001). ***See Appendices B.1 and B.2 for distribution and thicknesses of Waitemata rocks and depth to basement, and hydrogeological properties of Waitemata aquifers***.

## 6.3 General architecture of Motukorea volcano and local substrate setting

Motukorea volcano (also known as Browns Island) is an island located in the Waitemata Harbour in the northeast part of the AVF (Figs. 3.1 and 6.1). Based on an early Holocene high stand terrace built over lava flows (seen in the southern flat section of the island, Fig. 6.1), a minimum age of 7000-9000 y BP was estimated for the eruption (Bryner, 1991). The volcano erupted at a sea-level lower than that of the present day, pushing its minimum age back to >15 ka. This is broadly consistent with a recent Ar-Ar age determination on juvenile material of 14.3 ±5.5 ka (Graham Leonard., written communication 2014). Motukorea is located along a ridge of Waitemata Group rock, an extension of Musik Point (Fig. 3.1) (Searle and Mayhill, 1981), flanked to the west and southwest by the Tamaki Stream (now an estuary), a tributary of the ancestral Waitemata River (now the main harbour) (Searle and Mayhill, 1981). The Waitemata ridge and the channel may have been part of an N-trending fault, which is down-thrown to the west (Bucklands Beach fault, Fig. 3.1) (Kenny et al., 2011, 2012).

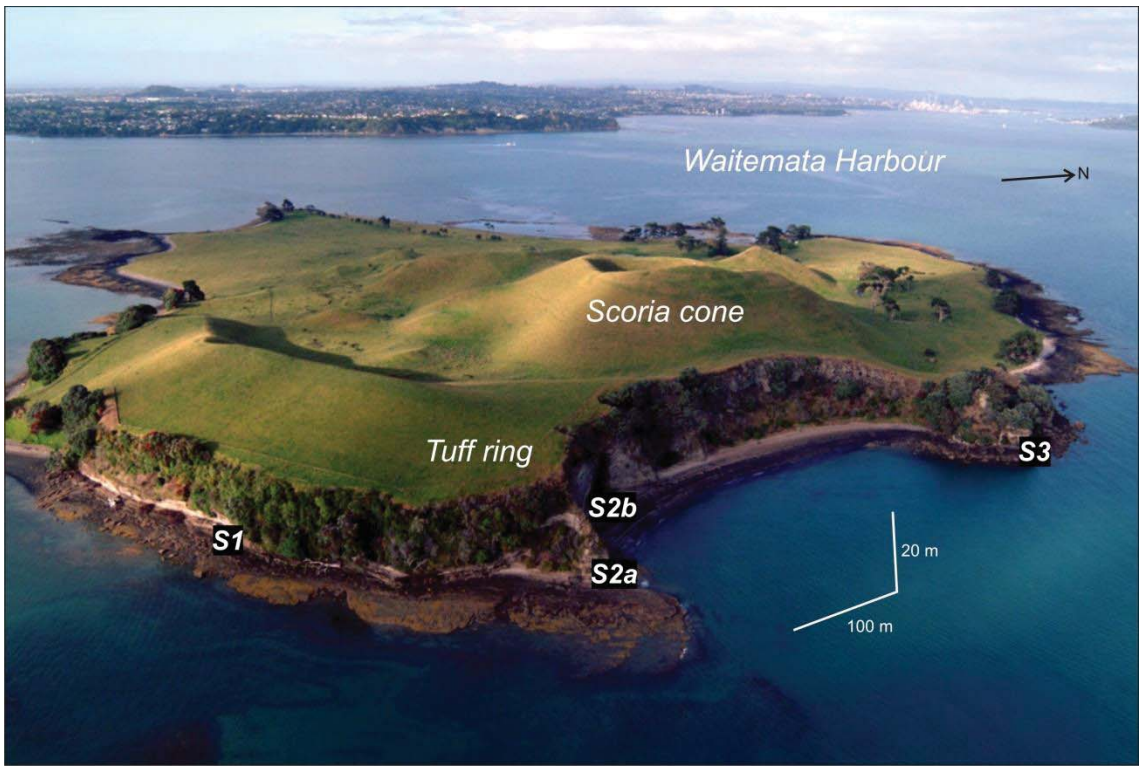


**Fig. 6.1**. Aerial photograph of Motukorea volcano. The exposed tephra ring deposits are clearly seen on the northern-eastern side of the island; the locations of the four key sites are labelled. The horizontal/vertical scale is approximate. ***See Appendix D.1 for location of complete number of sites and detailed stratigraphic logs.***

Motukorea Island has an area of 0.75 $km^2$. The initial volcanic activity was characterized by dominantly phreatomagmatic explosions that formed a tuff ring (Bryner and Grant-Mackie, 1993; Allen et al., 1996; McGee et al., 2012). Partially eroded by the sea, the ejecta ring is up to 40 m-high on the northeast section of the island (Fig. 6.1). Tephra was preferentially deposited to the ENE, but this may also reflect emplacement on a higher pre-eruptive surface on the up-thrown side of the fault. If the tuff ring was complete its full crater was likely <1 km in diameter. Tephra beds dip <20° away from the crater. The next phase of the eruption was magmatic, producing a scoria cone and related mounds, followed by lava extrusion. By using Light Detection and Ranging (LiDAR) Digital Surface Model in combination with geological mapping, the bulk volume estimated for the tuff ring is $3.1\times10^6$ $m^3$ and the DRE volumes of the scoria cone and lava flows are $1.3\times10^6 m^3$ and $2.3\times10^6 m^3$ respectively (Kereszturi et al., 2013).

Apart from the Waitemata lithics, other deeper substrate rocks found in the tuff ring are Waipapa greywacke lithic fragments. This observation confirms field and borehole data that indicate that the Waitemata sequence sits directly on the Waipapa Terrane basement below the volcano. Waipapa rocks consist of thinly bedded, alternating fine-grained sandstone and argillite, and thicker massive argillite and jointed greywacke sandstone. These basement rocks are typically hard to very hard, and densely fractured and sheared.

The contact between Waitemata Group rocks and underlying basement greywacke rocks is inferred from borehole data to successively deepen west of Motuihe and Motutapu islands (~ 4.5 km NE and 6 km N of Motukorea, respectively; Fig. 3.1), where it outcrops at the surface (Kenny et al., 2011). The maximum depth to basement in the Auckland isthmus (in West Auckland, about 16 km southwest of Motukorea Island) was estimated at~600 m. Seismic reflection studies in the Waitemata Harbour, 3-4 km east of Motukorea Island were interpreted to indicate Waitemata Group thicknesses of 200 to 300 m (Davy, 2008). Based on the above, we infer that the thickness of the Waitemata rocks beneath Motukorea (and thus the depth to basement) is 200-300 m, or shallower (agreed by Berhard K. Spörli, expert on basement of AVF, written communication), given its proximity to the location where greywacke outcrops at the surface.

***See Appendix B.1 for the distribution and thicknesses of the Waitemata rocks and configuration of the basement (Waipapa rocks).***

## 6.4 General terminology

Phreatomagmatism occurs when magma explosively interacts with groundwater (Stearns, 1953). This process fragments magma to form juvenile particles (e.g. Wohletz, 1983, 1986; Kokelaar, 1986; Zimanowski et al., 1991, 1997), although magmatic-gas expansion driven fragmentation probably also occurs to variable degrees during these eruptions. Pyroclasts (after Fisher and Schmincke, 1984) include all fragments ejected from volcanoes through the air, including juvenile (fresh erupted magma) and

country-rock clasts (lithics). White and Houghton (2006) are more specific classifying pyroclast as clasts deposited from subaerial, subaqueous, or subsurface jets, plumes, or currents. Then all particles transported in a system triggered by magmatic energy and found in pyroclastic deposits are named pyroclasts, irrespective of their origin. Here, particles were grouped using the pyroclast size terms of Sohn and Chough (1989) (see Table 6.1). Sedimentary units of <1 cm-thickness are termed laminae, with beds describing thicker units (following Ingram, 1954). Unconsolidated volcaniclastic deposits are termed ash or lapilli, whereas consolidated equivalents are termed *tuff* if composed of ash-sized-pyroclasts, or *lapilli-tuff* if composed dominantly of lapilli-sized pyroclasts (after Schmid, 1981). Lapilli-tuff also indicates a consolidated, poorly-sorted mixture of both lapilli and ash-sized grains.

Although not equivalent, base surge, surge, current, or flow are all frequently used as synonyms for dilute pyroclastic density currents (PDCs); a highly expanded, low-particle-concentration, gas + particle-laden flow, sometimes containing steam or water droplets (Cas and Wright, 1987). These are characterized by strong vertical density stratification (Valentine, 1987; Sulpizio et al., 2007). Base surge is the most common type of PDC associated with phreatomagmatic eruptions.

Ejecta rings form from the accumulation of pyroclasts (mostly base surge and subordinate fall deposits) around maar-diatreme craters. Some authors describe the deposits around maars as tuff rings (Bryner and Grant-Mackie, 1993; Allen et al., 1996; McGee et al., 2012; Geshi et al., 2011), therefore using “tuff ring” (*sensu lato*) referred to such deposits is possible. Tuff rings (*sensu stricto*) may be underlain by a shallow diatreme, but their craters lie above the pre-eruptive surface (White and Ross, 2011). The diatreme is a pyroclast-filled pipe (or inverted cone) structure, cut into the substrate (Lorenz and Kurszlaukis, 2007). It is unknown whether the Motukorea phreatomagmatic crater cuts the pre-eruptive surface, but from the lithic contents and ejecta ring size, it is evident that it formed a maar-diatreme volcano.

## 6.5 Methodology

### 6.5.1 Field work and deposit characterization

Remnants of the Motukorea tuff ring occur along the north-eastern side of the island (Fig. 6.1) and contain proximal to medial deposits from a centrally located crater. Within a coastal cliff, site 1 (*S1*) runs roughly parallel to the crater rim (Figs. 6.1, 6.2). Site 2 represents a 60 m long slice through the ejecta ring from near rim (*S2b*) to outer flanks (*S2a*) (Figs. 6.1, 6.3). Site 3 (*S3*) is another proximal locality (Figs. 6.1, 6.4). The small area over which exposures occur allows no useful analysis of proximal to distal variations. No contact is exposed between the ejecta ring deposit and the pre-eruptive surface even at low tide, thus it must rest a few meters below sea-level; however, the exact depth of this boundary is unknown. ***Appendix D.1 contains the complete number of sites and detailed stratigraphic logs***.

The entire maar ejecta ring is a phreatomagmatic unit, which was subdivided using sedimentary structures and juvenile fragment abundances into: the lower tuff sequence (*LTS*), the mid scoria unit (*MSU*), and the upper tuff sequence (*UTS*) (Figs. 6.2, 6.3, 6.4). We retain the nomenclature of McGee et al. (2012) for these units for clearest comparison to the stratigraphical and geochemical data published in that work. Magmatic deposits above the phreatomagmatic unit represent the upper scoria unit (Fig. 6.3) and indicate the initiation of the late-stage magmatic activity at Motukorea volcano. Field mapping and the analyses of sedimentary structures were used to correlate between sites (Fig. 6.5). The sites are aligned roughly parallel to the rim of the tuff ring. Slightly non-symmetrical impact sags and dune bedform(s) with distinguishable stoss and lee sides show that the eastern cliff faces (at *S1*, Fig. 6.1) are sub-perpendicular to the direct radial travel path from the crater.

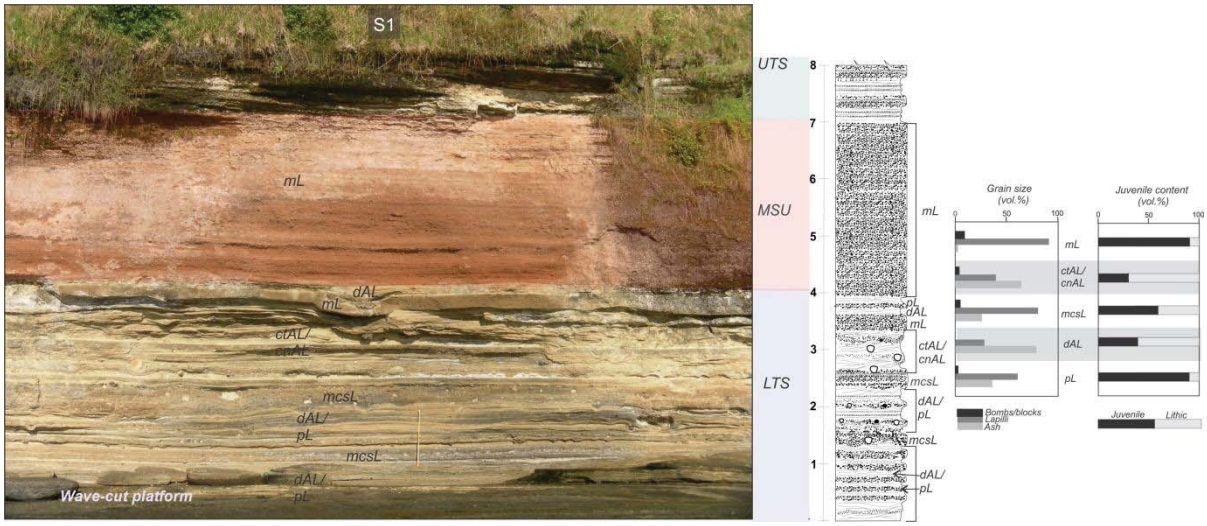


**Fig. 6.2**. Stratigraphic sequence at *S1* (see Fig. 6.1 for location). *LTS* and *MSU* sequences characterize this site (see section 6.7 for description of sequences). The lithofacies that constitute *S1* are displayed (for more details on lithofaces see Table 6.2 and ***Appendix D.2***). The volume percentage of grain size and juvenile content of the lithofacies that appear within the sequence are presented in the graphs on the right. The boxes containing the grain size and juvenile content are not to scale and do not represent stratigraphic columns. The base of the sequence intersects a wave-cut platform that marks approximately the highest tide sea level in the area. Thickness of sequence (in metres) corresponds to thickness in photograph.

**Table 6.1** Grain size nomenclature and its volumetric proportion in the entire phreatomagmatic deposit. ***This classification was made in part with the results and analysis and of grain zise distribution of sieved samples (see Appendix D.1 for more information on grain size results and distribution, as well as the componentry results of analysed samples).***

| Pyroclast size | ~Vol.% of this grain size range within entire deposit | ~Proportion of lithic to juvenile clasts within this size range | Characteristics of lithic fragments | Characteristics of juvenile fragments |
|---|---|---|---|---|
| Block/bomb *(-6 to -8 ϕ) (64-256 mm)* | <10 | 2:3 | -Sub-rounded Wiatemata sandstone blocks | Dense to poorly-vesicular, sub-angular, fragments. Some breadcrust-type and cauliflower bombs. Bombs may have small inclusions of non-juvenile fragments. |
| Coarse lapilli *(-4 to -6 ϕ) (16-64 mm)* | 20-25 | 3:7 | -Sub-angular to rounded fragments of Waitemata sandstone -Sand/silt aggregates of Plio-Pleistocene sediments (soft aggregates do not show plastic deformation or internal structures) (<10 vol.% of non-juvenile).<br><br>-Angular greywacke fragments (<10 vol.% of non-juvenile)<br><br>-Scarce shell fragments | Moderately to poorly vesicular, angular to sub-angular fragments. Particles may be coated by lithic fine ash. Palagonization is present, but not pervasive. |
| Medium lapilli *(-2 to -4 ϕ) (4-16 mm)* | | | | |
| Fine lapilli *(-1 to -2 ϕ) (2-4 mm)* | 25-30 | 1:4 | -Subrounded particles of Waitemata sandstone (40-50 vol.%) (dominant between 1 to 3 ϕ size)<br><br>-Blocky, opaque individual grains of quartz and feldspar (30-40 vol.%) (dominant down 3 ϕ size)<br><br>-Minor amount of fine ash/silt, round aggregates<br><br>-Scarce shell fragments | Angular to sub-rounded, poorly vesicular sideromelane/tachylite fragments with adhered lithic, fine ash particles. Rare surficial cracks are present. |
| Coarse ash *(1 to -1 ϕ) (0.5-2 mm)* | | | | |
| Medium ash *(4 to 1 ϕ) (0.625-0.5 mm)* | 40 | 9:1 | | |
| Fine ash <4 ϕ | | | | |

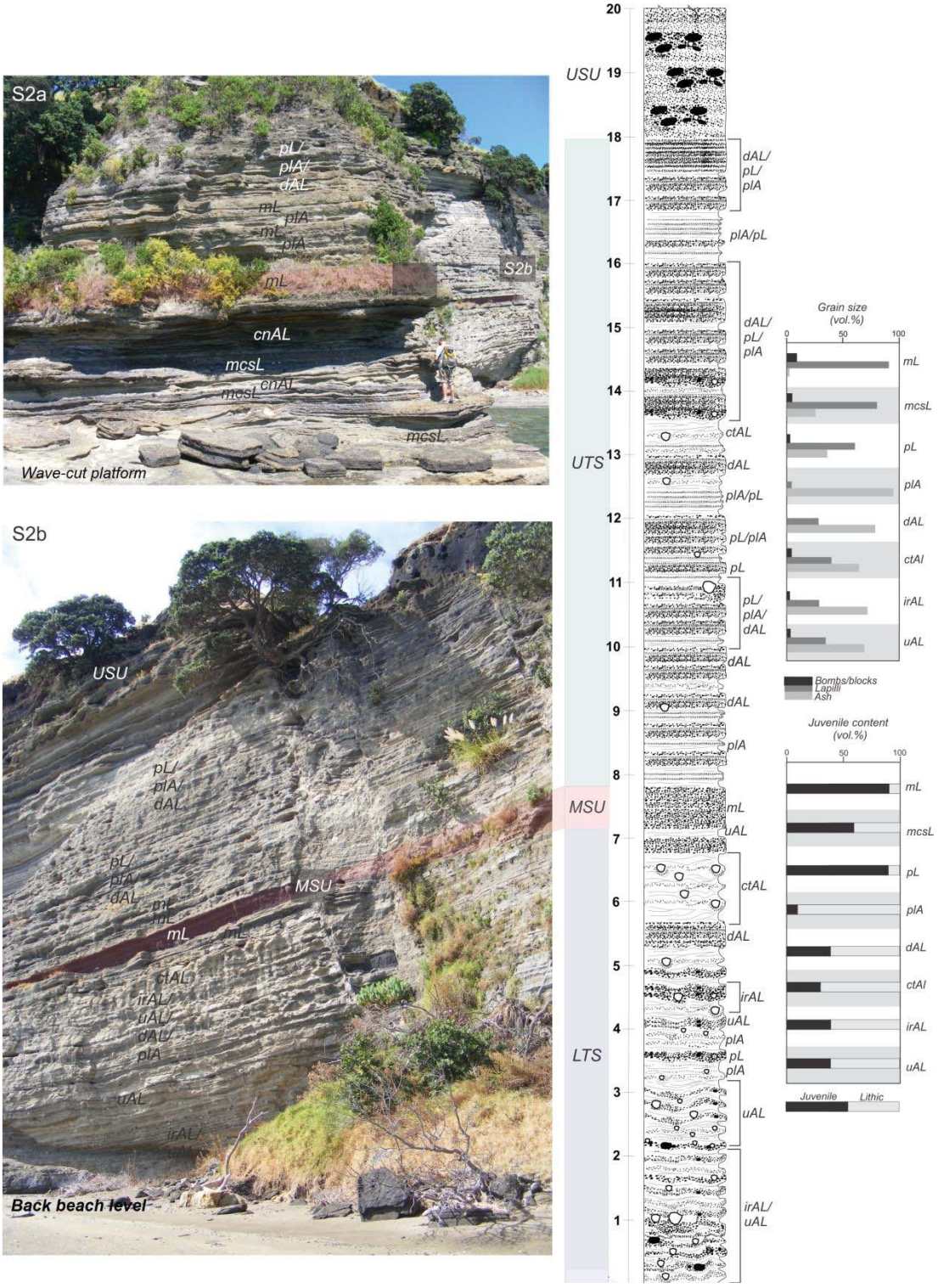


**Fig. 6.3**. Stratigraphic sequence at S2a/S2b (see Fig. 6.1 for location). LTS, MSU, UTS, and scoriacious unit USU sequences characterize this site (see section 6.7 for description of sequences). The lithofacies that constitute S2a/S2b are displayed (for more details on lithofacies see Table 6.2 and Appendix D.2). The volume percentage of grain size and juvenile content of the lithofacies that appear within the sequence are presented in the graphs on the right. The boxes containing the grain size and juvenile content are not to scale and do not represent stratigraphic columns. The base of the S2a sequence intersects a wave-cut platform that marks approximately the highest tide sea level in the area, whereas the base of S2b sequence intersects the back beach level. Thickness of log (in metres) corresponds to thickness of sequence in photograph S2b. Person in photograph S2a is 1.8 m high.

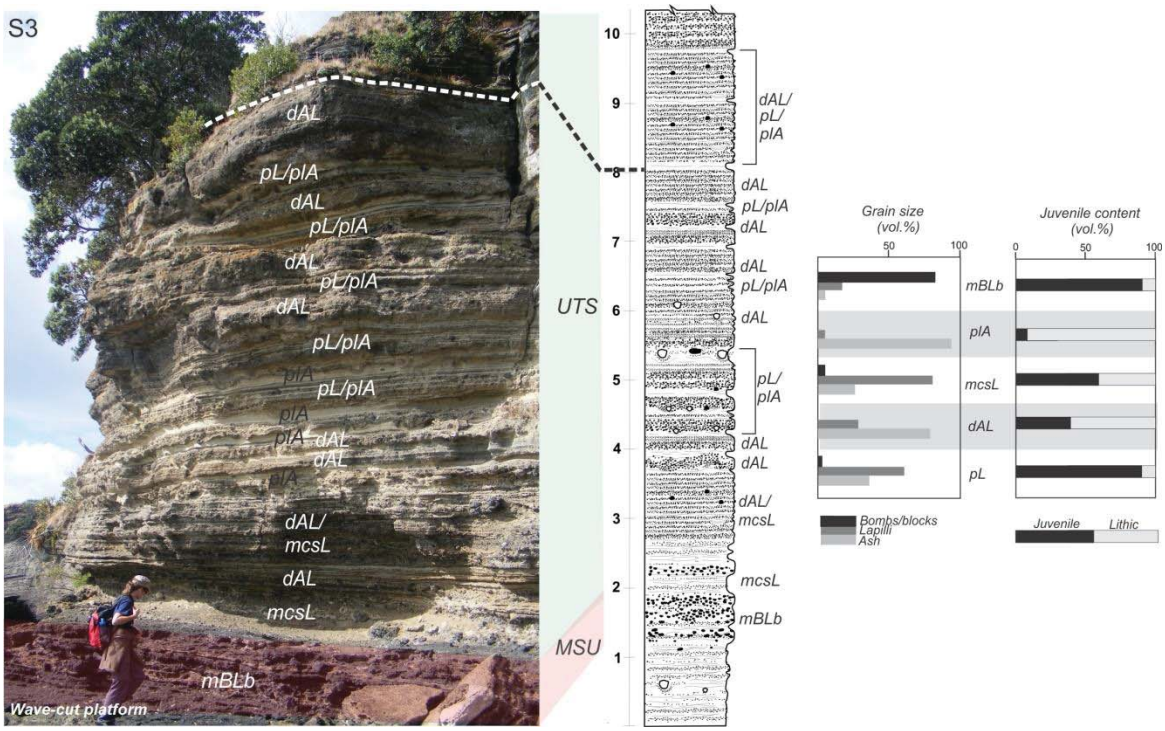


**Fig. 6.4**. Stratigraphic sequence at *S3* (see Fig. 6.1 for location) *MSU* and *UTS* sequences characterize this site (see section 6.7 for description of sequences). The lithofacies that constitute *S3* are displayed (for more details on lithofacies see Table 6.2 and ***Appendix D.2***). The volume percentage of grain size and juvenile content of the lithofacies that appear within the sequence are presented in the graphs on the right. The boxes containing the grain size and juvenile content are not to scale and do not represent stratigraphic columns. The base of the sequence intersects a wave-cut platform that marks approximately the highest tide sea level in the area. Thickness of log (in metres) corresponds to thickness in sequence of photograph

### 6.5.2 Sample preparation and analysis

Most accessible deposits are moderately consolidated and unsuitable for sieving, although some less consolidated tuff samples were disaggregated by soaking in water, before drying and sieving (***the results of grain size distribution and location of sieved samples is presented in Appendix D.1***). Manual disaggregation adds a considerable error in grain size distribution calculations, hence approximate grain size distribution and sorting of deposits were best estimated by field observations, as well as photograph and thin section analyses (using a petrographic microscope and the JMicrovision software). Since the size of juveniles formed by FCI explosions in experiments is usually less than 0.2 mm (Wohletz, 1983; Zimanowsky, 1997) but bigger than 0.125 mm (3 $\phi$) , samples from the 2 and 3 $\phi$ fractions (0.25-0.125 mm) were used for grain morphology analyses of juveniles. These particles were cleaned with 10% HCl and rinsed with acetone in an ultrasonic bath for 30-60 s. Counts of 500 grains were performed in the 2 and 3 $\phi$ fraction sizes of 16 samples (taken from different stratigraphic levels where tuff was present) for the componentry analyses (***see Appendix D.1 for location of samples and componentry graph***). The morphological features and componentry of pyroclasts were also identified by direct observation of deposits, hand specimens in the field and by viewing loose and thin sectioned small lapilli/ash-sized grains

(smaller than 1 ϕ, 0.5 mm) under binocular/stereo and transmitted polarised light microscopy and scanning electron microscopy (FEI Qanta 200 environmental scanning electron microscope operated at 20 kV, Massey University Microscope Centre). Juvenile samples (2 and 3 ϕ, 0.25-0.125 mm) were also analysed by energy-dispersive spectrometry (EDS) (Edax 10 $mm^2$ detector with data processed by Edax Genesis 5.21 software). Volume percentage of vesicles was calculated based on 500 point counts on 5-6 coarse ash to fine lapilli-sized juveniles per thin section image using the JMicrovision software (a total of five thin sections from different stratigraphic levels belonging to the *LTS* and *UTS* were analysed).

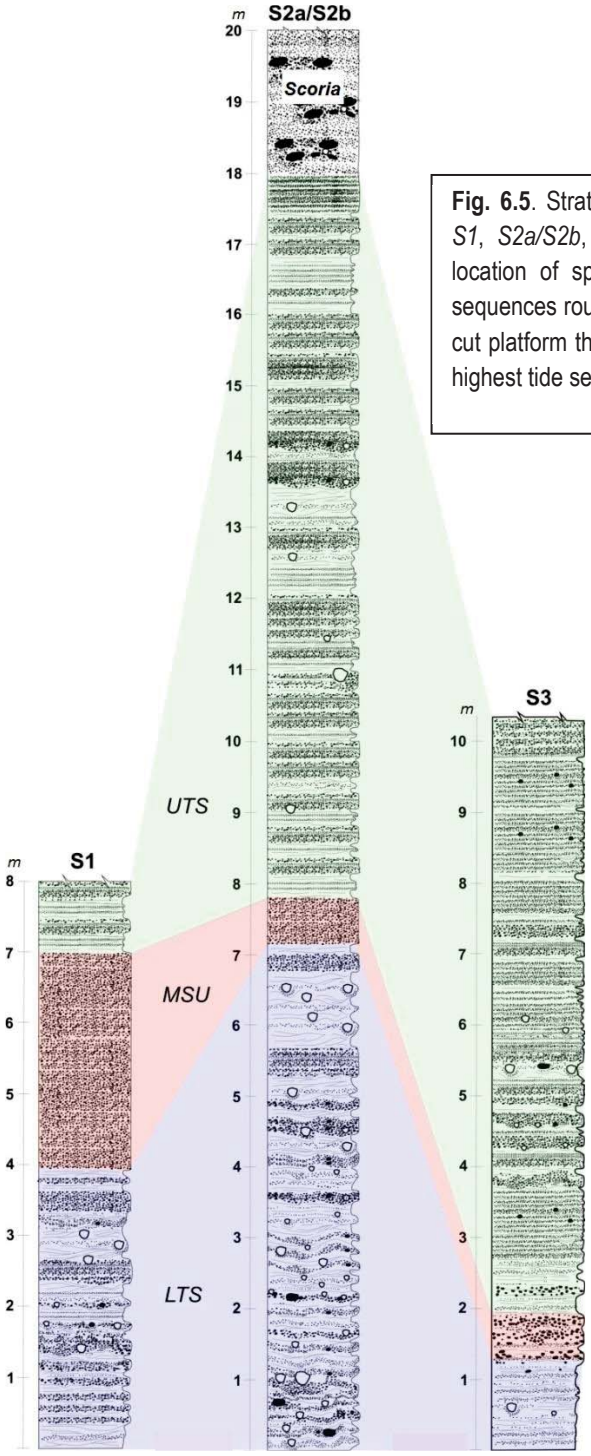


**Fig. 6.5**. Stratigrapic correlation between *S1*, *S2a/S2b*, and *S3* (see Fig. 6.1 for location of specific sites). The base of sequences roughly correspond to a wave-cut platform that marks approximately the highest tide sea level in the area

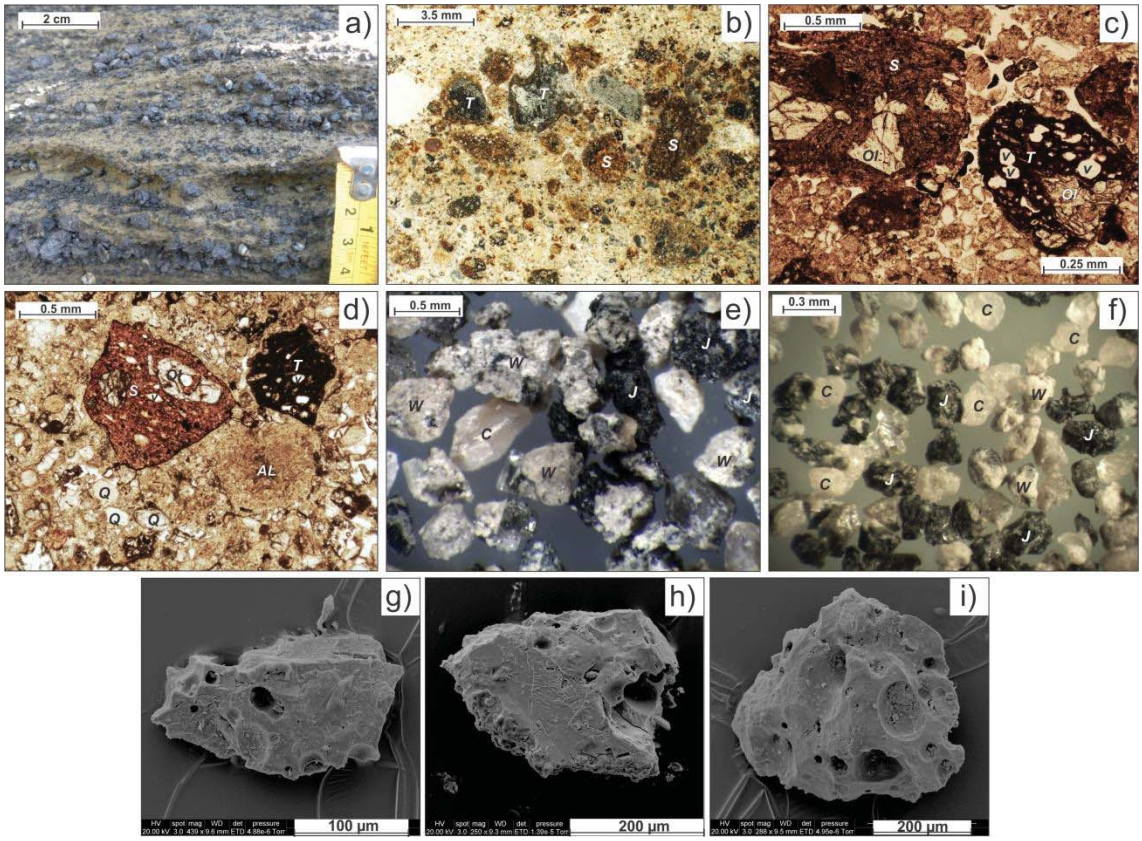


**Fig. 6.6**. a) Characteristics of pyroclasts. a) Close-up view of tuff. Note the contrast between the dark, angular, juvenile fragments and the finer grained, light-brown, lithic ash. b) Polished surface of tuff sample. (*T* = tachylite, *S* = sideromelane). The contrasts between coarser, juvenile fragments and lithic ash are observable. Sideromelane particles show palagonitization. c) and d) Plane-polarised, transmitted light photomicrographs (*AL* = accretionary lapilli, *Ol* = Olivine, *Q* = quartz, *V* = vesicles). Poor vesicularity and thick walls between spherical/sub-spherical vesicles are widespread. e) and f) Stereo light microscope images of 2 and 3 ϕ (0.25-0.125 mm) fractions (*C*= quartz/feldspar crystal, *J* = juvenile fragment, *W* = Waitemata Group rock fragment). Blocky and equant juvenile fragments dominate. g), h), i) Scanning electron microscope images of typical juvenile grain morphologies in the 2 and 3 ϕ (0.25-0.125 mm) fractions. Low vesicular, blocky, angular fragments dominate.

## 6.6 Results: Pyroclast characteristics

The whole exposed maar-ejecta ring deposit is poorly sorted and is dominated by fragments of fine lapilli to medium ash (60-70 vol.%) (Table 6.1), with a juvenile content of 40-45 vol.%. The proportions of lithic to juvenile for each pyroclast size-category are shown in Table 6.1. The juvenile fraction is mostly within the lapilli size, while the lithic fragments are mainly ash grade (Table 6.1) (Fig. 6.6a,b,c,d). ***See Appendix D.1 for information (graphs and table) on the volume percentage values for ϕ fractions of selected sieved Motukorea samples.***.

Based on major element contents, Motukorea rocks range from basanite to nephelinite with low $Al_2O_3$ (McGee et al. 2012). Samples from the tuff ring sequence have higher total alkalis and lower $SiO_2$ than the scoria mounds and lava (McGee et al., 2012). Vesicles are sub-spherical to spherical with diameters <80 µm and separated by thick walls (Fig 6.6c,d,g,h,i). In general all juvenile clasts show low vesicularity (Fig.

6.6c,d,g,h,i) (median of 8 vol.% from the analysed samples). Vesicle distribution in the juvenile samples (both sideromelane and tachylite) is variable within particles of either the same of different stratigraphic levels. This observation points to the difficulty of establishing changes in particle vesicularity in relation to stratigraphic position. Bryner (1991) reports distinct mean vesicularity values of juveniles (coarse ash to fine lapilli) within specific beds suggesting subtle vertical patterns. Re-analysis of this data shows that mean-analysis is unsuited to the strongly skewed patterns or bimodal distributions in the data, commonly with two domains of the same juvenile fragment having distinctively different vesicle distribution.

Thin section analysis shows that tachylite particles are more vesicular than sideromelane fragments in these deposits (Fig. 6.6c). Tachylite fragments are also more abundant in the upper tuff sequence (*UTS*) compared to the lower tuff sequence (*LTS*). Sideromelane shows the reverse pattern.

Morphological characteristics of juvenile pyroclasts of different sizes are described in Table 6.1. Fragments are angular, sub-angular, and sub-rounded (Fig. 6.6a,b,c,d,e,f,g,h,i). Fine lapilli to ash size juvenile fragments may be coated by lithic fine ash. Bread-crust-type and cauliflower bombs are present, but not abundant (Table 6.1). The morphology of juvenile fragments in the 2-3 $\phi$ fraction (0.25-0.125 mm) is characterized by blocky, equant, angular to sub-angular, sideromelane/tachylite pyroclasts with poor vesicularity and fine vesicles <50 µm (Fig. 6.6e,f,g,h,i). Some palagonitization is present (Fig. 6.6b).

Lithic fragments are mostly contained in the medium to fine ash fraction (Table 6.1; Fig. 6.6a,b,c,d; ***Appendix D.1***). In the lithic lapilli fraction, Waipapa Terrane greywacke fragments constitute <10 vol.% with Waitemata rock fragments dominant. The medium to fine ash fraction is dominated by up to 85 vol.% of lithics, dominantly Waitemata fragments (Fig. 6.6e,f) along with individual grains of quartz and feldspar, minor amount of spherical ash/silt aggregates, and scarce shell fragments (Fig. 6.6e,f). The medium to fine ash fraction makes up approximately 40 vol.% of the total deposit (Table 6.1). The block and coarse lapilli-sized lithics often form symmetrical to slightly asymmetrical impact sags or are embedded within the sequences (Fig. 6.7c,g,h,i). Accretionary lapilli are rare (Fig. 6.6d). Waitemata fragments comprise approximately 90 vol.% of lithics considering all particle sizes, with Waipapa lithics making up <10 vol.%.

## 6.7 Sedimentary characteristics and maar ejecta ring formation

Based on changes in the size, composition, and distribution of pyroclasts, as well as distinct sedimentary characteristics, a total of 10 lithofacies were recognized (Table 6.2, Fig. 6.7) (***see Appendix D.2 for detailed of lithofacies***). Each phreatomagmatic sequence (i.e. *LTS*, *MSU*, and *UTS*) comprises a distinctive set of lithofacies (Figs. 6.2, 6.3, 6.4) as described below

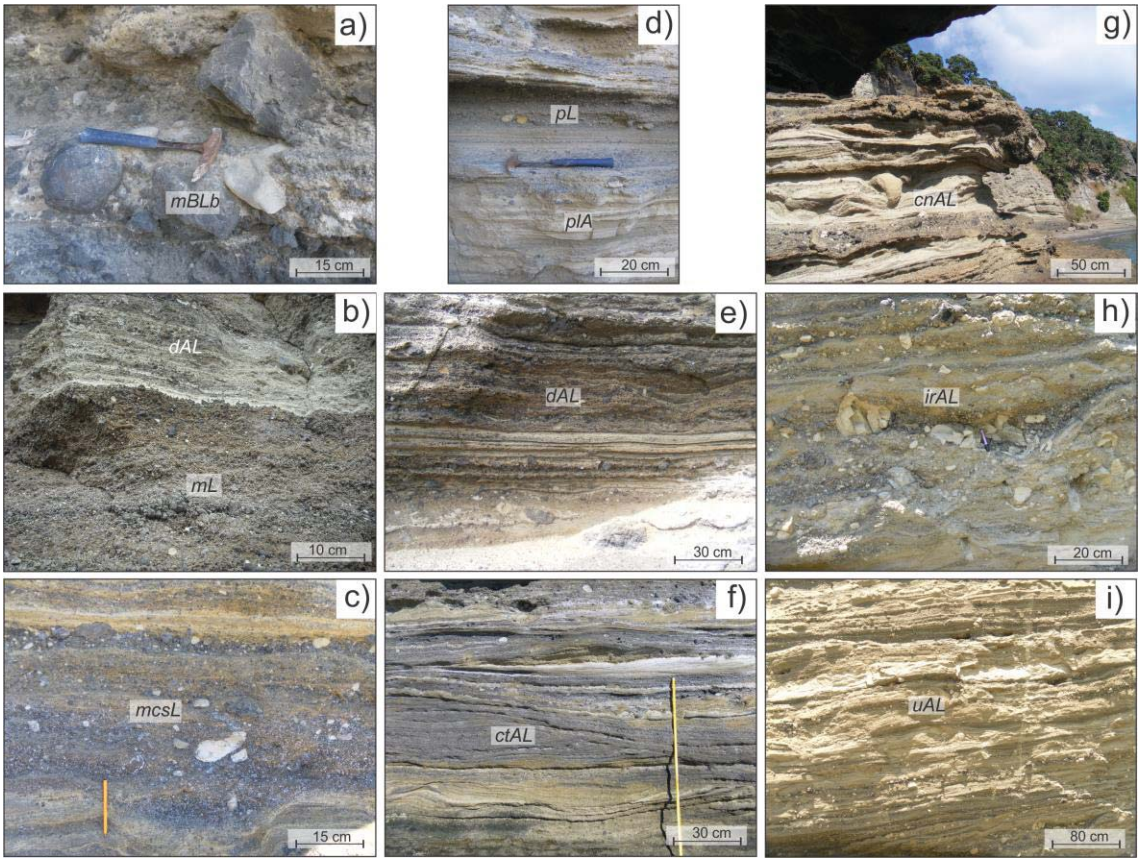


**Fig. 6.7**. Close-up view of lithofacies. See Table 6.2 and ***Appendix D.2*** for description and interpretation of each lithofacies and Figs. 6.2, 6.3, and 6.4 for their distribution within the stratigraphic sequences.

### 6.7.1 Lower Tuff Sequence (*LTS*)

The base of *LTS* is inferred to be several metres below the basal observable units. *LTS* is~7 m thick at *Sb2* (Fig. 6.3) and ~4 m at *S2a* and *S1*. At *S3* only the uppermost 1 m of *LTS* is visible (Fig. 6.4). The lowermost part of *LTS* at *S2b* is characterized mainly by *irAL* beds (Fig. 6.3), but *uAL* beds are also present. *irAL* lithofacies are formed by a crudely stratified tuff composed of a combination of lapilli-rich and ash-rich layers (Fig. 6.7h; Table 6.2). Individual layers pinch and swell and there is evidence of subtle cross-stratification and clear cross-lamination. Fragments larger than coarse lapilli are embedded within the sequences, with rare impact structures also observed (Figs. 6.3, 6.7h). In the lowermost part of the sequence the bedding is disorganized and diffuse, resembling the “dune bedded lapilli tuff” lithofacies at Orakei maar (in the AVF) (Németh et al., 2012a). These deposits at Orakei overlie a tuff breccia that is interpreted as a vent-opening facies by Németh et al. (2012a). However, although a distinct coarse-grained, chaotic explosion breccia (Wohletz and Sheridan, 1979) is not observable at Motukorea, these lowermost deposits may represent deposits resulting from the stages following the very first phreatomagmatic explosions. The characteristics of lithofacies *irAL* suggest moderately turbulent base surges (Table 6.2). Increasing turbulence of base surges upwards in *LTS* is attested by the presence of *uAL* and the prominence of *ctAL/cnAL* in upper segments of *LTS* (Figs. 6.2, 6.3) where low-angle cross

**Table 6.2** Nomenclature, grain size/sedimentary characteristics, and interpretation of lithofacies identified for the Motukorea phreatomagmatic deposits. ***Appendix D.2 contains detailed description of lithofacies.***

| | *Lithofacies* | ▪ *Thickness,*<br>▪ *Grain size (vol.% of this grain size)*<br>▪ *Approximate juvenile to lithic proportion* | *Sedimentary characteristics* | *Interpretation* |
|---|---|---|---|---|
| *Juvenile, clast-suported* | ***mBLb*** (*Fig. 6.7a*)<br>Massive bomb/lapilli breccia | ▪ up to 40 cm<br>▪ Bombs (up to 90)<br>▪ 9:1 | Poorly sorted, dominantly massive, ungraded, consolidated beds. Incipient matrix in some sections. | Scarcity of lithic fragments and coarse-juvenile-rich, poorly sorted beds suggest deposition by fall from magmatic activity. |
| | ***mL*** (*Fig. 6.7b*)<br>Massive lapilli tuff | ▪ cm to ~3 m<br>▪ coarse/medium lapilli (70-90)<br>▪ 9:1 | Moderately sorted, dominantly massive, ungraded, laterally parallel, continuous beds with transitional boundaries. | Ungraded, massive, and moderately-sorted beds of juvenile lapilli point to deposition by fall from magmatic activity. |
| *Variable juvenile to lithic, matrix - supported* | ***mcsL*** (*Fig. 6.7c*)<br>Massive to crudely stratified lapilli tuff | ▪ <1 m<br>▪ lapilli/coarse ash (up to 90)<br>▪ 6:4 | Poorly sorted, consolidated, ungraded to crudely stratified beds whose thickness may vary laterally and may show basal scour surfaces. Shallow impact structures. Scarce accretionary lapilli. | Poor sorting, relatively massive beds with coarse fragments embedded, and scour surfaces at their base imply dense, relatively erosive pyroclast density currents (high shear stresses at their basal boundary) with high sedimentation rates. |
| | ***pL /plA*** (*Fig. 6.7d*)<br>Parallel bedded lapilli/ laminated ash | ***pL***<br>▪ <1 m<br>▪ medium lapilli/coarse ash (>40)<br>▪ 9:1<br>***plA***<br>▪ <1 m<br>▪ medium to fine ash (>90)<br>▪ 1:9 | Poorly consolidated, rhythmic sequences composed by the combination of juvenile-rich (**pL**) with lithic-rich (**plA**) layers with sharp, but gradational boundaries. Juvenile-rich layers are reversed graded, whereas lithic strata are non-erosive, non-graded and laminated. Scarce subtle plastic deformation is present. | Reverse grading of juvenile-rich layers with moderate sorting are related to deposition from grain flows that originated from rapidly falling pyroclasts from a cloud. Laminated nature of lithic-rich layers and some presence of juvenile trains indicate low sedimentation rate from turbulent diluted base surges with tractional flow boundaries. |
| *Dominantly lithic,, matrix supported* | ***dAL*** (*Fig. 6.7e,b*)<br>Diffusely bedded ash/lapilli | ▪ <1 m<br>▪ lapilli/coarse ash (<40), medium/fine ash (>60)<br>▪ 4:6 | Poorly sorted, poorly consolidated, diffusely stratified, ash-rich beds with laterally continuous, reverse graded trains of juvenile lapilli. Beds may be relatively plane parallel to slightly wavy and vary in thickness laterally. Gradational boundaries | Crude bedding, diffuse stratification, and reverse grading of juveniles suggest tractional flow boundaries in turbulent base surges with relatively high rate of deposition. The lack of erosive boundaries suggests flows with low shear stresses at the basal boundaries. |
| | ***ctAL*** (*Fig. 6.7f*)<br>Cross-stratified ash/lapilli tuff | ▪ up to <2 m<br>▪ Lapilli (<40), Medium/fine ash (>60)<br>▪ 3:7 | Consolidated, stoss-side truncated, cross-stratified dune bedforms. Height of dune bedforms is <0.5 m and their length within a range of 2 m. Formed by a rhythmic alternation of lithic-rich (ash) with relatively juvenile-rich (fine lapilli) layers. Dune bedforms may be plastically deformed and show basal erosive boundaries. | ***ctAL/cnAL***. Cross-stratification indicates transport in the turbulent regime of dilute base surges with tractional flow boundaries. Truncation and erosive basal boundaries point to flows with high shear stresses, wherea soft deformation characteristics are related to the presence of water during deposition.<br><br>***cnAL***. Pervasive soft deformation characteristics are related to the presence of relatively abundant water during deposition. |
| | ***cnAL*** (*Fig. 6.7g*)<br>Convoluted, cross-bedded ash/lapilli tuff | ▪ <1.5 m<br>▪ Lapilli (<40), medium/fine ash (>60)<br>▪ 3:7 | This consolidated lithofacies share similar sedimentary characteristics as ***ctAL***, but dune bedforms show clearly more evidence of soft deformation: impact structures, bed-load structures, and high angle undulations. | |
| | ***irAL*** (*Fig. 6.7h*)<br>Crudely stratified, irregularly bedded ash/lapilli | ▪ ~1 m<br>▪ fine lapilli (<40), medium/fine ash (>60)<br>▪ 4:6 | Poorly sorted, poorly consolidated, rhythmic sequence formed by the combination of reversed-graded, juvenile-rich (fine lapilli) and cross-laminated, lithic-rich (ash) layers. Individual layers subtly pinch and swell and may exhibit subtle "ripple-type" undulations. Contacts between layers are gradational. | ***irAL/uAL***. Separation of upper finer material from reversed-graded, lower, coarser material indicates flow segregation with a tractional denser basal flow. Cross lamination suggests that the upper diluted part of the flow travelled in the turbulent regime at low rates of sedimentation of low-energy base surges.<br><br>***uAL.*** Thicker fine-ash beds and dune bedforms with symmetrical undulations suggest the presence of a thicker suspended load and more energetic flow in comparison to the base surges that formed ***irAL.*** |
| | ***uAL*** (*Fig. 6.7i*)<br>Undulating cross-laminated ash/lapilli | ▪ <50 cm<br>▪ Lapilli (<40), medium/fine ash (>60)<br>▪ 4:6 | This lithofacies shares most sedimentary characteristics with ***irAL***. The main difference is that ***uAL*** does not exhibit "ripple-type" structures. In addition, the dune bedforms show symmetrical and rhythmic undulations. Height of "crests" is <40 cm and distance between crests is about 2 m. | |

stratification, as well as low-angle-cross lamination is widespread. In addition, scour surfaces and truncation of dune bedforms are common in lithofacies *ctAL* (Table 6.2; Figs. 6.2, 6.3, 6.7f), but less so in lithofacies *uAL* (Fig. 6.7i). Soft sediment impact structures are evident in *ctAL*, but pervasive in *cnAL* (Fig. 6.7g). The presence of soft-sediment deformation in *cnAL* at *S2a* beds is evidence for more condensed water at the deposition of currents, in comparison to the more proximal *S2b* site. For the entire eastern cliff (*S1*) *ctAL* is present throughout.

Lithofacies *mcSL* is characterized by ungraded and poorly sorted beds (Table 6.2; Fig. 6.7c) and is also present within *LTS* at *S1* and *S2a* (Figs. 6.2, 6.3). Scour surfaces at the basal boundaries of *mcSL* imply an erosive base surge. Scarce accretionary lapilli attest to the presence of some water at the time of deposition. The *mcSL* is interpreted to be the result from the deposition of erosive, denser pyroclastic density currents (Table 6.2) that are transitional to fall from lithic-rich, wet, discrete tephra jets.

Thin, subordinate inter-bedded sections of *LTS* at all sites are characterized by lithofacies *plA* and *dAL* (Figs. 6.2, 6.3), deposited likely from turbulent base surges. These show extensive plane parallel lamination (indicating low sedimentation rates) and non-erosive gradational boundaries implying low basal shear stress and lower-energy currents.

### 6.7.2 Mid Scoria Unit (*MSU*)

*MSU* marks the boundary between *LTS* and *UTS* (Figs. 6.2, 6.3, 6.4, 6.5). Lithofacies *mL* and *mBLb*, which are part of *MSU* (Figs. 6.2, 6.3, 6.4), are related to the deposition by fall from magmatic activity. The transition from *LTU* to *MSU* is relatively sharp (Figs. 6.2, 6.3).

From *S1* to *S2a*/*S2b*, *MSU* is formed by lithofacies *mL* (clast-supported, moderately sorted, ungraded, dominantly juvenile-lapilli beds) (Table 6.2; Fig. 6.7b). Yet at S3, *MSU* is composed dominantly by lithofacies *mBLb* (clast-supported, poorly sorted beds of dominantly coarse-lapilli/bombs of juvenile origin) (Table 6.2; Fig. 6.7a). North to south along the eastern cliff wall *MSU* thickens from <1 m to up to 3 m implying a source towards the south of the main scoria cone (Fig. 6.1). The coarser juvenile fragments of *mBLb* at *S3* indicate that the vent for this magmatic unit was located further north, closer to *S3*. This may imply that two, or more, vents were active with simultaneous dry eruptions (e.g. Houghton et al., 1999). Although the fall out origin for *MSU* is obvious from its sedimentary character, the moderate vesicularity of *mL* fragments may indicate that fragmenting magma was chilled by water during the eruption. The transition from *MSU* to *UTS* is sharp, but non-erosive.

### 6.7.3 Upper Tuff Sequence (*UTS*)

*UTS* is amply visible at *S2a*, *S2b*, and *S3* (Figs. 6.3, 6.4). Part of the 10 m of UTS exposed at *S2a*/*S2b* can be correlated to 7 m of the unit at*S3* (Fig. 6.5). Exact bed to bed correlation between these two segments was not possible, but both segments are dominantly composed of lithofacies *pL* and *plA* with

subordinated *dAL* and minor *ctAL* beds (Figs. 6.3, 6.4). The crude parallel bedding of *dAL* (Table 6.2; Fig. 6.7e), cross lamination of lithofacies *plA* (Table 6.2), the lack of distinct erosive surfaces or truncations (within *dAL* and *plA* beds), and the reverse grading of coarser juvenile fragments all suggest tractional flow boundaries in turbulent base surges with low shear stresses at their bases. The widespread presence of *pL* inter-beds (moderately sorted, reversely graded, juvenile-rich) (Table 6.2; Fig. 6.7d) indicates that fall-out, although not dominant, was important in this phase of the phreatomagmatic eruption. Moderate vesicularity of *pL* fragments may indicate water chilling/fragmentation in the formation of these pyroclasts. Soft sediment deformation and the presence of coarse lapilli/bomb/block size-fragments are not as common as in *LTS*. These characteristics and the unconsolidated nature of *UTS* suggest that less water was involved during the process of deposition compared to *LTS*. The succession of *pL* with *plA* (but also with *dAL* and *ctAL*) is marked by gradational contacts (Figs. 6.3, 6.4, 6.7d), and suggests the alternation of deposition of base surges with fallout from a magmatic eruption column. This indicates multiple vent sites with simultaneous magmatic and phreatomagmatic activity, similar to that seen at Surtsey Island, Iceland (Thórarinsson, 1964); Ukinrek East Maar, Alaska (Büchel and Lorenz, 1993); Crater Hill maar/scoria cone volcano, AVF (Houghton et al., 1999); Capelinhos and Capelas tuff cone, Azores (after Cole et al. 2001; Solgevik et al. 2007).

There is no evidence for pauses during this eruption in the form of a widespread unconformity or other weathering/erosion horizon.

## 6.8 Discussion

### 6.8.1 Depth of explosions associated with the opening of the vent and magma fragmentation

Despite Waitemata aquifers having poor hydraulic conductivity, they host considerable deep ground water along fractured zones, from which a few $m^3$ to over 1000 $m^3$water/day can be supplied (Crowcroft and Smaill, 2001). Waitemata rocks in the Motukorea area have a thickness of around 200-300 metres. Considering that the lowermost exposed deposits may represent the result of phreatomagmatic stages close to the initiation of the eruption, and the fact that Waitemata rock lithics dominate from the base of the Motukorea phreatomagmatic sequence, it may be suggested that the phreatomagmatic explosions involved in the opening of the vent were predominantly caused by the explosive interaction of magma with groundwater (Fig. 6.8a,b) at depths shallower than the maximum thickness of the Waitemata rocks (300 metres). The maximum depth of these explosions is thus at or close to the inferred interface between Waitemata and Waipapa rocks. This implies that Waipapa rocks may have also been disrupted during the first explosions; however, Waipapa lithics are very scarce within the lower parts of *LTS*, which rule out any relevant involvement of Waipapa rocks during the first eruptive stages.

#### 6.8.1.1 Magma fragmentation

By comparison with experimentally derived pyroclasts, which are non-vesicular or poorly-vesicular, equant, blocky, medium ash–size (2-3 phi; 0.25-0.125 mm), juvenile pyroclasts (usually sideromelane with coatings of fine ash) result from explosive fuel-coolant interaction (FCI) (brittle magma fragmentation) when magma contacts water (Sheridan and Wohletz, 1983; Wohletz, 1983; Zimanowski et al., 1997). FCI processes are thought to dominate in phreatomagmatic eruptions when ascending magma interacts explosively with groundwater. The juvenile sideromelane particles in the ash component of the *LTS* and *UTS* from Motukorea ejecta ring show such typical characteristics. The overall lower vesicularity in the juvenile particles of the phreatomagmatic deposit than those in to the overlying magmatic unit is also consistent with phreatomagmatic fragmentation.

Abundant medium-ash grade tachylite particles with similar morphologies and vesicularities to sideromelane occur in the Motukorea deposits. Tachylite is common in scoria deposits of Strombolian eruptions, and is associated with relatively slow cooling rates of magma (Fisher and Schmincke, 1984; Tadeucci et al., 2004). This could suggest that FCI fragmentation occurred alongside magmatic fragmentation in the Motukorea eruption. However, mixed and mingled populations of both sideromelane and tachylite have been found in deposits of both exclusively phreatomagmatic (or underwater) eruptions (e.g. Schipper et al., 2010; Murtagh et al., 2011; Ross et al., 2011; Murtagh and White, 2013), and exclusively Strombolian eruptions (e.g. Sable et al., 2006; Andronico et al., 2009; Lautze et al., 2013). These mixed juvenile populations are explained by complex and dynamic conduit processes during the final magma ascent before fragmentation. Juvenile fragments (either tachylite or sideromelane) may also be the result of “secondary (brittle) fragmentation” as shock waves produced in the FCI process disrupt magma away from the zone of water contact (Zimanowski et al., 1991; Raue, 2004). Zimanowski et al. (1991) describe the particles resulting from secondary fragmentation as dominant in their experiments, and explain that they can show very similar shapes and sizes to the “interactive” fragments produced by FCIs. Additionally, recycling of juvenile (and lithic clasts) may have occurred (e.g. Houghton and Smith, 1993). Upwards into the phreatomagmatic sequence at Motukorea sideromelane is scarcer, suggesting a decreasing involvement of water in magma fragmentation.

### 6.8.2 Assumptions of substrate disruption based on inferred volumes and nature of lithics: evidence for shallow-seated explosions

The deposits of the Motukorea ejecta ring comprise approximately 55-60 vol.% lithics. Considering $3.1\times10^6$ $m^3$ the total (bulk) volume of the tuff ring (Kereszturi et al., 2013), an approximate average of $1.78\times10^6$ $m^3$ of lithics are contained in the ejecta ring if the previous 55-60 vol.% lithics is assumed. Of these approximately 90 vol.% are Waitemata rock fragments, which make up 35 vol.% of the entire medium to fine ash fraction (Table 6.1). The remaining 10% of lithic fragments include Waipapa

greywacke, which are dominantly lapilli size-clasts. Then roughly a maximum $1.6\times10^6$ $m^3$ of Waitemata rock fragments are contained in the ejecta ring and less than $0.17 \times 10^6$ $m^3$ of Waipapa lithics. The crater diameter is not known and difficult to estimate, but it must be <1 km. Although a diatreme is not exposed, the possible extent of disruption of the substrate will be estimated by equating the diatreme with an inverse cone. The range of potential diatreme wall angles is between 60 and 80° (White and Ross, 2011; Valentine, 2012; Lefebvre et al., 2013), for less consolidated to more competent substrate, respectively. Specifically, Lefebvre et al. (2013) assume a 60° angle wall for the uppermost poorly consolidated substrate, and 80° for the deeper competent rocks. Therefore, considering the Waitemata rocks as a moderately consolidated substrate and the Waipapa rocks as more consolidated, angles of 70° and 80°, respectively, were assumed for inwardly dipping diatreme walls. Assuming a surface crater diameter of 500 m (which is roughly the average diameter for AVF phreatomagmatic craters), the total diatreme beneath Motukorea ejecta ring equates to approximately $55\times10^6$ $m^3$. If a reliable thickness of 300 m is assumed for the Waitemata sediments (from Davy. 2008; Kenny et al., 2011; Bernhard Spörli, written communication 2015), then the approximate volume of disrupted Waitemata rocks would be around $44\times10^6$ $m^3$ and the approximate volume of the underlying disrupted Waipapa basement would be approximately $11 \times 10^6$ $m^3$. This approximate 4:1 ratio is far lower than 9:<1, in the tuff ring. Similar discrepancies between known substrates and tuff rings were also noted for two maar volcanoes in the San Francisco Volcanic Field by Valentine (2012). The tephra deposits studied at Motukorea also reflect shallow-seated explosions without the progressive deposition of deeper rock fragments. From field observations, Bryner (1991) reported an increasing proportion of Waipapa greywacke fragments upward within the tuff ring sequence, but this is not clearly seen in the field. A constant content of lapilli-sized lithics from the deeper greywake substrate beneath Motukorea can be best explained by its early explosive disruption followed by mixing into the upper diatreme via debris jetting (Ross and White, 2006). The differences in the proportions of Waitemata to Waipapa lithics found in the ejecta ring (9:<1) compared to the proportions of Waitemata to Waipapa rocks that were disrupted (4:1) may indicate that the Waipapa clasts in the ejecta ring can be explained by an upper diatreme fill that is progressively filled by debris-jet-transported Waipapa lithics, which are later ejected by shallow explosions. On the other hand, it could be argued that the overwhelming presence of Waitemata fragments in the tuff ring was the result of a very shallow excavation into the upper 200-300 m Waitemata rocks. However, how shallow a diatreme may be beneath and approximately 500 m-diameter crater at Motukorea? A very clear cross-section of a small maar-diatreme volcano is reported by Geshi et al. (2011). In their example a surface crater of approximately 200 m excavated into 220 m from the surface of the crater. In another case, Lefebvre et al. (2013), combining the information of a partially exposed diatreme and nearby tuff rings (with not exposed diatremes) reconstruct a maar-diatreme volcano with a surface crater of 300 m in diameter and a diatreme structure that extended downwards 700 m from the paleosurface. In addition, Lorenz (1986) suggests a linear relationship between crater size and diatreme size. The above may indicate the presence of a diatreme cut beyond the 200-300 m-thick Waitemata rocks at Motukorea.

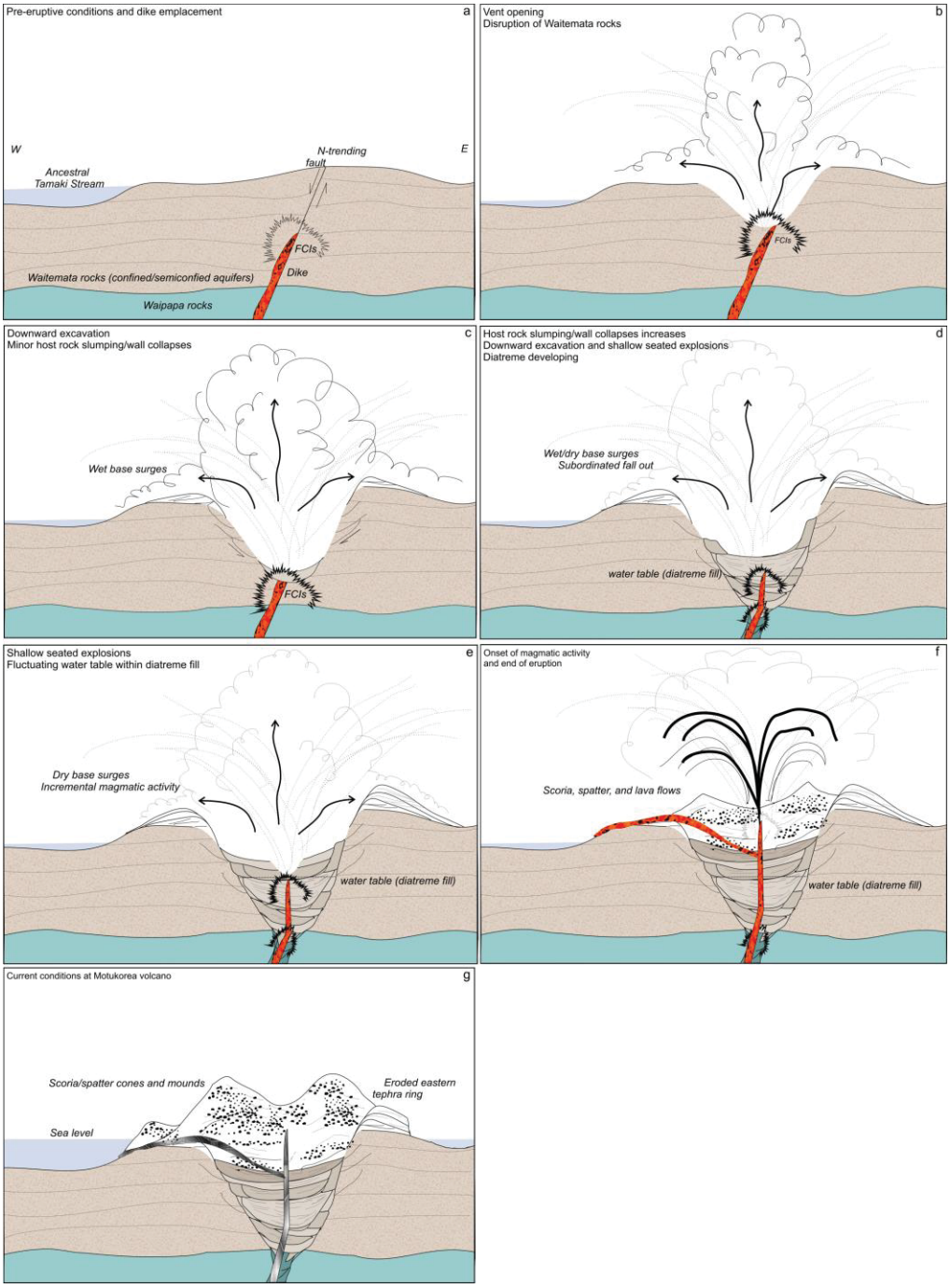


**Fig. 6.8**. Cartoons representing a simplified model of the Motukorea eruption history and construction. Figures are not so scale. The real morphometric parameters of the cone (height, crater depth, and bed slopes) are distorted in the figures. Dike intrusion and position is hypothetical. For a more detailed sequence of the eruption see section 6.8.3 in the text. a) Hypothetical pre-eruptive conditions. The dip of the normal fault, which is unknown, is shown only for illustrative purposes. b) Initial explosions at shallow depth and disruption of predominantly Waitemata Group rocks with some disruption of Waipapa Terrane greywacke, and opening of the crater. c) Downward excavation and onset of diatreme formation. Relatively wet base surges are generated. d) Crater and diatreme enlargement. The diatreme is filled dominantly with Waitemata rock fragments. e) Drier, relatively less energetic base surges are generated in shallow-seated explosions within the diatreme fill. Subordinate, but progressively dominant magmatic activity is present. Waipapa lithics are transported to the upper diatreme by debris jets. f) Final magmatic stage of eruption with dominance of magmatic activity (scoria/spatter structures, tephra bed deposition, and lava flow emplacement). g) External current conditions with hypothetical diatreme fill and frozen dike.

In recent experimental studies (Graettinger et al., 2014), in which deep-seated explosions do not expel material to the ejecta ring because the explosions were confined., the final deposition of material in the ejecta ring is the result of the interaction between the locus depth and energy of explosions, as well as the vent geometry. Lefebvre et al. (2013) and Agustín-Flores et al. (2014) also propose that shallow-seated explosions dominated in tuff ring construction based on lithic proportions in ejecta rings compared with the proportion of substrate rocks disrupted. Other examples in the AVF (Crater Hill, Houghton et al., 1999; Németh et al., 2012a) also appear to show similar shallow-dominated explosions. Deep explosions occur, but although they can move material within the diatreme, they do not excavate the crater or contribute to the ejecta ring (P.-S. Ross, written communication 2015).

### 6.8.3 The construction of Motukorea maar

#### 6.8.3.1 The first phreatomagmatic stage (*LTS*)

After vent opening, the confining pressure of the underlying aquifers may have dropped, increasing the depth of the most effective FCI explosions, which are highly dependent on the combination of induced fracturing and original and enhanced hydraulic properties of aquifers at this stage. Explosive fracturing of Waitemata rocks may have increased their hydraulic conductivity (e.g. Aranda-Gómez and Luhr, 1996), sustaining limited deeper locus explosions. *LTS* sequences were formed by dominantly erosive, wet base surges (Fig. 6.8b,c). The common Waitemata-coarse lapilli/blocks (either ballistics or within currents) suggest strong vent excavation through Waitemata rocks.

#### 6.8.3.2 A change in eruptive style (*MSU*)

A sudden change in eruptive style is marked by the deposition of *MSU* (Fig. 6.8d). The gradual deepening of the locus and widening of the crater may have caused slumping of crater walls and further disruption of shallow substrate (Fig. 6.8c,d). In addition, magma intruded into or beside the crater/diatreme fill in dikes (Fig. 6.8d,e) to form at a further magmatic eruption vent or series of vents.

#### 6.8.3.3 The second phreatomagmatic phase (*UTS*) and termination of phreatomagmatism

Later in the eruption, low-energy, relatively dry base surges occurred alongside increasingly dominant juvenile tephra fall associated with magmatic activity. The overwhelming presence of Waitemata lithics suggest that base surges were generated by shallow-seated explosions (Fig. 6.8e). Intensive chilling of magmatic juvenile particles rules out pure fire fountaining or Strombolian activity during this stage. Drier activity may be attributed to an increase in magma flux (e.g. Houghton and Nairn, 1991; Houghton et al., 1999). However, the relative homogeneity in vesicularity and textures of the juvenile pyroclasts within *UTS* do not suggest this. Instead the dryer magmatic activity could relate to explosions within dry domains within an upper diatreme and crater fill. Hence, dryer and wetter eruptive styles might thus be the result of consecutive or coeval explosions at loci of different depths or/and sites within the diatreme fill

characterized by domains with different water contents (as predicted by the Valentine and White´s model, 2012). Progressively drier deposits in the Motukorea ejecta ring sequence may be the result of progressive drying of the upper parts of the diatreme, which in turn suggest that the external aquifer was drying up (P.-S. Ross, written communication 2015). This contrasts with the overall "wet" tephra deposits of Maungataketake volcano erupted through water-saturated, soft sediments to the south of the same volcanic field (Agustín-Flores et al., 2014). Unlike Motukorea, the continuous presence of water provided by the sediments may have contributed to the "wet" nature of Maungataketake tephra deposits.

The transition to the onset of the final magmatic phase is distinct (Fig. 6.3). As expected for a magmatic gas-expanding eruption, the vesicularities of the magmatic phase juveniles are higher than those within the underlying phreatomagmatic sequences. McGee et al. (2012) proposed a geochemical model characterized by two distinct magma batches for Motukorea volcano. They state that the phreatomagmatic stage of the eruption was terminated by the arrival at the surface of higher flux, more voluminous magmas with a different chemical composition (McGee et al., 2012) which led to magmatic activity and scoria/spatter structures, and lava flows (Fig. 6.8f).

Considering that there were no time breaks in the Motukorea eruption an eruption rate estimate of 5 $m^3/s$ (estimation by Kereszturi et al., 2013 using data from other basaltic eruptions comparable to the AVF), suggests an eruption-duration of 10 days (Kereszturi et al., 2013). Although the complete run-out distance of base surges is not evident, Bryner (1991) reported tuff from drill holes up to 1 km from the vent. Other examples in the AVF may have had base surges travelling up to 2 km radially from the vent (e.g. Maungataketake volcano in the AVF; Agustín-Flores et al., 2014; Brand et al., 2014). Any similar explosive, short-lived phreatomagmatic eruption on the Waitemata Group substrate is likely to affect~4 – 16 $km^2$ with base surges. These substrate geological conditions are prevalent throughout the highest populated areas of the central Auckland isthmus and the North Shore peninsula (Fig 3.1).

## 6.9. Conclusions

I propose a model for the Motukorea phreatomagmatic eruptions based on the study of lithics and the sedimentary characteristics of deposits, combined with hydrological and lithological information of the substrate. Juvenile particle morphology, composition, and its distribution within the tuff ring deposits added information to infer eruption dynamics.

The pre-eruptive substrate is composed of~200-300 m of the aquifer-bearing Waitemata sedimentary rocks underlain by the Waiapapa Terrane-greywacke basement rocks. The first phreatomagmatic explosions are inferred to have taken place within the Waitemata rocks. The calculated approximate proportions of hypothetically disrupted Waitemata and Waipapa rocks (~4:1) compared with the proportions of these rock lithics actually found in the ejecta ring(~9:<1) show that Waipapa lithics are strongly under-represented in the ejecta ring. The proportion would be expected to be higher, considering

the location of Waipapa terrane at relatively shallow levels beneath the volcano, if the Lorenz (1986) model of downward excavation is applied. Instead, we infer that the maar ejecta ring was constructed by deposition of material from shallow-seated explosions in the dominantly Waitemata lithic-rich diatreme fill as in the revised model by Valentine and White (2012). It is likely that underlying Waipapa fragments were transported upwards into the diatreme by debris jetting as the model envisages.

Sedimentary characteristics suggest that the *LTS* was relatively wetter than the upper sequences and was formed when water was relatively more abundant during the early stages of the eruption when the first explosions took place within the Waitemata aquifers. Once a diatreme was established, the eruption was characterized by a combination of lower energy, turbulent base surges and fall-out generated through shallow seated explosions within the diatreme fill. Phreatomagmatic fragmentation occurred together with magmatic fragmentation, indicating multiple explosion sites were active and a complex plumbing network of feeder dikes. Eventually water was exhausted, leading to a shift to an exclusively magmatic phase.

These results shed light into the possible eruption dynamics of future phreatomagmatic eruptions through areas with similar substrate to Motukorea within the highest populated parts of central Auckland. The most dangerous hazard related to this type of eruptions is the generation of base surges. Therefore even a short-lived and small phreatomagmatic eruption like Motukorea would pose a high risk to the largest city of New Zealand.

DRC 16

MASSEY UNIVERSITY
GRADUATE RESEARCH SCHOOL

## STATEMENT OF CONTRIBUTION
## TO DOCTORAL THESIS CONTAINING PUBLICATIONS

(To appear at the end of each thesis chapter/section/appendix submitted as an article/paper or collected as an appendix at the end of the thesis)

We, the candidate and the candidate's Principal Supervisor, certify that all co-authors have consented to their work being included in the thesis and they have accepted the candidate's contribution as indicated below in the *Statement of Originality*.

**Name of Candidate:** Javier Agustín Flores

**Name/Title of Principal Supervisor:** Karoly Németh

**Name of Published Research Output and full reference:**

Agustín-Flores J., Németh K., Cronin S., Lindsay J., Kereszturi, G., 2015. Shallow-seated explosions in the construction of the Motukorea tuff ring (Auckland, New Zealand: evidence from lithic and sedimentary characteristics. Journal of Volcanology and Geothermal Research, 304: 277-286.Doi 10.1016/j.jvolgeores.2015.09.013

**In which Chapter is the Published Work:** Chapter 6

Please indicate either:

- The percentage of the Published Work that was contributed by the candidate:

  and / or

- Describe the contribution that the candidate has made to the Published Work:

  Organization and completion of the whole field work and most laboratory work, main contributor on writing and editing of manuscript draft, and subsequent correcting and editing for final version

Javier Agustin-Flores
Digitally signed by Javier Agustin-Flores
DN: cn=Javier Agustin-Flores, o=Massey University, ou=Institute of Agriculture and Environment, email=kiaoranet@yahoo.co.nz, c=NZ
Date: 2015.04.23 15:13:43 -06'00'

Candidate's Signature

24/09/2015
Date

Karoly Nemeth
Digitally signed by Karoly Nemeth
DN: cn=Karoly Nemeth, o=Massey University, ou=Institute of Agriculture and Environment, email=k.nemeth@massey.ac.nz, c=NZ
Date: 2015.09.25 10:45:19 +12'00'

Principal Supervisor's signature

25/09/2015
Date

# Chapter 7. Reconstruction of the North Head (Maungauika) Surtseyan eruption and implications of the hydrological conditions

## 7.0 Preface

This chapter includes the reconstruction of the eruptive history of the North Head tuff cone, situated in the northern AVF (Fig. 3.1). The study is based on collected stratigraphic, sedimentary, and pyroclast data from the tuff cone deposits. The main objective of the research was to understand the causes of the deposition of a sequence that resembles a tuff cone, in contrast with the widespread tephra ring deposits in the Auckland Volcanic Field associated to the interaction of magma with groundwater (e.g. Chapters 5 and 6). The evidences seem to indicate the interaction of magma with shallow surface water (~12 m), a situation likely to have occurred during the Last Interglacial.

**Contents** Page



**Chapter 7 comprises the published article (*Appendix E*):**

**Construction of the North Head (Maungauika) tuff cone: a product of Surtseyan volcanism, rare in the Auckland Volcanic Field, New Zealand**

**Authors**: Agustín-Flores J., Németh K., Cronin S., Lindsay J., Kereszturi, G., 2015. Bulletin of Volcanology, 77: 11. Doi 10.1007/s00445-014-0892-9

**The contribution of each author is as follows:**

**Javier Agustín-Flores (PhD candidate)**: Organization and completion of the whole field work and most laboratory work, main contributor on writing and editing of manuscript draft, and subsequent correcting and editing for final version.

**Karoly Németh (main supervisor)**: Oversight of the research process, assistance in the field and laboratory work, as well as in manuscript revision and discussion from the initial draft to the final version.

**Shane J. Cronin (supervisor)**: Discussions during the whole research project and assistance in manuscript revision and discussion from the initial draft to the final version.

**Jan M. Lindsay (supervisor)**: Discussions during the whole research project and assistance in manuscript revision and discussion from the initial draft to the final version.

**Gábor Kereszturi**: Overall field assistance, manuscript revision and discussion.

## 7.1 Introduction

The Auckland Volcanic Field (AVF) of northern New Zealand comprises at least 52 individual eruption centres dispersed over a roughly elliptical area of ~360 $km^2$ (Allen and Smith 1994; Spörli and Eastwood 1997; Kereszturi et al. 2013) (Fig. 3.1). These eruptive centres consist mostly of maar-diatreme volcanoes formed by subaerial phreatomagmatic eruptions, scoria cones formed by magmatic (dry) explosive activity, and combinations thereof (Allen and Smith 1994; Kereszturi et al. 2013). North Head (also known as Maungauika), is the only known tuff cone formed by Surtseyan activity in the AVF. One reason for the paucity of Surtseyan eruptions may be that the field's activity, since its inception c. 250 k.y. ago, coincides in approximately 90% of this time with glacio-eustatic sea levels lower than today (Pillans, 1983; Siddall et al., 2006; Hannah et al., 2011) with >60% of the eruptions occurring within these lower sea-level intervals (Bebbington and Cronin, 2011). However, about 35% of the AVF now lies below shallow water (0-30 m) (Fig. 7.1a), and sea levels are expected to rise (Hannah et al., 2011) so present or future Surtseyan activity may occur in the AVF (Lindsay et al., 2010) within the submerged areas. This must be considered in hazard planning for the City of Auckland (population of 1.4 million), which has enormous wealth concentrated in coastal properties, as well as one of the most economically important harbours in New Zealand.

The North Head tuff cone case study provides valuable insights into the sedimentary and lithological features that can be used to identify Surtseyan activity, and also highlights the volcanic processes expected when small-volume basaltic magmas erupt through shallow marine basins. The sedimentology, as well as the morphological and textural characteristics of pyroclasts are described and compared with those of other tuff cones. From this, eruption mechanisms are interpreted and the surface water conditions for the eruption elucidated. North Head provides a unique and valuable scenario for future Surtseyan eruptions in the Auckland region and other volcanic fields in the world with shallow subaqueous settings.

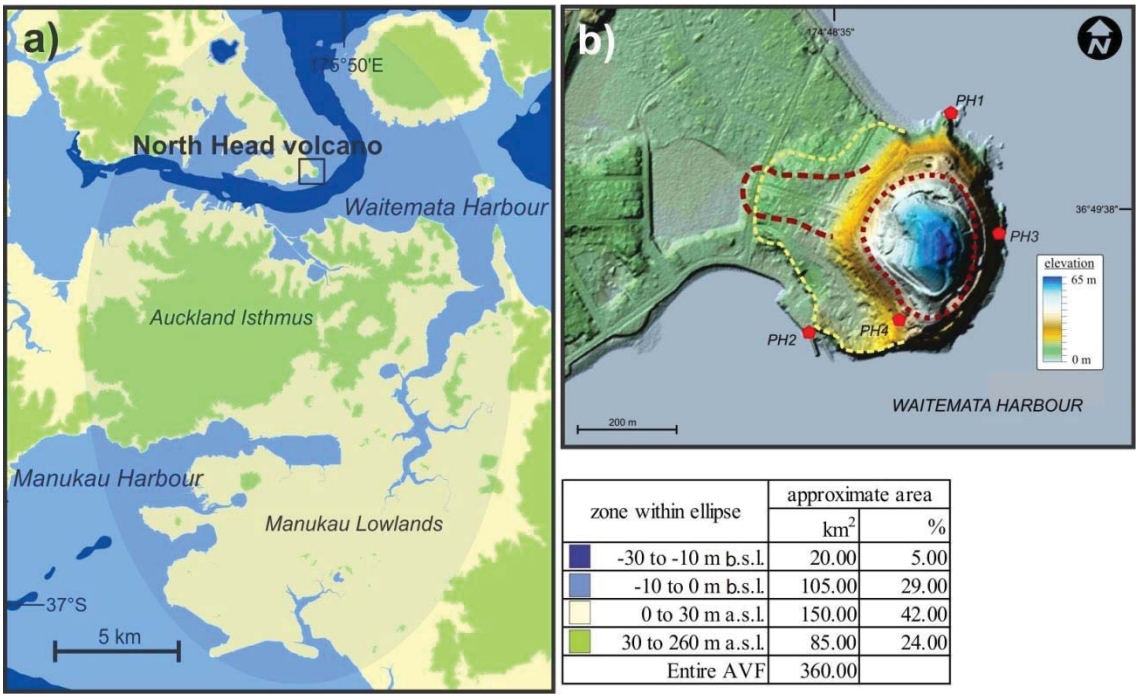


| zone within ellipse | approximate area | |
|---|---|---|
| | km$^2$ | % |
| -30 to -10 m b.s.l. | 20.00 | 5.00 |
| -10 to 0 m b.s.l. | 105.00 | 29.00 |
| 0 to 30 m a.s.l. | 150.00 | 42.00 |
| 30 to 260 m a.s.l. | 85.00 | 24.00 |
| Entire AVF | 360.00 | |

**Fig. 7.1** a) Approximate areas associated with four different ranges of elevations with respect to sea level (with respect to Chart Datum for depths and drying above Chart Datum for heights) (from -30 m b.s.l. to 260 m a.s.l.) in the Auckland Volcanic Field (ellipse) Note the prevalence of submerged and low land areas. b) Shaded relief model of the light detection and ranging (LiDAR) -derived digital surface model of the North Head volcano. The location of the four key sites (representing the four phreatomagmatic subunits) (PH1-4) is shown (for the exact elevation of each site see Figs. 7.2, 7.3, 7.4, and 7.5). The red dashed line indicates the possible extent of the lava flow and the red broken line roughly marks the transition from phreatomagmatic to magmatic deposits, i.e. approximately 40 m above sea level. The yellow broken line delineates what appears to be a broad platform (***Appendix E.1 contains information of complete sites for North Head***).

## 7.2 Surtseyan volcanism

Many tuff cones comprise the emergent portion of volcanoes initiated in subaqueous settings (either marine or lacustrine) (White, 1991b), with a distinction made between the pre-emergent and emergent eruption stages (e.g. White, 1996, 2001; Brand and Clarke, 2009). In general, the pre-emergent (subaqueous) stage produces shallow-dipping sequences of well-bedded tephra fall deposits, intercalated with massive, diffusely bedded gravity flow units that form a broad platform. The emergent stage, which forms a capping tuff cone, involves abundant water in the eruption site, but mostly in the form of slurry of basalt fragments and water (Kokelaar, 1983). In this phase, tephra jets and phases of continuous tephra up-rushing are dominant (Kokelaar, 1986; Belousov and Belousova, 2001). Jets of tephra contain water (Kokelaar, 1986) and may be spreading (cock's tail) or directed (cypressoid) (Thórarinsson, 1964; Belousov and Belousova, 2001; Németh et al., 2006). Water in tephra jets is provided by the condensation of steam and as ejected un-vaporised sea or lake water (Kokelaar 1983). Continuous up-rush generates tephra and steam plumes reaching up to 1 km in height or higher and causes rapid proximal tephra

accumulation (Kokelaar 1986; Cole et al. 2001). Close to the vent, grain flows and/or debris flows may result from rapidly piled-up tephra and slopes greater than the material repose angle (e.g. Kokelaar, 1986; Sohn and Chough, 1992, 1993). These generate massive or weakly stratified beds with over 90% moderately-vesicular, ash-lapilli size, juvenile pyroclasts. This implies that fragmentation occurs above ground level, with little or no excavation into the eruptive surface. From proximal to distal locations cross stratification may be present showing high-velocity lateral flows and base surges (e.g. Lorenz, 1974a; Solgevik et al., 2007), but crude, planar, or lenticular beds with reverse grading related to tephra fall are dominant at some tuff cones (e.g. Sohn and Chough, 1992, 1993; White, 2001; Solgevik et al., 2007). Armoured lapilli/accretionary lapilli may also occur (e.g. Lorenz, 1974a; Solgevik et al., 2007). Many tuff cones contain yellow palagonitized and indurated beds (Wohletz and Sheridan 1983; Solgevik et al. 2007). Palagonitization and induration occurred progressively at Surtsey within a few years after deposition due to mild hydrothermal alteration (Jakobsson, 1972, 1978; Lorenz, written communication 2014). Lorenz (1974a,b) also reports vesicular tuff at Surtsey, evidencing water in liquid form at the time of deposition. The pyroclastic succession may contain bedforms typical of deposition influenced by tidal and wave action (i.e. erosion surfaces, ripples, remobilized deposits, as well as slumps and slides (Sohn et al., 2012). If tephra piles grow and water becomes excluded from the vent, magmatic eruptions follow (lava fountaining and/or Strombolian phases, Kokelaar, 1986).

## 7.3 The AVF and the North Head (Maungauika) tuff cone

### 7.3.1 The Auckland Volcanic field

A minimum of 1.7 $km^3$ of DRE magma has been erupted in the AVF so far (Kereszturi et al., 2013) in the form of olivine-rich alkali basalts and basanites (Smith et al., 2009). Eruptions have been sporadic since 250 ka, but with a noticeable flare-up within the last ~40 k.y. (Molloy et al. 2009; Bebbington and Cronin 2011). An intriguing feature of the AVF is the fact that approximately 75% of the volcanoes experienced a phreatomagmatic, maar-forming phase at the onset of eruptions. Unlike North Head, all of the other exposed sites are dominated by lithic-rich tuff and lapilli tuff units indicating magma fragmentation as the result of the explosive interaction between ground-water and rising magma (e.g. Allen et al., 1996; Houghton et al., 1999; Németh et al., 2012a; Agustín-Flores et al. 2014) when the sea level was mostly lower than today. Maar-forming phreatomagmatic eruptions producing violent base surges (dilute pyroclastic density currents) are considered to be the most hazardous volcanic events expected to threaten the inhabitants and infrastructure of the City of Auckland (Allen and Smith, 1994; Németh et al., 2012a; Sandri et al., 2012). Explosive Surtseyan eruptions (or a combination of maar-forming and Surtseyan eruptions) may be more likely in the future of the AVF, because approximately 35% of the field is now covered by surface water (using boundaries from Spörli and Eastwood 1997) (Fig. 7.1a).

### 7.3.2 North Head (Maungauika) tuff cone

North Head is a small basaltic volcano (alkali olivine basalt) located at the tip of the Devonport Peninsula in North Shore City (part of greater Auckland) (Fig. 3.1). This volcano lies on an eroded surface of late Miocene-aged Waitemata Group rocks as evidenced from nearby drill core data (Searle, 1959). Waitemata rocks comprise >300 m-thick inter-bedded turbiditic sandstones and pelagic siltstones with subordinate breccia and conglomerate units (Ballance, 1974; Hayward, 1979, 1993; Raza et al., 1999). Waitemata rocks are weakly indurated with a compressive strength of ~5 MPa (Spörli and Rowland, 2007) and host heterogeneous and anisotropic aquifers (Crowcroft and Smaill, 2001). The tuff cone deposits of North Head (without the capping magmatic deposits) rise to 45-50 m above the present mean sea level (~50-60 m above the pre-eruptive surface) (Allen and Smith, 1994). From the outcrops available it is possible to observe that the beds dip outwards from the cone centre at approximately 10° at most of locations, but bedding planes increase to up to 20° in sequences 40-45 m above sea level. The bulk volume estimated by Kereszturi et al. (2013) for the tuff cone is $1.1x10^6$ $m^3$. Scoria and spatter deposits of the magmatic stage of the eruption are exposed at the top. A small lava flow (tens of m long) was emplaced west of the volcano, but it is now concealed beneath houses (Hayward et al., 2011). The total edifice stands 65 m above sea level (Fig. 7.1b) (approximately 72 m above the pre-eruptive surface) (Allen and Smith 1994) and has a DRE minimum volume of $2.6x10^6$ $m^3$ (Kereszturi et al. 2013). Marine erosion has exposed tuff beds on the eastern/southern slopes of the volcanic edifice (Fig. 7.1b). Hayward et al. (2011) report that a small crater was present (dimensions unknown) at the summit of the cone, but is now infilled and covered by buildings. Based on the point of transition from phreatomagmatic to magmatic deposits (Fig. 7.1b), the maximum tuff cone crater diameter is estimated to be 220-280 m.

## 7.4 General terminology and methodology

Although *sensu stricto* phreatomagmatism refers to the interaction of magma with groundwater, following Stearns (1953), we use it more broadly to include explosive magma-water interaction with surface or groundwater. Pyroclasts in this study are defined as juvenile (freshly erupted magma) and explosively erupted, non-juvenile country-rock lithic fragments (following Fisher and Schmincke, 1984). Country rock fragments at North Head consist of ash to block size fragments of the underlying Waitemata Group rocks. Grainsize and textural nomenclature follows Sohn and Chough (1989) (see Table 7.1). Base surge is used as a synonym for dilute, radially travelling, ground-hugging pyroclastic density currents. Base surges are a signature process of explosive phreatomagmatic eruptions.

### 7.4.1 Field work

The deposits related to the Surtseyan activity at North Head were examined in detail at four sites (PH1-4) (Fig 7.1b) (***Appendix E.1 contains information of complete number of sites and corresponding stratigraphic logs***). These represent vertical variations of proximal cone facies. PH1, PH2, and PH3 are

located respectively at the northern, southern, and eastern side of the eroded tuff cone, (Fig. 7.1b), whereas PH4 is located at approximately 30-35 m above sea level (Fig. 7.1b). Deposits at PH1 are heavily indurated and slightly palagonitized, whereas deposits at PH2-4 are dominantly unconsolidated or poorly-consolidated. The precise transition from tuff into spatter/scoria deposits (the magmatic unit) is concealed by vegetation, but the latter occur first distinctively above 40 m above sea level (Fig. 7.1b). PH1 deposits do not represent the lowermost tuff cone deposits, which lie 7-8 m below the current sea level (c.f. Allen and Smith 1994). No information about these underwater deposits is available.

**Table 7.1**. Grain size nomenclature and its volumetric proportion in the entire phreatomagmatic deposit. ***This classification was made in part with the results and analysis and of grain size distribution of sieved samples (see Appendix E.1 for more information on grain size results and distribution, as well as the componentry results of analysed samples)***.

| Piroclast size | ~Vol-% within entire deposit | ~Vol.% of juvenile pyroclasts |
|---|---|---|
| Block/bomb (-6 to -8 ϕ) (64-256 mm | <5 | 90 |
| Coarse lapilli (-4 to -6 ϕ) (16-64 mm) | 15-25 | 95 |
| Medium lapilli (-2 to -4 ϕ) (4-16 mm) | | |
| Fine lapilli (-1 to -2 ϕ) (2-4 mm) | 65-75 | 95 |
| Coarse ash (1 to -1 ϕ) (0.5-2 mm) | | |
| Medium ash (4 to 1 ϕ) (0.625-0.5 mm) | <5 | 70 |
| Fine ash <4 ϕ (<0.625 mm) | | |

### 7.4.2 Laboratory work

Unconsolidated samples from lithofacies L1 (present in PH1 and PH2) and L2 (present in PH4) (see lithofacies in section 7.5.2) were sieved between -4.0 and 4.0 ϕ (16-0.0625 mm) at 0.5 ϕ intervals. Grain size distribution parameters (Inman, 1952; Folk and Ward, 1957) were calculated using the SFT (Sequential Fragmentation/Transport) program (http://www.ees1.lanl.gov/Wohletz/SFT.htm). Particles from the 2 ϕ and 3 ϕ fractions (0.25-0.125 mm) were cleaned with 10% HCl and rinsed with acetone in an ultrasonic bath for 30-60 s. Morphological characteristics of fragments were characterized by viewing loose grains and thin sectioned grains under binocular/stereo and transmitted polarised light microscopy and scanning electron microscopy (FEI Quanta 200 environmental scanning electron microscope operated at 20 kV, Massey University Microscope Centre). The grain size data (percentage area) and componentry of the consolidated lithofacies LT1 were obtained from field observations and thin section analyses under petrographic microscope and using the JMicrovision v.1.2.7software for image analysis. The vesicularity index of some 2-4 mm-lapilli grains (30 grains each of a total of 4 samples representing lithofacies L1 and L2) was obtained following the methods of Houghton and Wilson (1989). The density of these grains was calculated using a Micromeritics GeoPyc 1360 envelope density pycnometer. For the lithofacies LT1, a vesicle percentage volume was calculated using point counting (600 points) in juvenile grains (10 grains) from thin section images.

Glass microprobe analyses were carried out on selected North Head samples (***see Appendix C for glass microprobe results***).

## 7.5 Results: North Head eruptive products

In general, the entire deposit displays crude bedding that may be ungraded or reverse graded, and is composed of >90 vol.% of juvenile lapilli and coarse ash (15-25 vol.% of coarse and medium lapilli; 65-75 vol.% of fine lapilli and coarse ash; Table 7.1). It is moderately to poorly sorted (from sieving analysis and visual estimates). (***Appendix E.1 shows a table and graph representing the volume percentage values for phi fractions of selected sieved-North Head samples (histograms are presented in Figs. 7.3, 7.4, 7.5***). These results contributed to the estimation of grain size percentage volumes and the proportions of lithic and juvenile pyroclasts.

Accretionary/armoured lapilli are rare. Each site (PH1-4) defines a phreatomagmatic subunit (also represented by PH1-4) (Figs. 7.2, 7.3, 7.4, 7.5) (hencefort PH indicates a subunit, otherwise stated). Six lithofacies are distinguished based on sedimentary and grain size characteristics (Table 7.2) (Fig. 7.6). A phreatomagmatic subunit represents a separate segment in the vertical stratigraphy with respect to other phreatomagmatic subunits and is characterized by distinct overall sedimentary and grain size features (determined by a single or multiple lithofacies) (Figs. 7.2, 7.3, 7.4, 7.5). PH1 (Fig. 7.2) is formed exclusively by lithofacies LT1 and may reach up to 6 m in thickness. PH2 (Fig. 7.3) attains about 6 m in thickness and contains an alternating sequence of lithofacies LT2 and L1. PH3 (Fig. 7.4) forms an approximately 5 m-thick sequence and is constituted by lithofacies L1, LB, and T. PH4 (Fig. 7.5) is wholly composed by lithofacies L2 and has a maximum thickness of 25 m. (***Appendix E.1 contains information of additional sites***)

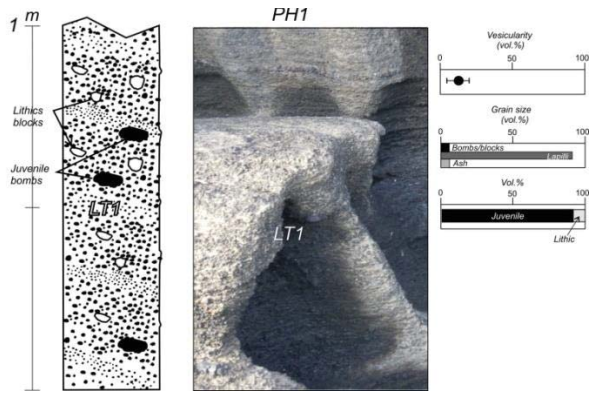


**Fig. 7.2**. Segment of the phreatomagmatic subunit PH1 (see location in Fig. 7.1b). Observe the crude bedding and the prevalence of juvenile fragments. The sequence is solely constituted by lithofacies LT1 (see section 7.5.2 in the text, Table 7.2 and Fig. 7.6 for details on lithofacies). PH1 lies at the bottom of the studied deposits and comprises up to 6 m in thickness. Base of exposed sequence is approximately at Chart Datum which is approximately Lowest Astronomical Tide (from data in nautical chart 5322, Land Information New Zealand). Estimates of vesicularity (mean ±1SD), grain size, and juvenile content of LT1 within the displayed segment are representative values for the entire PH1.

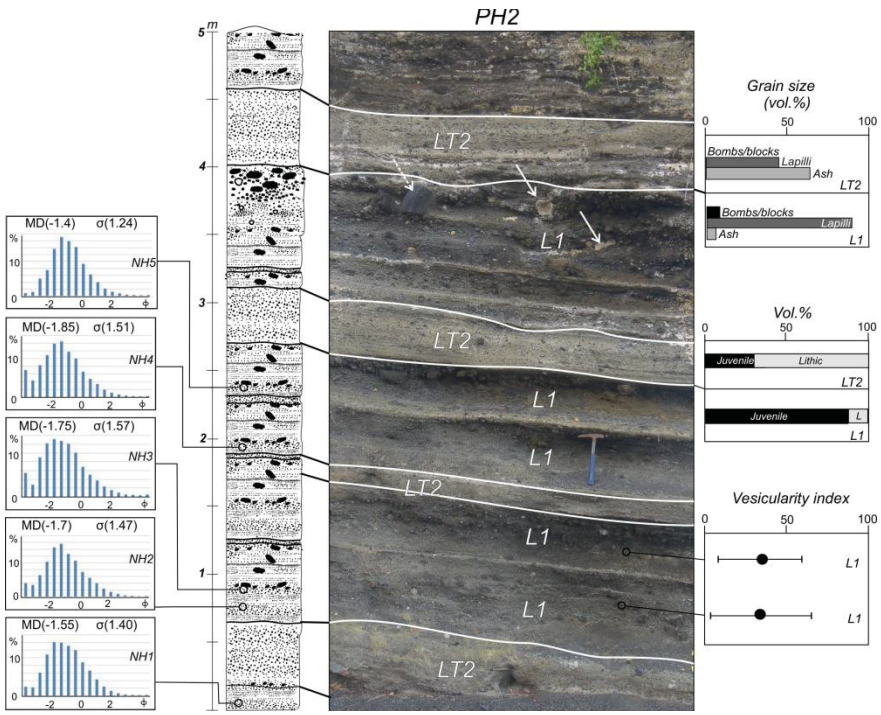


**Fig. 7.3**. Stratigraphic sequence that contains the phreatomagmatic subunit PH2 (see location in Fig. 7.1b). PH2 is formed by the alternation of lithofacies LT2 and L1 (white fonts) (see section 7.5.2 in the text, Table 7.2 and Fig. 7.6 for more details on lithofacies). Base of exposed sequence is approximately at 3-4 m above Chart Datum which is approximately Lowest Astronomical Tide (from data in nautical chart 5322, Land Information New Zealand). Scale indicates thickness in metres. Grain size histograms of five samples of the same lithofacies L1 at different stratigraphic levels are shown on the left side [MD= median diameter; σ= sorting; the horizontal and vertical axes are the phi diameter (ϕ) versus frequency (%)]. Estimates of grain size and juvenile content represent values of lithofacies LT2 and L1 at all levels within the entire sequence. Vesicularity estimates (mean ±1SD) are exclusively for lithofacies L1 located at the indicated level. White arrows point to rare Waitemata blocks. Broken white arrow points to a juvenile bomb.

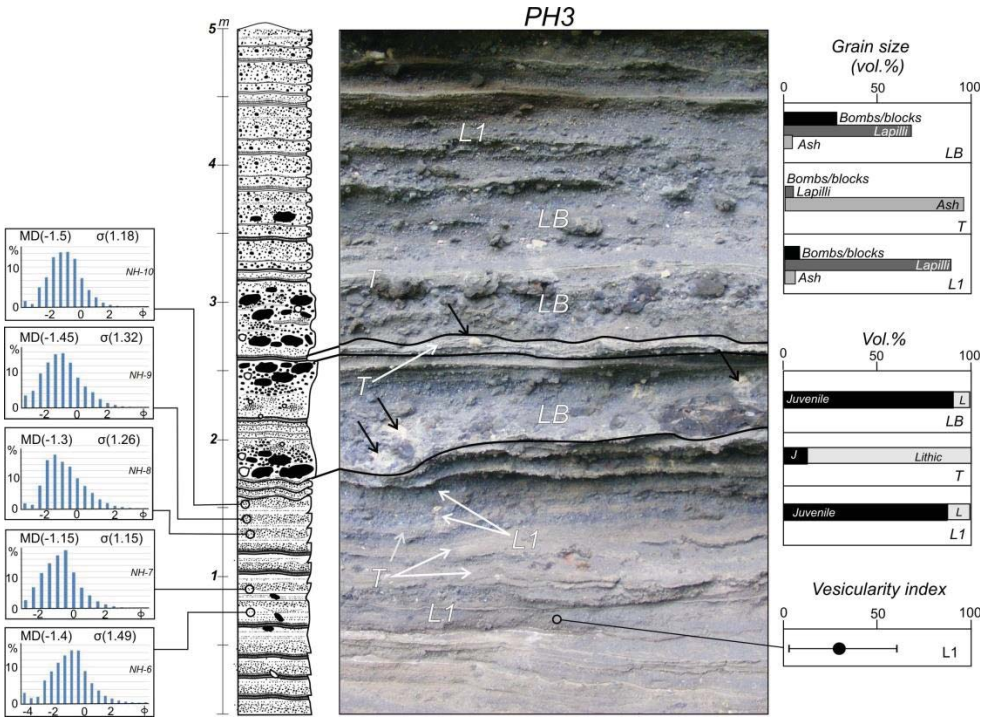


**Fig. 7.4**. Stratigraphic sequence that contains the phreatomagmatic subunit PH3 (see location in Fig. 7.1b). PH3 is formed by the alternation of lithofacies LB, T, and L1 (white fonts) (see section 7.5.2 in the text, Table 7.2 and Fig. 7.6 for more details on lithofacies). Base of exposed sequence is approximately at 7-8 m above Chart Datum which is approximately Lowest Astronomical Tide (from data in nautical chart 5322, Land Information New Zealand). Scale indicates thickness in metres. Grain size histograms of five samples of the same lithofacies L1 at different stratigraphic levels are shown on the left side [MD= median diameter; σ= sorting; the horizontal and vertical axes are the phi diameter (ϕ) versus frequency (%)]. Estimates of grain size and juvenile content represent values of lithofacies LB, T, and L1 at all levels within the entire sequence. Vesicularity estimates (mean ±1SD) are exclusively for lithofacies L1 located at the indicated level. Black arrows point to rare Waitemata blocks.

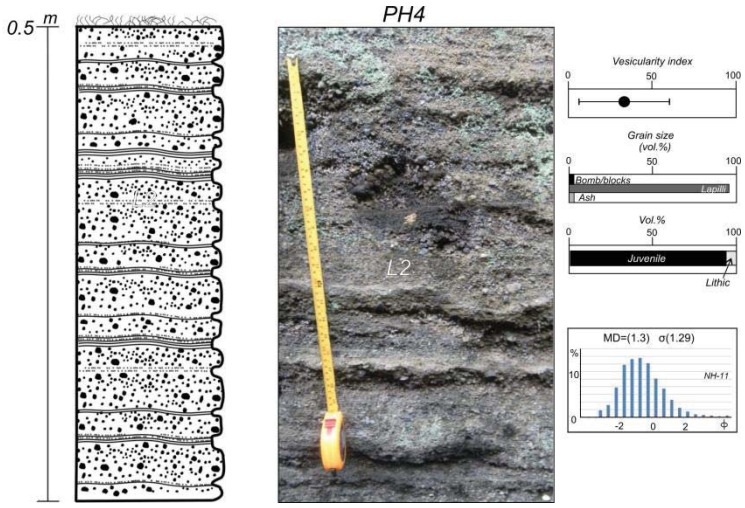


**Fig. 7.5**. Segment of the phreatomagmatic subunit PH4 (see location in Fig. 7.1b). Observe the prevalence of juvenile fragments. PH4 is solely constituted by lithofacies LT2 (see section 7.5.2 in the text, Table 7.2 and Fig. 7.6 for details on lithofacies). PH4 comprises about 25 m in thickness of a very homogeneous sequence. Base of exposed sequence is approximately at 35-40 m above Chart Datum which is approximately Lowest Astronomical Tide. Estimates of vesicularity (mean ±1SD), grain size, and juvenile content of LT2 within the displayed segment are representative values for the entire PH4.

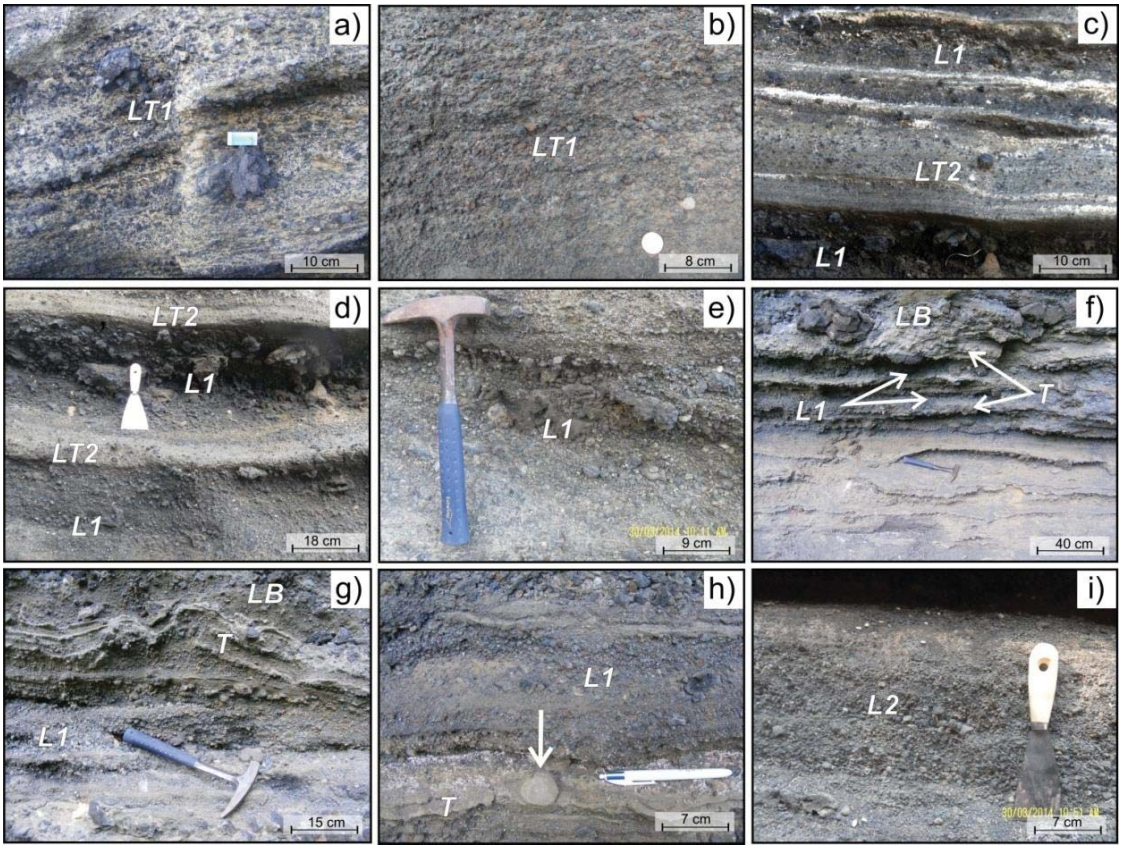


**Fig. 7.6**. Close-up view of the six lithofacies identified within the North Head sequence. For the specific characteristics, descriptions and interpretations of lithofacies see section 7.5.2 in the text and Table 7.2. See in Figs. 7.2, 7.3, 7.4, and 7.5 for detail on the distribution of lithofacies within each phreatomagmatic subunit (PH1-4): LT1 occurs within PH1; LT2 is part of PH2; L1 is included in PH2 and PH3; LB and T are found in PH3; and L2 in PH4.

### 7.5.1 Pyroclast characteristics

In the samples from lithofacies LT1 (PH1) the vesicularity of juvenile pyroclasts is between 6-20 vol.%, (Fig. 7.2) with sub-spherical to spherical vesicles <60 μm in diameter (Fig. 7.7b,c). Thick walls between vesicles (usually >50 μm) dominate (Fig. 7.7b,c). Vesicularity index ranges from approximately 5 to 65% (from non-vesicular to highly vesicular; Houghton and Wilson, 1989) in the four groups of samples from lithofacies L1 (present in PH1/PH3) and L2 (present in PH4) (Figs. 7.3, 7.4, 7.5), with sample group averages of 31-37%. The vesicularity of juvenile fragments in the consolidated LT1 is relatively more homogeneous than those composing the overlying sequences (where subordinate scoria pyroclasts are present; Fig. 7.7d). Since the vesicularity calculations were carried out on coarse ash/fine lapilli and the entire deposit is dominated by juveniles within this grain-size range (Table 7.1), these results may approximate the overall vesicularity of juvenile pyroclasts.

The dominant coarse ash to lapilli juvenile pyroclasts of the entire phreatomagmatic phase have sub-angular to angular shapes (Figs. 7.6a,d, 7.7a,b,h,i,). Similarly, coarse lapilli and small bombs are either sub-angular or angular blocky fragments (Fig. 7.6a,d,e,f). The large bombs may show cauliflower surface patterns. Some of the bombs show flattened fluidal forms produced on landing. The 2-3 $\phi$ fraction (0.25-0.125 mm) comprises 85 vol.% juvenile fragments (Fig. C.7, ***Appendix E.1***). These fragments range from poorly vesicular to dense, and have irregular equant to sub-angular shapes (Fig. 7.7e,f,g,h,i). This fraction only represents <3 vol.% of the pyroclastic deposit and it may represent recycling rather than direct production by phreatomagmatic fragmentation (Kokelaar, 1983). A ubiquitous feature of juvenile grains in the 2-3 $\phi$ (0.25-0.125 mm) fraction is a few μm-thick yellowish palagonite coatings (Fig. 7.7e,f).

Juvenile fragments contain olivine phenocrysts and Ca-rich pyroxene microcrysts and microlites embedded in a sideromelane groundmass (Fig. 7.7b). Glass compositions of all juvenile grains from analysed samples show a tight compositional range, with $SiO_2$ ranging from 47.9 to 48.7 wt.% (from normalized data; Appendix B, section B.2) (Fig. 7.7j).

Lithic components are scarce (<<10 vol.%) throughout and consist of ash and few coarse lapilli to block-sized fragments derived from the Waitemata Group (section 3.2). This contrasts strongly with phreatomagmatic deposits from other AVF sites where the lithic content may reach 65 to 80 vol.% (Allen et al., 1996; Németh et al. 2012a; Agustín-Flores et al., 2014). In the 2-3 $\phi$ fraction (0.25-0.125 mm), lithic particles (comprising less than 15 vol.% within these fractions) are mainly individual quartz and plagioclase grains (Fig. 7.7f) derived from the Waitemata rocks, which were probably broken up by vent explosions and/or recycling into the vent.

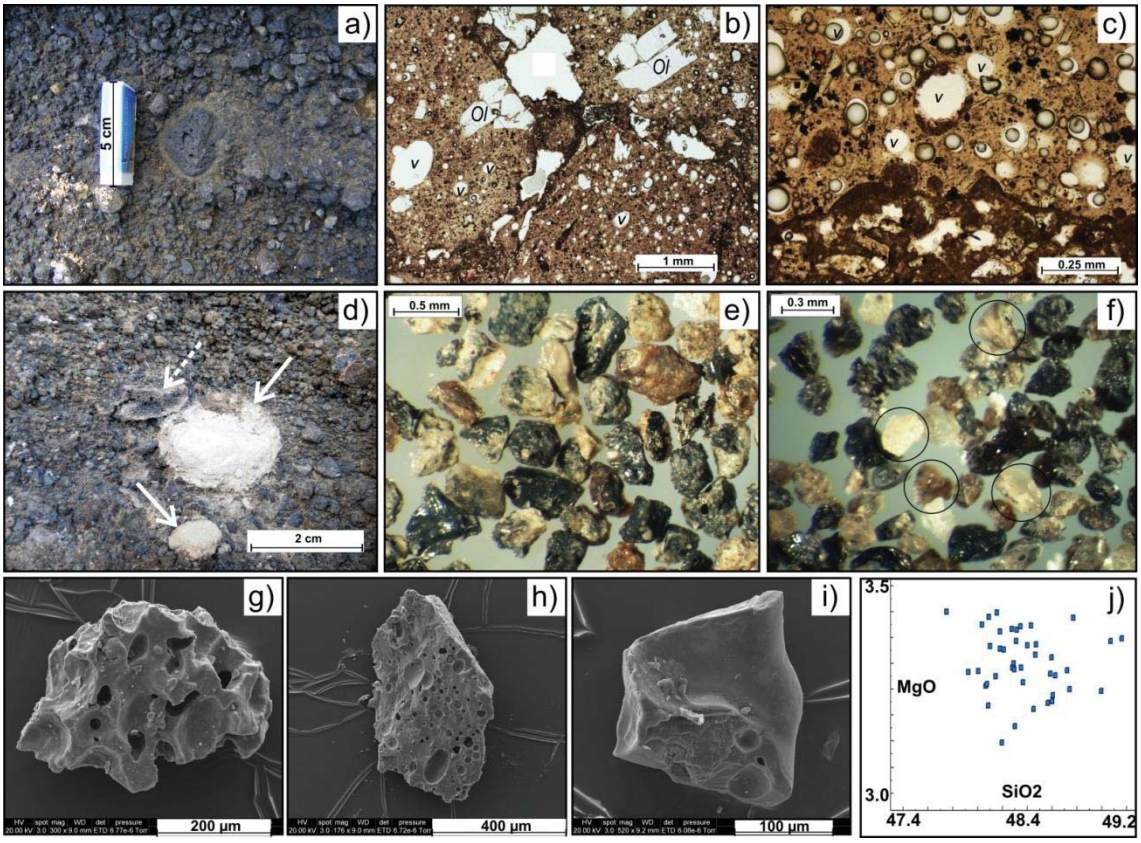


**Fig. 7.7**. a) Pyroclast characteristics of consolidated lithofacies LT1 present in PH1. Note the prevalence of sub-angular to angular, low vesicularily, juvenile fragments. b) and c) Plane-polarised, transmitted light photomicrographs of juvenile fragments from LT1. Thick walls between spherical/sub-spherical vesicles ("*V*") are widespread (Ol= olivine). d) Sub-angular to angular, juvenile fragments characterize lithofacies L1. Continuous, white arrows point at two sub-spherical lithic fragments; dashed, white arrow indicates a scoriaceous fragment. e) and f) Stereo microscope images of the 2 and 3 $\phi$ (0.25-0.125 mm) fractions representing lithofacies L1 and L2 respectively. Blocky and equant juvenile fragments dominate. Some fragments exhibit a thin, yellowish layer of palagonite. The encircled fragments in f) are rare quartz and plagioclase accidental crystals. g), h), i) Scanning electron microscope images of typical juvenile grain morphologies in the 2 $\phi$ (0.25 mm) fraction. Low vesicularity, angular fragments dominate. j) Scatter graph of the $SiO_2$ wt.% and MgO wt.% (normalized values; Appendix C, section C.2) showing a narrow range of glass compositions for both elements in the selected samples from different sites (Appendix C, section C.2).

### 7.5.2 Lithofacies

*Consolidated, lapilli-rich lithofacies (LT1 and LT2)*. LT1 (up to 5 m-thick) is contained in the entire PH1 (Fig. 7.2), whereas LT2 (up to 0.3 m-thick) is present in parts of PH2 (Fig. 7.3). LT1 (Fig. 7.6a,b) is dominantly clast-supported, massive to crudely-bedded, moderately sorted, ungraded, and mainly composed of juvenile coarse ash and fine lapilli (Table 7.2). Open framework textures occur in the coarser-grained beds and vesicular tuff (vesicles of sub-millimetre to millimetre) in the finer ones is also present (e.g. Lorenz 1974b). LT2 (Fig. 7.6c,d) is matrix-supported, massive, poorly sorted, ungraded, juvenile-rich coarse ash and fine lapilli (40-50 vol.%) and lithic-rich ash (up to 50 vol.%) (Table 7.2). No internal bedding or lamination is observed. Beds of both lithofacies dip outwardly from the crater at 10° or

**Table 7.2**. Nomenclature, grain size/sedimentary characteristics, and interpretation of lithofacies identified for the North Head phreatomagmatic deposits

| | *Lithofacies*<br><br>*(thickess)* | ➢ Grain size (approx. vol.% content in lithofacies)<br><br>➢ *Total juvenile vol. % in lithofacies* | ➢ Sorting<br><br>➢ Grading | Sedimentary characteristics | Interpretation |
|---|---|---|---|---|---|
| Consolidated, lapilli rich | *LT1*<br>(Figs. 3, 7a,b)<br><br>*(up to 5 m)* | ➢ Coarse ash-to-fine lapilli (>90%)<br><br>➢ *>90%* | ➢ Moderate<br><br>➢ Ungraded | Massive to crudely-parallel bedded sequences. No ripple or cross bedding are observed. Dominantly clast-supported, but fragments may be embedded in an incipient matrix composed of accidental ash. Some sections of the lapilli tuff is vesicular and/or palagonitized (Fig. 4b). | Sub-aerial deposition by fall from dense tephra jets and phases of continuous up-rush |
| | *LT2*<br>(Figs. 4, 7c,d)<br><br>*(up to 0.3 m)* | ➢ Coarse ash-to-fine lapilli (30-40%)<br>Matrix composed of lithic-rich ash (up to (60%)<br><br>➢ *40%* | ➢ Poor<br><br>➢ Ungraded | Massive beds with no internal bedding or laminations. Matrix supported. | Sub-aerial deposition by fall from non-juvenile particle-rich, discrete tephra jets. |
| Unconsolidated, clast-supported, open framework, lapilli rich | *L1*<br>(Figs. 4, 5, 7c,d,e,f,g,h)<br><br>*(up to 0.5 m)* | ➢ Coarse ash-to-coarse lapilli (>90%).<br><br>➢ *>90%* | ➢ Moderate to poor<br><br>➢ Reverse (dominates), normal | Crudely-bedded sequences containing internal layers with irregular contacts. Lenses of fine-to-medium lapilli occur within beds, as well as rare non-juvenile, lapilli-size fragments. Beds dip outward from the crater at 10°. Some degree of palagonitization is observed (Fig. 4e,f). | Deposition formed when pyroclasts falling from a slightly drier (compared to the activity that generated LT1 and LT2) column produced syn-impact grain flows. |
| | *L2*<br>(Figs. 6, 7i)<br><br>*(up to 25 m)* | ➢ Coarse ash to coarse lapilli juvenile fragments (>90%).<br><br>➢ *>90%* | ➢ Moderate<br><br>➢ Ungraded | Diffusely-bedded sequences. Rare mm-scale laminae of juvenile ash layers occur within the more dominant lapilli-rich beds. Beds dip outward from the crater at approximately 20° and 10° at the upper and lower beds respectively. Incipient palagonitization is observed (Fig. 4e,f). | Deposition from unmodified fallout deposits from slightly drier (compared to the activity that generated LT1 and LT2, sustained, low eruption columns. |
| | *LB*<br>(Figs. 5, 7f,g)<br><br>*(up to 0.5 m)* | ➢ Bombs (up to 25%)<br>Coarse ash to coarse lapilli (up to 75%)<br><br>➢ *>90%* | ➢ Poor<br><br>➢ Ungraded (dominates), reverse, normal | Crudely-bedded sequences with irregular and diffuse boundaries. Tens of cm-scale lenses of coarse lapilli occur. | Deposition of pyroclasts ballistically ejected and falling from an eruption column, with some modification by rare grain flows |
| Semi-Consolidated, ash rich | *T*<br>(Figs. 5, 7f,g,h)<br><br>*(less than 0.2 m)* | ➢ Coarse ash (up to 30%)<br>Lithic-rich medium to fine ash (up to 70%)<br><br>➢ *Up to 20%* | ➢ Poor<br><br>➢ Ungraded to subtly reverse | Diffusely-bedded, matrix-supported, laterally-continuous beds constituted by accidental ash and trains of coarse ash, juvenile lapilli. Layers exhibit undulations due to the irregularities on deposition surface and subtle soft-sediment deformation occurs at irregular intervals. No accretionary lapilli | Deposition from a combination of fall out and short run-out, low-energy base surges related to the collapse of non-spreading tephra jets |

*Interpretation*. LT1 is interpreted to be sub-aerially deposited tephra fall from frequent dense jets and phases of continuous up-rush (Kokelaar, 1986; Sohn and Chough, 1992), whereas LT2 likely resulted from sub-aerial fall deposition of discrete, lithic (ash)-rich, tephra jets.

*Unconsolidated, lapilli-rich, open framework, clast-supported lithofacies (L1, L2, and LB)*. L1 (Fig. 7.6c,d,e,f,g,h) (up to 0.5 m-thick) is crudely-bedded, moderately to poorly sorted with dominant reverse grading and internal layering with irregular contacts (lenses may occur) (Table 7.2). It contains beds dipping outwardly from the crater at 10°, and is dominantly composed of juvenile coarse ash to coarse lapilli. L1 occurs in PH2 (Fig. 7.3) and PH3 (Fig. 7.4). L2 (Fig. 7.6i) (up to 25-m thick) is diffusely-bedded, moderately sorted, ungraded, and constituted principally by juvenile coarse ash to coarse lapilli (Table 7.2). This lithofacies is contained entirely in PH4 (Fig. 7.5) and its lower and upper beds dip respectively at approximately 10° and 20° outwardly from the crater. LB (Fig. 7.6f,g) (up to 0.5 m-thick) is crudely-bedded, poorly sorted, dominantly ungraded (but reverse and normal grading is present), and composed of approximately 25 vol.% of juvenile bombs (up to 25 cm in size) and juvenile coarse ash to coarse lapilli (75 vol.%) (Table 7.2). LB is included in PH3 (Fig. 7.4) and exhibits lenses of coarse lapilli. Bombs do not form impact sags. Some degree of palagonization is observed in the fine fraction of these three lithofacies (Fig. 7.7e,f).

*Interpretation.* L1 lithofacies may represent deposits formed when pyroclasts falling from a slightly drier column (compared to the initial activity that generated LT1 and LT2) produced syn-impact grain flows (cf. Sohn and Chough, 1993). It is possible that the coarser pyroclasts were ballistically ejected. L2 beds appear to be unmodified fallout deposits from slightly drier (compared to the initial activity that generated LT1 and LT2), sustained, low eruption columns. LB lithofacies were probably the result of deposition of pyroclasts ballistically ejected and/or falling from an eruption column, with some modification by rare grain flows on landing.

*Semi-consolidated, ash-rich lithofacies (T).* This lithofacies (Fig. 7.6f,g,h) (up to 0.2 m-thick), which is contained in PH3 (Fig. 7.4), comprises diffusely-bedded, matrix supported, poorly sorted, weakly reversely graded to ungraded, laterally continuous beds composed mainly of lithic-rich ash and trains of juvenile coarse ash (up to 30 vol.%) (Table 7.2). Subtle soft-sediment deformation is present but not widespread (Fig. 7.6g).

*Interpretation*: Lithofacies T likely resulted from the deposition of a combination of tephra fall and short run-out, low-energy base surges related to the collapse of non-spreading tephra jets (e.g. Belousov and Belousova, 2001).

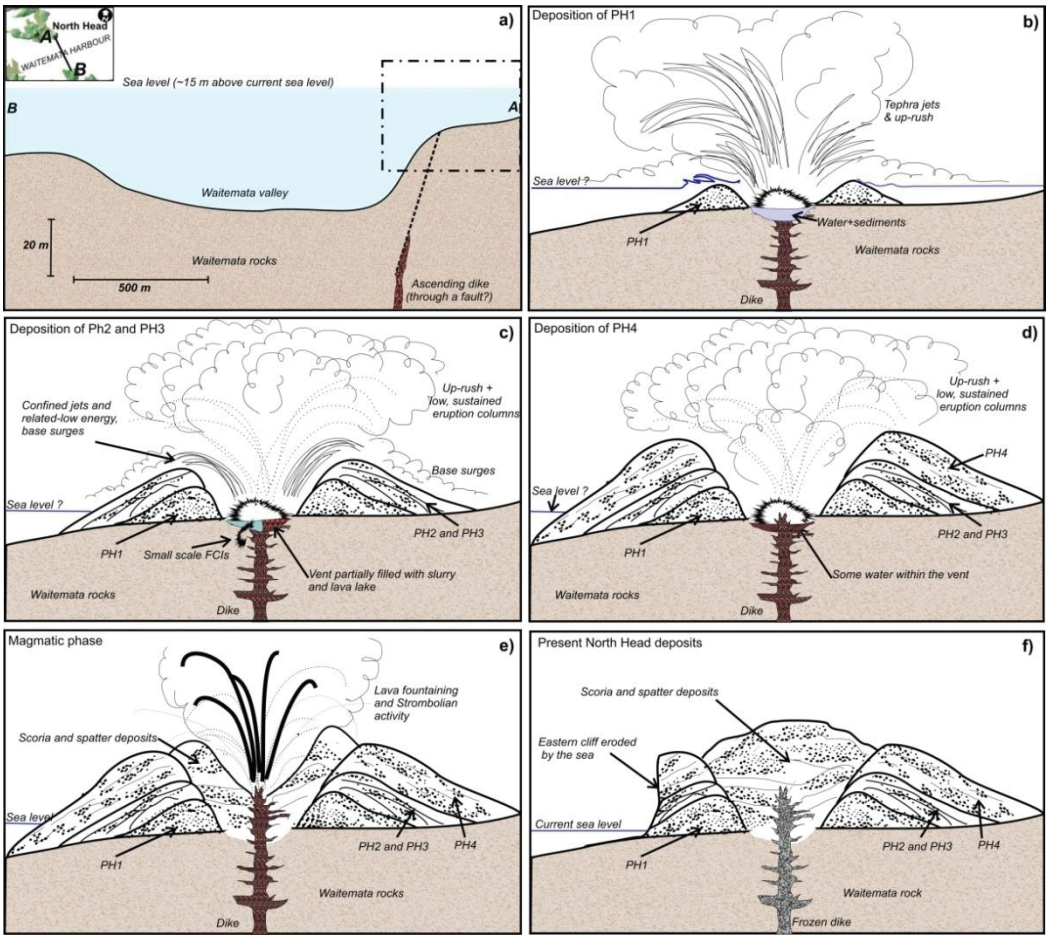


**Fig. 7.8**. Cartoons representing a simplified model of the North Head eruption history and construction. Figures are not to scale. The real morphometric parameters of the cone (height, crater depth, and bed slopes) are distorted in the figures. Dike intrusion and position is hypothetical. For a more detailed eruption sequence see section 7.6 in the text. a) Hypothetical pre-eruptive conditions. The broken line rectangle represents the area for the following figures. b) Deposition of phreatomagmatic subunit 1 (PH1) in deepest water. c) Deposition of phreatomagmatic subunit 2 (PH2) and phreatomagmatic subunit 3 (PH3) when water partially filled the vent. It is possible that lava ponds were contemporaneous. d) Deposition of phreatomagmatic subunit 4 (PH4) as more stable up-rush and eruption columns dominated. e) Water was cut off finally from the vent and fire-fountaining and Strombolian activity completed the eruption sequence. f) Current conditions of North Head volcano. The sea ward, eastern coastal flank of the volcano has been partially eroded by waves.

## 7.6 Tuff cone construction and eruption dynamics

### 7.6.1 Phreatomagmatic subunit PH1

The first phase of the North Head eruption that can be inferred from deposits (LT1 in PH1; Fig. 7.2) was dominated by tephra jets and phases of up-rush (section 7.5.2; Table 7.2) (Fig. 7.8b). These deposits are very close to the inferred vent, consistent with Kokelaar's (1986) observation of discrete jets from Surtsey halting almost immediately with little lateral transport (cf., traction features described by Sohn and Chough, 1992). Vesicular tuff beds show that abundant liquid water was present within the jets (section 7.5.2; Table

7.2) (cf., Lorenz, 1970, 1974a, 1974b). PH1 exhibits no other sign of water excess (e.g. mudflow channels, gravity flow ripples, bedding sags). LT1 units (c. 8 m above the basal surface) show no characteristics consistent with subaqueous mass flow or inter-tidal and wave action, suggesting that they were deposited subaerially due to the tephra pile building up and possibly forming a barrier to the shallow surrounding water (cf., Martin and Németh, 2005).

### 7.6.2 Phreatomagmatic subunit PH2

As the tuff cone grew upward sub-aerially, PH2 (Fig. 7.3) was deposited and comprises an alternating sequence of lithofacies LT2 and L1 (Section 7.5.2; Table 7.2). LT2 may represent the deposits of discrete, lithic-rich jets (Fig. 7.8c), or slurry flows that splashed out of the crater (Belousov, written communication, 2014). Either way, abundant water was available during deposition (Fig. 7.8c). Also, lithic-rich ash in LT2 suggests some fragmentation and excavation of country-rock fragments (section 7.5.2; Table 7.2), which formed a muddy slurry in the vent area for a short period (Fig. 7.8c). L1 represents tephra fall during periods when more stable eruption columns formed (section 7.5.2; Table 7.2) (Fig. 7.8c). Coarser lapilli and bombs were ejected ballistically. The fine grainsize in these proximal deposits (coarse ash to fine lapilli) and low vesicularity of juvenile fragments in L1 (section 7.5.1) show the continued dominance of water-magma interaction.

### 7.6.3 Phreatomagmatic subunit PH3

In the PH3 (Fig. 7.4), lithofacies T (poorly sorted and diffusely-bedded, ash rich beds) deposition began via low-energy base surges (section 7.5.2; Table 7.2). These are envisaged as weak base surges resulting from the collapse of 100-150 m high narrow jets (e.g. Belousov and Belousova, 2001). Continued deposition of L1 beds also indicates the formation of a relatively stable eruption column (Fig. 7.8c). The absence of LT2 beds shows that less water was available to form tephra jets.

The fall-deposited lithofacies LB is dominant in PH3 (Section 7.5.2; Table 7.2), showing a greater degree of magmatic gas-expansion fragmentation alongside the magma-water interaction (cf., Valentine and Gregg, 2008) (section 7.5.2). Common fluidal bombs and the presence of both LB and T beds may indicate that a small lava lake had filled parts of the crater or a “dry” vent had formed alongside the main eruption centre (Fig. 7.8c). Coarse lithics and bombs appear to slightly deform L beds (Fig. 7.6f,g), or are embedded within ash (Fig. 7.6h). Overall, PH3 deposits suggest that less water was available in the eruption centre.

### 7.6.4 Phreatomagmatic subunit PH4

The transition upward from PH3 to PH4 is gradational, with PH4 (Fig. 7.5) being entirely composed of lithofacies L2 (section 7.5.2; Table 7.2). At this stage, tephra jets had stopped and grain flows were rare or absent. The continued fine grain size (coarse ash to fine lapilli) and the low vesicularity of the proximal

juvenile fragments in L2 and L1 (section 7.5.1), show that magma-water fragmentation remained dominant (cf., Kokelaar, 1986). There was a stable eruption column also formed during this phase with tephra fall dominating (Fig. 7.8d). This phase led to exclusion of water from the vent, and a subsequent change to magmatic eruptions, producing scoria and spatter (Fig. 7.8e). The small total volume of the entire volcano and the lack of discontinuities and unconformities in the entire sequence indicate a continuous eruption that may have lasted hours to days (e.g. ~6 days for a typical average eruption rate of 5 $m^3/s$; c.f., Kereszturi et al., 2013).

## 7.7 Water influence on magma fragmentation

The range in vesicularity of pyroclasts in lithofacies L1 and L2 (5-65%) (section 7.5.1) is broad and lower than that of typical magmatic "dry" eruptions (70-80%; Houghton and Wilson, 1989). Clast vesicularity is lowest in lithofacies LT1 and highest in L1/L2. The broad vesicularity range may indicate that the magma was chilled and fragmented at varied degrees of vesiculation, such as in the Surtseyan eruptions at Karymskoye (e.g. vesicularity of 7 to 63%, Belousov and Belousova, 2001), the Capelas tuff cone (18 to 59%, Mattsson, 2010), or Black Point volcano (4 to 89%, Murtagh and White, 2013). Water-magma driven fragmentation throughout the tuff cone construction is also supported by vesicles being small (mean ~60 μm) with thick walls (>50 μm) (section 7.5.1), and pyroclasts having dominantly equant, blocky, angular to sub-angular pyroclast morphologies (section 7.5.1) (cf., Wohletz, 1983; Zimanowski et al., 1991). The palagonitization of the deposits (section 7.5.1) and the presence of sideromelane in thin section also indicate rapid quenching of magma with water (Fisher and Schmincke 1984). Lithofacies LT1, LT2 and T (section 7.5.2) suggest the highest water to magma ratios, whereas there may have been less-efficient water-magma interaction during deposition of L1, L2, and LB (section 7.5.2).

Magma fragmentation in Surtseyan eruptions is triggered by explosively expanding steam as magma rises into water, and there is little heat exchange by direct contact such as in fuel-coolant interactions (Kokelaar, 1986). Mastin (2007) and Mastin et al. (2009) show that such fragmentation occurs via the growth and breakage of glassy rinds on deforming magma surfaces during turbulent mixing and impact of tephra jets on the volcano slopes. In Surtseyan eruptions, jets up to 500 m-high enhance particle surface cooling and subsequent breakage on landing.

## 7.8 North Head volcano and Surtseyan activity in the AVF context and hazard implications

The Waitemata Harbour (Fig. 3.1) was formed by the post-glacial rise in sea level, from 14-10 k.y. B.P. (Searle, 1959). From 5.5 to 3 k.y. B.P., the sea stood at 0.5 m-1.0 m above present day levels (Hannah et al., 2011). Siddall et al. (2006) suggest that approximately from 128 to 116 ka, global sea levels were 2-4 m higher than current sea levels. Other high-stands in New Zealand are: ~101 ka (~11 m below present sea level), ~81 ka (~20 m below present sea level), and 60 ka (~24 m below present sea level) (Pillans, 1983). Global interglacial highstands prevailed from 190 to 240 ka, but these were 5-15 m below current

sea level (Siddall et al., 2006). Given the absence of post 14 ka. B.P. tephra layers corresponding to North Head in nearby sediment cores (Molloy et al., 2009; Bebbington and Cronin, 2011), and recognising the tectonic stability in the AVF area (Beavan and Litchfield, 2012), the most likely time for North Head eruption falls between 128 and 116 ka when the sea level was 10-12 m above the current sea level. This equates to a water depth of 10-12 m, which is shallower than most other examples of Surtseyan activity: 130 m at Surtsey (Thórarinsson, 1964); 70 m at Capelinhos (Machado, 1958); 40-50 m at Karymskoye Lake, Kamchatka (Belousov and Belousova, 2001); and 55 m at Capelas tuff cone, Azores (Solgevik et al., 2007). Recognising this, however, even though the base of the eruptive surface was 130 m below sea level at Surtla (Iceland), tephra jets broke the water when the volcanic pile was just ~5 m below sea level (Kokelaar, 1986). Tephra jets (the dominant deposit emplacement mechanism recognised for lithofacies LT1 and LT2; section 7.5.2; Table 7.2) rarely pierce the surface from more than a few meters depth (White, 1996; Németh et al., 2006) as the explosive processes become more vigorous with shallowing. This may indicate that the North Head eruption started at very shallow water depths of <15 m and LT1, which was emplaced sub-aerially (section 7.5.2), may represent the emergent stage of the eruption. Interestingly, Ilchulbong and Udo tuff cones (Jeju Islands, South Korea) (Sohn and Chough, 1992, 1993) appeared to have been constructed over a basalt plateau covered with shallow sea water (exact depth is not provided, but several meters are inferred). Additionally, 17 tuff cones located on Marion and Prince Edward islands (Indian Ocean) are inferred to be built from Surtseyan eruptions close to or at sea level (Verwoerd and Chevallier, 1989).

The processes during formation of the North Head tuff cone can only be interpreted from exposures of proximal deposits (section 7.4.1), which only show minor evidence of base surges (section 7.5.2). Medial to distal deposits from other Surtseyan eruptions show more distinct base surge deposits compared to proximal sites (e.g. Capelas tuff cone, Azores; Solgevik et al., 2007), so it is reasonable to assume that North Head produced these also. The Surtseyan base surge deposits lack climbing ripples, antidunes, and long wavelength beds, implying that they were of lower energy compared to some produced during maar/tuff ring formation (Solgevik et al. 2007). The onset of North Head activity involved ejection of tephra jets, but it subsequently produced more stable eruption columns, with both weak base surges and tephra falls, until eventually water was excluded from the vent and scoria/spatter was produced.

In the emergent stage of Surtsey, Capelinhos, and Karymskoye Lake eruptions, multiple major tephra jets were ejected at varied angles, reaching heights of tens of metres up to ~1 km, and at Capelinhos ~1.4 km (Kokelaar, 1986; Belousov and Belousova, 2001). Collar-type, pyroclast-poor surges spread radially for several hundred metres from the base of the emerging jets also at these volcanoes (Machado, 1958; Thórarinsson, 1964; Belousov and Belousova, 2001). Collapse of particularly large jets produced ground-hugging base surges that travelled radially up to 600 m from the vent. At Capelinhos surges reached >2 km (Cole et al., 2001), while reaching 1.3 km at Karymskoye. Up-rush tephra columns up to 2 km in height were documented at Surtsey and Capelinhos. In the latter, ash fall at approximately 1.2 km northwest of

the eruption reached up to 1.9 m thick during single nights of the eruption, (Cole et al., 2001). Belousov and Belousova (2001) report bombs (10 cm to 2 m) ejected out to 1.3 km from the vent from similar eruptions. The Karymskoye eruption also generated local tsunamis (Belousov and Belousova, 2001), with large concentric radiating waves having wavelengths of ~100 m. The run-up of these tsunamis reached 20-30 m near the eruption and 2-3 m around 4 km away.

The exact location of the next eruption in the AVF is unknown (cf., Bebbington and Cronin, 2011). Assuming that the next eruption may occur at any site inside the ellipse shown in Fig. 7.1a, and considering that an ascending magma interacting with a body of water may promote a Surtseyan eruption (as the examples illustrated above), any volcano erupting nowadays within the area covered by water (~35%) may display Surtseyan dynamics. With the forecast of rising in sea-level in the future in Auckland (Hannah et al., 2011), the submerged area will be progressively enlarged with the consequence that any future eruption taking place in this area may exhibit Surtseyan activity. Certainly, the styles of phreatomagmatism may vary and it will depend on many factors such as the amount of water relative to that of magma and the efficiency with which water and magma mix (White and Houghton, 2000). The calculations of the probability of the occurrence of Surtseyan eruption in the AVF however is beyond the scope of this study.

The proximal hazards related to such an eruption could be very destructive within the Auckland area. A large proportion of the Auckland population, the central business district (CBD), the largest New Zealand shipping port and the Auckland airport are located on the coast within the AVF (Fig 3.1). Hazards related to Surtseyan eruptions are not explicitly considered in models related to hazard assessment for the AVF (e.g. Sandri et al., 2010; Kereszturi et al., 2014), an oversight that should be remedied with urgency.

## 7.9 Conclusions

The North Head edifice was first constructed by a Surtseyan phase that likely lasted hours as magma emerged through shallow water of the proto-Waitemata Habour. The eruption started with tephra jetting that was later entirely replaced by semi-continuous tephra uprush and the formation of more stable tephra columns, with collar-like base surges throughout. Water was eventually excluded from the vent, leading to a magmatic phase filling the crater of the Surtseyan cone with spatter/scoria. Based on inferred paleo sea-levels in Auckland, the age of North Head is likely to be between 128-116 ka, when the sea level was at least 12 m above the pre-eruption surface.

The North Head eruptive scenario contrasts with those for other phreatomagmatic eruptions in the AVF, where magma-groundwater interaction produced violent base surges and built broad tephra rings. Lower sea levels during most AVF eruptions explain the lack of Surtseyan tuff cones. Now that approximately 35% of the field is covered by up to 30 m of water (mostly <5 m) and with sea rise forecasted, the occurrence of future AVF eruptions within the submerged area may display Surtseyan dynamics similar to

North Head. Such eruptions, based on observed analogues, would be characterized by ash fall, ballistically emplaced pyroclasts, and low-energy base surges. Further, local wave-generation and tsunami may also occur. Given the concentration of high-value housing, the major seaport and airport of Auckland along the low coastline, the hazards associated to such eruptions must be considered.

DRC 16

MASSEY UNIVERSITY
GRADUATE RESEARCH SCHOOL

## STATEMENT OF CONTRIBUTION
## TO DOCTORAL THESIS CONTAINING PUBLICATIONS

(To appear at the end of each thesis chapter/section/appendix submitted as an article/paper or collected as an appendix at the end of the thesis)

We, the candidate and the candidate's Principal Supervisor, certify that all co-authors have consented to their work being included in the thesis and they have accepted the candidate's contribution as indicated below in the *Statement of Originality*.

**Name of Candidate:** Javier Agustín Flores

**Name/Title of Principal Supervisor:** Karoly Németh

**Name of Published Research Output and full reference:**

Agustín-Flores J., Németh K., Cronin S., Lindsay J., Kereszturi, G., 2015. Construction of the North Head (Maungauika) ruff cone: a product of Surtseyan volcanism, rare in the Auckland Volcanic Field, New Zealand. Bulletin of Volcanology, 77: 11. Doi 10.1007/s00445-014-0892-9

**In which Chapter is the Published Work:** Chapter 7

Please indicate either:

- The percentage of the Published Work that was contributed by the candidate:

  and / or

- Describe the contribution that the candidate has made to the Published Work:

  Organization and completion of the whole field work and most laboratory work, main contributor on writing and editing of manuscript draft, and subsequent correcting and editing for final version

Javier Agustin-Flores — Digitally signed by Javier Agustin-Flores DN: cn=Javier Agustin-Flores, o=Massey University, ou=Institute of Agriculture and Enviroment, email=kiaoranet@yahoo.co.nz, c=NZ Date: 2015.04.23 15:13:43 -05'00'

Candidate's Signature — 08/05/2015 — Date

Karoly Nemeth — Digitally signed by Karoly Nemeth DN: cn=Karoly Nemeth, o=Massey University, ou=Institute of Agriculture and Environment, email=K.nemeth@massey.ac.nz, c=NZ Date: 2015.05.11 16:32:49 +12'00'

Principal Supervisor's signature — 11/05/2015 — Date

# Chapter 8. Discussion and conclusions

**Contents** Page



## 8.1 Introduction

The three main case studies of the Auckland Volcanic Field (AVF) presented in this thesis emphasize how differences in substrate geology and hydrogeology strongly impact on the processes and deposits of phreatomagmatic eruptions. The three eruptive scenarios treated in chapters 5, 6, and 7 are summarized in the first section of this chapter. The consolidation of these scenarios is the consequence of the integration of the results obtained in the development of this study. These key results comprise the information regarding the stratigraphy and sedimentary characteristics of deposits, the characterization of pyroclasts and the insights into the understanding of the substrate conditions. The three studied cases are then seen in a wider geological setting context (the AVF and worldwide), analysing their possible contribution regarding small basaltic phreatomagmatic eruptions.

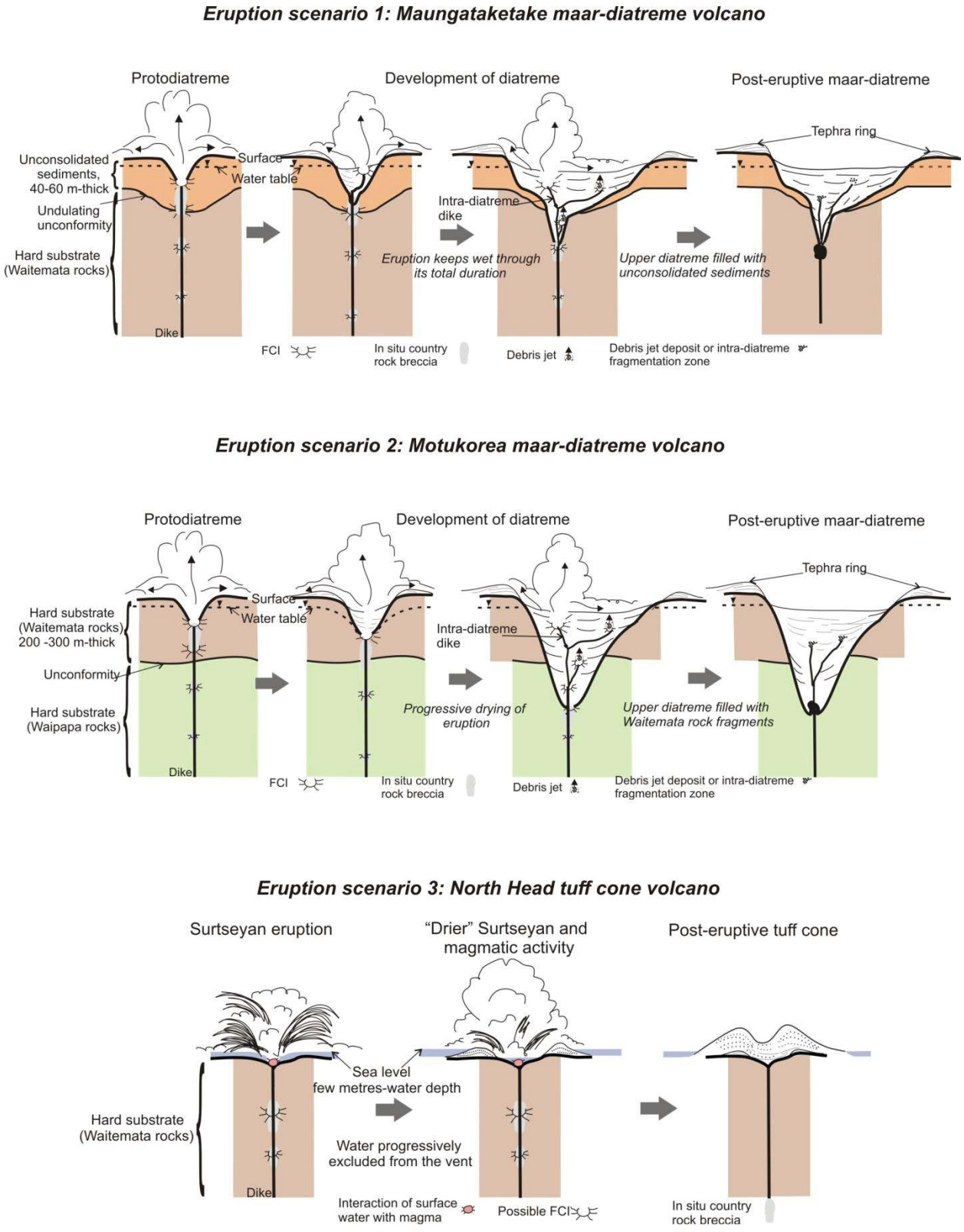


**Fig. 8.1** Schematic and simplified representation of the three phreatomagmatic eruption scenarios for different settings in the Auckland Volcanic Field. The concluding magmatic phases are not included. Scenario 1 and Scenario 2 follow closely the model of Valentine and White (2012), in which shallow seated explosions formed the ejecta rings. Scenario 3 represents a Surtseyan eruption, which is not typical of the AVF. Unlike the base surge-dominated eruptions scenarios 1 and 2, the evidence shows that the tuff cone in Scenario 3 was formed by pyroclast fall out.

## 8.2 Highlights of the studied cases (chapters 5, 6, and 7)

### 8.2.1 Eruption scenarios

#### 8.2.1.1 Scenario 1: the formation of Maungataketake maar-diatreme volcano (Fig. 8.1)

In the Manukau Lowlands (Fig. 3.1) when hydrogeological conditions where similar to the current ones (>125 ka), magma interacted with groundwater contained in both water-saturated, unconsolidated sediments (Tauranga Group and Kaawa Formation) and confined aquifers (Waitemata Group). The initial crater was opened at shallow depth within the unconsolidated sediments (<100 m). Due to the unconsolidated nature of the sediments crater wall collapse was pervasive in the initial stages of the eruption. The contrast between the soft and hard substrate and the soft nature of the overlying sediments itself, may have caused the emplacement of diverted and splayed dikes. This generated phreatomagmatic explosions located at shallow levels and displaced from a central locus. Crater wall collapse continued at this stage and caused enlargement of the crater. Relative deepening of phreatomagmatic explosions occurred when Waitemata rocks were disrupted as evidenced from the mid-section of the tephra ring. A mature diatreme was formed whose infill was composed dominantly of the unconsolidated sediments. The most abundant presence of this material and the sedimentary characteristics in the ejecta ring suggests that it was built from material deposited from base surges generated by shallow-seated explosions. Base surges were of moderate energy and travelled <2 km from the vent, and due to the moisture content, had a high sedimentation rate. Subordinate fall also occurred. Water-saturated, unconsolidated sediments filling the diatreme probably promoted uninterrupted phreatomagmatic explosions until the onset of the concluding magmatic phase. This change could have been brought about by a change in magma flux and/or magma lining and sealing the walls of the shallow conduit. The phreatomagmatic eruptive phase lasted for few days.

#### 8.2.1.2 Scenario 2: the formation of Motukorea maar-diatreme volcano (Fig. 8.1)

During the late Pleistocene when sea level was lower than today in the northern AVF (Fig. 3.1), magma interacted with groundwater contained in the 200-300 m-thick Waitemata rocks, which overlie the Waipapa greywacke rocks. An initial crater was opened at shallow depths. Semi-confined and confined aquifers provided water for phreatomagmatic explosions to occur at deeper levels promoting the enlargement of the crater by ejection of disrupted material and crater wall collapse. A mature diatreme was eventually formed and filled with fragments of the disrupted Waitemata rocks. Deeper explosions within the Waipapa rocks are not ruled out, but these fragments contributed little to the tephra ring construction as shown by the componentry analyses of ejecta ring deposits. This observation implies that at this stage, the ejecta ring was built by the deposition of material transported by base surges generated in shallow-seated explosions within the diatreme fill. The base surges travelled 1-2 km from the vent. Fall out was progressively more abundant as the eruption developed, but never dominant. The eruption was

characterized by a progressive drying until the eruption became dominantly magmatic. The phreatomagmatic eruptive phase probably lasted for few days

#### 8.2.1.3 Scenario 3: the formation of North Head tuff cone volcano (Fig. 8.1)

This eruption was through shallow water (~12 m) within the northern AVF probably at the end of the Last Interglacial (128-116 ka). No evidence for systematic, important excavation into the Waitemata rocks was found. Initially, the tephra cone was constructed from the deposition of material contained in tephra jets. "Wet" pyroclastic fall out (from up-rush clouds and low eruptive columns) was dominant until water was prevented from entering the vent. Eventually, "drier" Surtseyan activity followed. At this stage, periods of purely magmatic activity occurred simultaneously or at intervals. Subsequently, water was not available for sustaining phreatomagmatic explosions and the eruption shifted to a magmatic phase. Fall out was the dominant mechanism of deposition of pyroclasts, but associated low energy, base surges were also present. Considering base surges in North Head-type eruptions are not energetic, which is consistent with the examples reported in the literature (e.g. Belousov and Belousova, 2001), it is possible that their run-out distances were in the range of hundreds of meters. The tephra cone was probably formed in the course of hours to a few days.

### 8.2.2 Integration of results

Table 8.1 shows a summary of the different characteristics for the three studied volcanoes, compiled from the results of chapters 5, 6, and 7. Some of the most relevant aspects of these results are next described in a comparative manner between the three scenarios.

#### 8.2.2.1 Eruptive centres and types of deposits

Maungataketake shows a very broad crater surrounded by a roughly irregular ejecta ring with a low rim and gentle slopes (Table 8.1). The entire shape and extent of the Motukorea ejecta ring and crater is not possible to distinguish. Although it is not directly observable that Maungataketake and Motukorea phreatomagmatic craters are cut beneath the pre-eruption ground surface, the evidence gathered during this study (moderate size crater diameter, lithic-rich ejecta ring deposits, and geophysical inference of magmatic bodies infilling a deep crater) point to the fact that those are maar craters underlain by a diatreme. North Head's tuff cone has relatively steeper slopes and a narrow crater typical of tuff cones.

Fall deposits dominate North Head, whereas base surge units characterize Maungataketake and Motukorea ejecta ring deposits (Table 8.1). The wettest deposits were emplaced at Maungataketake where the most abundant accretionary lapilli and soft-sediment deformation features occur. Unlike Motukorea base surge deposits, erosive boundaries are not pervasive at Maungataketake ejecta ring exposures. "Wetness" of deposits diminishes upwards the Motukorea phreatomagmatic sequence, with increasing evidence of pyroclastic fall. Conversely, "wetness" is relatively pervasive within the entire

Maungataketake phreatomagmatic units. North Head deposits exhibit progressively drier sedimentary characteristics upwards.

**Table 8.1** Summary of the general morphometric, stratigraphic, sedimentary, and pyroclast characteristics of the studied volcanoes

| | Maungataketake | Motukorea | North Head |
|---|---|---|---|
| Morphological type | Maar | Maar | Tuff cone |
| Volume of tephra ring/cone ($m^3$) | $4.3\times10^6$ | $3.1\times10^6$ | $1.1\times10^6$ |
| Crater diameter (m) | 1300×1100 | Partial tephra ring, ~<1000 | ~220-280 m |
| Crater depth | Unknown | Unknown | Unknown |
| Maximum rim height (m) | 25 | 40 | ~50-60 |
| Dip of outer beds | Nearly horizontal to less than 20° | Few degrees to less than 20° | Lower beds: up to 10°<br>Upper beds: up to ~22° |
| Dominant stratification | Plane parallel bedded, cross-lamination | Cross- to plane- parallel- bedded | Massive to crudely stratified |
| Sedimentary features | Overall accretionary lapilli and soft sediment deformation | Dominant soft sediment deformation and erosive surfaces in the lower deposits | Common open framework, non erosive surfaces |
| Vesiculated tuff | Yes | No | Yes |
| Main transport mode of pyroclasts | Wet base surges, minor fallout | Wet/dry base surges, fallout | Fallout, minor base surges |
| Dominant grain size | Fine lapilli to fine ash | Medium lapilli to medium ash | Coarse lapilli to coarse ash |
| Dominant juvenile grain size | Coarse ash to medium lapilli | Coarse ash to medium lapilli | Coarse ash to medium lapilli |
| Juvenile content (vol.%) | 35 | 40-45 | >90 |
| Juvenile vesicularity | Poor (<30 %) | Poor (<30%) | Variable (5-65%) |
| General juvenile morphology | Sub-angular, sub-rounded, blocky | Sub-angular, angular, blocky, fluidal | Angular, blocky, fluidal |
| Adhering particles | Yes | Yes | No |
| Dominant lithic type | Plio-Pleistocene sediments | Waitemata rock fragments | N/A |
| Substrate type | Waitemata rocks + 60-m Plio-Pleistocene sediments | Waipapa rocks + 200/300 m of Waitemata rocks | Waitemata rocks |
| Water involved | Groundwater | Groundwater | Superficial water |
| Underlain by diatreme | Yes possible, inferred | Yes possible, inferred | No, inferred |
| Followed by dry activity | Yes | Yes | Yes |
| Length of phreatomagmatic eruption | Few days | Few days | Hours to very few days |

.

### 8.2.2.2 Characteristics, percentage contents and distribution of pyroclasts

North Head tuff cone deposits differ strongly from the other centres in being dominated by juvenile fragments (>90 vol.%) compared to ~45 vol.% at Motukorea and ~35 vol.% for Maungataketake ejecta ring deposits (Table 8.1), which is typical of maar-diatreme volcanoes. The bulk of juvenile pyroclasts are in the range size of medium lapilli-to-coarse ash in all of the studied deposits.

North Head juvenile pyroclasts are the most angular: The Motukorea juvenile fragments are angular-to-subangular with some having fluidal shapes, while Maungataketake ones are blocky and sub-angular to sub-rounded (Table 8.1). Adhering, fine lithic-ash on the surfaces of juveniles is widespread on Maungataketake and Motukorea fragments, but not on North Head clasts. The general range in vesicularity of North Head juveniles is broader (~5 to 65%) than at the other two sites (usually <30%) (Table 8.1). Both sideromelane and tachylite occur in all volcanoes, with Motukorea containing the highest proportions of sideromelane (>50 vol.%). Palagonitization is not pervasive, but most evident in North Head and Motukorea.

North Head tuff cone deposits contain very few substrate-derived lithics (<10 vol.%), compared to Maungataketake (~65 vol.%) and Motukorea (~55 vol.%) ejecta ring deposits (Table 8.1). The lithics are concentrated in the medium-to-fine ash-size range in Maungataketake (~50-60 vol.%) and Motukorea (~30-40 vol.%). The Maungataketake lithic ash is mainly made up of particle aggregates of individual crystals of quartz and feldspar (>80 vol.%) sourced from the Plio-Pleistocene sediments (Table 8.1). By contrast, Waitemata fragments dominate Motukorea lithic ash (> 80 vol.%).

### 8.2.2.3 Local eruptive settings and environmental conditions

Three distinct general eruption settings are recognized (Fig. 8.1): a) >60 m-thick soft Plio-Pleistocene sediments onto hard Waitemata Group rocks (Scenario 1); b) Waitemata rocks onto basement (Scenario 2); and c) a shallow submarine setting (Scenario 3). Waitemata rocks are the most common lithology in the AVF area and these host low yield, anisotropic, heterogeneous, confined or semi-confined aquifers. Thickness of the Waitemata rock sequence is not known at Maungataketake, but beneath Motukorea and North Head it reaches at least 200-300 m.

The Auckland area has remained tectonically more stable than many parts of New Zealand since the onset of the AVF activity (250 ka) (Alloway et al., 2004; Beavan and Litchfield, 2012; Kenny et al., 2012). A paleo-environmental reconstruction at Maungataketake (Marra et al., 2006) suggests that general environmental conditions were similar to the present during the Maungataketake phreatomagmatic eruption (in the Manukau Lowlands). Cover-bed stratigraphy and dating imply that the eruption is older than 125 ka.. At Motukorea (in the northern AVF), an Ar-Ar age determination on juvenile material of 14.3 ±5.5 ka was recently obtained (Leonard Graham, written communication 2014). This is consistent with a

mid-Holocene beach-level on the island and indicates the eruption occurred when sea level was possibly up to 30 metres lower than today. The eruption site lay above sea level near the banks of the ancestral Tamaki River. When sea level was lower during both Maungataketake and Motukorea eruptions, the now submerged area of the AVF was irrigated by ancestral hydrological networks. It is very likely that the hydrogeolgical conditions by the time of such eruptions where similar to the ones prevailing nowadays.

Sea level reconstructions indicate that the most likely age for North Head eruption was between 128 and 116 ka when the sea level was 2-4 m above current sea level. The presence of surface water set the conditions for the formation of a tuff cone.

#### 8.2.2.4 The inferences on eruptive styles and the ending of the phreatomagmatic phase

Considering the general morphometric, morphological, and sedimentary characteristics of small basaltic volcanoes (which includes tuff rings, tuff cones, and maars) (chapter 2), the studied phreatomagmatic volcanoes (Table 8.1) are within the range of medium to small size phreatomagmatic volcanoes, similarly to other phreatomagmatic vents in the AVF. Although all the cases are relative small eruptions in volume [for example individual AVF ejecta rings usually comprise much less than 0.02 $km^3$ in volume and are related to similar volumes of magma involved (for the exact figures see Kereszturi et al., 2013)], the stratigraphic sequences, the sedimentary structures, and the pyroclast distribution are varied within each case. These observations imply varied modes of transport of pyroclasts and changes in their rates of sedimentation and deposition

Changes in phreatomagmatic dynamics can be inferred from the bedforms, bedding transitions, lamination characteristics and the presence and absence of accretionary lapilli. It has been mentioned that the phreatomagmatic sequence of each volcano shows changes in eruptive styles from subtle changes in the Maungataketake ejecta ring formation to more distinct shifts characterized by drier upward sequences (Motukorea, Scenario 2) or transient magmatic phases (North Head, Scenario 3). However, juvenile pyroclast morphology and vesicularity suggest that in the construction of the entire ejecta rings and tuff cone water played a role to a greater or lesser extent.

The study of lithics within the sequences added important information about the type of substrate involved in the phreatomagmatic eruptions. Maungataketake and Motukorea ejecta rings are dominated by lithics sourced from shallow depths. These observations, paired with the inferred substrate conditions at the time of eruption provided information on the role of the substrate in the changing eruption dynamics. Shallow-seated explosions dominated in the construction of the Maungataketake and Motukorea ejecta rings (sections 8.2.1.1, 8.2.1.2; Fig. 8.1), while a Surtseyan eruption characterized the formation of North Head (section 8.2.1.3; Fig. 8.1).

All eruptions eventually shifted to a magmatic phase with the accumulation of spatter, scoria, and the emplacement of small lava flows. The relative homogeneity in vesicularity and textures of the juvenile pyroclasts during the Motukorea ejecta ring construction do not indicate a change in magma flux. In this case, it is however likely that water became progressively scarcer due to the low permeability and water content of Waitemata Group rocks. At North Head, the transition from phreatomagmatic to magmatic phase is coupled with an increase in vesicularity of juvenile lapilli. This could indicate a change in magma flux or sealing of the vent area from water ingress, or both, as in the Maungataketake scenario.

## 8.3 Discussion

Maar and tuff cone eruptions in historical times are poorly documented. Even in the case where the chronology of a maar eruption exists (e.g. Ukinrek maars; Kienle et al., 1980) it does not record the step-by-step tephra ring construction. Despite this hindrance, it was still possible here to infer the distinct eruptive styles and the mechanisms of transport and deposition of pyroclasts in the formation of the ejecta ring (or cone) of each studied volcano (section 8.2) by using typical stratigraphic and sedimentary methodology.

These findings are in agreement with most of previous eruptive reconstructions of phreatomagmatic eruptions in the AVF (Allen et al., 1996; Houghton et al., 1999; Németh et al., 2012a) and worldwide (e.g. Verwoerd and Chevallier, 1987; Chough and Sohn, 1989; Sohn and Chough, 1989, 1992, 1993; White, 1990, 1991b; 2001; Büchel and Lorenz, 1993; Németh et al., 2001, 2008, 2012a; Auer et al., 2007; Ross et al., 2011; Lefebvre et al., 2013; van Otterloo et al., 2013).

### 8.3.1 What do pyroclasts reveal?

#### 8.3.1.1 Juvenile fragments: witnesses of magma fragmentation?

The morphological and textural characteristics of juvenile fragments provide information on the dynamics of magma fragmentation (Heiken, 1972; Wohletz, 1983; Zimanowski et al., 1997; Büttner et al., 1999). According to experimental and field observations, FCIs generates medium and fine ash with one or more of the following characteristics: blocky particles with flat surfaces (medium ash) and particles with irregular, “moss” like-surfaces (fine ash); poorly vesicular, glassy fragments of sideromelane that may be coated by fine ash on their surfaces. Except for the “moss” like surfaces of particles, the above characteristics are prevalent in medium-to-fine ash juvenile particles of Maungataketake and Motukorea deposits (Table 8.1). Low vesicularity of juveniles, which is commonly reported in tephra ring and/or diatreme deposits elsewhere, is ubiquitous in particles of the three volcanoes (Table 8.1). The wider range of vesicularity at North Head tuff cone may suggest that the magma must have been chilled and fragmented at various depths, such as at the Surtseyan eruptions at Karymskoye (e.g. vesicularity of 7 to 63%, Belousov and

Belousova, 2001); the Capelas tuff cone (18 to 59%, Mattsson, 2010), or Black Point volcano (4 to 89%, Murtagh and White, 2013).

The above features point to rapid chilling and brittle fragmentation of the magma that is best explained by the explosive interaction of magma with water. However, magma may fragment by, either direct FCI processes or shock waves produced by them (Zimanowski et al., 1991; Raue, 2004), producing particles of similar appearance (Zimanowski et al., 1991). Although, in general, the juvenile particle morphology of Maungataketake, Motukorea, and North Head somehow resembles the ones experimentally obtained, some of these fragments may have been not the direct result of FCIs. In addition, for North Head-Surtseyan eruption, magma fragmentation may have been also caused by explosively expanding steam as magma rises into water (Kokelaar, 1986) or via the growth and breakage of glassy rinds on deforming magma surfaces during turbulent mixing and impact of tephra jets on the volcano slopes (Mastin, 2007; Mastin et al., 2009).

Juvenile pyroclast characteristics indeed provide insights into the evidence for explosive interaction of magma with water. However, juvenile fragments contained within a specific bed were not necessarily fragmented in the phreatomagmatic explosion(s) that generated the particle-laden base surges that eventually formed that specific bed (c.f., Valentine and White, 2012). Experimental studies by Graettinger et al. (2014) suggest the final deposition of material in the tephra ring is the result of a complex interaction between the locus depth and energy of explosions, as well as the vent geometry. Therefore caution must be taken when interpreting magma fragmentation of juveniles within specific horizons. For the studied cases, the characterization of juvenile pyroclasts was done considering the entire deposit and the phreatomagmatic origin of juveniles could be attested.

#### 8.3.1.2 Lithics: a window to the substrate

Phreatomagmatic eruptions depend on many factors (chapter 2). One factor is the substrate hydrogeological and geological conditions, whose role has been addressed by different studies (e.g. White, 1990, 1991b; Aranda-Gómez and Luhr, 1996; Sohn, 1996; Németh et al., 2001, 2008; Lorenz, 2003; Lorenz and Haneke, 2004; Martin and Németh, 2004; Auer et al., 2007; Carrasco-Núñez et al., 2007; Ort and Carrasco-Núñez, 2009). Few studies have concentrated on the calculation of the proportions of lithics in the tephra ring and to what extent this reflects the conditions, distribution and type of substrate lithologies (e.g. Auer et al., 2007; Ross et al., 2011; Valentine, 2012; Lefebvre et al., 2013).

The ejected lithics in tuff and tephra rings provide samples of the substrate materials fragmented and ejected by phreatomagmatic eruptions (Auer et al., 2007; Ross et al., 2011; Valentine, 2012; Lefebvre et al., 2013). While ejected material is more likely to over-represent shallow explosions (Valentine, 2012; Lefebvre et al., 2013; Graettinger et al., 2014; Valentine et al., 2015), deeper phreatomagmatic explosions may slowly move material upward within the diatreme to be later ejected.

North Head shows very little evidence for substrate excavation. Conversely, Plio-Pleistocene, unconsolidated sediment compose >80% of the lithic fragments in Maungataketake ejecta ring deposits (Table 8.1), with subordinate deeper Waitemata Group rock fragments. Similarly, Waitemata fragments are widespread within all size grades within Motukorea ejecta ring deposits, with subordinate deeper Waipapa greywakes. These patterns indicate that the construction of Maungataketake and Motukorea ejecta rings was from material dominantly sourced from the shallowest segments of the substrate, that is, from the Plio-Pleistocene sediments and the Waitemata rocks respectively.

In other examples in the AVF the prevalence of fragments from shallow segments of the substrate is also reported. Houghton et al. (1999) report the dominant presence of lithic fine ash in Crater Hill phreatomagmatic deposits. The origin of this fine ash was the shallow Plio-Pleistocene sediments, which may comprise around 80-100 m of thickness beneath Crater Hill. Similarly, Orakei maar ejecta ring deposits are characterized by up to 70% by volume of lithics, dominantly derived from the shallower Plio-Pleistocene valley filling sediments and the underlying Waitemata rocks (Nemeth et al., 2012a). These explosions were thus likely concentrated at the contact between the overlying sediments and the fractured Waitemata Group sediments below, tens of metres below the pre-eruptive surface (Németh et al., 2012a).

### 8.3.2 Deep versus shallow excavation (Valentine and White model and Lorenz model)

The referred examples document the dominant presence of fragments from shallow substrates within the ejecta ring, which is the evidence of the prevalence of shallow-seated explosions in the construction of ejecta rings as proposed by Valentine and White (2012) (Fig. 8.2). This is a revised maar-diatreme model that suggests that shallow explosions are more likely to erupt than deep ones (Valentine and White, 2012). At one end of the spectrum, when the diatreme is not well mixed, tephra ring deposits are characterized by particles from shallow country rocks. When the diatreme fill is well mixed, the tephra ring deposits exhibit a range of country rock lithologies disrupted. The lithics from deeper locations may have been “transported” upwards by debris jets produced by explosions at depth (Ross and White, 2006), mixed within the upper diatreme material, and eventually ejected by shallow seated explosions. The lithic data from Maungataketake, Motukorea, Crater Hill, and Orakei tephra rings, as well as other examples outside the AVF (Valentine and Groves, 1996; Ross et al., 2011; Valentine, 2012; Lefebvre e al., 2013) show a high proportion of shallow country rocks (the former end of the spectrum), but with small proportions of deeper-seated lithics. In addition, experiments with scaled-energy/depth blasts (Graettinger et al., 2014) suggest that shallow blasts are more likely to eject material above the blast loci than deep seated ones, which may not eject material at all. From an experimental and theoretical review, Valentine et al. (2014) conclude that maar ejecta rings are built by material deposited from explosions that are likely to erupt within the uppermost ~200 m, and even shallower (<100 m).

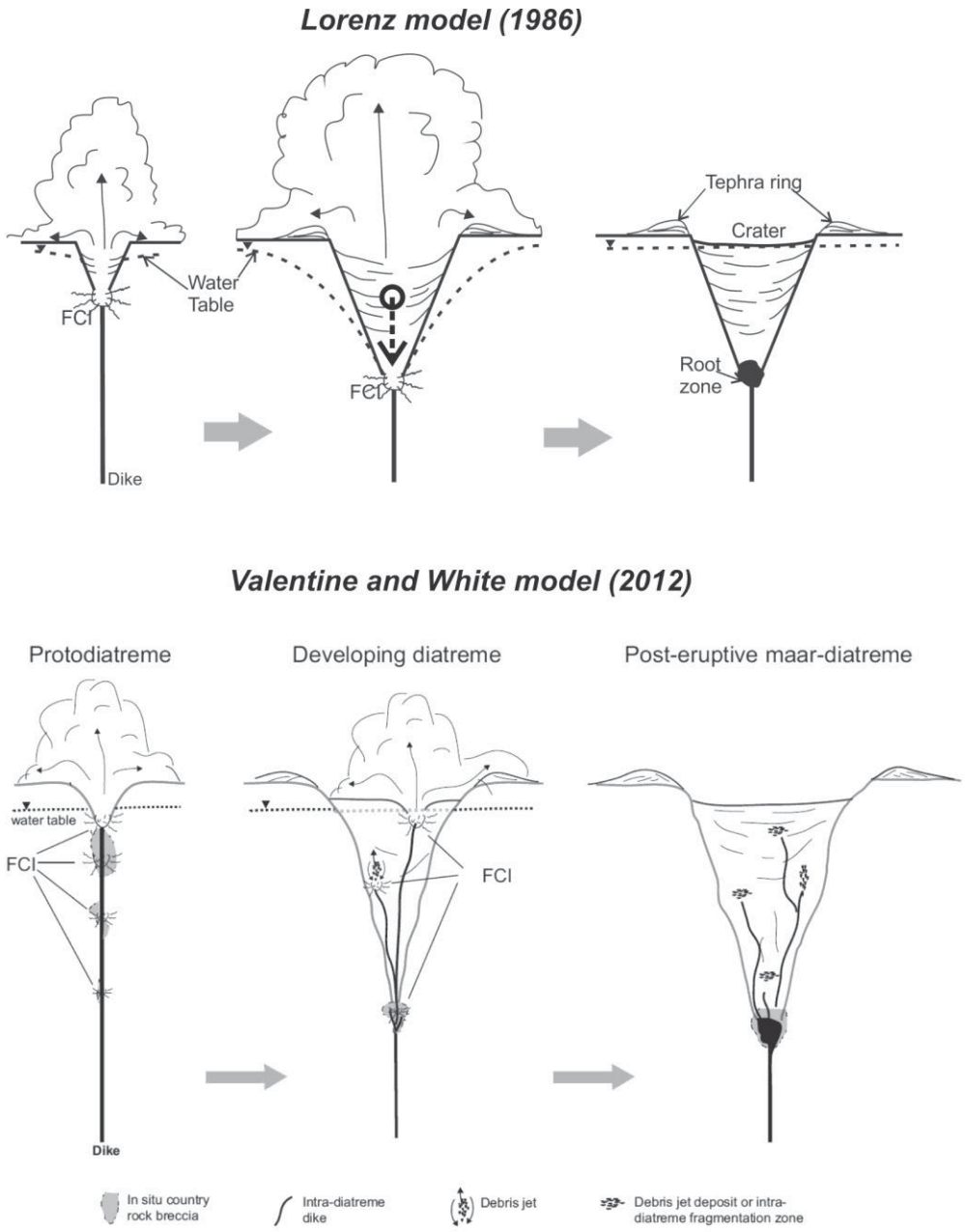


**Fig. 8.2** Schematic and simplified representation of Lorenz model (1986) and its revised version proposed by Valentine and White (2012) (after Valentine and White, 2012). In the former, water first interacts explosively with magma via fuel-coolant interaction (FCI) near the water table. As a consequence, a vent opens and diatreme formation initiates. Once water at shallow levels is used, the water table drops, then the locus of explosive activity progressively deepens and the diatreme widens by subsidence. In the revised model, FCI take place over a range of depths (the country rock surrounding the explosions is brecciated), but being more effective at shallow depths. The upper part of the diatreme widens and dikes rise to various levels and sometimes FCI occur, creating intra-diatreme fragmentation zones and debris jets that circulate the diatreme fill, but only shallow or especially powerful explosions erupt.

This view contradicts some aspects of the model of maar-diatreme formation proposed by Lorenz (1986) (Fig. 8.2). The initial explosive interaction of water with magma creates a small crater with an ejecta rim and initial diatreme. The usage of water in the explosions results in water table drawdown, and as magma continues to flow into the system, the locus of explosive activity progressively deepens and the diatreme widens by subsidence. Deepening of the explosion locus results in progressively deeper-seated country rocks lithics in the tephra deposits. Examples of an inverted tephra ring stratigraphy are found in the literature (e.g. Lorenz, 1986; Németh et al., 2001). The revised model contemplates the presence of relatively more abundant fragments from deeper-seated lithogies when eventually more and more of this material is carried up into the upper part of the diatreme by debris jets. But it does not imply the direct transport from depths to the surface. In the Valentine and White (2012) model, as well as in the Maungataketake and Motukorea eruption scenarios (Fig. 8.1), deepening of the explosion is not ruled out, but the water table drawdown appears not to be a condition for the deepening of the loci of explosions.

For the North Head eruption excavation into the underlying substrate was not relevant, but the surface hydrological conditions promoted a Surtseyan scenario, rare in the AVF. The dynamics and implications of this type or eruption will also be treated in the next sections.

### 8.3.3 The relevance of the substrate and surface hydrological conditions

The component analysis has shown that the presence of lithics in the tephra ring does not realistically represent the proportions of the disrupted substrates where lithics originated (e.g. Valentine, 2012; Lefebvre et al., 2013, this study). This suggests lithics of the uppermost part of the substrate substrate involved in the phreatomagmatic explosions are over-represented in the ejecta ring. The implications of this observation are best explained by the dominance of shallow-seated explosions in the tephra ring construction as the Valentine and White model (2012) predicts. In turn, the lithological and hydrogeological conditions of the substrate may be inferred or known (as it is the case the studied volcanoes). When all the available information is integrated, the role of the substrate in the eruptive styles and course of a phreatomagmatic eruption can be assessed.

For the eruptive scenarios depicted for Maungataketake (Scenario 1) and Motukorea (Scenario 2), the differences seen in their deposit characteristics, that is, the relatively homogeneous wet sequence of Maungataketake compared to the upward-drying sequence of Motukorea, is evident. The lithics found in their ejecta ring deposits indicate that they were sourced chiefly from the water-saturated sediments in the Scenario 1 and the Waitemata rocks in the Scenario 2. These lithologies represent the uppermost levels of the substrat and their thicknesses and hydrogeological condition at the time of the eruption were inferred. On the integration of results it is clear that, although impermeable, the water-saturated nature of the Plio-Pleistocene sediments provided water (probably through liquefaction) to fuel phreatomagmatic explosions at Maungataketake until the change to the magmatic phase due to the lining and sealing of conduits and

changes in magma flux. The 60+ m thickness of these sediments suggests that explosions kept very shallow throughout the eruption (similar to the example reported by Ort and Carrasco-Núñez, 2009) and the diatreme may have been dominantly filled with these sediments. On the other hand, the 200-300 m-thick Waitemata rocks were the host for phreatomagmatic explosions at Motukorea. The initiation of explosions before the opening of a crater may have taken place in a substrate that was characterized by a hydrogeology similar to the current Waitemata aquifer conditions. Once the diatreme was formed, this was probably filled with Waitemata rock fragments. Water was relatively not abundant within the diatreme fill due to the low to moderate water supply from the low permeable, low yield Waitemata aquifers. This caused the progressive diminishing of water supply, which is reflected in the alternating "wet" and "dry" Motukorea upper sequence and the eventual shift to the magmatic phase.

Although size and geometry of a diatreme beneath the studied volcanoes is not possible to envisage, the general formation of a Motukorea and Maungataketake diatreme, from the criteria compiled in this study, appears to be plausible. However, the generation of shallow-seated explosions are not dependant on size and geometry of the diatreme. Indeed, the existence of a diatreme is not even a pre-requisite for shallow-seated explosions to occur. Actually, the opening of a crater in the onset of a phreatomagmatic eruption is not within a diatreme fill, but the substrate itself (the Valentine and White model call it the proto-diatreme stage, Fig. 8.2). Interestingly, Valentine et al. (2014) states that despite their conclusions made on simple theoretical argument and limited experimental data under specific laboratory conditions, it is apparent that phreatomagmatic eruptions are likely sourced mostly by explosions in the uppermost ~200 m and shallower-seated explosions (<100 m) are expected to dominate the emplacement of material unto ejecta rings. Then, considering that ~60 m-thick unconsolidated sediments and 200-300 m-thick Waitemata rocks characterize the pre-eruptive shallowest substrate at Maungataketake and Motukorea eruption scenarios, it is possible that the first explosions were within those depths. The study results show that the lithics contained in the ejecta rings are composed dominantly of those shallower lithogies. Therefore, following Valentine et al. (2014) rationale, explosions kept occurring within those depths. The formation of the current Maungataketake and Motukorea crater size from a single explosion is ruled out from the sedimentary characteristics of their ejecta ring deposits (multiple bedding and lamination of base surge deposits, which attest for the occurrence of series of explosions). It means that the crater was enlarged progressively. Thus the material that filled the crater floor or the upper diatreme, either if a deep diatreme was formed of not, was sourced from those shallower substrates. Since substrates differ in hydrogeological conditions, the differences seen in the course and style of phreatomagmatic eruptions between scenarios 1 and 2 are linked to the specific hydrological conditions of the shallowest host substrate that charaterized each eruption (if magma flux is kept constant).

The evidence in the AVF and other monogentic fields (see above) supports the relationship between substrate conditions and the dynamics of eruptive processes in phreatomagmatic volcanoes. A general

stament from this study would be that magma that interacts with moderate water-content aquifers in hard substrates would promote relatively more energetic eruptions than magma that encounters tens of metres water-saturated, unconsolidated substrate overlying a hard substrate. However, the thickness of the unconsolidated sediments may be an influential factor that has to be taken into account. Also, a difference would be marked if those unconsilidated sediments are permeable or impermeable or the hard substrate has good hydraulic properties. Therefore the detailed characterization of the shallower substrates (<200 m depth) and the study of their lithological, rheological, and hydrogeological conditions associated with phreatomagmatic vents are relevant to get insights into the volcano construction.

Norht Head (Scenario 3) was formed by the interaction of magma with surface water (few meters deep) and the substrate did not play an important role in the construction of the cone. Setting of North Head within a few metres water depth resembles the Ilchulbong and Udo tuff cones (Jeju island, South Korea) (Sohn and Chough, 1992, 1993) that appeared to have been constructed over a basalt plateau covered with shallow sea water (exact depth is not provided, but several meters are inferred). Additionally, 17 tuff cones located on Marion and Prince Edward islands are inferred to be built from Surtseyan eruptions close to or at sea level (Verwoerd and Chevallier, 1987). North Head is the only case of a Surtseyan eruption so far documented in the AVF and indicates that this eruption occurred when sea levels where higher during the Last Interglacial (128-116 ka).

### 8.3.4 Hazard implications

Only few phreatomagmatic eruptions have been observed world-wide, hence little is known about the range and intensity of hazards associated with these events. Lorenz (2007) identified base surges, which may cause damage up 5 km from the vent, as the main hazard related to the eruption of maar-diatreme volcanoes. Base surges of lower energy and shorter run-out distances are associated with Surtseyan eruptions (Belousov and Belousova, 2001; Cole et al., 2001; White, 2001). Secondary hazards include earthquakes, tephra fall, ballistically ejected blocks and bombs, tephra jets and lahars. For example, eruption clouds in phreatomagmatic eruptions may rise to 20 km (Lorenz, 2007). However, even the relatively modest phreatomagmatic eruption of the Eyjafjallajökull volcano in Iceland (0.18 $km^3$ DRE and eruptive columns <10 km; Gudmundsson et al., 2010) produced serious short and long-distance effects, which disrupted the air traffic in northern Europe. The distribution and volume of medial to distal tephra fall from the three studied volcanoes is unknown, but the evidence of other hazards (base surges, ballistic projectiles, proximal tephra fall) is imprinted in their deposits. The area affected by these hazards expands only for a few square kilometres (roughly the area of the ejecta ring or tuff cone distribution). However, the city of Auckland, with 1.4 million people, is the largest city in New Zealand, and located almost perfectly across the AVF. In addition, the studied phreatomagmatic eruptions probably lasted for hours to a few days. Even in the case that an eruption lasted for only few hours, the violent onset in the opening of a phreatomagmatic vent, and subsequent explosions, may cause considerable damage to infrastructure and

people in minutes (e.g. phreatomagmatic eruption on Ambrym, Vanuatu, in 1913; Németh and Cronin, 2011). Therefore the impact of any phreatomagmatic-related hazard on Auckland would be immediate, direct, and high-powered.

The hazards associated with the Maungataketake and Motukorea eruptions are those linked to the eruption of maar-diatreme volcanoes, whereas those of North Head relate to the formation of a tuff cone. In general, the extent of hazards in relation to all studied eruptions differs slightly. Qualitatively speaking, the energy associated with the eruption of North Head was lower than that of the Maungataketake or Motukorea events. The eruptive styles and dynamics of each eruption, which were connected to the substrate hydrogeological and surface hydrological conditions, reflect the eruptive energy.

**Maungataketake eruption**. Ballistic bombs and blocks are distributed within the area comprised by the ejecta ring (roughly 3 $km^2$). Blocks up to 30 cm in diameter and lithics of medium-to-coarse size occur up to 1 km from the vent, but they are not abundant. The run-out distance of base can be measured up to 2 km from the vent. At the base of the exposed deposits there are some tree remnants that were snapped by the base surges. These indicate dynamic pressures of 35 to 80 kPa within 0.5 km from the vent, decreasing to 10 kPa beyond 1 km (Brand et al., 2014). Considering that the onset of structural damage begins around 7 kPa (Valentine, 1998), these dynamic pressures would damage or destroy most buildings. These quantitative findings are a step ahead in the estimation of hazards of base surges for the AVF.

The current substrate conditions and those that prevailed when the Maungataketake eruption took place were probably similar, so the Maungataketake scenario provides a guide to future eruptions in the southern AVF (Manukau Lowlands, Fig. 3.1), where shallow unconsolidated sediments overlie Waitemata rocks.

**Motukorea eruption**. The scarcity of bombs and blocks bigger than 20 cm is evident, but lithics of medium-to-coarse lapilli are relatively common in the entire phreatomagmatic deposits. The lack of exposures from proximal to distal locations prevents an estimate of the extent of fall of larger blocks, but those blocks may have fallen within the ejecta ring area. The lateral extent of base surges is difficult to evaluate, but run out distance may have been within 1-2 km from the vent, similarly to the base surges generated at Maungataketake eruption. Motukorea base surges appeared to have been more energetic than those of Maungataketake, with common erosive surfaces indicating high basal shear of the base surge deposits. In contrast, Maungataketake base surges were wetter, and showed steady deposition with mostly planar-parallel bedding.

Considering that the current hydrogeological conditions of Waitemata rocks may resemble those that dominated at the time of the Motukorea eruption, the Motukorea example is diagnostic of the present dry areas in the Auckland Isthmus and the northern AVF (Waitemata rocks) (Fig. 3.1).

**North Head eruption**. Due to the nature of exposures, the hazards associated with the North Head eruption are difficult to estimate; however, documented observed examples can be used as an analogy. The distinctive feature of Surtseyan eruptions is the formation of tephra jets. These can reach up to 1.4 km height (e.g. Belousov and Belousova, 2001), but typically land close to the vent (Kokelaar, 1986). Low energy base surges are engendered by the landing of tephra jets with run-out distances of hundreds of meters (Kokelaar, 1986; Belousov and Belousova, 2001). Therefore, minor, low energy base surges are envisaged for North Head eruption. Heavy fall was dominant in proximal areas during the North Head tuff cone eruption. In an analogous case, thick tephra deposits (1.9 m) are documented up to 1.2 km beyond the cone at Capelinhos (Cole et al., 2001). Similar Surtseyan eruptions generated columns of 4 to 7.6 km in height over 3-5 days at Hunga Ha´apai in Tonga (Vaughan and Webley, 2010), producing considerable airborne tephra. Local tsunamis may also be associated with Surtseyan eruptions (e.g. Belousov and Belousova, 2001).

Considering that 35% of the AVF is covered by up to approximately 30 m of water, the occurrence of a Surtseyan eruption like that of North Head appears possible. Although the extent of hazards related to Surtseyan eruptions are relatively less than those associated to maar-diatreme volcanoes, if taking place in the Waitemata Harbour or in shallow water close to the airport, the impact of these eruptions may be considerable.

### 8.3.5 Conclusions

- Lithics of the shallower substrates are over-represented in the ejecta ring deposits. This suggests that shallow-seated explosions dominated in the construction of Maungataketake and Motukorea maar ejecta rings (Scenario 1 and Scenario 2). Deep explosions can occur, but they do not tend to eject material beyond the crater. This is in agreement with the dominance of shallow-seated explosions in the eruption model as described by Valentine and White (2012).
- Either a deep diatreme was formed or not, the eruptive styles and dynamics of eruptive scenarios 1 and 2 were influenced by the hydrogeological and lithological conditions of the shallowest substrates (<200 m depth) that characterized each area. Unconsolidated, water-saturated sediments appeared to generate relatively moderate energy, wet base surges during the entire Maungataketake eruption (southern AVF). Conversely, during the Motukorea eruption (northern AVF), the changes in eruptive styles are more distinct with the upwards drying of the sequence, which seemed to be controlled by the poor to moderate hydraulic properties of the Waitemata rocks. The transition to the concluding and steady magmatic phases is due to the lack of water availability during the Motukorea eruption and the sealing of conduits and changes in magma flux in the Maungataketake event, where water was probably always available.

- A general concluding stament from this study would be that magma that interacts with moderate water-content aquifers in hard substrates would promote relatively more energetic eruptions than magma that encounters tens of metres water-saturated, unconsolidated substrate overlying a hard substrate. However, other factors must be taken into account: thickness of the unconsolidated sediments overlying a hard substrate, as well as the physical, hydrogeological, hydraulic, and rheological properties of unconsolidated sediments and hard rocks. Therefore the detailed characterization of the shallower substrates (<200 m depth), and the study of their conditions, associated with phreatomagmatic vents are relevant to get insights into the volcano construction.
- North Head (Scenario 3) marks a watershed in the phreatomagmatic eruptions in the AVF as it is the only volcano that shows evidence of a Surteyan eruption in its initial stage. The substrate did not play an important role in the eruption dynamics. The eruption started through shallow superficial water (around 12 m). The tuff cone starts with a relatively wet sequence that eventually becomes drier, until a concluding magmatic phase ensued.

- The reconstruction of the substrate hydrogeological and geological conditions and superficial hydrological conditions of the past may be achieved from the study of the current hydrogeological and hydrological condition, the knowledge of the tectonic and structural history of the area, the information of the paleoclimate, and the inclusion of paleoenvironmental reconstructions. As long as the substrate conditions are similar to the ones that prevailed at the time of the studied eruptions, the replication of similar phreatomagmatic eruption styles and dynamics are expected to occur in the AVF. Scenario 1 (Maungataketake, maar-diatreme eruption within soft substrate) may be replicated in the southern Manukau Lowlands. Scenario 2 (Motukorea, maar-diatreme eruption within hard substrate) may be reproduced in the northern AVF (Auckland Isthmus). Scenario 3 (North Head, Surtseyan within shallow water) may occur in the submerged areas of the AVF.
- Although similar, the extent and impact of hazards for each eruption scenario is controlled by their distinct characteristics of their phreatomagmatic eruptive styles and dynamics, which in turn are dependent on the type of substrate or the surface hydrological conditions. The relatively most hazardous eruptions would be those through hard Waitemata rocks, and the less hazardous would be those through shallow water. Although the areal extent of hazards associated with these eruptions is confined to a few square kilometres, any eruption occurring in the AVF would have a negative impact on the city of Auckland.
- Most maar-diatreme eruptions in the AVF occurred when the sea level was lower than today. Since sea level is currently higher and global trends in sea level point to further rises, the occurrence of an initial phreatomagmatic phase, triggered by groundwater or surface water, in

AVF appears very likely. Considering that the site of the next eruption in the AVF is unknown, all areas within the AVF have the same probability to host a future eruption.

The three eruptive scenarios presented here are single cases of three different substrate and environmental conditions. By no means, they are defined models that unambiguously characterize the eruptive dynamics of each substrate/environmental conditions. An exhaustive testing is necessary, so these models can be improved and refined. The application of different techniques, methodologies, and theoretical background is necessary to disclose the factors that control phreatomagmatic eruptions individually and in the regional and global context.

Specific propositions for future work in the AVF:

- Where possible, reconstruction of the phreatomagmatic eruptions at other vents in the AVF using the typical sedimentary and stratigraphical methodology, emphasizing on the characterization of lithics.
- Pairing recent hydrogeological and volcanological studies at specific phreatomagmatic vents. For example, the hydrogeological conditions of the substrate at the Three King area are well known, but there is not a study on the phreatomagmatic phase of this volcano (apparently the largest maar in the AVF).
- Study of the changes in the hydraulic and physical properties of Waitemata rocks when fracturing is induced.
- Obtention of reliable dating of volcanoes in the AVF.
- Characterization of the exact thickness of the unconsolidated sediments beneath phreatomagmatic vents in the Manukau Lowlands, so a reliable correlation between eruption dynamics and thickness of the unconsolidated sediments can be obtained.
- Due to the lack of good ejecta ring exposures in the AVF, the characterization of ejecta ring deposits can be made using drilling and/or indirect methods like ground penetrating radar techniques.
- Use of drilling and/or indirect high resolution geophysical techniques for the study of possible diatreme structures in the field.
- An interdisciplinary work that includes geologists, hydrogeologists, hydrologists, geophysicists, climatologists, physicits and specialist of other fields is necessary in order to obtain the best results.

## References


Adams, C.J., Maas, R., 2004. Age/isotopic characteristics of the Waipapa Group in Northland and Auckland, New Zealand, and implication s for the status of the Waipapa Terrane. New Zealand J Geol Geophys, 47: 173-178.

Affleck, D.K., Cassidy, J., Locke, C.A., 2001.Te Pouhawaiki Volcano and pre-volcanic topography in central Auckland: Volcanological and hydrogeological implications. New Zealand J Geol Geophys, 44: 313-321.

Agustín-Flores, J., Németh, K., Cronin, S., Lindsay, J., Kereszturi, G., Brand, B., Smith, I.E.M., 2014. Phreatomagmatic eruptions through unconsolidated coastal plain sequences, Maungataketake, Auckland Volcanic Field (New Zealand). J Volcanol Geotherm Res, 180: 203-224.

Agustín-Flores, J., Németh, K., Cronin, S., Lindsay, J., Kereszturi, G., 2015a. Construction of the North Head (Maungauika) tuff cone: a product of Surtseyan volcanism, rare in the Auckland Volcanic Field, New Zealand. Bulletin of Volcanology, 77: 11. Doi 10.1007/s00445-014-0892-9.

Agustín-Flores J., Németh K., Cronin S., Lindsay J., Kereszturi, G, 2015b. Shallow-seated explosions in the construction of the Motukorea tuff ring (Auckland, New Zealand): evidence from lithic and sedimentary characteristics. Journal of Volcanology and Geothermal Research, 304: 272-286. Doi 10.1016/j.jvolgeores.2015.09.013

Allen, S.R., Smith, I.E.M., 1994. Eruption styles and volcanic hazard in the Auckland Volcanic Field, New Zealand. Geoscience reports of Shizuoka University, 20: 5-14.

Allen, S.R., Bryner, V.F., Smith, I.E.M., Ballance, P.F., 1996. Facies analysis of pyroclastic deposits within basaltic tuff-rings of the Auckland volcanic field, New Zealand. New Zealand J Geol Geophys, 39: 309-327.

Alloway, B., Westgate, J., Pillans, B., Pearce, N., Newnham, R., Byrami, M., Aarburg, S., 2004. Stratigraphy, age and correlation of middle Pleistocene silicic tephras in the Auckland region, New Zealand: A prolific distal record of Taupo Volcanic Zone volcanism. New Zealand J Geol Geophys, 47: 447-479.

Andronico, D., Cristaldi, A., Del Carlo, P., Taddeucci, J., 2009. Shifting styles of basaltic explosive activity during the 2002-03 eruption of Mt. Etna Italy. J Volcanol Geotherm Res, 180: 110-122.

Aranda-Gómez, J.J., Luhr, J.F., 1996. Origin of the Joya Honda mar, San Luis Potosí, México. J Volcanol Geotherm Res, 74:1-18.

Auer, A., Martin, U., Németh, K., 2007. The Fekete-hegy (Balaton Highland Hungary) “soft-substrate” and “hard-substrate” maar volcanoes in an aligned volcanic complex – Implications for vent geometry, subsurface stratigraphy and the paleoenvironmental setting. J Volcanol Geotherm Res, 159: 225-245.

Austin-Erickson, A., Büttner, R., Dellino, P., Ort, M.H., Zimanowski, B., 2008. Phreatomagmatic explosions of rhyolitic magma: experimental and field evidence. J Geophysic Res – Solid Earth 113 (B11).

Ballance, P.F., 1974. An Inter-Arc Flysch Basin in Northern New Zealand: Waitemata Group (Upper Oligocene to Lower Miocene). J Geol, 82: 439-471.

Barnett, W.P., 2008. The rock mechanics of kimberlite volcanic pipe excavation. J Volcanol Geotherm Res, 174: 29-39.

Beavan, R.J., Litchfield, N.J., 2012. Vertical movement around New Zealand coastline: implications for sea-level rise. GNS Science Report 2012/29, September 2012, 41 pp.

Bebbington, M.S., Cronin, S.J., 2011. Spatio-temporal hazard estimation in the Auckland Volcanic Field, New Zealand, with a new event-order model. Bull Volcanol, 73: 55-72.

Belousov, A., Belousova, M., 2001. Eruptive processes, effects and deposits of the 1996 and the ancient basaltic phreatomagmatic eruptions in Karymskoye Lake, Kamchatcka, Russia. In: White JDL, Riggs, NR (eds.), Volcaniclastic Sedimentation in Lacustrine Settings: International Association of Sedimentologists Special Publication, 30: 35-60.

Berry, K.A., 1984. Stratigraphic, structural, and geophysical studies of the Neogene sediments of the Manukau Lowlands. M.Sc. Thesis, The University of Auckland, New Zealand, 89 pp.

Booden, M.A., Smith, I.E.M., Black, Philippa M., Mauk, J.L., 2011. Geochemisty of the Early Miocene volcanic succession of Northland, New Zealand, and implications for the evolution of subduction in the Southwest Pacific. J Volcanol Geotherm Res, 199, 25-37.

Berghuijs, J.F., Mattsson, H.B., 2013. Magma ascent, fragmentation and depositional characteristics of "dry" maar volcanoes: Similarities with vent-facies kimberlite deposits. J Volcanol Geotherm Res, 252: 53-72.

Brand, B.D., White, C.M., 2007. Origin and stratigraphy of phreatomagmatic deposits at a Pleistocene Sinker Butte Volcano, Western Snake River Plain, Idaho. J. Volcanol Geotherm Res, 160: 319-339.

Brand, B.D., Clarke, A.B., 2009. The architecture, eruptive history, and evolution of the Table Rock Complex, Oregon: From a Surtseyan to an energetic maar eruption. J Volcanol Geotherm Res, 180: 203-224.

Brand, B.D., Clarke, A.B., Semken, S., 2009. Eruptive conditions and depositional processes of Narbona Pass Maar, Navajo volcanic field, Navajo Nation, New Mexico (USA). Bull Volcanol, 71: 49-77.

Brand, B.D., Gravley, D., Clarke, A., Lindsay, J., Boomberg, S.H., Agustin-Flores, J., Németh, K., 2014. A combined field and numerical approach to understanding dilute pyroclastic density current dynamics and hazard potential: Auckland Volcanic Field, New Zealand. J Volcanol Geotherm Res, 276, 215-232.

Branney, M.J., Kokelaar, P., 2002. Pyroclastic density currents and the sedimentation of Ignimbrites. Memoir, vol. 27. Geological Society, London, 143 pp.

Brenna, M., Cronin, S.J., I.E.M., Smith, Sohn, Y.K., Németh, K., 2010. Mechanisms driving polymagmatic activity at a monogenetic volcano, Udo, Jeju Island, South Korea. Contrib Mineral Petrol, 160: 931-950.

Briggs, R.M., Goles, G.G., 1984. Petrological and trace element geochemical features of the Okete Volcanics, western North Island, New Zealand. Contrib Mineral Petrol, 86: 77-88.

Briggs, R.M., Utting, A.J., Gibson, I.L., 1990. The origin of alkaline magmas in an intraplate setting near a subduction zone: the Ngatutura Basalts, North Island, New Zealand, 40: 55-70.

Briggs, R.M., Okada, T., Itaya, T., Shibuya, H., Smith, I.E.M., 1993. K-Ar ages, paleomagnetism, and geochemisty of the South Auckland volcanic field, North Island, New Zealand. New Zealand J Geol Geophys, 37: 143-153.

Briggs, R.M., Middleton, M.P., Nelson, C.S., 2004. Provenance history of a Late Triassic-Jurassic Gondwana margin forearc basin, Murihiku Terrane, North Island, New Zealand. Petrographic and Geochemical constrains. New Zealand J Geol Geophys, 47, 589-602.

Brooker, M.R., Houghton, B.F., Wilson, C.J.N., Gamble, J.A., 1993. Pyroclastic phases of a rhyolitic dome-building eruption: Puketarata tuff ring, Taupo volcanic zone, New Zealand. Bull Volcanol, 55: 395-406.

Bryner, V.F., 1991. Motukorea: The evolution of an eruption centre in the Auckland volcanic field. M.Sc. Thesis, The University of Auckland, New Zealand, 126 pp.

Bryner, V.F., Grant-Mackie, J.A., 1993. The bivalve Anadara Trapezia and other macrofossils in the tuffs of Motukorea volcano, Auckland. Tane, 34: 123-131.

Büchel G, Lorenz V, 1993. Syn- and post-eruptive mechanism of the Alaska Kinrek Maars in 1977. In Negendank, JFW and Solitschka B (eds.) Paleolimnology of European Maar Lakes. Lecture Notes in Earth Sciences, Springer, Berlin, Heidelberg, 49, 15-60.

Büttner, R., Zimanowski, B., 1998. Physics of thermohydraulic explosions. Physical Review E, 57: 5726-5729.

Büttner, R., Dellino, P., Zimanowski, B.., 1999. Identifying magma-water interaction from the surface features of ash particles. Nature, 401: 688-690.

Büttner, R., Dellino, P., La Volpe, L., Lorenz, V., Zimanowski, B., 2002. Thermohydraulic explosions in phreatomagmatic eruptions as evidenced by the comparison between pyroclasts and products from Molten Fuel Coolant Interaction experiments. J. Geophys Res, 107: Art. 2277.

Carey, S.N., 1991. Transport and deposition of tephra by pyroclastic flows and surges. In: Fisher, R.V. and Smith, G.A. (eds.), Sedimentation in volcanic settings, SEPM, Special Publications, 45: 39-57.

Cano-Cruz, M, Carraco-Núñez, G., 2008. Evolution of a rhyolitic explosion crater (maar): Joya de Estrada, Valle de Santiago volcanic field Guanajuato, Mexico. Revista Mexicana de Ciencias Geologicas, 25: 549-564.

Carrasco-Núñez, G., Ort, M.H., Romero, C., 2007. Evolution and hydrological conditions of a maar volcano (Atexcac crater, Eastern Mexico). J Volcanol Geotherm Res, 159: 179-197.

Cas, R.A.F., Wright, J.V., 1987. Volcanic successions: Modern and ancient. Allen and Unwin, London, 528 pp.

Cas, R.A.F., Hayman, P., Pittari, A., Porrit, L., 2008. Some major problems with existing models and terminology associated with kimberlite pipes from a volcanological perspective, and some suggestions. J Vocanol Geotherm Res, 174: 209-225.

Cassidy, J., Locke, C.A., 2010. The Auckland volcanic field, New Zealand: Geophysical evidence for structural and spatio-temporal relationships J Volcanol Geotherm Res, 195: 127-137.

Chough, S.K., Sohn, Y.K., 1990. Depositional mechanics and sequences of base surges, Songaksan tuff ring, Cheju Island, Korea. Sedimentology, 37: 1115-1135.

Cioni R., Sbrana, A., Vecci, R., 1992. Morphologic features of juvenile pyroclasts from magmatic and phreatomagmatic deposits of Vesuvius. J Volcanol Geotherm Res, 51: 61-78.

Cole, P.D., Guest, J.E., Duncan, A.M., Pacheco, J.M., 2001. Capelinhos 1957-1958, Faial, Azores: deposits formed by an emergent Surtseyan eruption. Bull Volcanol, 63: 204-220.

Connor, C.B., Stamatakos, J.A., Ferrill, D.A., Hill, B.E., Ofoegbu, G.I., Conway, F.M., Sagar, B., Trapp, J., 2000. Geologic factors controlling patterns of small-volume basaltic volcanism: Application to a volcanic hazard assessment at Yuca Mountain, Nevada. J Geophys Res, 105: 417-432.

Conybeer, M., 1995. Physical volcanology of Maungataketake volcano. M.Sc. Thesis, The University of Auckland, New Zealand, 100 pp.

Crowcroft, G., Smaill, A., 2001. Auckland. In: Groundwaters of New Zealand. M.R. Rosen and P.A. White (eds.). New Zealand Hydrological Society Inc., Wellington, New Zealand: 303-313.

Crowcroft, G., Bowden, D., 2002. Auckland Water Resource Quantity Statement 2002; Surface water and groundwater resource information availability and location. Technical Publication Number 171, Auckland Regional Council, 44 pp.

Davy, B., 2008. Marine seismic reflection profiles from the Waitemata-Whangaparaoa region, Auckland. New Zealand J Geol Gephys, 51:161-173.

Delaney, P, 1986. Field relations between dikes and joints: emplacement processes and paleostress analysis. J Geophys Res, 91: 4929-4938.

Dellino, P., Frazzetta, G., La Volpe, L., 1990. Wet surge deposits at La Fossa di Vulcano: Depositional and eruptive mechanisms. J Volcanol Geotherm Res, 43:215-233.

Dellino, P., Isaia, R., Veneruso, M., 2004. Turbulent boundary layer shear flow as an approximation of base surge at Campi Flegrei. J Volcanol Geotherm Res, 133: 211-228.

Dellino, P., Mele, D., Sulpizio, R., La Volpe, L., Braia, G., 2008. A method for the calculation of the impact parameters of dilute pyroclastic density currents based on deposits particle characteristics. J Geophys Res, 113, B07206.

Douillet, G.A., Pacheco, D.A., Kueppers, U., Letort, J., Tsang-Hin-Sun, E., Busitllos, J., Hall, M., Ramón, P., Dingwell, D.B., 2013. Dune bedforms produced by dilute pyroclast density currents from the August 2006 eruption of Tungurahua volcano, Ecuador. Bull Volcanol, 75, 762.

Druitt, T.H., Brenchley, P.J., Gökten, Y.E., Francaviglia, V., 1995.Late Quaternary rhyolitic eruptions from the Acigöl Complex, central Turkey. J Geol Soc, 152(4): 655-667.

Edbrooke, S.W., 2001. Geology of the Auckland area. Insitute of Geological and Nuclear Sciences 1:250 000 Geological map 3.3.

Edbrooke, S.W., Crouch, E.M., Morgans, H.E.G. Sykes, R., 1998. Late Eocene-Oligocene Te Kuiti Group at Mount Roskill, Auckland, New Zealand. New Zealand J Geol Geophys, 41: 85-93.

Edbrooke, S. W., Mazengarb, C., Stephenson, W., 2003. Geology and geological hazards of the Auckland urban area, New Zealand. Quaternary International, 103: 3-21.

Erlund, E.J., Cashman, K.V., Wallace, P.J., Pioli, L., Rosi, M., Johnson, E., Delgado Granados, H., 2010. Compositional evolution of magma from Parícutin volcano, Mexico: The tephra record. J Volcanol Geotherm Res, 197: 167-187.

Fisher, R.V., Schmincke, H.-U., 1984. Pyroclastic Rocks. Springer-Verlag, Berlin, 472 pp.

Folk, R.L., Ward, W.C., 1957. Brazos river bar: a study in the significance of grain size parameters. J Sed Petrol, 27: 3-26.

Fröhlich, G., Zimanowski, B., Lorenz, V., 1993. Explosive thermal interactions between molten lava and water. Experimental Thermal and Fluid Science 7(4): 319-332.

Geshi, N., Németh, K., Oikawa, T., 2011. Growth of phreatomagmatic explosion craters: A model inferred from Suoana crater in Miyakejima Volcano, Japan. J Volcanol Geotherm Res, 201: 30-38.

Gilbert, J.S., Lane, S.J., 1994. The origin of accretionary lapilli. Bull Volcanol, 56: 398-411.

Graettinger, A.H., Valentine, G.A., Sonder, I., Ross, P.-S., White, J.D.L., Taddeucci, J., 2014. Maar-diatreme geometry and deposits: Subsurface blast experiments with variable explosion depth. Geochem Geophys Geosyst, 15: 740-764.

Gudmundsson, M., Pedersen, R., Vogfjörd, K., Thorbjarnardóttir, B., Jakobsdóttir, S., Roberts, M.J., 2010. Eruptions of Eyjafjallajökull Volcano, Iceland. EOS, 91, 190-191.

Hannah, J., Bell, R., Paulik, R., 2011. Auckland: A case study in the regional assessment of long-term sea level change. FIG Working Week 2011, Bridging the gap between cultures, Marrakech, Morocco, 18-22 May 2011, 16 pp.

Hayward, B.W., 1979. Eruptive history of the early to mid Miocene Waitekere Volcanic arc and paleogeography of the Waitemata Basin, northern New Zealand. J Royal Soc New Zealand, 9: 297-320.

Hayward, B.W., 1993. The tempestuous 10 million year life of a double arc and intra-arc basin – New Zealand's Northland Basin in the early Miocene. In: Sedimentary Basins of the World, vol 2, South Pacific Sedimentary Basis, P.F. Balance (eds.), Elsevier, Amsterdam, pp 113-142.

Hayward, B.W., 2004. Foraminifera-based estimates of palaeobathymetry using modern Analogue Technique, and the subsidence history of the early Miocene Waitemata Basin. New Zealand J Geol Gephys, 47: 749-767.

Hayward, B.W., Murdoch, G, Maitland, G., 2011. Volcanoes of Auckland, the essential guide. Auckland University Press, New Zealand, 234 pp.

Hayward, J.J. and Hayward, B.W., 1995. Fossil forest preserved in volcanic ash and lava at Ihumatao and Takapuna, Auckland. Tane, 35: 127-142. Heiken, G., 1974. An atlas of volcanic ash. Smithsonian Contr Earth Sciences, 12: 1-101.

Heiken, G.H., 1972. Morphology and petrography of volcanic ashes. Geol Soc Amer Bull, 83: 1961-1988.

Heiken, G.H., 1974. An atlas of volcanic ash. Smithsonian Contr Earth Sc, 12: 1-101.

Hochstein, M.P., Ballance, P.F., 1993. Hauraki Rift: A young active intra-continental rift in a Back-Arc Setting. In: South Pacific Sedimentary Basins, Sedimentary basins of the world, Balance, P.F. (eds.), Elsevier, 2: 295-305.

Hodder, A.P.W., 1984. Late Cenozoic rift development and intraplate volcanism in northern New Zealand inferred from geochemical discrimination diagrams. Tectonophysics, 101: 293-318.

Houghton, B.F., Wilson, C.J.N., 1989. A vesicularity index for pyroclastic deposits. Bull Volcanol 51:451-462.

Houghton, B.F., Nairn, I.A., 1991. The 1976-82 Strombolian and phreatomagmatic eruptions of White Island, New Zealand: eruptive and depositional mechanisms at a "wet" volcano. Bull Volcanol, 54:25-49.

Houghton, B.F., Smith, R.T., 1993. Recycling of magmatic clasts during explosive eruptions: estimating the true juvenile content of phreatomagmatic volcanic deposits. Bull Volcanol, 55: 414-420.

Houghton, B.F., Wilson, C.J.N. and Smith, I.E.M., 1999. Shallow-seated controls on styles of explosive basaltic volcanism: a case study from New Zealand. J Volcanol Geotherm Res, 91: 97-120.

Ingram, R.L., 1954. Terminology for the thickness of stratification and parting units in sedimentary rocks. Geol Soc Am Bull, 65: 130-165.

Inman, D.L., 1952. Measures for describing the size distribution of sediments. J Sedimen Petrol, 22: 125-145.

Irwin, M., 2009. Synthesis of existing structural data for the Auckland Volcanic Field. Institute of Earth Science and Engeneering Technical Report 1-2009.01. The University of Auckland, 207 pp.

Jakobsson, S.P., 1972. On the consolidation and palagonitization of the tephra of the Surtsey volcanic Island, Iceland. Surtsey Res Progr Rep, 6: 121-128.

Jakobsson, S.P., 1978 Environmental factors controlling the palagonitization of the Surtsey tephra, Iceland. Bull Geol Soc Denmark, 27: 91-105.

Kenny, J.A., Lindsay, J.M., Howe, T.M., 2011. Large-scale faulting in the Auckland region. Institute of Earth Sciences and Engineering Report 1-2011.04, Auckland, New Zealand, 95 pp.

Kenny, J.A., Lindsay, J.M, Howe, T.M., 2012. Post-Miocene faults in Auckland: insights from borehole and topographic analysis. New Zealand J Geol Geophys, 55: 323-343.

Kereszturi, G., Németh, K., Csillag, G., Balogh, K., Kovács, J., 2011. The role of external environmental factors in changing eruption styles of monogenetic volcanoes in a Mio-Pleistocene continental volcanic field in western Hungary. J Volcanol Geotherm Res, 201: 227-240.

Kereszturi, G., Németh, K., Cronin, J.S., Agustin-Flores, J., Smith, I.E.M., Lindsay, J., 2013. A model for calculating eruptive volumes for monogenetic volcanoes – Implication for the Quaternary Auckland Volcanic Field, New Zealand. J Volcanol Geotherm Res, 266: 16-33.

Kereszturi, G., Németh, K., Cronin, J.S., Procter, J., Agustin-Flores, J., 2014. Influences in the variability of eruption sequences and style transitions in the Auckland Volcanic Field. J Volcanol Geotherm Res, 286:101-115.

Kermode, L.O., 1992. Geology of the Auckland Urban Area. Scale 1:50,000. Institute of Geological and Nuclear Sciences geological map 2, 1 sheet and 63p. Institute of Geological and Nuclear Sciences Ltd., Lower Hutt, New Zealand.

Kienle, J., Kyle, P.R., Self, S., Motyka, R.J., Lorenz, V., 1980. Ukinrek Maars, Alaska, I. April 1977 eruption sequence, petrology and tectonic setting. J Volcanol Geotherm Res, 7: 11-37.

Kokelaar, P., 1983. The mechanism of Surtseyan volcanism. J Geol Soc (London), 140: 939-944.

Kokelaar, P., 1986. Magma-water interactions in subaqueous and emergent basaltic volcanism. Bull Volcanol, 48: 275-289.

Kurszlaukis, S., Fulop, A., 2013. Factors controlling the internal facies architecture of maar-diatreme volcanoes. Bull Volcanol, 75: 761.

Lautze, N., Taddeucci, J., Andronico, D., Houghton, B., Niemeijer, A., Scarlato, P., 2013. Insights into explosion dynamics and the production of ash at Stromboli from samples collected in real-time, October 2009, in Rose, W.I., Palma, J.L., Delgado Granados, H., and Varley, N. (eds.), Understanding Open-Vent Volcanism and Related Hazards: Geological Society of America Special Paper 498, p. 125–139.

Leat, P.T., Thompson, R.N., 1988. Miocene hydrovolcanism in NW Colorado, USA, fuelled by explosive mixing of basic magma and wet unconsolidated sediment. Bull Volcanol, 50: 229-243.

Le Corvec, N., 2013. Age, distance, and geochemical evolution within a monogenetic volcanic field: Analyzing patterns in the Auckland Volcanic Field eruption sequence. Geochem Geophys Geosyst, 14. Doi: 10.1002/ggge.20223.

Lefebvre, N., Kurszlaukis, S., 2008. Contrasting eruption styles of the 147 Kimberlite, Fort à la Corne, Saskatchewan, Canada. J Volcanol Geotherm Res, 174: 171-185.

Lefebvre, N.S., White, J.D.L., Kjarsgaard, B.A., 2013. Unbedded diatreme deposits reveal maar-diatreme-forming eruptive processes: Standing Rocks West, Hopi Buttes, Navajo, Nation, USA. Bull Volcanol, 75:739. DOI 10.1007/s00445-013-0739-9.

Lewis, J.D., 1990. Chapter 5: Diatremes. In: Geology and mineral resources of Western Australia Geological Survey Memoir, 3: 565-589.

Lindsay, J.M., Marzocchi, W., Jolly, G., Constantinescu, R., Selva, J., Sandri, L., 2010. Towards real-time eruption forecasting in the Auckland Volcanic Field: application of BET_EF during the New Zealand National Disaster Exercise 'Ruaumoko'. Bull Volcanol, 72: 185-204.

Lindsay, J.M., Leonard, G.S., Smid, E.R., Hayward, B.W., 2011. Age of the Auckland Volcanic Field: a review of existing data. New Zealand J Geol Geophys, 54: 379-401

Lorenz, V., 1970. Some aspects of the eruption mechanism of the Big Hole maar, central Oregon. Bull Geol Soc Am, 81: 1823-1830.

Lorenz, V., 1974a. Studies of Surtsey tephra deposits. Surtsey Res Progr Rep, 7: 72-79

Lorenz, V., 1974b. Vesiculated tuffs and associated features. Sedimentology, 21: 273-291.

Lorenz, V., 1986. On the growth of maars and diatremes and its relevance to the formation of tuff rings. Bull Volcanol, 48: 265-274.

Lorenz, V., 2003. Maar-diatreme volcanoes, their formation, and their setting in hard-rock or soft-rock environments. GeoLines, 15: 72-83.

Lorenz, V., 2007. Syn- and post- eruptive hazards of maar–diatreme volcanoes. J Volcanol Geotherm Res, 159: 285-312.

Lorenz V., Haneke J., 2004. Relationship between diatremes, dykes, sills, laccoliths, intrusive–extrusive domes, lava flows and tephra deposits with unconsolidated water-saturated sediments in the late Variscan intermontane Saar-Nahe Basin, SW Germany. In: Breitkreuz C, Petford N (eds.) Physical Geology of Subvolcanic Systems — Laccoliths, Sills, and Dykes. Blackwell Sciences, Oxford, pp 75-124.

Lorenz, V., Kurszlaukis, S., 2007. Root zone in the phreatomagmatic pipe emplacement model and consequences for the evolution of maar-diatreme volcanoes. J Volcanol Geotherm Res, 159: 4-32.

Luhr, J.F., Simkin, T., 1993. Paricutin: The volcano born in a Mexican cornfield. Geoscience Press, Inc, Phoenix Arizona.

Machado, F., 1958. Acitividade Vulcanica da Ilha do Faial (1957-1958) Atlantida v II: 225-236.

Marra, M.J., Alloway, B.V., Newnham, R.M., 2006. Paleoenvironmental reconstruction of a well-preserved Stage 7 forest sequence catastrophically buried by basaltic eruptive deposits, northern New Zealand. Quaternary Sci Rev, 25: 2143-2161.

Martin, U., Németh, K., 2007. Blocky versus fluidal peperite textures developed in volcanic conduits, vents, and crater lakes of phreatomagmatic volcanoes in Mio/Pliocene volcanic fields of Western Hungary. J Volcanol Geotherm Res, 159:164-178.

Mastin, L.G., 1997. Evidence for water influx from a caldera lake during the explosive hydromagmatic eruption of 1790, Kilauea volcano, Hawaii. J Geophys Res, 102: 20,093-20,109.

Mastin, L.G., 2007. Generation of fine hydromagmatic ash by growth and disintegration of glassy rinds.J Geophys Res, 112, B02203.doi:10.1029/2005JB003883.

Mastin, L.G., Christiansen, R.L., Thornber, C., Lowenstern, J., Besson, M., 2004. What makes hydromagmatic eruptions violent? Some insights from the Keanakako'i Ash, Kilauea volcano, Hawaii. J Volcanol Geotherm Res, 137: 14-31

Mastin, L.G., Spieler, O., Downey, W.S., 2009. An experimental study of hydromagmatic fragmentation through energetic non-explosive magma-water mixing. J Volcanol Geotherm Res, 180: 161-170.

Mattsson, H.B., 2010. Textural variation in juvenile pyroclasts from an emergent, Surtseyan-type, volcanic eruption: The Capelas tuff cone: São Miguel (Azores). J Volcanol Geotherm Res, 189: 81-91.

McDougall, I., Polach, H.A., Stipp, J.J., 1969. Excess radiogenic argon in young sub-aerial basalts from the Auckland volcanic field, New Zealand. Geochimica Cosmochimica A, 33: 1485-1520.

McGee, L.E., Beier, C., Smith, I.E.M., Turner, S.P., 2011. Dynamics of melting beneath a small-scale basaltic system: a U-Th–Ra study from Rangitoto volcano, Auckland volcanic field, New Zealand. Contrib Mineral Petrol 162: 547-563.

McGee, L.E., Millet, M.-A., Smith, I.E.M., Németh, K., Lindsay, J.M., 2012. The inception and progression of melting in a monogenetic eruption: Motukorea volcano, the Auckland Volcanic Field, New Zealand. Lithos, 155: 360-374.

McGee, L.E., Smith, I.E.M., Millet, M.-A., Handley, H.K., Lindsay, A.M., 2013. Asthenospheric control of melting processes in monogenetic basaltic systems: a case study of the Auckland Volcanic Field, New Zealand. J Petrol, 54: 2125-2153.

McFadden, L.D., McDonald, E.V., Wells, S.G., Anderson, J.Q., Forman, S.L., 1998. The vesicular layer and carbonate collars of desert soils and pavements: formation, age, and relation to climate change. Geomorphology, 24: 101-145.

Molloy, C., Shane, P., Augustinus, P., 2009. Eruption recurrence rates in a basaltic volcanic field based on tephra layers in maar sediments: Implications for hazards in the Auckland volcanic field. Geol Soc Am Bull 121: 1666-1677.

Moore, J.G., Nakamura, K., Alcaraz, A., 1966. The 1966 eruption of Taal Volcano. Science, 151: 955-960.

Murtagh, R.M., White, J.D.L., 2013. Pyroclastic characteristics of a subaqueous to emergent Surtseyan eruption, Black Point volcano, California. J Volcanol Geotherm Res, 267:75-91.

Murtagh, R.M., White, J.D.L., Sohn, Y.K., 2011. Pyroclast textures of the Ilchulbong 'wet´ tuff cone, Jeju Island, South Korea. J Volcanol Geotherm Res, 201: 385-396.

Németh, K., Martin, U., 2007. Shallow sill and dike complex in western Hungary as a possible feeding system of phreatomagmatic volcanoes in "soft rock" environment. J Volcanol Geotherm Res, 159:138-152.

Németh, K., Cronin, S.J., 2009. Phreatomagmatic volcanic hazards where rift-systems meet the sea, a study from Ambae Island, Vanuatu. J Volcanol Geotherm Res, 180: 246-258.

Németh, K., Cronin, S.J., 2011. Drivers of explosivity and elevated hazard in basaltic fissure eruptions: The 1913 eruption of Ambrym Volcano, Vanuatu (SW-Pacific). J Volcanol Geotherm Res, 201: 194-209.

Németh, K., Martin, U., Harangi, S., 2001. Miocene phreatomagmatic volcanism at Tihany (Pannonian Basin, Hungary). J Volcanol Geotherm Res, 111(1–4): 111-135.

Németh, K., Cronin, S.J., Charley, D., Harrison, M., Garae, E., 2006. Exploding lakes in Vanuatu – "Surtseyan-style" eruptions witnessed on Ambae Island. Episodes, 29: 87-92.

Németh, K., Goth, K., Martin, U., Csillag, G., Suhr, P., 2008. Reconstucting paleoenvironment, eruption mechanism and paleomorphology of the Pliocene Pula maar (Hungary). J Volcanol Geotherm Res, 177: 441-456.

Németh, K, Cronin, S.J., Haller, M.J., Brenna, M., Csillag, G., 2010. Modern analogues for Miocene to Pleistocene alkali basaltic phreatomagmatic fields in the Pannonian Basin: "soft substrate" to "combined" aquifer controlled phreatomagmatism in intraplate volcanic fields. Cent Eur J Geosci, 2: 339-361.

Németh, K., Cronin, S.J., Smith, I.E.M., Agustín-Flores, J., 2012a. Amplified hazard of small-volume monogenetic eruptions due to environmental controls, Orakei Basin, Auckland Volcanic Field, New Zealand. Bull Volcanol, 74: 2121-2137.

Németh, K., Risso, C., Nullo, F., Smith, I.E:M., Pécskay, Z., 2012b. Facies architecture of an isolated long-lived, nested polygenetic silicic tuff ring erupted in a braided river system: The Los Loros volcano, Mendoza, Argentina. J Volcanol Geotherm Res, 239: 33-48.

Ort, M.O., Carrasco-Núñez, G, 2009. Lateral vent migration during phreatomagmatic and magmatic eruptions at Tecuitlapa, east-central Mexico. J Volcanol Geotherm Res, 181: 67-77.

Pattle Delamore and Partners LTD, 2003. Groundwater modelling of the Waitematas near Three Kings Quarry. Unpublished internal report prepared for Winstone Aggregates, February 2003, New Zealand.

Pillans, B., 1983. Upper Quaternary marine terrace chronology and deformation, South Taranaki, New Zealand. Geology, 11: 292-297.

Pittari, A., Cas, R.A.F., Lefebvre, N., Robey, J., Kurszlaukis, S., Webb, K., 2008. Eruption processes and facies architecture of the Orion Central kimberlite volcanic complex, Fort à la Corne, Saskatchewan; kimberlite mass flow deposits in a sedimentary basin. J Volcanol Geotherm Res, 174: 152-170.

Polach, H.A., Chapell, J., Lovering, J.F., 1969. Australian National University radiocarbon date list. Radiocarbon, 11: 245-262.

Raue, H., 2004. A new model for the fracture energy budget of phreatomagmatic explosions. J Volcanol Geotherm Res, 129: 99-108.

Raza, A., Brown, R.W., Ballance, P.F., Kamp, P.J.J., 1999. Thermal history of the early Waitemata Basin and adjacent Waipapa Group, North Island, New Zealand. New Zealand J Geol Geophys, 42: 469-488.

Ross, P.-S., White, J.D.L., 2006. Debris jets in continental phreatomagmatic volcanoes: a field study of their subterranean deposits in the Coombs Hills vent complex, Antarctica. J Volcanol Geotherm Res, 149: 62-84.

Ross, P.-S., Delpit, S., Haller, M.J., Németh, K., Corbella, H., 2011. Influence of the substrate on maar-diatreme volcanoes – An example of a mixed setting from the Pali Aike volcanic field, Argentina. J Volcanol Geotherm Res, 210: 253-271.

Ross, P.-S., White, J.D.L., Valentine, G.A., Taddeucci, J., Sonder, I., Andrews, R., 2013. Experimental birth of a maar-diatreme volcano. J Volcanol Geotherm Res, 260: 1-12.

Rottas, K.M., Houghton, B.F., 2012. Structure, stratigraphy, and eruption dynamics of a young tuff ring: Hanauma Bay, O´ahu, Hawai´i. Bull Volcanol, 74: 1683-1697.

Sable, J.E., Houghton, B.F., Del Carlo, P., Coltelli, M., 2006. Changing conditions of magma ascent and fragmentation during Etna 122 BC basaltic Plinian eruption: evidence from clast microtextures. J Volcanol Geotherm Res, 158: 333-354.

Sandri, L., Jolly, G., Lindsay, J., Howe, T., Marzocchi, W., 2012. Combining long- and short-term PVHA with cost-benefit analysis to support decision making in a volcanic crisis from the Auckland Volcanic Field, New Zealand. Bull Volcanol 74: 705–723.

Schipper, C.I., White, J.D.L., Houghton, B.F., 2010. Syn- and post-fragmentation textures in submarine pyroclasts from Lo´ihi Seamount, Hawai´i. J Volcanol Geotherm Res, 191: 93-106.

Schipper, C.I., White, J.D.L., Zimanowski, B., Büttner, R., Sonder, I., Schmid, A., 2011. Experimental interaction of magma and “dirty” coolants. Earth Planet Sci Lett, 303: 323-336.

Schmid, R., 1981. Descriptive nomenclature and classification of pyroclastic deposits and fragments: Recommendations to the IUGS Subcommision on the Systematics of Igneous Rocks. Geology, 9(1): 41-43.

Schumacher, R., Schmincke, H.-S., 1991. Internal structure and occurrence of accretionary lapilli – a case study at Laacher See Volcano. Bull Volcanol, 53: 612-634.

Scoble, R., Millar, A., 1995. Kumeu-Hobsonville groundwater resource assessment report (TP60). Auckland Regional Council (now Auckland Council) Technical Publication, Auckland Council, New Zealand, 70 pp.

Scolamacchia, T., Macías, J.L., Sheridan, M.F., Hughes, S.R., 2005. Morphology of ash aggregates from wet pyroclastic surges of the 1982 eruption of el Chichón Volcano, Mexico. Bull Volcanol, 68: 171-200.

Searle, E.J., 1959. The volcanoes of Ihumatao and Mangere, Auckland. New Zealand J Geol Geophys, 3: 870-888.

Searle, E.J., Mayhill, R.D., 1981. City of Volcanoes: a geology of Auckland. Longman Paul, Auckland, New Zealand, 195 pp.

Sherburn, S., Scott, B.J., Olsen, J., Miller, C.A., 2007. Monitoring seismic precursors to an eruption from the Auckland Volcanic Field, New Zealand. New Zealand J Geol Geophys, 50: 1-11.

Sheridan, G.J., 2006. The macroporosity and microporosity components of the Waitemata group rocks, Auckland, New Zealand. M.Sc. thesis, The University of Auckland, New Zealand, 105 pp.

Sheridan, M.F., Wohletz, K.H., 1983. Hydrovolcanism: Basic considerations and review. J Volcanol Geotherm Res, 17: 1-29.

Siddall, M., Chappell, J., Potter, E-K., 2006. Eustatic sea level during the past Interglacials. In: Sirocko F, Litt T, Claussen M, Sanchez-Goni M-F (eds), The climate of past Interglacials, Elsevier, Amsterdam: 75-92.

Simpson, K.A., 1987. Rock properties and slope processes of the Waitemata group soft rock, along sections of the east coast of Auckland, New Zealand. M.Sc. thesis, The University of Auckland, 144 pp.

Smith, I.E.M., 1989. North Island. Intraplate volcanism in New Zealand, In: Johnson, R.W., Taylor, S.R. (eds.). Intraplate volcanism in Australia and New Zealand. Cambridge University Press, pp 157-162.

Smith, I.E.M., Okada, T., Itaya, T., Black, P.M., 1993. Age relationships and tectonic implications of Late Cenozoic basaltic volcanism in Northland, New Zealand. New Zealand J Geol Geophys, 36: 385-393.

Smith, I.E.M., Blake, S., Wilson, C.J.N., Houghton, B.F., 2008. Deep-seated fractionation during the rise of a small-volume basalt magma batch: Crater Hill, Auckland, New Zealand. Contrib Mineral Petrol 155: 511-527.

Smith, I.E.M., McGee, L.E., Lindsay, J.M., 2009. Review of the petrology of the Auckland Volcanic Field. Institute of Earth Science and Engineering Report 1-2009.03, Auckland, New Zealand, 36 pp.

Sohn, Y.K., 1996. Hydrovolcanic processes forming basaltic tuff rings and cones on Cheju Island, Korea. Geol Soc Am Bull, 108: 1199-1211.

Sohn, Y.K., 1997. On traction-carpet sedimentation. J Sedimentary Research, 67: 502-509.

Sohn, Y.K., Chough, S.K., 1989. Depositional processes of the Suwolbong tuff ring, Cheju Island (Korea). Sedimentology, 36: 837-855.

Sohn, Y.K., Chough, S.K., 1992. The Ichulbong tuff cone, Cheju Island, South Korea; depositional processes and evolution of an emergent, Surtseyan-type tuff cone. Sedimentology, 39: 523-544.

Sohn, Y.K., Chough, S.K., 1993. The Udo tuff cone, Cheju Island, South Korea: transformation of pyroclastic fall into debris flow and grain flow on a steep volcanic cone slope. Sedimentology, 40: 769-786.

Sohn, Y.K., Park, K.H., 2005. Composite tuff ring/cone complexes in Jeju Island, Korea: possible consequences of substrate collapse and vent migration. J Volcanol Geotherm Res, 141: 157-175.

Sohn, Y.K., Son, M., Jeong, J.O., Jeon, Y.M., 2009. Eruption and emplacement of a laterally extensive, crystal-rich, pumice-free ignimbrite (the Cretaceous Kusandong Tuff, Korea). Sedim Geol, 2009: 190-203.

Sohn, Y.K., Cronin, S.J., Brena, M., Smith, I.E.M., Németh, K., White, J.D.L., Murtagh, R.M., Jeon, Y.M., Kwon, C.W., 2012. Ichulbong tuff cone, Jeju Island, Korea, revisited: A compound monogenetic volcano involving multiple magma pulses, shifting vents, and discrete eruptive phases. Geol Soc Am Bull, 124: 259-274.

Solgevik, H., Mattsson, H.B., Hermelin, O., 2007. Growth of an emergent tuff cone: Fragmentation and depositional processes recorded in the Capelas tuff cone: São Miguel, Azores. J Volcanol Geotherm Res, 159: 246-266.

Sparks, R.S.J., 1976. Grain size variation in ignimbrites and implications for the transport of pyroclastic flows. Sedimentology, 23: 147-188.

Spörli, K.B., 1978. Mesozoic tectonics, North Island, New Zealand. Geol Soc of Am Bull, 89: 415-425.

Spörli, K.B., Eastwood, V.R., 1997. Elliptical boundary of an intraplate volcanic field, Auckland, New Zealand. J Volcanol Geotherm Res, 79: 169-179.

Spörli, K.B., Rowland, J.V., 2007. Superposed deformation in turbidites and syn-sedimentary slides of the tectonically active Miocene Waitemata Basin, northern New Zealand. Basin Res, 19: 199-216

Spörli, K.B., Black, P.M., 2013. Catalogue of crustal xenoliths from the St Heliers volcanoes, Auckland Volcanic Field, New Zealand. Institute of Earth Science and Engineering Report 1-2013.01, Auckland New Zealand, 67 pp.

Stearns, H.T., 1953. Causes of basaltic explosions. Bull Geol Soc Amer, 64: 599.

Stirling, M.W., McVerry, G.H., Berryman, K.R., 2002. A new seismic hazard model for New Zealand. Bull Seism Soc of Am, 92: 1878-1903.

Stoppa, F., 1996. The San Venanzo maar and tuff ring, Umbria, Italy: eruptive behavior of a carbonatite-melilitite volcano, Bull Volcanol, 57: 563-577.

Stroncik, N.A., Schmincke, H-U., 2002. Palagonite – a review. J Earth Sci (Geol Rundsch), 91: 680-697.

Sulpizio, R., Dellino, P., 2008. Sedimentology, depositional mechanisms and pulsating behaviour of pyroclastic density currents. In: Gottsman, J., Marti, J. (eds.). Caldera Volcanism: analysis, modelling, and response. Developments in volcanism, 10: 57-96. Elsevier, Amsterdam.

Sulpizio, R., Mele, D., Dellino, P., La Volpe, L., 2007. Deposit and physical properties of pyroclast density currents during complex Subplinian eruptions: the AD 472 (Pollena) eruption of Somma-Vesuvius, Italy. Sedimentology, 54: 607-635.

Sulpizio, R., De Rosa, R., Donato, P., 2008. The influence of variable topography on the depositional behaviour of pyroclastic density currents: The examples of the Upper Pollara eruption (Salina Island, southern Italy). J Volcanol Geotherm Res, 175: 367-385.

Taddeucci, J., Pompilio, M., Scarlato, P., 2004. Conduit processes during the July-August 2001 explosive acitivity of Mt Etna (Italy): inferences from glass chemistry and crystal size distribution of ash particles. J Volcanol Geotherm Res, 137: 33-54.

Taddeucci, J., Sottili, G., Palladino, D.M., Ventura, G., Scarlato, P., 2010. A note on maar eruption energetics: current models and their application. Bull Volcanol, 72: 75-83.

Taddeucci, J., Valentine, G.A., Sonder, I., White, J.D.L., Ross, P.-S., Scarlato, P., 2013. The effect of pre-existing crater on the initial development of explosive volcanic eruptions: An experimental investigation. Geophys Res Lett, 40: 507-510.

Tait, M.A., Cas, R.A.F., Viramonte, J.G., 2009. The origin of an unusual tuff ring of perlitic rhyolite pyroclasts: The last explosive phase of the Ramadas Volcanic Centre, Andean Puna, Salta, NW Argentina. J Volcanol Geotherm Res, 183: 1-16.

Thórarinsson, S.,1964. Surtsey, the new island in the North Atlantic, Almenna Bókafélagith, Reykjavík, pp 1-63.

Valentine, G.A., 1987. Stratified flow in pyroclastic surges. Bull Volcanol, 49: 616-630.

Valentine, G.A., 1998. Damage to structures by pyroclastic flows and surges, inferred from nuclear weapon effects. J Volcanol Geotherm Res, 87: 117-140.

Valentine, G.A., 2012. Shallow plumbing systems for small-volume basaltic volcanoes, 2: Evidence from crustal xenoliths at scoria cones and maars. J Volcanol Geotherm Res, 223–224: 47-63.

Valentine, G.A., Groves, K.R., 1996. Entrainment of country rock during basaltic eruptions of the Lucero volcanic field, New Mexico. J Geol, 104: 71-90.

Valentine, G.A., Fisher, R.V., 2000. Pyroclastic surges and blasts. In: Sigurdsson, H., Houghton, B.F. McNutt, S., Rymer, H., Stix, J. (eds.), Encyclopedia of Volcanoes. Washington D.C., Smithsonian Inst Press, pp. 571-580.

Valentine, G.A., Perry, F.V., 2007. Tectonically controlled, time-predictable basaltic volcanism from a lithospheric mantle source (central Basin and Range Province, USA). Earth and Planetary Science Letters 261(1-2): 201-216.

Valentine, G.A., Gregg, T.K.P., 2008. Continental basaltic volcanoes –processes and problems. J Volcanol Geotherm Res, 177:857-873.

Valentine, G.A., White, J.D.L., 2012. Revised conceptual model for maar-diatreme: Subsurface processes, energetics, and eruptive products. Geology, 40: 1111-1114.

Valentine, G.A., Wyk de Vries, 2014. Unconventional maar-diatreme and associated intrusions in the soft sediment-hosted Mardoux structure (Gergovie, France). Bull Volcanol, 76: 807.

Valentine, G.A., Shufelt, N.L., Hintz, A.R.L., 2011. Models of maar volcanoes, Luna Crater (Nevada, USA). Bull Volcanol, 73: 753-765.

Valentine, G.A., Graettinger, A.H., Sonder, I., 2014. Explosion depth for phreatomagmatic eruptions. Geophys Res Lett, 41: 3045-3051.

Valentine, G.A., Graettinger, A.H., Marcorps, E., Ross, P-S., White, J.D.L., Döhring, E., Sonder, I., 2015. Experiments with vertically and laterally migrating subsurface explosions with applications to the geology of phreatomagmatic and hydrothermal explosions craters and diatremes. Bull Volcanol, 77: 15. DOI 10.1007/s00445-015-0901-7.

Van Otterloo, J., Cas, R.A.F., Sheard, M., 2013. Eruption processes and deposit characteristics at the monogenetic Mt. Gambier Volcanic Complex, SE Australia: implications for alternating magmatic and phreatomagmatic activity. Bull Volcanol, 75: 737.

Vaughan, R.G., Webley, P.W., 2010. Satellite observations of a Surtseyan eruption HungaHa'apai, Tonga. J Volcanol Geotherm Res, 198: 177-186.

Vazquez, J.A., Ort, M.H., 2006. Facies variation of eruption units produced by the passage of single pyroclastic surge currents, Hopi Buttes volcanic field, USA. J Volcanol Geotherm Res, 154: 222-236.

Verwoerd, W.J., Chevallier, L., 1989. Contrasting types of Surtseyan tuff cones on Marion and Prince Edward islands, southwest Indian Ocean. Bull Volcanol, 49: 399-417.

Viljevac, Z., Murphy, G., Smaill, A., Crowcroft, G., Bowden, D., 2002. South Auckland groundwater, Kaawa aquifer recharge study and management of the Volcanic and Kaawa aquifers. Auckland Regional Council (now Auckland Council) Technical Publication, Auckland Council, New Zealand, Number 133, 193 pp.

Walker, G.P.L., 1984. Characteristics of dune-bedded pyroclastic surge bedsets. J Volcanol Geotherm Res, 20: 281-296.

Walker, G.P.L., Croasdale, R., 1972. Characteristics of some basaltic pyroclasts, Bull Volcanol, 35: 303-17.

Walker, G.P.L., 1993. Basaltic-volcano systems. In: Prichards, H.M., Alabaster, T., Harris, N.B.W., Neary, C.R. (eds.), Magmatic processes and plate tectonics. Geol Soc Special Pub, 76: 3-38.

White, J.D.L., 1990. Depositional architecture of a maar-pitted playa: sedimentation in the Hopi Buttes volcanic field, northeastern Arizona, U.S.A. Sedim Geol, 67: 55-84.

White J.D.L., 1991a. The depositional record of small, monogenetic volcanoes within terrestrial basins. In: Fisher, R.V., and Smith, G.A. (eds.), Sedimentation in Volcanic Settings: Tulsa, SEPM (Society of Sedimentary Geology), 45: 155-171.

White, J.D.L., 1991b. Maar-diatreme phreatomagmatism at Hopi Buttes, Navajo Nation (Arizona), USA. Bull Volcanol, 53: 239-258.

White, J.D.L., 1996. Impure coolants and interaction dynamics of phreatomagmatic eruptions. J Volcanol Geotherm Res, 74: 155-170.

White, J.D.L., 2001. Eruption and reshaping of Pahvant Butte volcano in Pleistocene lake Bonneville. In: White JDL, Riggs, NR (eds.), Volcaniclastic Sedimentation in Lacustrine Settings: International Association of Sedimentologists Special Publication, 30: 61-80.

White, J.D.L., Houghton, B.., 2000. Surtseyan and related phreatomagmatic eruptions. In: Sigurdsson H, Houghton BF, McNutt SR, Rymer H, Stix J (eds.) Encyclopedia of Volcanoes. Academic Press, San Diego, pp 513-526.

White, J.D.L., Houghton, B., 2006. Primary volcaniclastic rocks. Geol Soc Am, 34: 677-680.

White, J.D.L. Ross, P.-S., 2011. Maar-diatreme volcanoes: A review. J Volcanol Geotherm Res, 201: 1-29.

Wilson L., Head, J.W., 1981. Ascent and eruption of basaltic magma on earth and moon. J Geophys Res, 86: 2971-3001.

Witte, L.C., Cox, J.E., Bouvier, J.E., 1970. The vapor explosion. J Metals, 22: 39-44.

Wohletz, K.H., 1983. Mechanisms of hydrovolcanic pyroclast formation: Grain-size, scanning electron microscopy, and experimental studies. J Volcanol Geotherm Res, 17: 31-63.

Wohletz, K.H., 1986. Explosive magma-water interactions: Thermodynamics, explosion mechanisms, and field studies. Bull Volcanol, 48: 245-264.

Wohletz, K.H., 1998. Pyroclastic surges and compressible two-phase flow. In: Freudt, A., Rosi, M. (eds.), From magma to tephra: modelling physical processes of explosive volcanic eruptions. Amsterdam, Elsevier Science Publications, pp. 246-312.

Wohletz, K.H., Sheridan, M.F., 1979. A model of pyroclastic surge. Geological Society of America Special Paper 180: 177-193.

Wohletz, K.H., McQueen, R.G., 1984. Experimental Studies of Hydrovolcanic Explosions. In: Explosive volcanism: Inception, evolution and hazards. National Academy Press, Washington D.C., USA, pp 158-169.

Wood, C.A., 1980. Morphometric evolution of cinder cones. J Volcanol Geotherm Res, 7: 387-413.

Wright, J.V., Walker, G.P.L., 1981. Eruption, transport and deposition of ignimbrite – a case-study from Mexico. J Volcanol Geotherm Res, 9: 111-131.

Zimanowski, B., Wohletz, K.H., 2000. Physics of phreatomagmatism-II. Terra Nostra, 6: 535-544.

Zimanowski, B., Fröhlich, G., Lorenz, V., 1991. Quantitative experiments on phreatomagmatic explosions. J Volcanol Geotherm Res, 48: 341-358.

Zimanowski, B., Büttner, R., Lorenz, V., Häfele, H-G., 1997. Fragmentation of basaltic melt in the course of explosive volcanism, J Geophys Res, 102:803-814.

## List of Appendices (information contained on CD)

***Chapter 3***

- **Appendix A.1** Thickness of substrate lithologies.
- **Appendix A.2** Hydrogeological information.

***Chapter 5***

- **Appendix B** Published article: Agustín-Flores J., Németh K., Cronin S., Lindsay J., Kereszturi, G., Brand, B., Smith I.E.M., 2014. **Phreatomagmatic eruptions through unconsolidated coastal plain sequences, Maungataketake, Auckland Volcanic Field (New Zealand). Journal of Volcanology and Geothermal Research**, 180: 203-224.
- **Appendix B.1** Maungataketake stratigraphic logs, frequency histrograms, and volume percentage values of phi fractions of 12 selected samples.
- **Appendix B.2** Lithofacies and units of Maungatatake volcano.

***Chapter 5 and 7***

- **Appendix C** Chemical Analyses.

***Chapter 6***

- **Appendix D** Published article: Agustín-Flores J., Németh K., Cronin S., Lindsay J., Kereszturi, G., 2015. **Shallow-seated explosions in the construction of the Motukorea tuff ring (Auckland, New Zealand): evidence from lithic and sedimentary characteristics**. **Journal of Volcanology and Geothermal Research**, 304: 272-286.
- **Appendix D.1** Motukorea stratigraphic logs, grain size distribution and juvenile/llithic content of selected samples.
- **Appendix D.2** Lithofacies of Motukorea volcano.

***Chapter 7***

- **Appendix E** Published article: Agustín-Flores J., Németh K., Cronin S., Lindsay J., Kereszturi, G., 2015. **Construction of the North Head (Maungauika) tuff cone: a product of Surtseyan volcanism, rare in the Auckland Volcanic Field, New Zealand**. **Bulletin of Volcanology**, 77: 11.
- **Appendix E.1** North Head stratigraphic logs, frequency histograms, grain size distribution and juvenile/lithic content of selected samples.

## Appendix A.1. Thicknesses of substrate lithologies

This appendix is related to the information about the substrate beneath Auckland. The thicknesses and distribution of these lithologies, which are schematically and generically described in chapters 3, 5, 6, and 7 in the thesis, were taken principally from three sources in the literature: Kenny et al. (2011), Kenny et al. (2012), Kereszturi et al. (2014). In turn, these publications based their results in the use, analysis, and modelling of deep borehole data now in the PETLAB website (www.pet.gns.cri.nz). Apart from borehole data, Kenny et al. (2011, 2012) use geophysical data combined with structural information gleaned from current topography and exposed geology (the main objective of these authors was the mapping of unknown faults in the Auckland area). Since all authors have used a great deal of borehole data (Fig. A.1.1) (Kenny et al., 2011, 2012 used over 2000 borehole drill data and Kereszturi et al., 2014, used 421 borehole drill data), the specific borehole information will not be presented in this appendix. Instead the regional thicknesses of the lithologies in the southern volcanic field (Northern Manukau Lowlands or simply Manukau Lowlands) are shown in cross-sections and maps.

The presence of Waitemata rocks beneath North Head and Motukorea is attested by the exposures of this lithology around the volcanoes. North Head did not disrupt the underlying substrate (chapter 7), but Motukorea was erupted through 200-300 m of Waitemata substrate (chapter 6). The figures for the Waitemata thickness at Motukorea were also inferred from Kenny et al. (2011, 2012) data. The Auckland Volcanic Field (AVF) has been subdivided into the northern AVF (North Shore and Auckland Isthmus, Fig. A.1.1) and the southern AVF (Northern Manukau Lowlands, Fig. A.1.1). The former seats virtually on Waitemata rocks, whereas the latter overlies a combination of Waitemata rocks and Plio-Pleistocene sediments (Kaawa Formation + Tauranga Group) (see chapter 3 for descriptions of lithologies).

Fig. A.1.1 (figure modified from Kenny et al., 2012) shows the map of the Auckland region showing boreholes used in Kenny et al. (2011, 2012) study. Kereszturi et al. (2014) used boreholes located in the Manukau Lowlands. The locations of the studied volcanoes are shown.

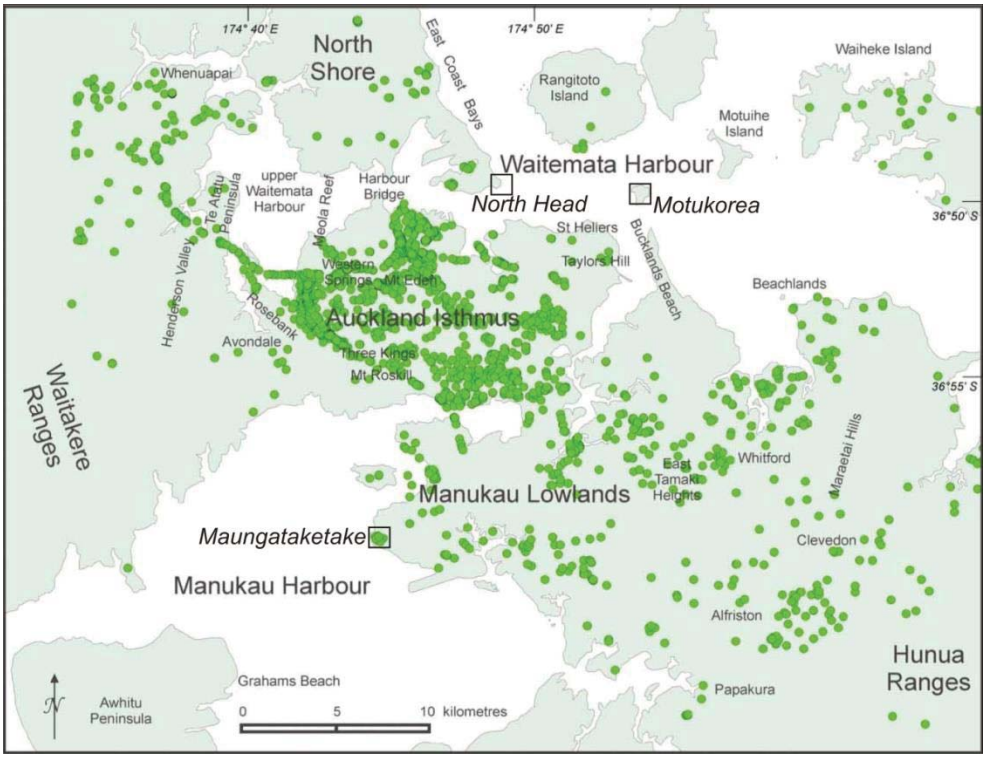


Fig. A.1.1

Fig. A.1.2 (from Kenny et al., 2012) shows the elevation map of current Auckland topography. It can be seen that the southern AVF is located in the low lying area known as the Manukau Lowlands.

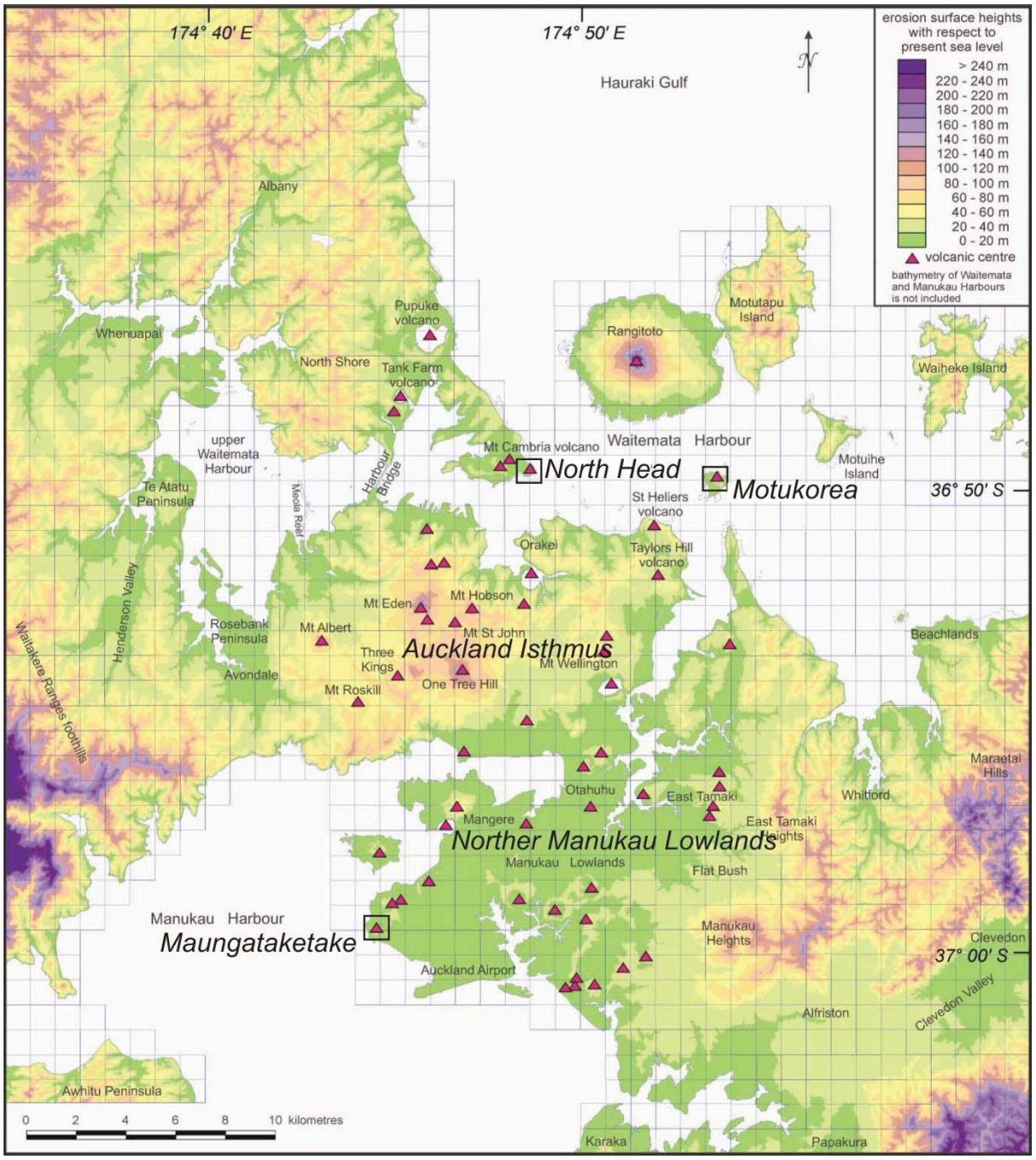


Fig. A.1.2

On the other hand, the erosion surface of the Waitemata Group rocks is now exposed or concealed beneath volcanics and sediments in the AVF. The erosion surface is the top of the Waitemata rocks as it exists at present time. Kenny et al. (2011, 2012) plotted the depths to the Waitemata Group from borehole log information and

also manually contouring the map. Fig. A.1.3 represents the erosion surface of the Waitemata Group rocks (Kenny et al., 2011, 2012). Although volcanoes post-date the erosion surface, they are shown to assist comparison with the Fig. A.1.2. Note the depth of the Waitemata rocks in the Manukau Lowlands (areas of white represent areas of unknown depths). The eroded surface is covered by Plio-Pleistocene sediments in this section of the AVF (see the cross-section by Kereszturi et al., 2014, Fig. 2.1.6). From the map is seen that the Waitemata rocks lie around 20 to 60 m below sea level. Conversely, in the Auckland Isthmus area the Waitemata eroded surface is generally higher and mostly covered by volcanics or exposed.

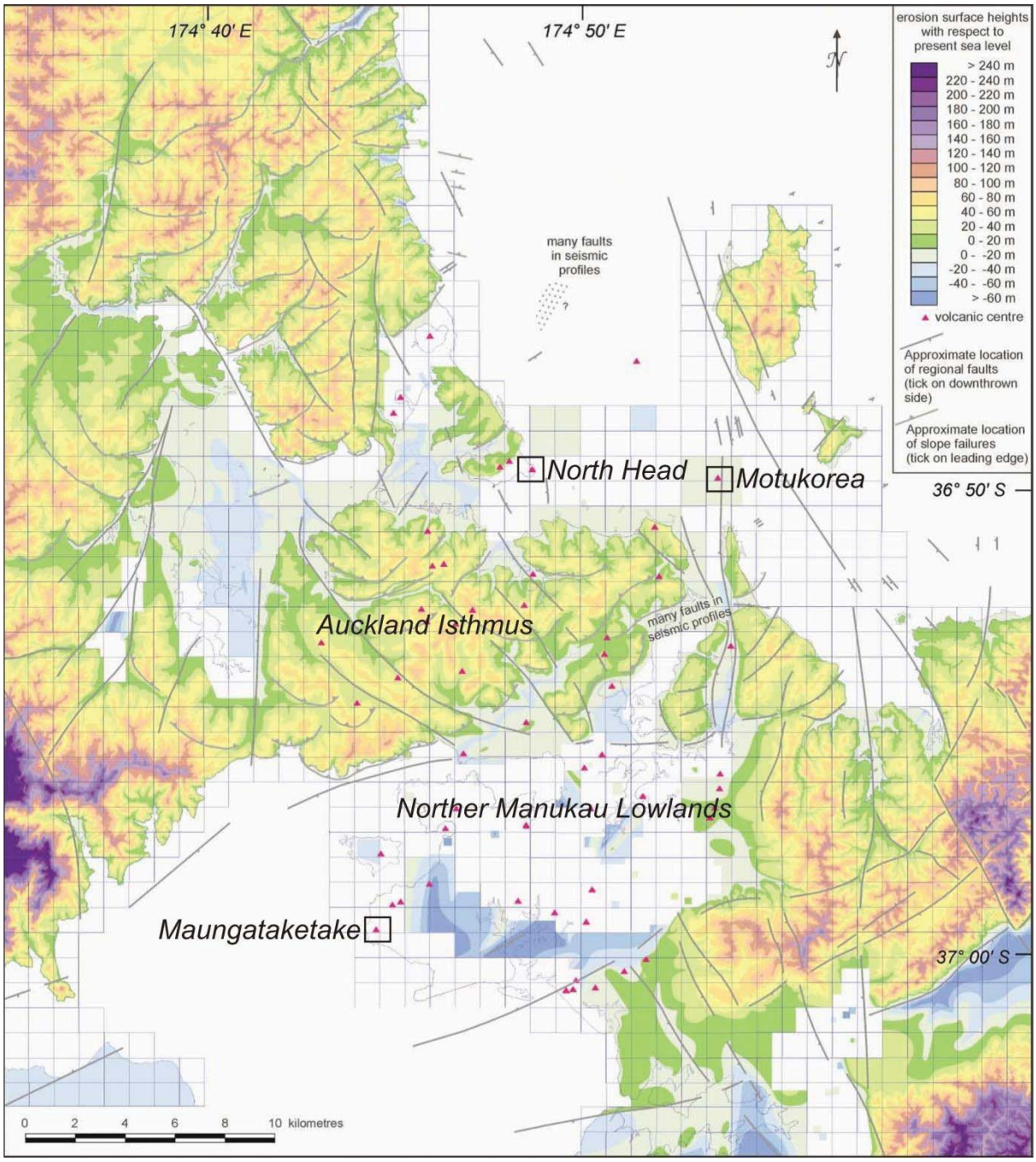


Fig. 2.1.3

This two previous map (2 1.2 and 2.1.3) give an idea of the distribution of the surface of the Waitemata rocks and its depth, which in turn provides clues on the type of the pre-eruptive surface at the time of the eruptions took place. This information was invoked in the reconstruction of the eruption of the three studied volcanoes.

According to Kenny et al. (2012) approximately 55% of the boreholes penetrated into the Waitemata rocks and further 5% reached the basement greywacke, either through the Waitemata rocks (and occasionally also Te Kuiti Group, see figure 3.2 in the main thesis text) or directly beneath superficial post-Miocene sediments. Of the remaining 40% just under half ended in post-Miocene sediments of fill. Due the relatively limited of drill holes reaching the basement, the thickness of the Waitemata Group rocks is difficult to assess. However, with the borehole information gathered and analysed by Kenny et al. (2011, 2012) it was possible to plot a map with locations of boreholes reaching greywacke (basement) (Fig. 2.1.4 from Kenny et al., 2011) ,where the depths are written in black numbers, or extending deep into Waitemata Group rocks without penetrating greywacke (grey numbers with a > 'deeper than' symbol). Greywacke is encountered in successively deeper boreholes in a westward direction (Fig. 2.1.4), but is deep under most of Auckland and yet to be penetrated (Kenny et al., 2011). Geophysical information analysed by Kenny et al. (2011) showed that the interface between the basement and the Waitemata rocks dips westward at different areas in the Auckland area. This information was used in chapter 6 to infer the thickness of the Waitemata rocks beneath Motukorea.

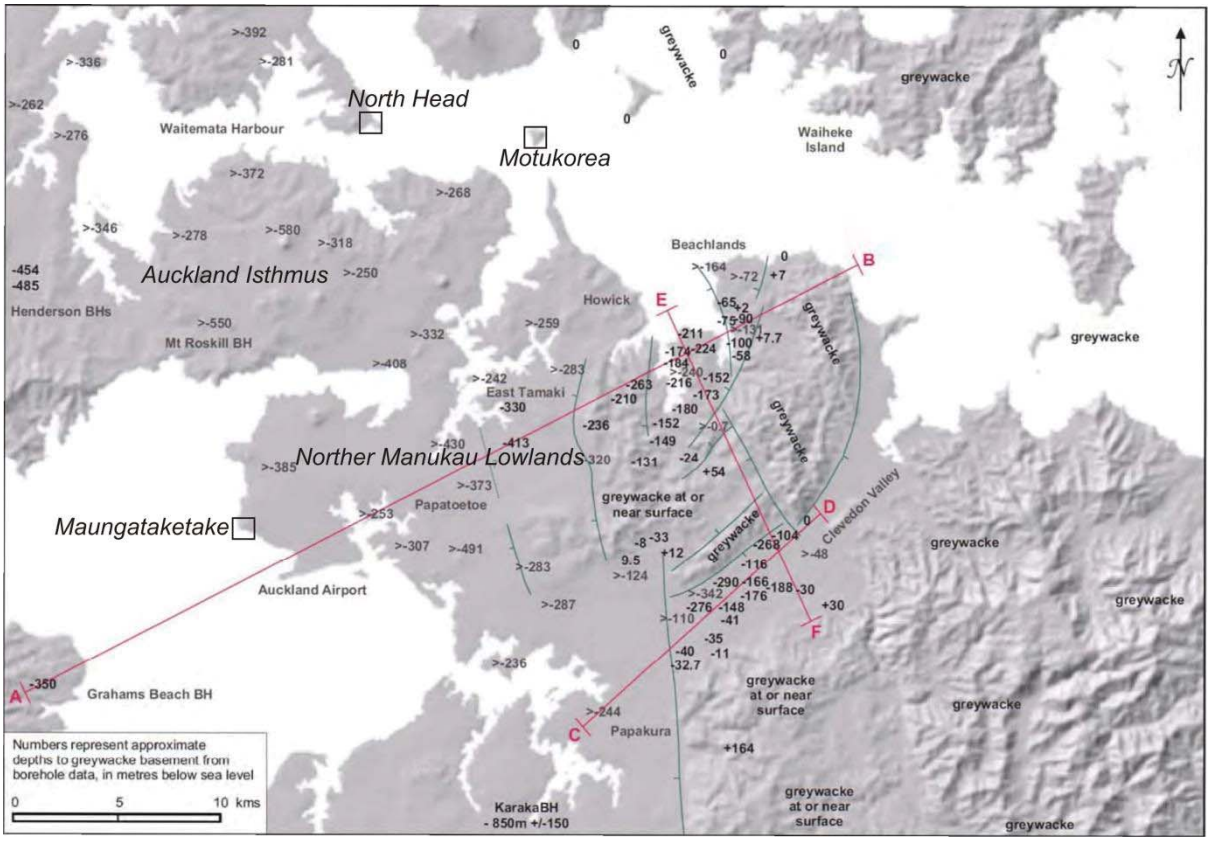


Fig. 2.1.4

A simplified cross-section A-B (Fig. 2.1.4) is shown in Fig. 2.1.5 (from Kenny et al., 2012). This cross-section corresponds to the Manukau Lowlands area and gives a general idea of the distribution of lithologies beneath the volcanics in this part of the AVF.

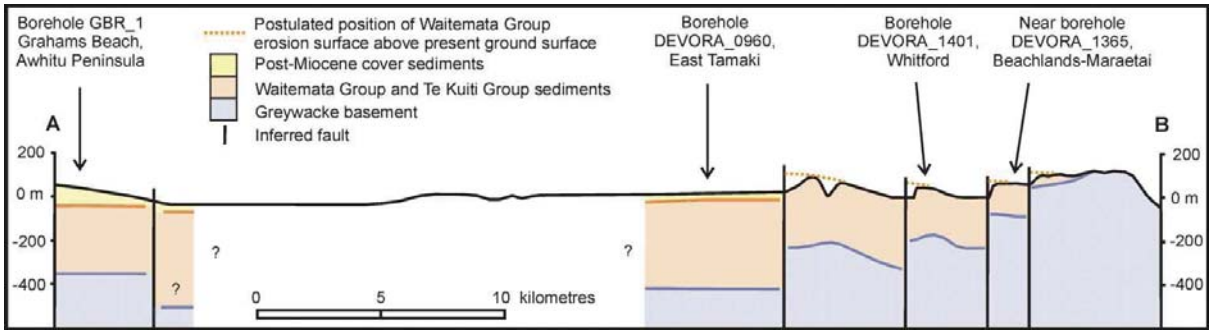


Fig. 2.1.5

The Plio-Pleistocene sediments, that is Tauranga Group and Kaawa Formation (see Fig. 3.2 and main thesis text in chapter 3 for description of such lithogies), are named Post-Miocene cover sediments by Kenny et al. (2012).

Kereszturi et al. (2014) presents a more detailed cross-section from the Manukau Lowlands (Fig. 2.1.6; modified from Kereszturi et al., 2014)). The maximum depth of the loose sediment cover (i.e. Tauranga Group and Kaawa Formation) at each drill core location was used to create an interpolated surface using natural neighbour interpolation method. In the AVF, the Manukau Lowlands host the largest thickness of post Waitemata soft-sediment cover within coastal alluvial basin. The cross-section are A-A' and B-B', both are within the Manukau Lowland areas. Unfortunately, none of the cross-sections cuts at Maungataketake volcano, but it provides with a clear picture of the distribution of substrate lithologies in the Manukau Lowlands. However, by extrapolating the thicknesses of the Tauranga Group from the borehole data, the thicknesses of these, water-saturated, unconsolidated sediments were mapped across the AVF (Fig. 2.1.7). Maungataketake lies in an area where the sediment cover is around 40-50 m. Note that the presence of the Tauranga sediments is scarce in the northern AVF. The Kaawa Formation is absent in the northern AVF, but still present in the southern AVF, and was not mapped. The thickness of the Kaawa formation in the Manukau Lowlands is variable, but probably of tens of metres. Kaawa Formation thickness beneath Maungataketake is unknown, but few drill holes attest the presence of lenses of Kaawa lithologies.

References

Kenny, J.A., Lindsay, J.M., Howe, T.M., 2011. Large-scale faulting in the Auckland region. Institute of Earth Sciences and Engineering Report 1-2011.04, Auckland, New Zealand, 95 pp.

Kenny, J.A., Lindsay, J.M, Howe, T.M., 2012. Post-Miocene faults in Auckland: insights from borehole and topographic analysis. New Zealand J Geol Geophys, 55: 323-343.

Kereszturi, G., Nemeth, K., Cronin, S.J., Procter, J., Agustin-Flores, J., 2014. Infuences on the variability of eruption sequences and style transitions in the Auckland Volcanic Field, New Zealand. J Volcanol Geotherm Res, 286: 101-115.

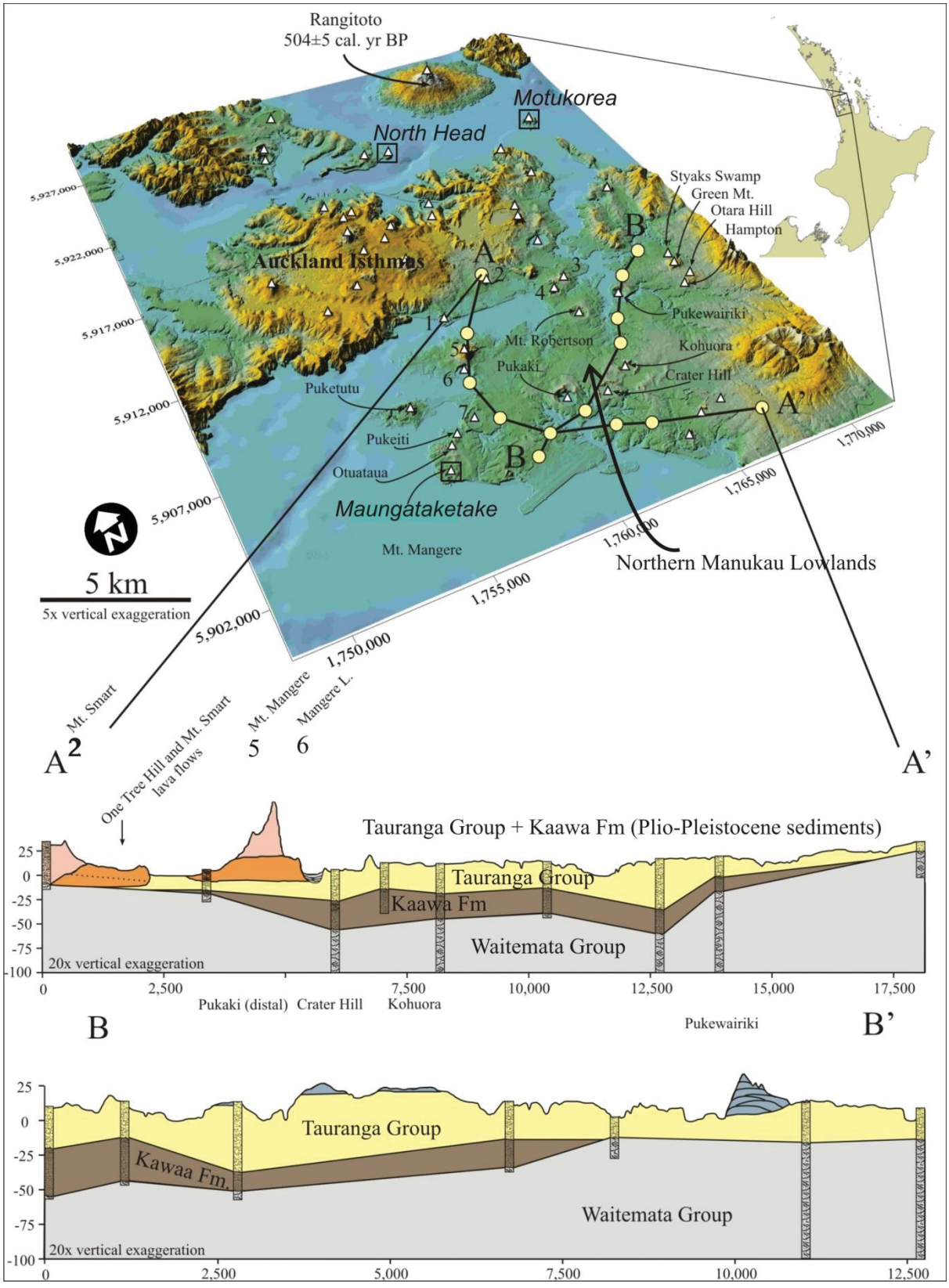


Fig. 2.1.6 The coordinates are in metres (New Zealand Transverse Mercator 2000.

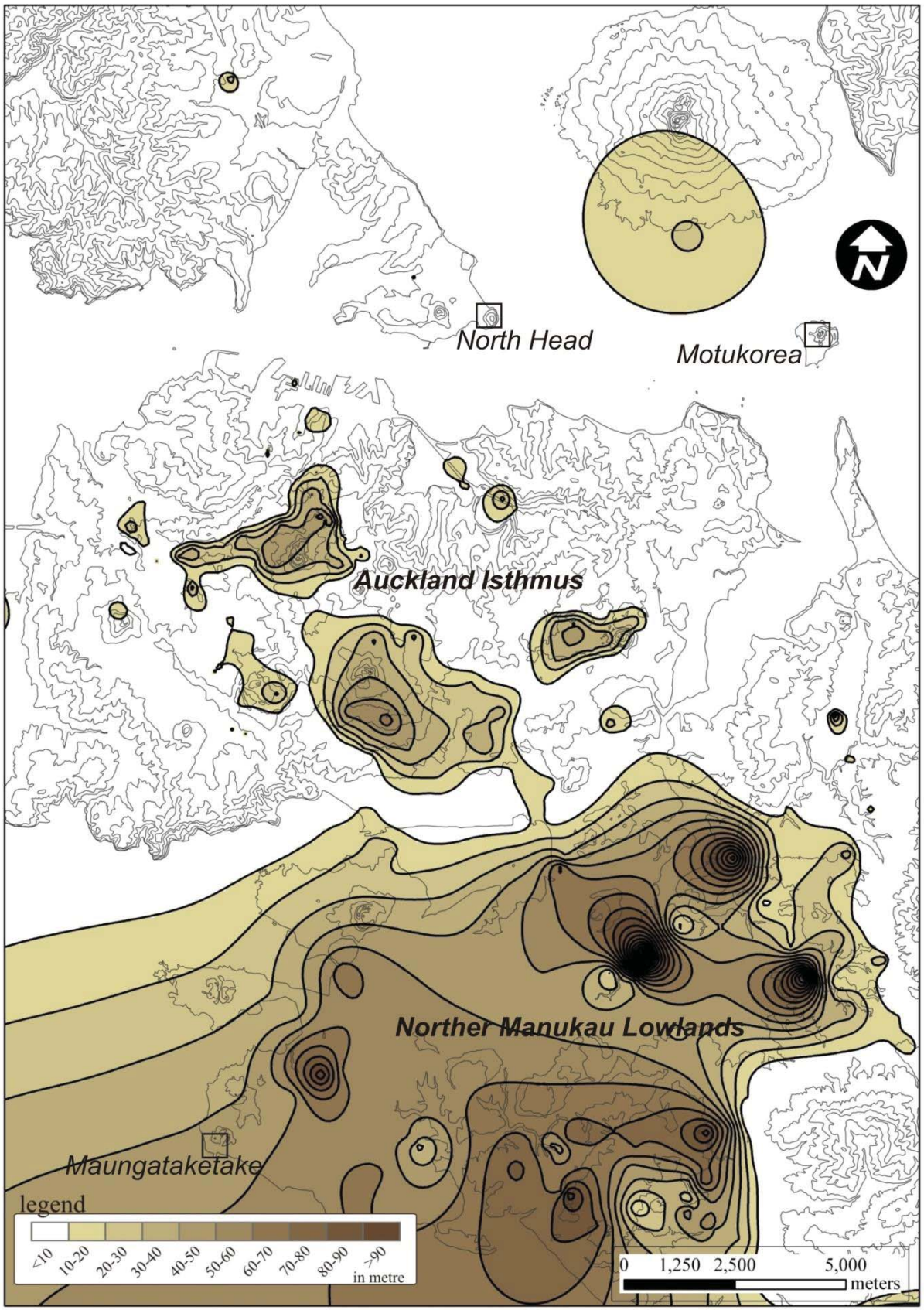
North Head
Motukorea
Auckland Isthmus
Norther Manukau Lowlands
Maungataketake
legend
<10
10-20
20-30
30-40
40-50
50-60
60-70
70-80
80-90
>90
in metre
0 1,250 2,500 5,000
meters

Fig. 2.1.7

## Appendix A.2 Hydrogeological information

Some of the hydrogeological properties and aquifers characteristics of aquifers within the Auckland Volcanic Field are listed in Table A.1. All data is sourced from reports and unpublished data. Note that the widespread lava flows in the field form fractured aquifers.

References for the data on Table A.1:


Auckland Regional Council, 1993: Draft Paraki geothermal groundwater resource statement and management plan.

Crowcroft, G., Smaill, A., 2001. Auckland. In: Groundwaters of New Zealand. M.R. Rosen and P.A. White (Eds.). New Zealand Hydrological Society Inc., Wellington, New Zealand: 303-313.

Crowcroft, G., Bowden, D., 2002. Auckland Water Resource Quantity Statement 2002; Surface water and groundwater resource information availability and location. Technical Publication Number 171, Auckland Regional Council, 44 pp.

Harding, B.C., Pattle, A., Harris, M.G., Twose, G., 2010. Groundwater response to the dewatering of a volcanic vent. IAEG Congress 2010. Presentation, 15 pp.

Moore, S.R., 1997. A combined geophysical and hydrogeological investigation of the Mt Richmond/McLennan Hills aquifer system, Auckland, New Zealand. M.Sc. thesis, The University of Auckland, 141 pp.

Namjou, P., 1996. Hydrogeological evaluation of proposed landfill sites in the greater Auckland area (New Zealand): Mt Wellington and Peach Hill Valley. M.Sc. thesis, The University of Auckland, 479 pp.

Namjou, P., Strayton, G., Pattle, A., Davis, M.D., Kinley, P., Cowpertwait, P., Salinger, M., Mullan, A., Patterson, G., 2005. Groundwater behavior in a fractured basalt aquifer under existing and future climate and land use in Auckland City (New Zealand). Impacts of Global Climate Change: 1-12.

Orgias, S., 2004. Groundwater flow characteristics of a low lying coastal aquifer system, Okahukura Peninsula, Norht Auckland. M.Sc. thesis, The University of Auckland, New Zealand,

Scoble, R. and Millar, A., 1995. Kumeu-Hobsonville groundwater resource assessment report (TP60). Auckland Regional Council (now Auckland Council) Technical Publication, Auckland Council, New Zealand, 70 pp.

Sheridan, G.J., 2006. The macroporosity and microporosity components of the Waitemata group rocks, Auckland, New Zealand. M.Sc. thesis, The University of Auckland, New Zealand, 105 pp.

Viljevac, Z., 1998. Western Springs Aquifer. Hydrogeological characteristics and computer model. M.Sc. thesis, The University of Auckland, 144 p.

Viljevac, Z., Murphy, G., Smaill, A., Crowcroft, G., and Bowden, D., 2002. South Auckland groundwater, Kaawa aquifer recharge study and management of the Volcanic and Kaawa aquifers. Auckland Regional Council (now Auckland Council) Technical Publication, Auckland Council, New Zealand, Number 133, 193 pp.

Table A.1

| Aquifer | Aquifer type | Locality | Thickness (m) | Porosity | Permeability |
|---|---|---|---|---|---|
| Waitemata | Confined-semiconfined | General | 200-400 (?) depth of bores | | |
| Auckland volcanics | Fractured, unconfined | Onehunga/Mt Wellington | <60 | | |
| Auckland volcanics | Fractured, unconfined | Western Springs | <50 | | |
| Auckland volcanics | Fractured, unconfined | Mt Richmond | <45 | | |
| South Auckland volcanics | Fractured, unconfined (?) | General | Boreholes drilled 30-60 | | |
| Kaawa | Confined porous | General | Shellbeds (up to 6 m) | | |
| Waitemata | Confined to semiconfined (?) | North-Western Region | Bores drilled 120-300 | | |
| Waitemata | Confined to semiconfined (?) | North-East Region (General) | 100-800 | | |
| Waitemata | Confined to semiconfined (leaky) | North-East Region (Toramata) | 100-150 | | |
| Waitemata | Confined to semiconfined (?) | Kaipara and North Shore Region | Boreholes drilled 50-370 | | |
| Auckland volcanics | Unconfined | One Tree Hill | <60 | | |
| Auckland volcanics | Unconfined | Mt Wellington-Mt Smart | | | |
| Auckland volcanics | Unconfined | Western Springs | <50 | | |
| Auckland volcanics | Unconfined | Mt Richmond | <45 | | |
| Auckland volcanics | Unconfined | McLaughlins/Wiri | <30 | | |
| Waitemata | Confined to semiconfined (?) | Manukau/Wiri | >500 | | |
| Waitemata | Confined to semiconfined (?) | East Tamaki | Up to 400 | | |
| Waitemata | Confined to semiconfined (?) | Clevedon East | Up tp 230 | | |
| Waitemata | Confined to semiconfined (?) | Clevedon West | Up to 300 | | |
| Waitemata | Confined (?) | South Auckland area | | | |
| Auckland volcanics | Unconfined | Mt Wellington | | | 3x10E-6-1x10E-3 m/s |
| Waitemata | Semiconfined | General | | | |
| Waitemata | Semiconfined | Three Kings (A) (Distrubed) | | | |
| Waitemata | Semiconfined | Three Kings (A) (Undistrubed) | | | |
| Waitemata | Semiconfined (?) | Britomart | 30 m (for practical purposes) | | |
| Auckland volcanics | Unconfined | Three Kings | | | |
| Waitemata | Semiconfined (?) | Kumeu-Hobsonville | >300 | | |
| Auckland volcanics | Unconfined-perched | Basaltic, South Auckland | up to 100 | Primary (up to 10%) Actual (>25%) | |
| Tuff | N/A | South Auckland area | | Welded (14%) Pumiceous (40%) | |
| Plio-Pleistocene sediments | N/A | South Auckland area | | | |
| Kaawa | Confined | South Auckland area | up to 240 | | |
| Waitemata | Confined-perched | South Auckland area | | | |
| Auckland volcanics | Unconfined-perched | South Auckland area (?) | | | |
| Kaawa | Confined-perched | South Auckland area (?) | | | |
| Waitemata | ? | South Auckland area (?) | | | |
| Waitemata | Fractured (?) | Paraki | | | |
| Auckland volcanics | Fractured | Auckland area | 38.3, 24, 34.3 | | |
| Waitemata | | Omaha Beach | | | |
| Auckland volcanics | Fractured (?) | McLennan Hills | up to 45 | | |
| Auckland volcanics | Fractured (?) | Mt Richmond | | | |
| Auckland volcanics | Fractured (?) | General | | | |
| Auckland volcanics | Fractured (?) | Onehunga (Royal Oak) | | | |
| Auckland volcanics | Fractured (?) | Onehunga (Penrose) | | | |
| Auckland volcanics | Fractured (?) | Onehunga (Mt Wellington) | | | |
| Auckland volcanics | Fractured (?) | Onehunga (Southdown) | | | |
| Auckland volcanics | Fractured (?) | Western Springs (Mt Eden) | | | |
| Auckland volcanics | Fractured (?) | Western Springs (Three Kings) | | | |
| Auckland volcanics | Unconfined, fractured | Mt Wellington | at least 40 | effective poros= 0.08 +/- 0.02 | |
| Auckland volcanics | Unconfined, fractured | Mt Wellington | at least 40 | effective poros= 0.08 +/- 0.02 | |
| Waitemata | Confined-unconfined | Mt Wellington (Waitemata) | 100 m for study purposes (local aquifer system; but deeper | ave. effective poros= 0.3; siltstone and sandstone 0.01-0.4 | |
| Waitemata | Confined-unconfined | Mt Wellington (siltstone) | 100 m for study purposes (local aquifer system; but deeper | ave. effective poros= 0.3; siltstone and sandstone 0.01-0.4 | |
| Plio-Pleistocene sediments | N/A | Mt Wellington | up to 10 | non-permeable | |
| Alluvial deposits | N/A | Western Springs | up to 20 | 25-60% | 10-100 darcys |
| Tuff | N/A | Western Springs | | 39, 40, 36, 14 % | 0.04, 11.5, 1.4, 0.33 mdarcys |
| Auckland volcanics | Unconfined | Western Springs | up to 21 (two parts) | | |
| Waitemata | Unconfined-semiconfined | Okahukura Peninsula | | | |
| Waitemata | Confined | ECBF/BHBF | outcrops (305 measured) | effective porosity (sandstone)=15.5% | |

Table A.1
Continuation

| Hydraulic conductivity (m/s) | Transmissivity (m2/day) | Storativity | Storage coeficient | Specific storage | Water availability (m3/year) | Yield (m3/day) | Aquifer fluctuation (m) |
|---|---|---|---|---|---|---|---|
| | 1-250 | | | | 2.7x10E6-105,000 | 30-300 (100mm diam bore) | 2m approx (seasonal fluct., ?) |
| | 108-260 | | | | 13.3x10E6 | | |
| | 28-7700 | | | | 9.6x10E6 | | |
| | 260(tuff)-800(basalt) | | | | 880,000 | | |
| | 7-5600 (10-500 typical) | 7x10E-5-4.2x10E-2 | | | 1xE6 (Pukekohe) | | |
| | 30-500 | 10E-2-10E-5 | | | 6.4xE6 | 800-1200 (100-150 mm diam bore) | |
| | 1-13. | | | | | 10-200 | |
| | 4-250 | | | | | | <1m to within 2 m (incl. water pumping) |
| | 44.5-278.5 | 10E-4-1.7x10E-5 | | | | | |
| | 0.1-10 | 10E-3-2x10E-5 | | | | | |
| | 152-2, 656 | | | | | | |
| | 111-1, 636 | | | | | | |
| | 103-7, 800 | | | | | | |
| | 260(tuff)-1,500(rock) | | | | | | |
| | | | | | | | |
| | 2-21. | | | | | | |
| | | | | | | | |
| | 1-8. | | | | | | |
| | 15-61, 360 | | | | | | |
| | 6-62. | 0.035-0.00012 | | | | 30-300 (90-100 mm borehole) | |
| | | | | | | | |
| | | | | | | 400 | |
| Kx= 8x10E-5-7x10E-9 (9.4x10E-7) | | | 0.1(Sy)/1x10E-5(Ss) | | | | |
| Kx= 4x10E-10-3x10E-8 (1.5x10E-8) | | | 0.1(Sy)/1x10E-5(Ss) | | | | |
| | | 1x10E-4-1x10E-3 | | 1x10E-5 | | | |
| Kx= 2x10E-4 | | | 0.1 | | | | |
| 9.027x10E-8-5.21x10E-10 | 2 | | | | | | 3 m (including pumping) |
| | 13.2-2026 (av=344.145)(med=226) | 4.84x10E-4-2x10E-4 | | | | | |
| | | | | | | | |
| Variable | | | | | | | |
| | 13.7-500 (shell=163.118) (Kaawa=179.46) | 3.3x10E-5-2.15x10E-5 | | | | | |
| 3.125x10E-7 average (?) | 1.17-205.2 (ave=85.242)(med=48.87) | | | | | | |
| 3.47x10E-6-3.6x10E-3 | 7-5600. | 7x10E-5-4.2x10E-2 | | | | | |
| 1.16x10E-5 | 255-350 | | | | | | |
| | 20-60; 1-10 (Auckland ?) | | | | | | |
| | 270-2434 (av=500) | 4x10E-3 | 4x10E-3 | | | | up to 3 m (including pumping) |
| | | | | | | | |
| | | | | | | | |
| | | | | | 337335 | | 0.3-5.7 |
| 5.78x10E-5-3.7x10E-3, 1.15x10E-3 | | | | | 316050 | | |
| 2x10E-1-5x10E-5 (mean 9x10E-4) | | | 0.03-0.2 | | | | |
| | | | | | | | |
| | | | | | | | |
| | | | | | | | |
| | | | | | | | |
| | | | | | | | |
| | | | | | | | |
| 8x10E-4-1x10E-3 (Roberts, 1980); 1x10E-5 (Pattle Delamore) | | | | | | 1420 (summer)-1640 (winter) | |
| 2.6x10E-6; 1.2x10E-5; 3.7x10E-6; 1.8x10E-6 (Basalt) >1x10E-4 (Scoria) | | | | | | | |
| calibrated=1.5x10E-6-1.4x10E-10; Kz= 5x10E-8 | | 1x10E-6 | 0.2b-3.3x10E-6b (confined, ?) | | | | |
| 1x10E-7 | | | | | | | |
| 3.2x10E-7; 2.9x10E-7 | | | | | | | |
| | | | | Specific yield 40% | | | |
| | | | | | | | |
| 6.71x10E-5-1.46x10E-3 (av.= 6.77x10E-4) | 28-4800 | | | | | | 0.7, 1.2, 1.4 (seasonal) |
| 2.18x10E-5-1.55x10E-5 | 32.2, 45 | | | | | 150 | |
| average: Kx=1x10E-6; Kz=1.5x10E-10 | | | | | | | |

Table A.1
Continuation

| Yield (m3/day) | Aquifer fluctuation (m) | Groundwater velocity (m/day) | Study source | Comments |
|---|---|---|---|---|
| 30-300 (100mm diam bore) | 2m approx (seasonal fluct., ?) | | Crowcroft and Smail, 2001 | |
| | | | Crowcroft and Smail, 2001 | |
| | | | Crowcroft and Smail, 2001 | |
| | | | Crowcroft and Smail, 2001 | |
| | | | Crowcroft and Smail, 2001 | Responds quickly to rainfall |
| 800-1200 (100-150 mm diam bore) | | | Crowcroft and Smail, 2001 | Approx 28x10E6 m3/y regional water use in all Auckland area |
| 10-200 | | | Crowcroft, and Bowden., 2002 | |
| | <1m to within 2 m (incl. water pumping) | | Crowcroft, and Bowden., 2002 | |
| | | | Crowcroft, and Bowden., 2002 | |
| | | | Crowcroft, and Bowden., 2002 | Poor properties in Henderson and North Shore |
| | | | Crowcroft, and Bowden., 2002 | |
| | | | Crowcroft, and Bowden., 2002 | |
| | | | Crowcroft, and Bowden., 2002 | |
| | | | Crowcroft, and Bowden., 2002 | |
| | | | Crowcroft, and Bowden., 2002 | |
| | | | Crowcroft, and Bowden., 2002 | |
| | | | Crowcroft, and Bowden., 2002 | |
| | | | Crowcroft, and Bowden., 2002 | |
| | | | Crowcroft, and Bowden., 2002 | |
| | | | Crowcroft, and Bowden., 2002 | |
| 30-300 (90-100 mm borehole) | | | Crowcroft, and Bowden., 2002 | |
| | | | Harding-Pattle et al., 2010 | Not significal horizontal/vertical anisotropy |
| 400 | | | Harding-Pattle et al., 2010 | |
| | | | Harding-Pattle et al., 2010 | Kz is at least one order of magnitude smaller than Kx |
| | | | Harding-Pattle et al., 2010 | |
| | | | Harding-Pattle et al., 2010 | |
| | | | Harding-Pattle et al., 2010 | |
| | 3 m (including pumping) | | Scoble and Millar, 1995 | 1000-4000 kPa (compresive strengh) |
| | | | Viljevac et al., 2002 | Recharged from soil moisture |
| | | | Viljevac et al., 2002 | Aquitard |
| | | | Viljevac et al., 2002 | Aquitard |
| | | | Viljevac et al., 2002 | |
| | | | Viljevac et al., 2002 | |
| | | | Viljevac et al., 2002 | Confusing origin of data (shown in the conceptual models) |
| | | | Viljevac et al., 2002 | Confusing origin of data (shown in the conceptual models) |
| | | | Viljevac et al., 2002 | Confusing origin of data (shown in the conceptual models) |
| | up to 3 m (including pumping) | | Paraki Geoth Ground 1993 | Hydrothermal aquifer |
| | | | Hong et al., 2002 | |
| | | | Thorley, 2004 | Separate shallow and deep water flows in the Waitemata, and confluence |
| | 0.3-5.7 | | Moore, 1996 | Average density of Waitema= 2200 kg/m3 |
| | | | Moore, 1996 | |
| | | | Namjou et al., 2006 | |
| | | 14.4 | Namjou et al., 2006 | |
| | | 17.6 | Namjou et al., 2006 | |
| | | 8.2 | Namjou et al., 2006 | |
| | | 0.8 | Namjou et al., 2006 | |
| | | 20.9 | Namjou et al., 2006 | |
| | | 7 | Namjou et al., 2006 | |
| 1420 (summer)-1640 (winter) | | | Namjou, 1996 | Heterogeneous horizontal aquifer (1x10E-3-1.8x10E-6) |
| | | | Namjou, 1996 | Other values for K=8.4x10E-4-1x10E-3; 3x10E-5-3.8x10E-3 |
| | | | Namjou, 1996 | |
| | | | Namjou, 1996 | |
| | | | Namjou, 1996 | Lowers the vertical permeability |
| | | | Viljevac, 1998 | |
| | | | Viljevac, 1998 | |
| | 0.7, 1.2, 1.4 (seasonal) | 1.2, 0.2-0.6 (upper aquifer);0.5, >2 (lower aquifer) | Viljevac, 1998 | |
| 150 | | | Orgias, 2004 | Permeability of Waitemata 2.7x10E-2 m/day (?); hydraulic gradient=0.002 |
| | | | Sheridan, 2006 | |

## Appendix B.1 Maungataketake stratigraphic logs, frequency histograms, and volume percentage values of phi fractions of 12 selected samples.

This appendix first presents the total of logs corresponding to Maungataketake volcano (Figs. B.1.1 to B.1.9). There are 3 extra logs included (MM1, MM2, and MM3).The logs showed in chapter 5 (M1, M2, M3, M4, and M5) are also included. Additionally, because Fig. 5.2 is not clear in the thesis, the correlation of logs is presented as Fig. B.1.10 without the frequency histograms (now included in the logs) and the graph with the percentages of grain size fractions (now presented as itself in Fig. B.1.11). Also, Table B.1.1 displays the volume percentage for phi fractions of the 12 selected sieved samples.

Fig. B.1.1 shows the plan view of Maungataketake volcano (modified from Brand et al., 2014). Alongside the 5 sites described in chapter 5, other 3 sites are included.

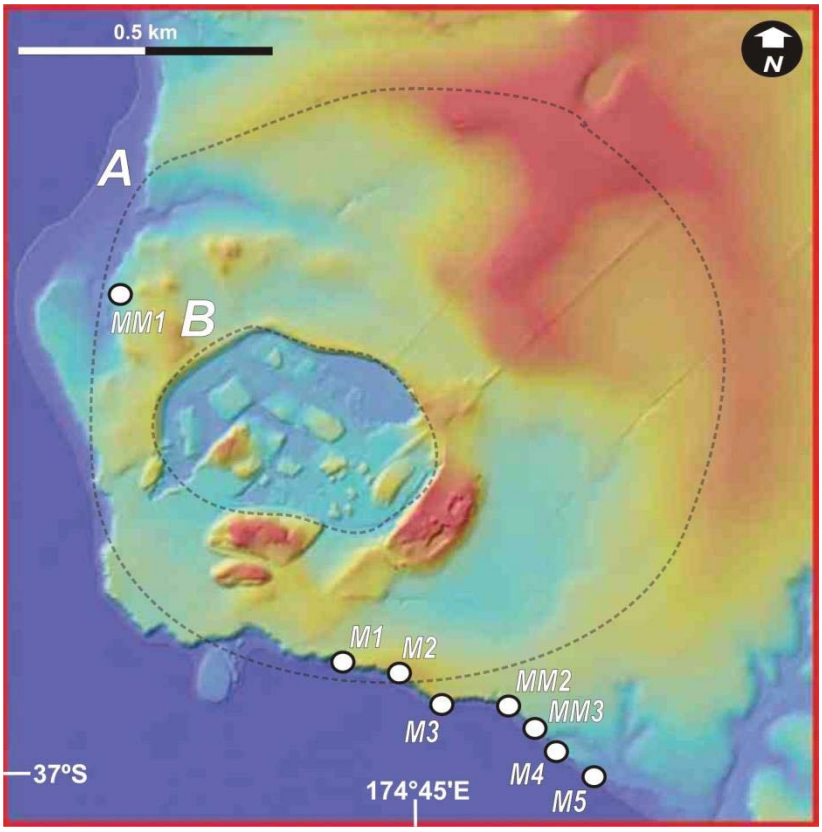


**Fig. B.1.1** Location of sites

The stratigraphic logs are presented in the order showed in Fig. B.1.1, from NW to SE. Except for exposures at sites M1 (3 metres above back beach level) and M2 (5 metres above back beach level), all exposures are virtually at back beach level. The scale at each log indicates thickness of exposures. A brief description of exposures is included. Specific descriptions of lithofacies are shown in Table 5.2 in the main text. A correlation and identification of units was not possible for site MM1. The letters at the upper right corner of some figures included in the main text are kept for identification in Fig. 5.5 in the main text. All histograms show grain size distribution of fine tuff and the sample number on histograms corresponds to the 12 sample numbers on Table B.1.1 and Fig B.1.11. Sample number on histograms is located at the upper left section (M followed by a number)

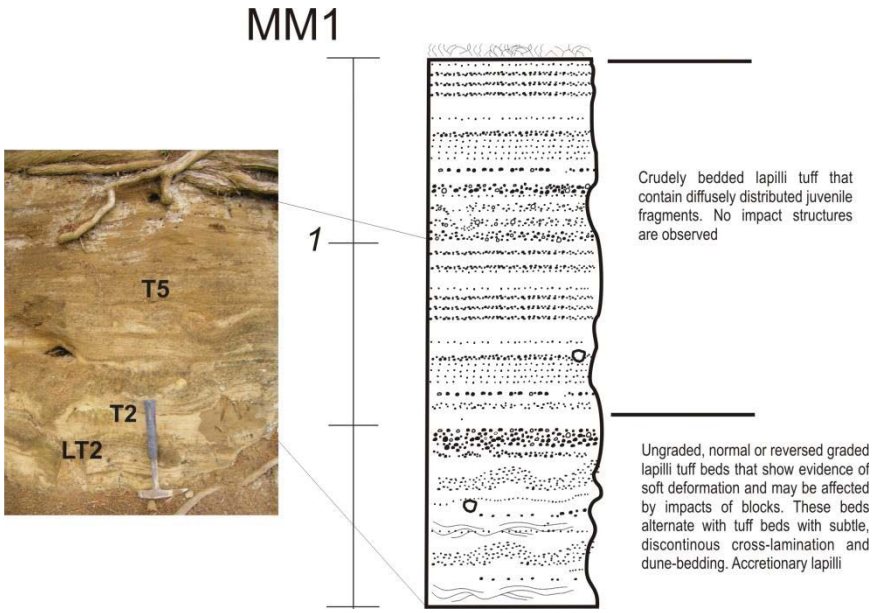


**Fig. B.1.2** Site MM1 (at back beach level)

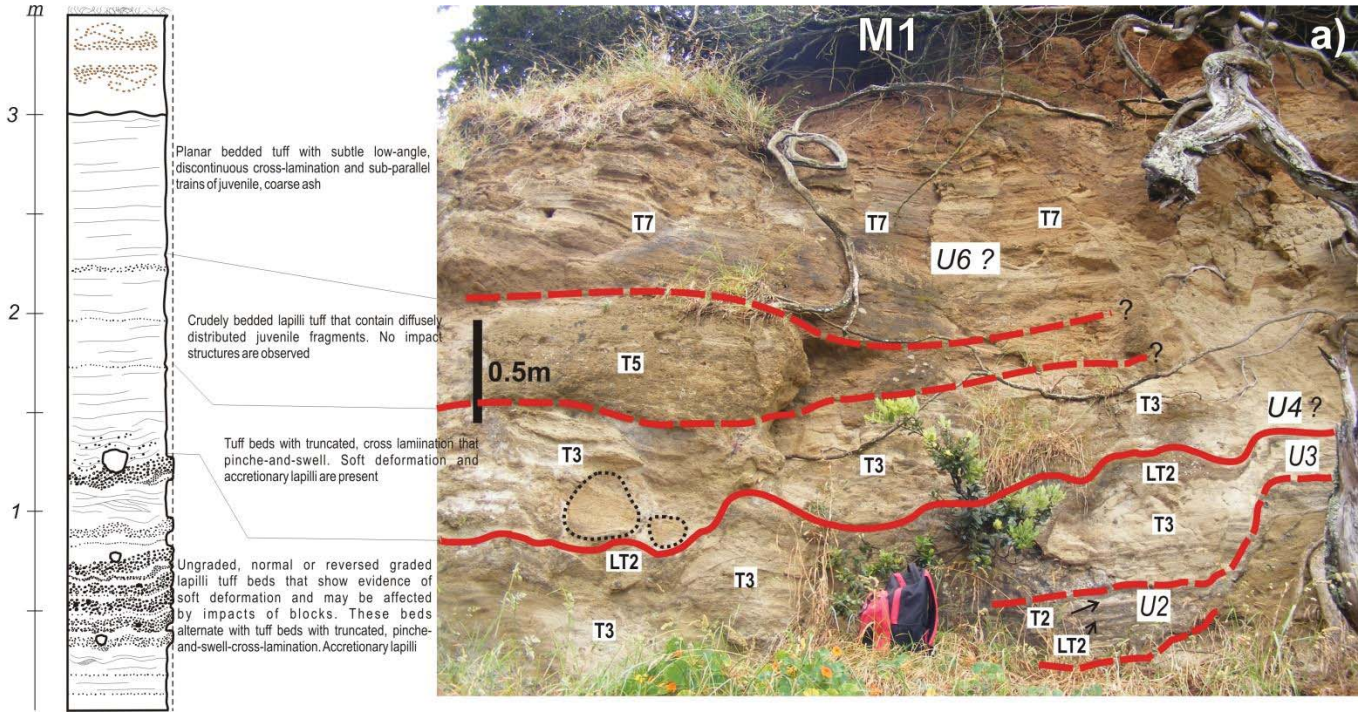


**Fig. B.1.3** Site M1. (3 metres above back beach level)

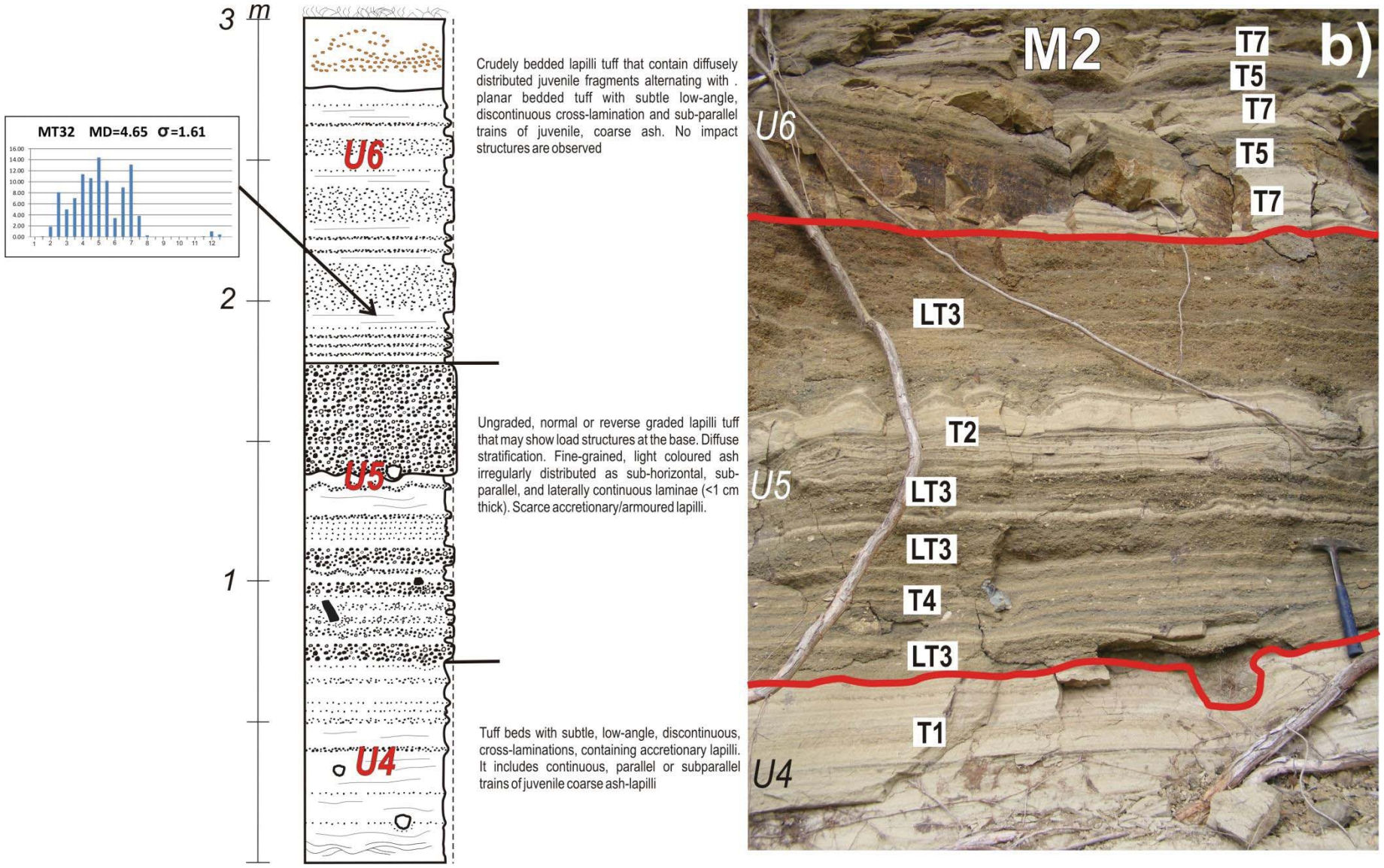


**Fig. B.1.4** Site M2 (at 5 metres above back beach level).

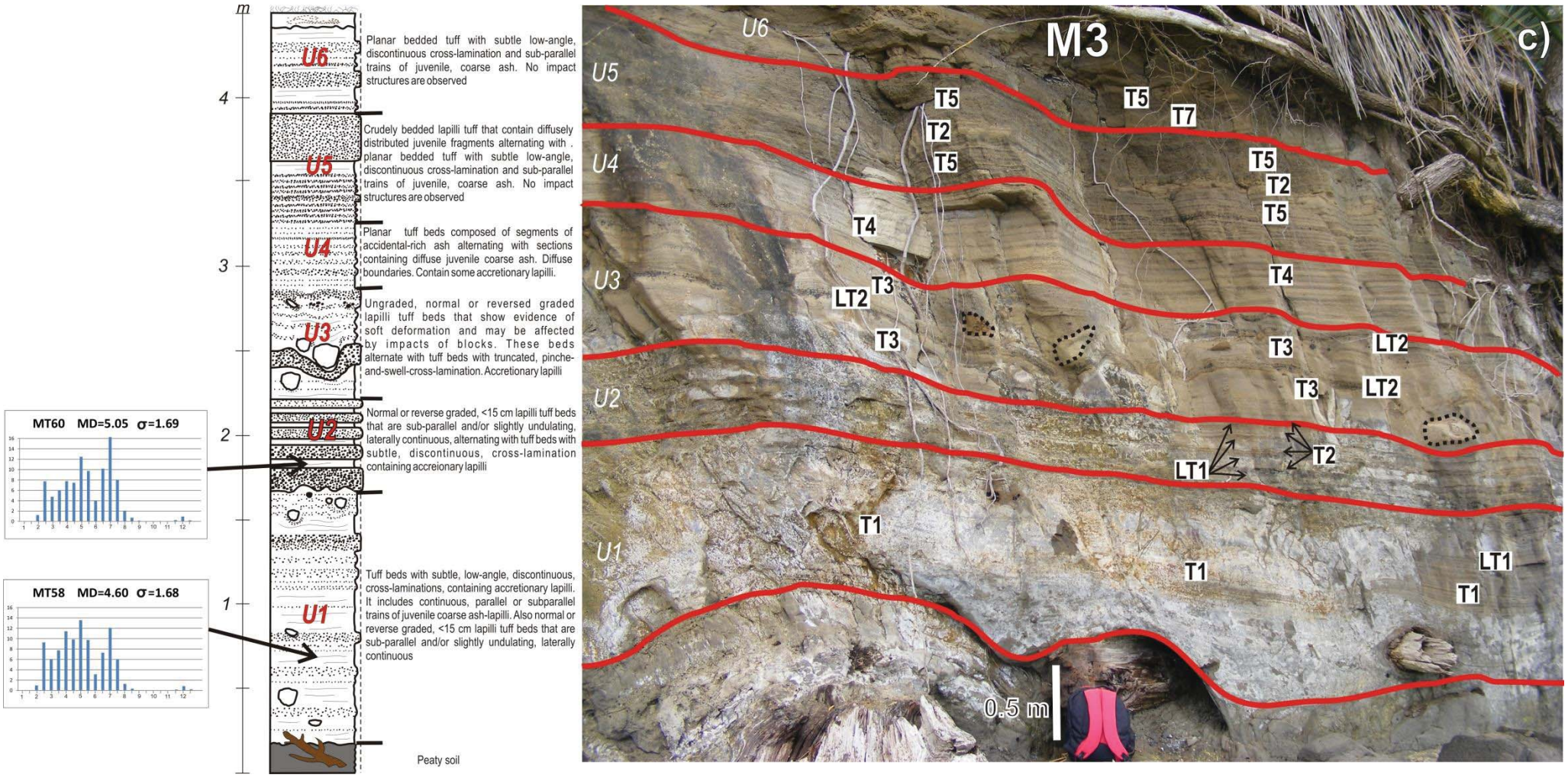


**Fig. B.1.5** Site M3 (at back beach level)

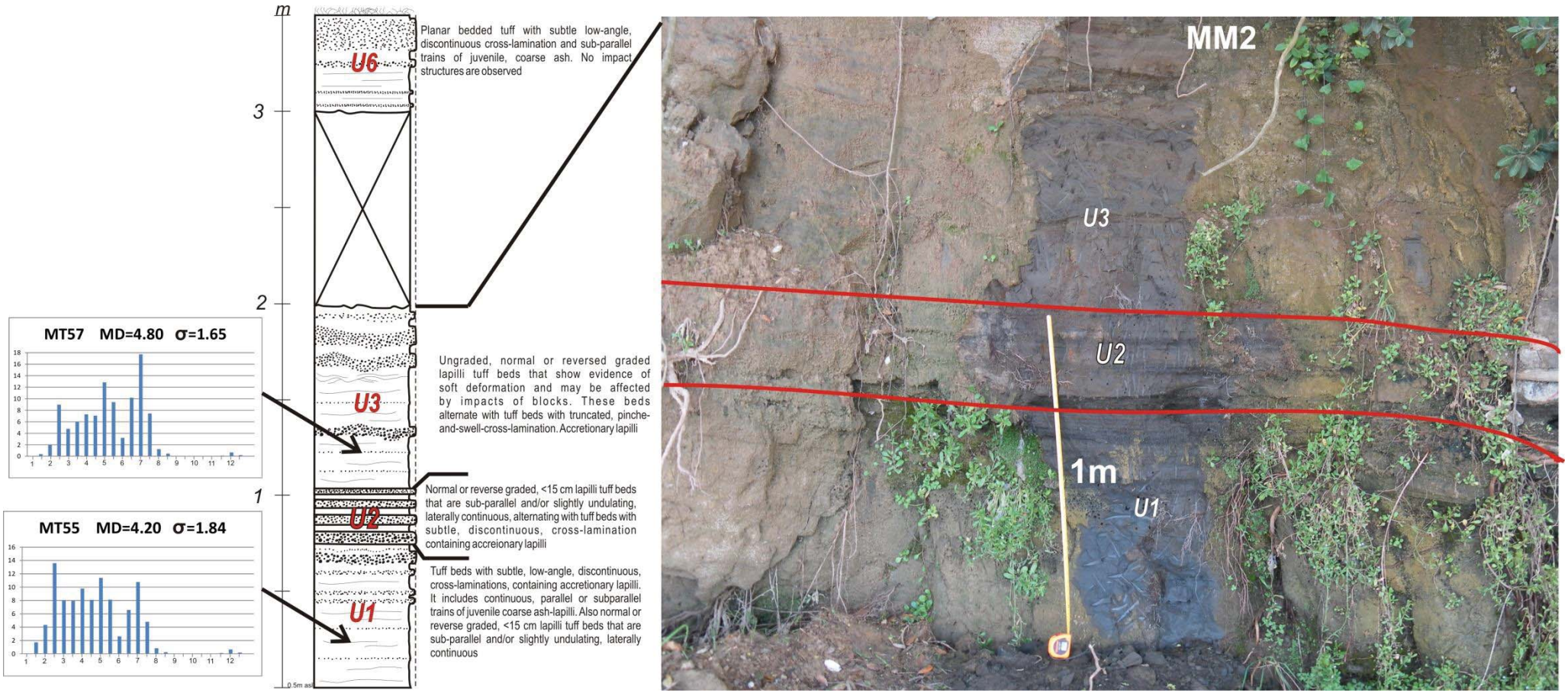


**Fig. B.1.6** Site MM2 (at back beach level)

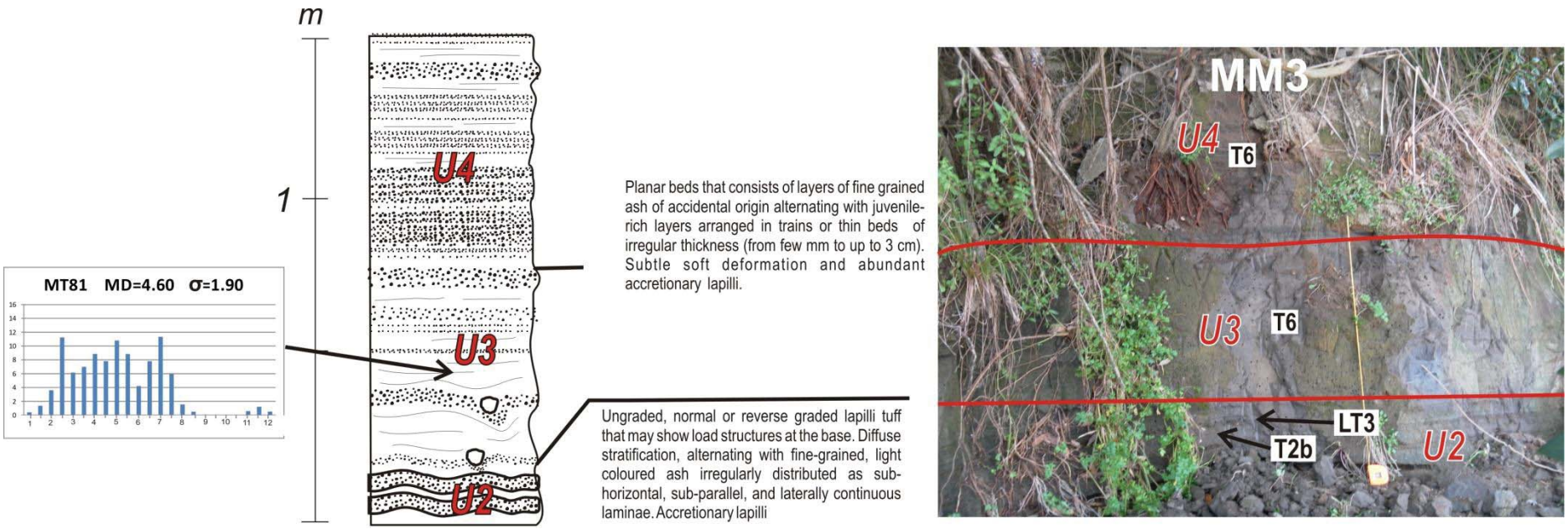


**Fig. B.1.7** Site MM3 (at back beach level)

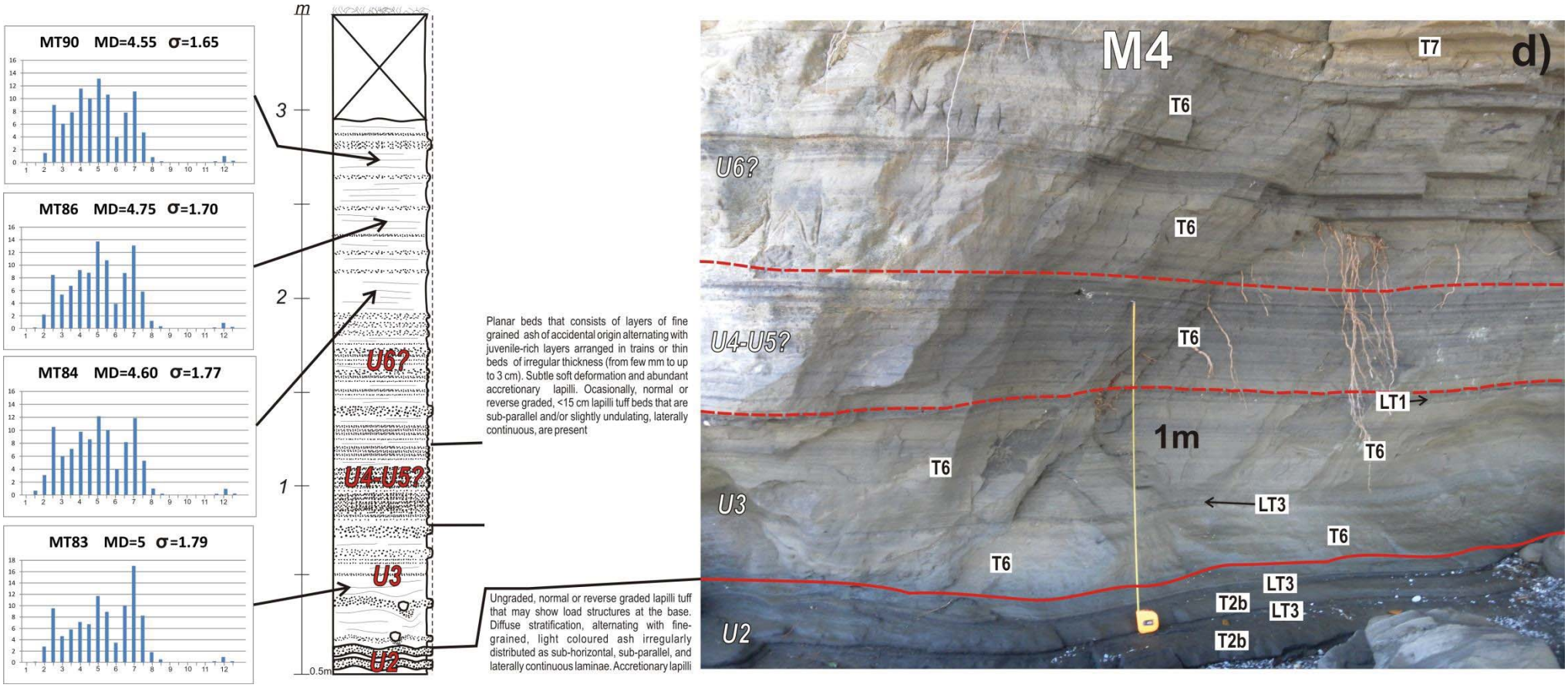


**Fig. B.1.8** Site M4 (at back beach level)

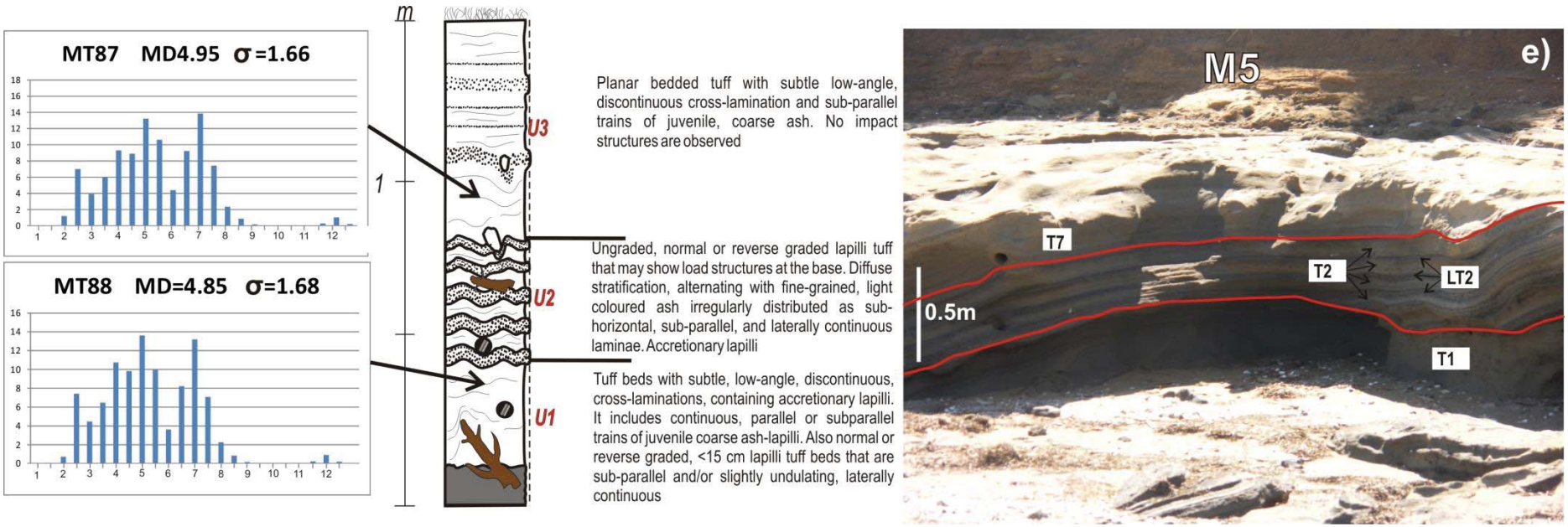


**Fig. B.1.9** Site M5 (at back beach level)

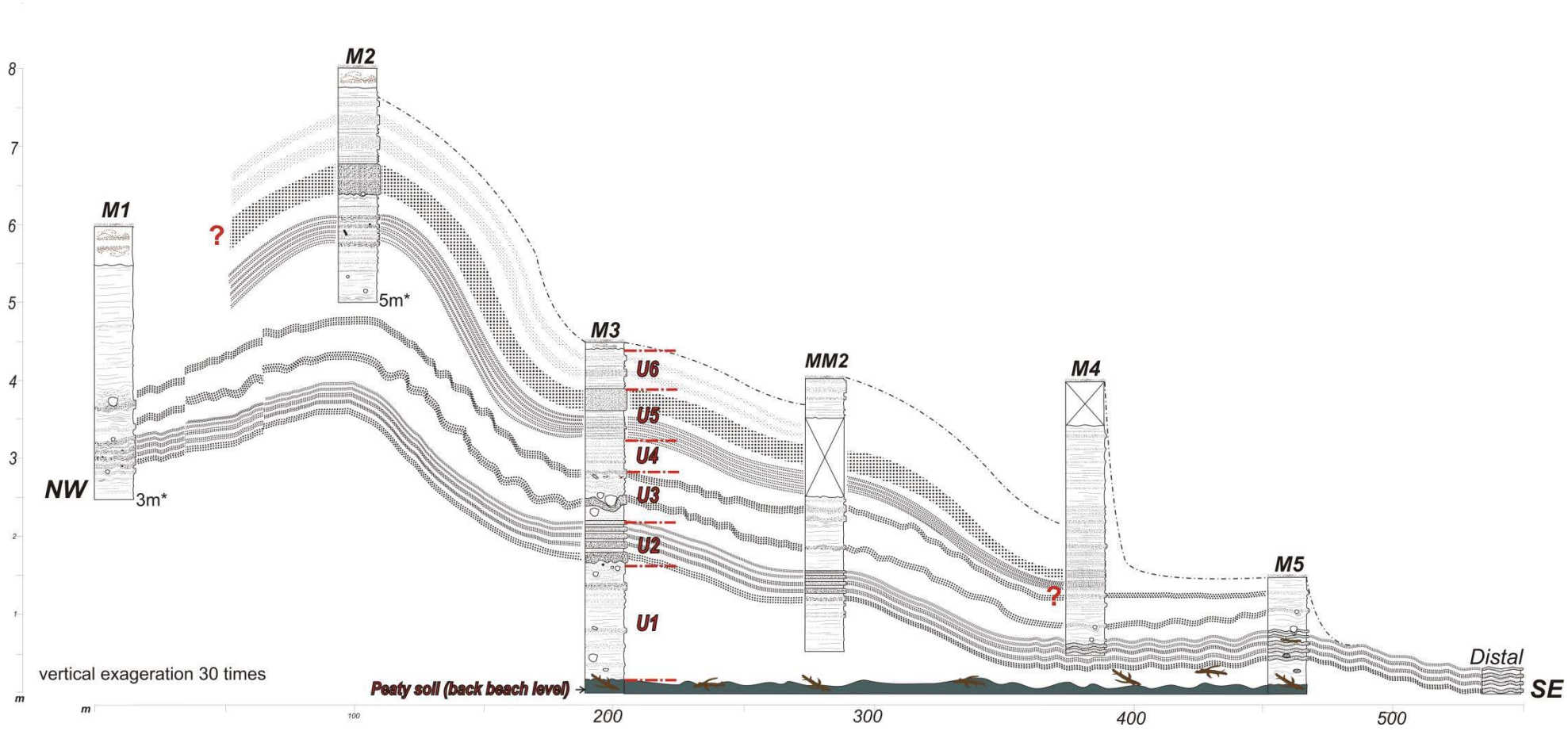


**Fig. B.1.10** Schematic correlation of logs and identified units. Note that site MM1 (Fig. B.1.2) is not included. Site MM3 (Fig. B.1.7) is located next to site M4. This correlation represents an approach of the cross-section of the ejecta ring from NW to SE. The vertical axis represents the maximum thickness of the exposed sequence. The peaty soil, when exposed, is at the base of the phreatomagmatic deposits and corresponds to the back beach level. Site M2 is located at the crater rim, whereas Site M1 is located at the inner slope of the ejecta ring.

Table B.1.1 displays the volume percentage values for phi fractions of the 12 sieved samples. The sample number is the same on the histograms shown with the logs and the graph of figure B.1.11

| Grain size | Phi | Sample / vol.% | | | | | | | | | | | |
|---|---|---|---|---|---|---|---|---|---|---|---|---|---|
| | | MT32 | MT55 | MT57 | MT58 | MT60 | MT81 | MT83 | MT84 | MT86 | MT87 | MT88 | MT90 |
| | 1 | 0.00 | 0.06 | 0.02 | 0.00 | 0.00 | 0.41 | 0.00 | 0.01 | 0.00 | 0.00 | 0.00 | 0.00 |
| | 1.5 | 0.13 | 1.72 | 0.37 | 0.00 | 0.00 | 1.35 | 0.16 | 0.68 | 0.18 | 0.00 | 0.00 | 0.00 |
| Coarse ash | | 0.13 | 1.78 | 0.39 | 0.00 | 0.00 | 1.76 | 0.16 | 0.69 | 0.18 | 0.00 | 0.00 | 0.00 |
| | 2 | 1.87 | 4.35 | 1.96 | 0.98 | 1.24 | 3.61 | 2.81 | 3.09 | 2.21 | 1.20 | 0.72 | 1.50 |
| | 2.5 | 8.09 | 13.59 | 8.98 | 9.28 | 7.74 | 11.25 | 9.54 | 10.52 | 8.46 | 7.00 | 7.43 | 9.02 |
| | 3 | 5.00 | 8.04 | 4.78 | 6.04 | 4.75 | 6.15 | 4.64 | 5.97 | 5.35 | 3.92 | 4.47 | 6.07 |
| | 3.5 | 7.03 | 7.93 | 6.01 | 7.75 | 5.99 | 7.00 | 5.82 | 7.14 | 6.75 | 5.97 | 6.47 | 7.87 |
| | 4 | 11.39 | 9.80 | 7.30 | 11.42 | 7.78 | 8.87 | 7.13 | 9.78 | 9.24 | 9.31 | 10.74 | 11.59 |
| Medium ash | | 33.37 | 43.71 | 29.02 | 35.47 | 27.50 | 36.88 | 29.94 | 36.49 | 32.00 | 27.40 | 29.83 | 36.05 |
| | 4.5 | 10.65 | 8.11 | 7.06 | 9.85 | 7.45 | 7.82 | 6.73 | 8.60 | 8.80 | 8.90 | 9.83 | 10.03 |
| | 5 | 14.40 | 11.39 | 12.85 | 13.56 | 12.47 | 10.80 | 11.71 | 12.16 | 13.74 | 13.22 | 13.62 | 13.13 |
| | 5.5 | 10.19 | 8.13 | 9.41 | 9.75 | 9.73 | 8.84 | 8.93 | 10.04 | 10.76 | 10.61 | 9.99 | 10.62 |
| | 6 | 3.43 | 2.62 | 3.20 | 3.12 | 3.97 | 4.23 | 3.48 | 3.98 | 3.89 | 4.39 | 3.62 | 4.01 |
| | 6.5 | 8.98 | 6.59 | 10.17 | 7.29 | 10.18 | 7.80 | 9.97 | 8.17 | 8.76 | 9.24 | 8.22 | 7.82 |
| | 7 | 13.13 | 10.77 | 17.71 | 12.10 | 16.30 | 11.34 | 17.01 | 11.88 | 13.10 | 13.87 | 13.19 | 11.12 |
| | 7.5 | 3.83 | 4.81 | 7.45 | 5.94 | 8.01 | 5.97 | 8.24 | 5.30 | 5.83 | 7.42 | 7.08 | 4.71 |
| Fine ash (silt) | | 64.61 | 52.43 | 67.85 | 61.62 | 68.11 | 56.80 | 66.06 | 60.13 | 64.89 | 67.66 | 65.55 | 61.44 |
| | 8 | 0.31 | 0.84 | 1.25 | 1.27 | 2.09 | 1.55 | 1.82 | 1.01 | 1.21 | 2.35 | 2.25 | 0.83 |
| | 8.5 | 0.00 | 0.25 | 0.46 | 0.35 | 0.73 | 0.50 | 0.54 | 0.23 | 0.36 | 0.87 | 0.84 | 0.20 |
| | 9 | 0.00 | 0.03 | 0.06 | 0.04 | 0.15 | 0.05 | 0.07 | 0.00 | 0.04 | 0.17 | 0.17 | 0.00 |
| | 9.5 | 0.00 | 0.00 | 0.00 | 0.00 | 0.00 | 0.00 | 0.00 | 0.00 | 0.00 | 0.00 | 0.00 | 0.00 |
| | 10 | 0.00 | 0.00 | 0.00 | 0.00 | 0.00 | 0.00 | 0.00 | 0.00 | 0.00 | 0.00 | 0.00 | 0.00 |
| | 10.5 | 0.00 | 0.00 | 0.00 | 0.00 | 0.00 | 0.00 | 0.00 | 0.00 | 0.00 | 0.00 | 0.00 | 0.00 |
| | 11 | 0.00 | 0.00 | 0.00 | 0.00 | 0.00 | 0.59 | 0.00 | 0.00 | 0.00 | 0.00 | 0.00 | 0.00 |
| | 11.5 | 0.13 | 0.12 | 0.11 | 0.17 | 0.25 | 1.20 | 0.23 | 0.21 | 0.17 | 0.29 | 0.23 | 0.20 |
| | 12 | 1.02 | 0.66 | 0.66 | 0.85 | 0.95 | 0.52 | 0.96 | 0.98 | 0.89 | 1.04 | 0.91 | 1.01 |
| | 12.5 | 0.43 | 0.20 | 0.20 | 0.23 | 0.21 | 0.09 | 0.23 | 0.25 | 0.25 | 0.22 | 0.21 | 0.28 |
| | 13 | 0.00 | 0.00 | 0.00 | 0.00 | 0.00 | 0.00 | 0.00 | 0.00 | 0.00 | 0.00 | 0.00 | 0.00 |
| Fine ash (clay) | | 1.89 | 2.09 | 2.73 | 2.91 | 4.39 | 4.50 | 3.84 | 2.68 | 2.93 | 4.95 | 4.62 | 2.51 |

**Table B.1.1**

With data from the grain size analyses, the phi fractions were plotted in regard to grain size classification. Note that all samples exhibit the prevalence of fine ash.

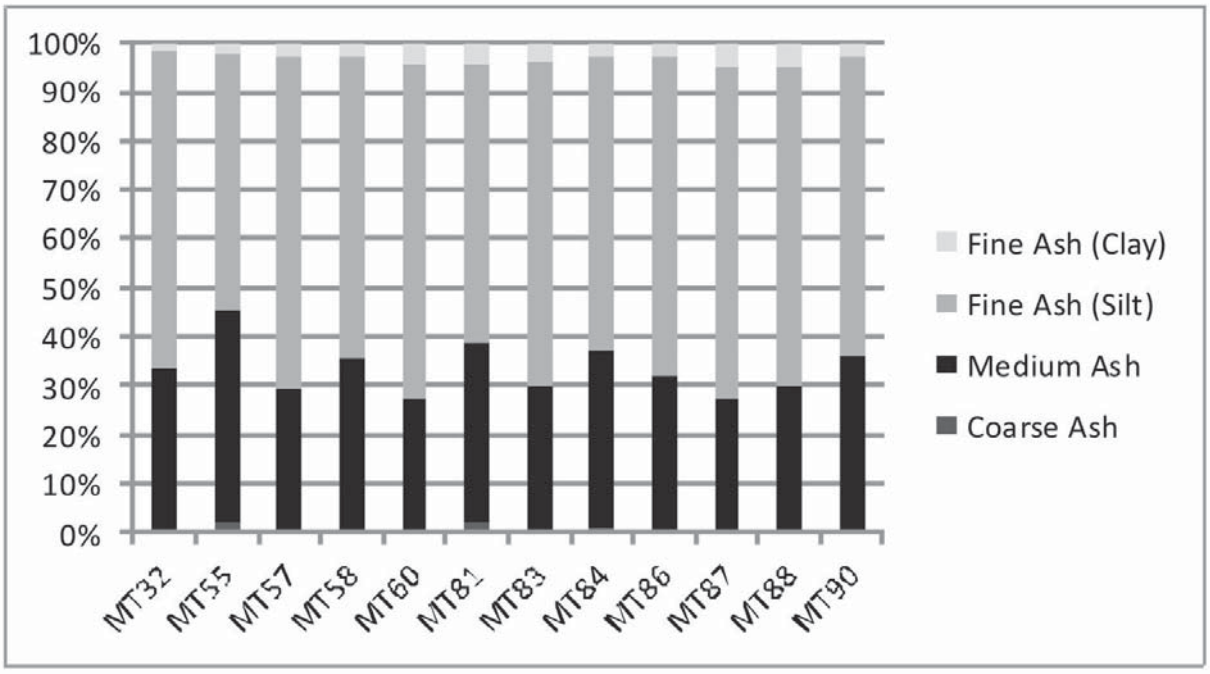


**Fig. B.1.11**

## Appendix B.2 Lithofacies and units of Maungataketake volcano

### 1. LITHOFACIES

The sedimentary criteria to group and describe the lithofacies are provided in chapter 5. The referred figures for lithofacies are also displayed in chapter 5. The summarized information of these lithofacies is presented in Table 5.2 in chapter 5.

**Tuff:**

**T1** *(Figs. 5.5c,b,e; 5.6a,b,f)*. Poorly consolidated, faintly laminated to massive, grey tuff sequences that have variable thickness (up to 0.5 m). It is poorly sorted and composed mainly of fine ash (~ up to 55 vol.%) and medium ash (~ up to 35 vol.%) of accidental origin. It contains continuous, parallel/sub-parallel trains composed of juvenile, coarse ash (<1 mm) (<10 vol.%).Randomly, at intervals, the juvenile fragments coarsen (up to fine-lapillus size) and are sparsely concentrated in bands (up to 10 cm thick) that exhibit vague inverse gradation. Subtle low-angle, discontinuous cross-lamination and dune bedding is present at intervals. <5 mm-diameter, spherical/oval accretionary lapilli are displayed along discontinuous horizontal trains at some segments or else scattered randomly in the tuff, but it is not pervasive. Small block/medium lapillus-size fragments of accidental origin are relatively scarce (<5 vol.%) and they are embedded in the tuff or forming impact structures. The finer ash is composed of quartz, feldspar, and smaller amounts of clay; the coarser juvenile grains consist of basaltic glass (tachylite or sideromelane) with some, individual or clustered, olivine/pyroxene phenocrysts and abundant Ca-rich pyroxene microlites/microcrysts.

Interpretation: Soft deformation, poor sorting and the presence of accretionary lapilli point to deposition of wet base surges. The presence of juvenile trains of variable thickness suggests transportation of the diluted PDCs as a combination of weak-turbulent suspended loads and bed loads/traction-carpets. With distance, the base surges may have become less concentrated and deposition is related to suspension. (Sohn, 1997; Sohn and Chough; 1989; Chough and Sohn, 1990).

**T2 (***Figs. 5.5a,b,c,d,e; 5.6a,b,c,d,e,f)*. Poorly consolidated, faintly laminated, grey to light brown, tuff beds up to ~10 cm in thickness. Poorly sorted and composed mainly of fine ash (~ up to 55 vol.%) and medium ash (~ up to 35 vol.%) of accidental origin. It contains parallel to subparallel trains composed of juvenile coarse ash (<1 mm) (<10 vol.%). Subtle cross-lamination is observed at times. Rare accretionary lapilli (<5 mm in diameter) is present. The finer ash is composed of quartz, feldspar, and smaller amounts of clay; the coarser juvenile grains consists of basaltic glass (tachylite or sideromelane) with some, individual or clustered, olivine/pyroxene phenocrysts and abundant Ca-rich pyroxene microlites/microcrysts.

Interpretation: Soft deformation, poor sorting, accretionary lapilli, subtle cross-lamination, and thin trains of juvenile fragments suggest the deposition of wet base surges transported as a low-energy, suspended load. T2 is associated with the deposition of LT2 probably as a bipartite base surge. (Sohn, 1997; Sohn and Chough; 1989; Chough and Sohn, 1990; Vazquez and Ort, 2006).

**T3** (*Figs. 5.5a,c; 5.6a,b,d,g)*. Poorly consolidated, faintly laminated, grey to light brown tuff sequences of variable thickness (up to 0.5 m). Poorly sorted and composed mainly of fine ash (~ up to 55 vol.%) and medium ash (up to 40 vol.%) of accidental origin. It contains twisted trains composed of juvenile coarse ash (<1 mm) (<10 vol.%). Laminations pinch and swell laterally and are often truncated by overlying laminations. Cross-lamination is not uncommon. <5 mm-diameter, spherical/oval accretionary lapilli are displayed along discontinuous horizontal trains at some segments or else scattered randomly in the tuff. In some sections this facies may contain coarse accidental blocks (up to 40 cm) either forming impact sags or embedded in the tuff without deforming the tuff beds. Soft deformation is pervasive. The diffuse distributed juvenile fragments (up to coarse lapilli) may form incipient reverse-grading layers The finer ash is composed of quartz, feldspar, and smaller amounts of clay; the coarser juvenile grains consists of basaltic glass (tachylite or sideromelane) with some, individual or clustered, olivine/pyroxene phenocrysts and abundant Ca-rich pyroxene microlites/microcrysts.

Interpretation: Intense soft deformation, poor sorting, accretionary lapilli, cross-lamination indicate the deposition of wet base surges that were transported in a low-energy, rapidly decelerating cloud. The presence of juvenile trains of variable thickness may suggest also traction carpet mode of transportation. (Sohn, 1997; Sohn and Chough; 1989; Chough and Sohn, 1990).

**T4** (*Figs. 5.5c, 5.6c)*. Poorly consolidated, diffusely stratified, light brown tuff sequences up to 0.5 m in thickness. It is poorly sorted and mainly composed of fine ash (~up to 40 vol.%) and medium ash (~ up to 30 vol.%) of accidental origin. It contains segments with concentration (30-40 vol.%) of diffusely distributed, inverse graded, juvenile coarse ash (<2 mm) which forms continuous, parallel/sub-parallel bands (up to 10 cm thick) with no distinct upper/lower boundaries. The bands thin upwards and the size of their juvenile fragments becomes finer. It also contains continuous, parallel/sub-parallel trains composed of juvenile, coarse ash (<1 mm) (<10 vol.%) randomly distributed. <5 mm-diameter, spherical/oval accretionary lapilli are displayed along discontinuous horizontal trains at some segments or else scattered randomly in the tuff. The finer ash is composed of quartz, feldspar, and smaller amounts of clay; the coarser juvenile grains consists of basaltic glass (tachylite or sideromelane) with some, individual or clustered, olivine/pyroxene phenocrysts and abundant Ca-rich pyroxene microlites/microcrysts

Interpretation: The presence of juvenile richer bands, accretionary lapilli, and poorly sorting point to the deposition of density stratified, wet, moderately diluted PDCs that were transported as a combination of low-turbulent suspended loads and traction carpets in a sustained fashion. The upwards thinning of juvenile richer bands may suggest progressively more suspended load mode of transport with the incorporation of finer and less abundant juvenile clasts. (Sohn, 1997; Sohn and Chough; 1989; Chough and Sohn, 1990; Dellino et al., 1990).

**T5** *(Figs. 5.5b,c; 5.6c,e)*. Moderately consolidated, poorly sorted, diffusely and/or crudely stratified tuff sequences up to 0.5 m in thickness. Composed of up to ~70 vol.% of juvenile clasts with grain sizes ranging from fine lapilli (4 mm) to more common coarse ash (usually 1 mm to 0.3 mm) embedded in a matrix composed of fine to medium-sized, light brown ash of accidental origin (up to 30 vol.%). Juvenile fragments are distributed across the sequence forming continuous parallel trains; up to ~3 cm-thick, continuous, parallel, diffuse bands; or else non-stratified, randomly scattered arrangements. Subtle

inverse grading is observed at times. Beds are not affected by impact structures. Accretionary lapilli were not observed, but some of the juvenile fragments are coated with a fine layer of accidental ash. The finer ash is composed of quartz, feldspar, and smaller amounts of clay; the coarser juvenile grains consists of basaltic glass (tachylite or sideromelane) with some, individual or clustered, olivine/pyroxene phenocrysts and abundant Ca-rich pyroxene microlites/microcrysts

Interpretation: Diffuse stratification, poorly sorting, ash-coated juvenile fragments suggest the deposition of moderately concentrated, low-energy, wet base surges that were transported mainly as bed loads/traction carpets in sustained manner. (Sohn, 1997; Sohn and Chough; 1989; Chough and Sohn, 1990).

**T6** *(Figs 5.5d; 5.6d,h)*. Moderately consolidated, poorly sorted tuff up to 1 m in thickness. Composed of a laterally continuous, parallel succession of segments composed of fine-to-medium sized, grey-light brown ash of accidental origin that alternate with sections that consist of medium-to-coarse, juvenile ash. The latter is arranged in trains, laminations, and thin beds or irregular thickness (from few mm to up to 3 cm). The accidental content is up to 60 vol.%. At intervals, the presence of dark layers becomes more dominant; however, no distinct layers boundaries are shown. The finer-grained segments contain moderate amounts of <5 mm-diameter, accretionary lapilli. The sequence is virtually devoid of lapillus and block size fragments either of lithic or juvenile origin Soft deformation is not intense. The finer ash is composed of quartz, feldspar, and smaller amounts of clay; the coarser juvenile grains consists of basaltic glass (tachylite or sideromelane) with some, individual or clustered, olivine/pyroxene phenocrysts and abundant Ca-rich pyroxene microlites/microcrysts

Interpretation: Accretionary lapilli, parallel bedding, juvenile-rich beds with diffuse boundaries indicate the deposition of density stratiified, weak-turbulent, rapidly decelerating, wet base surges that were mainly transported as suspended loads and bed loads. (Sohn, 1997; Sohn and Chough; 1989; Chough and Sohn, 1990; Dellino et al., 1990)

**T7** (*Figs. 5.5a,d,h)*. Poorly consolidated, faintly laminated, vesicular, unaltered (light brown to cream) to heavily altered tuff sequences up to 1.5 m in thickness. It is poorly sorted and composed mainly of fine-to-medium ash of accidental origin up to 70 vol.%. It contains continuous, sub-parallel trains composed of juvenile coarse ash (<1 mm). Subtle low-angle, discontinuous cross lamination is present at intervals. The presence of <5 mm-diameter, spherical/oval accretionary lapilli is ubiquitous. The sequence is virtually devoid of lapillus and block size fragments either of lithic or juvenile origin Soft deformation is not intense. The finer ash is composed of quartz, feldspar, and smaller amounts of clay; the coarser juvenile grains consists of basaltic glass (tachylite or sideromelane) with some, individual or clustered, olivine/pyroxene phenocrysts and abundant Ca-rich pyroxene microlites/microcrysts

Interpretation: Accretionary lapilli, cross-lamination, juvenile-rich beds with diffuse boundaries indicate the deposition of density stratiified, low-energy, rapidly decelerating, wet PDCs that were mainly transported as suspended loads and bed loads. (Sohn, 1997; Sohn and Chough; 1989; Chough and Sohn, 1990; Dellino et al., 1990)

**Lapilli-tuff:**

**LT1** (*Figs. 5.5c,d,e; 5.6a,b,d,f)*. Moderately consolidated tuff that forms beds that range from approximately 3 to 10 cm in thickness and form sub-parallel and/or slightly undulating, laterally continuous layers. The layers pinch and swell when encounter an obstacle. It is poorly sorted and composed of >80 vol.% of coarse ash to fine lapilli juvenile fragments. The beds are dominantly clast supported, ungraded, and normal or reverse graded, and may show scour surfaces of bed load structures. The poorly vesicular, sub-angular, juvenile fragments may be embedded in an incipient and irregularly widespread matrix of light coloured, fine-to-medium ash of accidental origin (<20 vol.%). Rare accidental/juvenile fragments bigger than fine lapillus size are present, as well as scarce <1 cm, accretionary/armoured lapilli. The finer ash is composed of quartz, feldspar, and smaller amounts of clay; the coarser juvenile grains consists of slightly to moderately palagonitized basaltic glass (tachylite or sideromelane) with some, individual or clustered, olivine/pyroxene phenocrysts and abundant Ca-rich pyroxene microlites/microcrysts.

Interpretation: The degree of consolidation, poorly sorting, pinch and swell, and variable grading may point to the deposition of a relatively high concentrated, wet PDCs transported dominantly in a traction carpet mode. These beds may have been part of a denser fraction of a PDC that became density segregated or decoupled. With distance, the flow was transformed into a granular fluid-based PDC. Grain addition of fall-out clasts into the already moving flow is not ruled out, but was probably never dominant. (Valentine, 1987, Fisher, 1995: Branney and Kokelaar, 2002; Vazquez and Ort, 2006)

**LT2** *(Figs. 5.5a,c; 5.6a,b,d,g)*. Moderately consolidated tuff beds that are laterally continuous, but notably vary in thickness (pinch and swell), exhibiting at times contorted and deformed beds. It is poorly sorted and composed of >80 vol.% of coarse to fine lapilli juvenile fragments. The beds are dominantly clast supported, ungraded, and normal or reverse graded. Intense soft deformation is evident and beds can be affected by impacts of blocks of accidental origin (up to 40 cm). Juvenile fragments are poorly vesicular and sub-angular and may be embedded in an incipient and irregularly widespread matrix of light coloured, fine-to-medium ash of accidental origin. Rare accretionary/armoured lapilli are present. The finer ash is composed of quartz, feldspar, and smaller amounts of clay; the coarser juvenile grains consists of slightly to moderately palagonitized basaltic glass (tachylite or sideromelane) with some, individual or clustered, olivine/pyroxene phenocrysts and abundant Ca-rich pyroxene microlites/microcrysts.

Interpretation: Intense soft deformation. The degree of consolidation, poorly sorting, and variable grading may point to the deposition of a relatively high concentrated, wet PDCs transported dominantly in a traction carpet mode and later deformed by impact fragments. These beds may have been part of a denser fraction of a PDC that became density segregated or decoupled. Grain addition of fall-out clasts into the already moving flow was probably more important than for LT1. (Valentine, 1987, Fisher, 1995: Branney and Kokelaar, 2002; Vazquez and Ort, 2006)

**LT3** *(Fig. 5.5b,e)*. Consolidated, massive-to-crude bedded tuff forming beds up to 0.5 m thick. It is poorly sorted and composed of >90 vol.% of coarse ash to fine lapilli juvenile fragments. The beds are dominantly clast supported, ungraded, and normal or reverse graded, and may show load structures at the base. The juvenile clasts are poorly to moderately vesicular, sub-angular, and slightly to moderately

palagonitized. It is possible to discern some fine, light coloured ash present as an incipient matrix and also irregularly distributed as subhorizontal, subparallel, and laterally continuous laminae (<1 cm thick). Rare accidental/juvenile fragments bigger than fine lapillus size are present, as well as scarce <1 cm, accretionary/armoured lapilli. The finer ash is composed of quartz, feldspar, and smaller amounts of clay; the coarser juvenile grains consists of slightly to moderately palagonitized basaltic glass (tachylite or sideromelane) with some, individual or clustered, olivine/pyroxene phenocrysts and abundant Ca-rich pyroxene microlites/microcrysts.

Interpretation: The high degree of consolidation, palagonitization, and juvenile clast morphology may suggest the deposition of a high concentrated, wet, non-turbulent PDC probably emplaced more like a Surtseyan tephra jet transported as a grain flow. The transformation into lithofacies T5 downhill may indicate that it was transformed into a more density stratified-like, diluted PDCs. The entrainment of further fall-out fragments is not discarded, but seems not to be the dominant process. (Kokelaar, ,1983; Sohn and Chough, 1992; Sohn and Chough, 1993).

## 2. LITHOSTRATIGRAPHIC UNITS

Stratigraphic and sedimentary criteria to describe the units are provided in chapter 5. The lithofacies included in the descriptions of units are described in the text above or briefly on Table 5.3. The condensed information of these units is presented in Table 3 in chapter 5. All referred figures are displayed in chapter 5.

### UNIT 1

U1 is defined within the lowest part of the tuff-ring basal deposits (Figs. 5.2 and 5.5c,e) and overlies pale brown muds and peaty paleosols with a sharp irregular contact (seen around sites M3 and M5). At site M3, the brownish-grey unit is ~1.5 m thick and characterized by crudely stratified, parallel-to-subparallel bedded, poorly consolidated tuff (lithofacies T1) and thin beds (<8 cm) of dominantly clast-supported, poorly-to-moderately consolidated, poorly sorted lapilli tuff (lithofacies LT1). Occasional rounded-subrounded <15 cm-diameter country rock ballistic clasts form impact structures, or are embedded in the tuff. They are formed by undeformed aggregates of Pliocene-Pleistocene (Kaawa and Tauranga Fm) sediments. The impact bedding sags are <10 cm deep, plastically deformed, and slightly asymmetric, with impact angles approximately ESE-WNW orientated. The tuff comprises >90% by volume of medium ash, that is >80% by volume of lithic. Randomly throughout the unit, horizontal trains of juvenile subangular, poorly-to-moderately vesicular, medium-lapilli occur. Variably abundant, but ubiquitous, <5 mm diameter, spherical and oval shaped accretionary lapilli are contained in the fine-grained beds throughout this unit, increasing in abundance upwards. At site M5, U1 is ~0.5 m thick (Fig. 5.5e), showing similar contacts with underlying peat/sediment, where lithofacies T1 becomes distinctively unbedded, massive, and composed of >95% in vol. of medium to fine ash.

Interpretation

The onset of the phreatomagmatic activity is represented by fine tuff (T1) dominantly comprising accidental feldspar and quartz grains derived from the Kaawa, Tauranga, and Waitemata lithologies (see section 2 in the main text for general descriptions of these Formations). The absence of massive,

country rock-rich, block or lapilli-bearing breccias characteristic of vent-clearing phases (e.g., Sohn and Chough, 1989) is due to the locus of initial explosions within shallow saturated and unconsolidated sediments. However, the lower tephra ring deposits do not necessarily represent the early ejecta from the maar (Valentine , 2012). These early explosions generated pyroclastic density currents (PDCs) containing ash-dominant particles. The PDCs were wet, either due to condensation of steam and/or original sediment pore water. Ash particles were cohesive, forming accretionary lapilli. The base surges rapidly decelerated and the lithofacies features represent weakly turbulent to laminar flow regimes (c.f., Zimanowski and Wohletz, 2000). Juvenile-clast trains in medial sites (site M3) with no distinct boundary layers indicate unsteady pulsatory base surges with variable grain size supply (c.f., Sohn, 1997; Sulpizio et al., 2008), and high rates of deposition. At this point, particles within the base surges travelled mostly in a tractional/saltational regime in which collisional mechanisms were practically absent (similar to fully dilute PDCs of Branney and Kokelaar, 2002). In distal locations (site M5, Fig. 5.5e), the base surges had degraded into fine-ash dominant, low-energy turbulent clouds, forming massive deposits mainly by particle settling (e.g., Wohletz and Sheridan, 1979; Sulpizio and Dellino, 2008).

**UNIT 2**

Along a segment from sites M3 to M4 (Fig. 5.2), U2 consists of a characteristic alternation of <10cm beds of coarse-ash to fine lapilli-sized, poorly-to-moderately vesicular, subangular, juvenile pyroclasts (lithofacies LT1), with inter-beds of pale brown-coloured, lithic dominated ash (lithofacies T2). At M1, U2 shows variable thickness (up to ~0.5 m), is faulted (Fig. 5.5a), and constituted by lithofacies LT2 and T2 (described above). At site M3, the lowermost LT1 bed shows a sharp contact with the underlying U1. At the contact, there are scour surfaces, load structures, impact structures from coarse lapilli/blocks that include both rounded, accidental lithics and poorly-vesicular, juvenile clasts (Figs. 5.5c and 5.6a,b). LT1 beds become thinner, finer grained, and have more diffuse contacts upwards (Fig. 5.6a,b). The distal sites, between M4 and M5 are characterized by a ≤0.5 m-thick U2, with 0.5 m-amplitude undulating layers of alternating lithofacies LT1 and T2 (Figs. 5.5e and 5.6d). At distal locations, hollow casts occur within U2 (up to 30 cm-thick across) from logs that have rotted out of the tuff virtually at sea level (Fig. 5.6d). Poorly-to-moderately abundant, <5 mm, spherical/oval accretionary lapilli/armoured lapilli occur in the finer-grained layers.

Interpretation

The presence of a coupled lower coarser-grained-rich bed (LT1) overlain by a finer-grained-laden layer (T2) suggests that U2 was formed by a series of density stratified PDCs (e.g. Valentine 1987) generated from both the collapse of small eruptive clouds as well as tephra jets (secondary and primary surges, respectively of Wohletz, 1998). These yielded concentrated and mostly wet flows. They were homogeneous very close to the vent, but were soon partitioned into two layers. The rather erosive basal part was concentrated in juvenile particles (lithofacies LT1) (e.g., Vazquez and Ort, 2006) and transported as a frictional/traction carpet (similar to the granular fluid-based PDCs of Branney and Kokelaar, 2002). By comparison, the less dense overlying portion was finer-grained and transported particles in a saltation-dominated bed load regime at its base, passing upward into a turbulent suspended load (lithofacies T2). Each PDC produced a deposit couplet (c.f., Vazquez and Ort, 2006). Following waning explosions produced pulsating successive PDCs. A fining upwards of juvenile

particles in U2 may indicated increasing efficiency of phreatomagmatic fragmentation (c.f., Sheridan and Wohletz, 1983), and/or possibly fall-back and re-fragmentation of recycled clasts (e.g., Houghton and Smith, 1993). Outward to medial distances the base surges were dominantly transported in the saltating to turbulent regime, producing more diffuse beds, but traction carpet mode of transport was still in effect. With distance from the vent, the pyroclastic currents became wetter and topographically controlled..

**UNIT 3**

In the most proximal location (M1, Fig. 5.5a) this unit is difficult to distinguish due to inner rim wall subsidence/faulting and weathering. With an average thickness of 0.7 m, U3 is best represented in the medial sites (M3) by layers of massive to crudely stratified, fine-to-medium ash tuff (with continuous subparallel trains) (lithofacies T3) and moderately consolidated, moderately sorted lapilli tuff (lithofacies LT2) (Fig. 5.5c). The lower and upper unit contacts and those between lithofacies are gradational. Accidental blocks (up to 25 cm in diameter) are mainly contained in the mid portions, plastically deforming the LT2 bed, the underlying T3, and at least in one location affecting slightly the uppermost part of the underlying U2 (Fig. 5.5c). >90 vol.% of sub-rounded to rounded blocks are composed of fragments of the Waitemata Group. Aggregates of Pliocene-Pleistocene sediments, which do not show plastic deformation and internal structures are also present (<10 vol.% of accidental blocks). Towards M4, the contact down to U2 is distinct but still gradational (Fig. 5.5d). Lithofacies T6 (moderately consolidated tuff composed of an alternation of thin layers of accidental-origin ash and relatively coarser, juvenile ash) and LT1 comprise this unit (Fig. 5.5d). Ballistic impacts are more subdued in distal outcrops. The thickness of U3 is roughly ~0.5 to ~0.7 m and varies little from proximal to distal locations (Fig. 5.2), although at the latter it lies at or near the sea level (Fig. 5.2). Accretionary lapilli (<1 cm diameter) occur scattered throughout.

Interpretation

This phase starts with lithofacies T3 deposits (sites M1 and M3, Fig. 5.5a,c), indicating PDCs with an unsteady and pulsatory behaviour, with multiple terminating trails of coarser juvenile fragments (c.f., Sulpizio and Dellino, 2008). This was followed by deposition of LT2 along with the first appearance of ballistic blocks derived sub-lithified Waitemata Group lithologies (Fig. 5.5c and 5.6a,b), which indicates a deepening locus of explosions and/or shifting of vent. Finally, a renewed series of unsteady and pulsating base surges (lithofacies T3) occurred. In medial to distal sites (at site M4, Figs. 5.5d and 5.6d), particles are transported mainly within bed loads. Towards the top of U3, coarse juvenile fragments were emplaced in a massive lapilli tuff, but very rare accidental blocks, possibly indicating that explosions did not progress further vertically or laterally into the Waitemata Group.

**UNIT 4**

At site M1 (proximal site), the tuff is weathered and comprises both undulating/deformed and undeformed beds of lithofacies T3 (Fig. 5.5a). At M2, the upper boundary with U5 is sharp and horizontal (Fig. 5.5b) and constituted of lithofacies T1. Unit 4 at site M3 stands at ~3 m above mean sea level (Fig. 5.2), is ~0.5 m-thick, and composed of poorly consolidated and moderately stratified ash tuff that contains continuously parallel and diffuse concentrations of trains (bands) composed of fine, juvenile lapilli (lithofacies T4) (Figs. 5.5c and 5.6c). At least at M2 to M4, the sequence is devoid of

coarse accidental clasts and its upper and lower boundaries are gradational. The rhythmically bedded T4 lithofacies become the diffusely stratified T6 lithofacies (moderately consolidated tuff composed of an alternation of thin layers of accidental-origin ash and relatively coarser, juvenile ash) at site M4 (Figs. 5.5d and 5.6d). Juvenile fragments reduce in size. U4 reduces in thickness by at least 30% from medial to distal sites. Sites M2 and M4 contain <5 mm-diameter, accretionary lapilli in the lithofacies T1 and T6.

Interpretation

The eruption proceeded without interruption as suggested from the gradational contact from U3 to U4. Lithofacies T4 indicates a rhythmic sequence of PDCs with progressively lower contents of finer-grained juvenile fragments. Juvenile-rich bands and trails are fine-grained and show no distinct boundary layers, which indicates that base surges were generated by the recurrent collapse of low eruption columns formed by semi-continuous eruptions (c.f, Dellino et al., 1990). Deposition in medial locations was from moderately-dilute, weakly-turbulent clouds, which rapidly deflated, reduced in turbulence and particle load, depositing lithofacies T6 (Fig. 5.6a). Soft-sediment deformation is more evident in proximal locations (Fig. 5.5a), corresponding to inner rim wall subsidence. The absence of Waitemata Group block/lapilli-sized accidentals may suggest that the deposited material did not originated from freshly excavated Waitemata host rock by deepening of the explosion locus or a shifting in the vent, but rather from shallow seated explosions (Valentine and White, 2012).

**UNIT 5**

This unit cannot be recognised in its entirety. At site M2, U5 comprises a sequence of moderately to poorly consolidated, crudely bedded, variably clast supported, juvenile lapilli tuff (lithofacies LT3 and ash tuff (lithofacies T2 and T4). The ~1 m-thick sequence, containing >5 mm accretionary lapilli, has continuous plane-parallel bedding with sharp contacts onto underlying ash-rich U4 that are deformed by load structures (Fig. 5.5b). Within the unit, contacts are sharpest between lithofacies T2 and LT3, but gradational between lithofacies LT3 and T4, (Fig 5.5b). Blocks and bombs are rare and small, bordering on coarse-lapilli-sized clasts that form roughly asymmetric shallow bedding sags (~5 cm) with low impact angles. At M3, U5 thins to ~0.7 m. Its lower and upper coarse-grained segments become two diffuse bedded succession (with no boundary layers) containing juvenile fragments interbedded with accidental-origin ash (lithofacies T5). At site M4, lower and upper unit boundaries are ill-defined with bounding units being characterized by similar plane-parallel bedded, diffusely stratified tuff sequences (lithofacies T6). At site M4 many of the lithofaces have merged and U5 is represented by <0.5 m of laminae of variable juvenile-content (lithofacies T6) (Figs. 5.5d and 5.6d). At distal sites, T6 lithofaces contain accretionary lapilli.

Interpretation

A sharp contact to the base of this unit, lithofacies LT5 shows that the eruption shifted suddenly to a phase of production of coarser and more common juvenile fragments, either due to a reduction of external water interaction (it is possible that it represents a very shallow explosion, where water was restricted), or an increase in magma ascent rate (c.f., Houghton et al., 1999). Deposition of this phase from PDCs was mainly via traction-carpet collisional regimes close to the vent. The sequences containing higher lithic content (lithofacies T2 and T4 -Fig. 5.5b) could possibly indicate inner vent-

wall/sediment slumping into the explosion locus (c.f., Houghton and Smith, 1993) causing transient variations in degrees of interaction of the magma with external water and/or changes in magma ascent rates (Houghton et al., 1999). The final stages of this phase produced again juvenile-rich beds (lithofacies LT5), similar to its onset. An outstanding feature of U5 is the progressive transformation of sediment character from proximal to distal sites (Figs. 5.5b,c,d). The coarse, juvenile-rich layers (Fig. 5.5b) become gradually more distinctly stratified, with diffuse boundaries and composed of finer-grained juvenile fragments, which are distributed scarcely (Figs. 5.5c,d). U5 at site M3 (Fig. 6c) may have been deposited following stepwise aggradations (Sulpizio and Dellinno, 2008) of a PDC (or PDCs) dominantly transported in a collisional regime. Although the number of layers deposited by the passage of a single base surge is to an extent uncertain (Dellino et al., 1990), the polymodal clast distribution and the lack of erosional breaks in a deposit could indicate closely-timed explosions (Dellino et al., 1990), which generated numerous PDCs that in turn may segregated into different pulses that travel independently from each other (Sulpizio and Dellino, 2008). In travelling away from the vent, the PDCs became less concentrated and transported in a combination of saltation/traction mode producing mainly plane parallel-bedded deposits (as described in Valentine, 1987) (Figs. 5.5d and 5.6d).

**UNIT 6**

U6 is the uppermost tuff-ring sequence, and is commonly eroded and weathered (Fig 5.2). There are at least three lithofacies preserved T5, T6, and T7 (accretionary lapilli-rich, vesicular, fine-grained, lithic ash tuff. At M1 the deposits are ~1.5 m thick and lithofacies T7 dominates (Fig. 5.5a). Beds are parallel, continuous and form a gentle syncline-like structure, and are not affected by faulting as in the lowermost units at this site. At site M2, U6 is <1 m thick and comprises lithofacies T7 and T5 (Fig. 5.5b). At medial locations around site M3, U6 is usually <1 m (Fig. 5.5c). At M4, however, the unit thickens again to ~1.5 m and comprises continuous, plane-parallel beds alternating between lithofacies T7 and T5 (Figs. 5.5d and 5.6c). The pale/cream tuff is dominantly finer than coarse ash (with rare fine lapilli), contains sub-mm, irregular-to-rounded vesicles and ≤5 mm-diameter, spherical/oval accretionary and armoured lapilli.

Interpretation

Along the cliff, it has an irregular thickness ranging from mostly <1m, with lenses up to 2 m, which may reflect its deposition in separate lobes rather than a continuous sheet.U6 is characterized by lithofacies T7 and T6 (Fig. 5.5a,d), which shows a regular pattern of deposition from PDCs. Although soft sediment deformation of beds is subdued (due to a paucity of fragments larger than coarse ash), the presence of abundant accretionary lapilli and the vesicularity of tuff indicates its depositing currents were wet, with condensed water (e.g. Dellino et al., 1990). The level of explosive fragmentation (e.g., the depth of the explosive eruption locus) probably remained shallow-seated as indicated from the widespread presence of fine-grained material possible sourced from an already comminuted fragmented host rock redeposited within the upper diatreme (Valentine and White, 2012). The thicker U6 accumulations at the inner rim and in the distal location could reflect either the topographic barrier of the inner rim (c.f., Sulpizio and Dellino, 2008), or the lofting and subsequent grounding of the currents as they accelerated over the rim (Sohn, 1996). In general, the succession exhibits regular deposition patterns that suggest stabilization of the vent with explosions remaining in the water-saturated poorly unconsolidated sediments.

## Appendix C. Chemical analyses

### C.1 Chemical analyses Maungataketake

#### C.1.1 Whole-rock analyses

Samples from Maungataketake Volcano analyzed for major and trace elements were collected from the ejecta ring (3 samples) and the central scoria/lava cone (16 samples) to represent the range of materials erupted from the volcano; these data are presented in Table A.1. The samples are juvenile bombs from within tuff sections, scoriaceous blocks and lava. Rock fragments were crushed in a tungsten carbide ring grinder to <200µ mesh. Major elements and some trace elements were analyzed by XRF on fused glass discs made using Lithium Borate Spectrachem 12-22 flux, using a Siemens SRS3000 sequential X-ray spectrometer with a Rh tube at the University of Auckland. Minor trace elements were measured on a Laser Ablation Inductively Coupled Mass Spectrometer (LA-ICP-MS) at the Australian National University using stacks of XRF discs following the procedure of Eggins et al (1998). NIST 612 was run every 15 samples and used for calibration, and the silica content obtained by XRF used in data reduction. BCR-2G was used as an external standard with every analytical session and 28 international standards provided a further check on the method. BCR-2 data (n=143) is <15% 2SD, and accuracy <10% for all elements except Cu, Y, Zr, Tb and Hf which are <17% and Cr which is <26%. XRF data is reported for Cr, Ni and Zr.

#### C.1.2 Glass analyses

10 juvenile grains were selected (from thin sections) for microprobe analyses. These grains represent 5 samples taken from different sites (see Fig. 5.2 in main text for location of units, U, and sites, M): sample 26 (from middle U3 at site M1) (2 grains), sample 28 (from upper U3 at site M1) (3 grains), sample 31 (from middle U5 at site M2)(2 grains), sample 40 (from lower U6 at site M5)(2 grains), and sample 41 (from upper U6 at site M5)(1 grain). 6 spot measurements per grain were run on different glass sites. An average glass composition of each grain is shown in Table A.2. These compositions have been plotted and are shown in Fig. 5c,d. Olivine phenocrysts (not shown) and Pyroxene microlites/microcrysts were also analyzed and are represented in Fig. 5e15 pyroxene crystals were analysed from the same 5 samples mentioned above.

The samples were analysed by a Jeol JXA-8900R electron microprobe at the Laboratorio Universitario de Petrología (LUPI), Instituto de Geofísica, UNAM, México City. Measuring conditions were a beam current of 10 nA, an accelerating potential of 20 kV, and a beam diameter of 15 µm for glass and 1-5 µm for crystal analyses. During analyses, Na and K were analysed using 10 s counting times, whereas a 40 s-counting-time was used for other elements.

| **Type** | SC | TR | SC | SC | TR | SC | TR | SC | TR | SC | SC | SC | SC | SC | SC | SC | TR | SC | SC | SC |
|---|---|---|---|---|---|---|---|---|---|---|---|---|---|---|---|---|---|---|---|---|
| **Sample** | AVF-238 | AVF-869 | AVF-247 | AVF-248 | AVF-870 | AVF-237 | AVF-859 | AVF-249 | AVF-863 | AVF-245 | AVF-240 | AVF-239 | AVF-246 | AVF-243 | AVF-244 | AVF-252 | AVF-861 | AVF-250 | AVF-242 | AVF-241 |
| **$SiO_2$** | 41.80 | 42.07 | 42.23 | 42.30 | 42.41 | 42.50 | 42.61 | 42.94 | 43.18 | 43.72 | 43.73 | 43.75 | 43.88 | 44.33 | 44.37 | 44.40 | 44.50 | 44.51 | 44.55 | 44.65 |
| **$TiO_2$** | 2.88 | 2.91 | 2.85 | 2.84 | 2.83 | 2.84 | 2.90 | 2.88 | 2.73 | 2.82 | 2.80 | 2.80 | 2.76 | 2.69 | 2.69 | 2.67 | 2.60 | 2.66 | 2.70 | 2.69 |
| **$Al_2O_3$** | 11.88 | 11.86 | 11.95 | 11.92 | 11.89 | 12.04 | 12.12 | 12.51 | 11.99 | 12.95 | 12.86 | 12.95 | 13.19 | 13.20 | 13.09 | 13.14 | 12.05 | 13.24 | 13.13 | 13.26 |
| **Fe2O3** | 2.23 | 2.29 | 2.21 | 2.22 | 2.24 | 2.24 | 2.28 | 2.24 | 2.26 | 2.23 | 2.22 | 2.22 | 2.23 | 2.20 | 2.20 | 2.20 | 2.15 | 2.18 | 2.21 | 2.21 |
| **FeO** | 11.17 | 11.43 | 11.04 | 11.11 | 11.19 | 11.21 | 11.39 | 11.21 | 11.32 | 11.14 | 11.09 | 11.09 | 11.16 | 10.99 | 11.00 | 10.99 | 10.74 | 10.92 | 11.03 | 11.03 |
| **MnO** | 0.21 | 0.20 | 0.20 | 0.20 | 0.20 | 0.20 | 0.20 | 0.21 | 0.19 | 0.20 | 0.20 | 0.20 | 0.20 | 0.20 | 0.20 | 0.20 | 0.18 | 0.20 | 0.20 | 0.20 |
| **MgO** | 12.38 | 11.66 | 11.75 | 11.81 | 11.68 | 11.37 | 11.92 | 11.05 | 11.33 | 10.70 | 10.78 | 10.25 | 10.32 | 10.27 | 10.31 | 10.46 | 10.43 | 10.21 | 10.53 | 10.31 |
| **CaO** | 11.40 | 11.48 | 11.31 | 11.34 | 11.29 | 11.34 | 11.52 | 11.32 | 10.76 | 11.11 | 10.97 | 11.07 | 10.84 | 10.63 | 10.71 | 10.76 | 11.27 | 10.67 | 10.68 | 10.72 |
| **$Na_2O$** | 3.76 | 4.37 | 4.21 | 4.13 | 4.20 | 4.13 | 3.18 | 3.47 | 4.07 | 3.34 | 3.37 | 4.18 | 3.84 | 3.67 | 3.77 | 3.45 | 3.89 | 3.64 | 3.24 | 3.11 |
| **$K_2O$** | 1.44 | 0.92 | 1.45 | 1.33 | 1.29 | 1.31 | 1.08 | 1.38 | 1.39 | 1.06 | 1.25 | 0.79 | 0.93 | 1.19 | 1.01 | 1.12 | 1.45 | 1.15 | 1.11 | 1.18 |
| **$P_2O_5$** | 0.84 | 0.82 | 0.79 | 0.79 | 0.79 | 0.82 | 0.80 | 0.79 | 0.77 | 0.73 | 0.72 | 0.71 | 0.67 | 0.64 | 0.63 | 0.62 | 0.73 | 0.62 | 0.63 | 0.65 |
| **Mg#** | 66.37 | 64.52 | 65.48 | 65.45 | 65.05 | 64.38 | 65.10 | 63.71 | 64.08 | 63.12 | 63.39 | 62.21 | 62.23 | 62.47 | 62.56 | 62.90 | 63.37 | 62.50 | 62.97 | 62.49 |
| | | | | | | | | | | | | | | | | | | | | |
| **Cs** | 0.31 | 0.28 | 0.33 | 0.30 | 0.34 | 0.30 | 0.40 | 0.17 | 0.38 | 0.32 | 0.20 | 0.17 | 0.32 | 0.26 | 0.20 | 0.53 | 0.57 | 0.20 | 0.23 | 0.21 |
| **Ba** | 264.9 | 309.8 | 310.4 | 309.9 | 331.0 | 314.9 | 336.1 | 226.1 | 309.6 | 268.8 | 235.4 | 266.7 | 314.9 | 229.6 | 271.7 | 317.6 | 310.9 | 223.5 | 233.6 | 234.9 |
| **Rb** | 20.1 | 20.9 | 21.5 | 20.8 | 24.4 | 22.1 | 18.5 | 15.8 | 21.7 | 16.9 | 17.4 | 16.8 | 22.7 | 15.1 | 16.6 | 24.9 | 24.4 | 15.4 | 16.9 | 16.1 |
| **Sr** | 680.6 | 771.6 | 743.0 | 727.0 | 764.3 | 745.6 | 704.8 | 613.4 | 672.0 | 677.7 | 621.7 | 673.6 | 748.0 | 615.8 | 700.6 | 678.1 | 671.7 | 617.8 | 619.1 | 621.8 |
| **Pb** | 1.67 | 5.35 | 2.64 | 2.56 | 3.66 | 2.59 | 7.74 | 2.07 | 4.07 | 2.25 | 2.17 | 1.95 | 1.48 | 0.75 | 1.41 | 2.99 | 5.33 | 2.06 | 2.13 | 2.26 |
| **Th** | 5.18 | 6.14 | 6.03 | 5.85 | 6.65 | 6.25 | 5.52 | 4.36 | 4.79 | 5.19 | 4.63 | 5.26 | 6.28 | 4.51 | 5.50 | 5.82 | 4.87 | 4.37 | 4.47 | 4.65 |
| **U** | 1.44 | 1.66 | 1.61 | 1.64 | 1.70 | 1.70 | 1.76 | 1.16 | 1.53 | 1.51 | 1.36 | 1.46 | 1.69 | 1.29 | 1.42 | 1.59 | 1.85 | 1.24 | 1.27 | 1.26 |
| **Zr** | 208.2 | 237.0 | 220.3 | 222.1 | 233.0 | 225.9 | 236.0 | 188.0 | 232.0 | 207.9 | 195.6 | 211.4 | 221.4 | 188.8 | 212.0 | 210.9 | 228.0 | 187.2 | 191.6 | 205.6 |
| **Nb** | 63.7 | 71.4 | 74.7 | 72.5 | 75.3 | 76.1 | 72.6 | 53.2 | 62.5 | 64.4 | 56.3 | 65.1 | 75.7 | 54.8 | 65.9 | 66.0 | 59.7 | 53.1 | 55.5 | 55.9 |
| **Hf** | 4.80 | 5.45 | 5.04 | 5.09 | 5.73 | 5.34 | 4.52 | 4.41 | 3.94 | 4.77 | 4.58 | 4.83 | 5.13 | 4.42 | 5.03 | 4.80 | 4.36 | 4.38 | 4.57 | 4.48 |
| **Ta** | 3.97 | 4.65 | 4.60 | 4.55 | 5.01 | 4.73 | 4.28 | 3.29 | 3.76 | 3.99 | 3.56 | 4.19 | 4.71 | 3.40 | 4.10 | 4.20 | 3.56 | 3.34 | 3.47 | 3.53 |
| **Sc** | 23.7 | 23.9 | 22.0 | 22.9 | 23.5 | 22.6 | 20.5 | 23.8 | 17.8 | 23.6 | 24.2 | 23.5 | 22.0 | 23.6 | 23.9 | 20.5 | 18.0 | 24.5 | 23.7 | 24.0 |
| **V** | 286.1 | 241.0 | 296.3 | 292.8 | 234.0 | 289.9 | 238.0 | 280.5 | 220.0 | 298.8 | 283.4 | 279.1 | 275.1 | 275.0 | 276.1 | 272.7 | 213.0 | 284.5 | 268.6 | 210.5 |
| **Cr** | 417.3 | 332.0 | 375.8 | 337.1 | 344.0 | 373.8 | 354.0 | 281.3 | 300.0 | 293.1 | 293.5 | 310.3 | 378.2 | 283.7 | 304.9 | 331.8 | 277.0 | 289.6 | 284.3 | 264.2 |
| **Co** | 62.4 | 69.6 | 64.8 | 69.8 | 72.9 | 70.3 | 70.3 | 58.2 | 76.7 | 63.7 | 65.0 | 68.3 | 66.4 | 59.4 | 70.1 | 77.0 | 76.5 | 69.8 | 67.7 | 68.9 |
| **Ni** | 185.6 | 300.0 | 235.1 | 213.3 | 308.0 | 218.4 | 318.0 | 193.8 | 317.0 | 205.8 | 194.1 | 197.8 | 237.7 | 196.7 | 208.4 | 240.7 | 306.0 | 199.5 | 196.2 | 228.4 |
| **Cu** | 52.7 | 88.7 | 53.9 | 55.0 | 1489.9 | 54.6 | 60.1 | 53.1 | 57.4 | 60.6 | 50.1 | 46.9 | 28.8 | 66.9 | 38.7 | 51.7 | 57.9 | 52.1 | 54.9 | 52.6 |
| **Zn** | 87.2 | 105.3 | 93.9 | 94.9 | 103.6 | 96.2 | 118.0 | 92.1 | 108.7 | 93.6 | 88.3 | 88.5 | 94.4 | 91.2 | 98.4 | 93.7 | 114.8 | 89.0 | 89.9 | 89.4 |
| **Ga** | 39.1 | 37.4 | 41.6 | 41.6 | 38.6 | 42.4 | 30.5 | 34.7 | 29.2 | 39.0 | 36.5 | 38.8 | 41.9 | 34.7 | 39.8 | 41.3 | 28.6 | 34.6 | 35.7 | 35.8 |
| **Y** | 22.5 | 24.3 | 22.3 | 23.4 | 24.4 | 22.9 | 19.9 | 22.0 | 17.9 | 22.8 | 22.6 | 22.7 | 22.7 | 21.9 | 23.0 | 21.4 | 18.8 | 22.0 | 22.0 | 22.3 |
| **La** | 42.7 | 52.4 | 49.5 | 48.4 | 52.4 | 50.2 | 46.0 | 36.2 | 41.6 | 43.6 | 39.0 | 44.6 | 49.5 | 37.1 | 44.9 | 44.3 | 41.4 | 36.3 | 37.9 | 38.6 |
| **Ce** | 82.6 | 97.5 | 93.5 | 92.2 | 96.8 | 94.9 | 96.5 | 71.9 | 87.8 | 83.5 | 75.8 | 84.8 | 93.7 | 73.2 | 85.7 | 85.0 | 86.6 | 71.4 | 74.1 | 74.6 |
| **Pr** | 9.73 | 11.29 | 10.91 | 10.84 | 11.23 | 11.16 | 10.54 | 8.45 | 9.41 | 9.73 | 8.87 | 10.01 | 11.02 | 8.69 | 10.02 | 9.91 | 9.30 | 8.52 | 8.73 | 8.80 |
| **Nd** | 39.76 | 45.67 | 44.80 | 44.26 | 46.19 | 45.66 | 40.02 | 34.95 | 37.76 | 40.04 | 36.80 | 40.23 | 44.41 | 35.67 | 41.54 | 40.36 | 36.83 | 35.09 | 36.28 | 36.49 |
| **Sm** | 7.95 | 9.01 | 8.75 | 8.80 | 9.12 | 8.63 | 7.72 | 6.97 | 7.40 | 7.90 | 7.56 | 8.25 | 8.51 | 7.17 | 8.28 | 8.08 | 7.68 | 7.15 | 7.30 | 7.33 |
| **Eu** | 2.52 | 2.78 | 2.75 | 2.70 | 2.74 | 2.79 | 2.59 | 2.26 | 2.41 | 2.54 | 2.36 | 2.62 | 2.68 | 2.33 | 2.64 | 2.48 | 2.33 | 2.37 | 2.38 | 2.32 |
| **Gd** | 7.33 | 7.95 | 7.51 | 7.34 | 8.13 | 7.73 | 6.84 | 6.60 | 5.98 | 7.07 | 6.87 | 7.08 | 7.66 | 6.56 | 7.27 | 7.01 | 5.89 | 6.66 | 6.56 | 6.85 |
| **Tb** | 0.98 | 1.05 | 0.99 | 1.02 | 1.04 | 1.04 | 0.87 | 0.93 | 0.75 | 1.02 | 0.96 | 1.00 | 1.01 | 0.93 | 1.02 | 0.93 | 0.82 | 0.93 | 0.92 | 0.94 |
| **Dy** | 5.28 | 5.75 | 5.57 | 5.55 | 5.90 | 5.37 | 5.12 | 4.99 | 4.07 | 5.29 | 5.16 | 5.19 | 5.40 | 5.10 | 5.43 | 5.20 | 4.29 | 5.02 | 5.17 | 5.05 |
| **Ho** | 0.94 | 0.96 | 0.90 | 0.92 | 0.99 | 0.95 | 0.77 | 0.87 | 0.70 | 0.94 | 0.91 | 0.91 | 0.91 | 0.87 | 0.92 | 0.87 | 0.75 | 0.88 | 0.89 | 0.88 |
| **Er** | 2.20 | 2.23 | 2.13 | 2.19 | 2.42 | 2.15 | 1.91 | 2.23 | 1.70 | 2.25 | 2.22 | 2.22 | 2.17 | 2.12 | 2.32 | 2.06 | 1.65 | 2.21 | 2.13 | 2.24 |
| **Tm** | 0.27 | 0.30 | 0.25 | 0.28 | 0.28 | 0.25 | 0.22 | 0.28 | 0.20 | 0.27 | 0.28 | 0.27 | 0.26 | 0.28 | 0.28 | 0.25 | 0.24 | 0.28 | 0.27 | 0.27 |
| **Yb** | 1.63 | 1.62 | 1.53 | 1.60 | 1.75 | 1.55 | 1.31 | 1.71 | 1.18 | 1.66 | 1.66 | 1.68 | 1.44 | 1.69 | 1.66 | 1.41 | 1.40 | 1.66 | 1.69 | 1.64 |
| **Lu** | 0.20 | 0.22 | 0.19 | 0.20 | 0.22 | 0.20 | 0.19 | 0.22 | 0.15 | 0.23 | 0.21 | 0.23 | 0.19 | 0.21 | 0.22 | 0.18 | 0.17 | 0.22 | 0.22 | 0.22 |

**Table C.1** Whole rock major and trace element analyses for Maungataketake samples. Mg# calculated as mole percent Mg/Mg+Fe x100. SC= scoria cone sample; TR= tuff ring sample.

| Sample | 26a | 26b | 28a | 28b | 28c | 31a | 31b | 40a | 40b | 41 |
|---|---|---|---|---|---|---|---|---|---|---|
| $SiO_2$ | 44.85 | 46.16 | 41.92 | 46.74 | 46.84 | 42.88 | 43.03 | 45.16 | 46.01 | 44.61 |
| $TiO_2$ | 3.32 | 3.30 | 3.27 | 3.04 | 3.16 | 3.41 | 3.43 | 3.39 | 3.13 | 3.44 |
| $Al_2O_3$ | 15.75 | 15.90 | 15.56 | 16.44 | 16.23 | 15.48 | 15.48 | 15.49 | 16.11 | 15.58 |
| FeO | 13.29 | 13.20 | 12.84 | 12.52 | 12.74 | 13.19 | 13.27 | 13.10 | 12.94 | 13.20 |
| MgO | 4.05 | 4.10 | 4.01 | 3.78 | 4.06 | 4.21 | 4.22 | 4.20 | 3.85 | 4.33 |
| CaO | 11.31 | 11.35 | 11.25 | 10.77 | 11.08 | 11.69 | 11.67 | 11.61 | 10.95 | 11.73 |
| $Na_2O$ | 5.16 | 5.04 | 4.91 | 5.12 | 4.95 | 3.88 | 3.86 | 4.04 | 4.20 | 4.11 |
| $K_2O$ | 1.93 | 1.93 | 1.86 | 1.99 | 1.93 | 1.92 | 1.87 | 1.89 | 1.89 | 1.89 |
| Total | 99.67 | 100.98 | 95.63 | 100.40 | 100.98 | 96.67 | 96.82 | 98.88 | 99.09 | 98.89 |
| Mg# | 35.22 | 35.63 | 35.77 | 36.21 | 35.01 | 36.28 | 36.20 | 36.38 | 35.22 | 36.90 |

**Table C.2** Average glass composition of selected juvenile clasts from Maungataketake volcano. Mg# calculated as mole percent Mg/Mg+Fe x100. Each sample number (see Appendix 2 for sample details) can be represented by one up to three single grains which are indicated by letters (*a,b,c*).

## C.2 Glass analyses of North Head

Groundmass glass compositions were analysed at the University of Auckland with a JEOL JXA-840 electron microprobe microanalyser (EPMA) interfaced with a Princenton Gamma Tech Prism 2000 Si (Li) EDS X-ray detector at an accelerating voltage of 15 kV, a beam current of 800 pA and a total count time of 100 s. 17 juvenile sideromelane grains were selected (representing different levels from PH1, PH3, and PH4); up to three spots were analysed on each grain. The characteristics and location of each unit PH are explained in Chapter 7.

| Sample | PH1-1a | PH1-1b | PH1-1c | PH1-2a | PH1-2b | PH1-2c | PH1-3a | PH1-3b | PH1-3c | PH1-4a | PH1-4b | PH1-5a | PH1-5b | PH1-6a | PH1-6b | PH1-7a | PH1-7b | PH1-7c | PH3-1a | PH3-1b | PH3-1c |
|---|---|---|---|---|---|---|---|---|---|---|---|---|---|---|---|---|---|---|---|---|---|
| $SiO_2$ | 46.8 | 46.5 | 46.9 | 46.6 | 46.4 | 46.6 | 46.8 | 46.6 | 46.4 | 47.3 | 47.0 | 47.1 | 46.9 | 46.8 | 47.0 | 46.4 | 46.1 | 46.9 | 46.7 | 46.8 | 46.4 |
| $TiO_2$ | 2.9 | 3.0 | 2.9 | 3.2 | 3.1 | 2.7 | 2.6 | 2.7 | 2.6 | 2.8 | 2.7 | 2.6 | 2.8 | 2.6 | 2.7 | 2.5 | 2.5 | 2.6 | 2.7 | 2.7 | 2.9 |
| $Al2O_3$ | 17.1 | 16.7 | 17.0 | 16.7 | 17.0 | 16.9 | 17.3 | 17.1 | 17.1 | 17.1 | 16.9 | 17.1 | 17.1 | 17.2 | 17.1 | 17.0 | 16.8 | 16.7 | 17.1 | 17.1 | 16.9 |
| FeO | 10.6 | 10.8 | 10.9 | 10.6 | 10.6 | 10.3 | 10.5 | 10.4 | 10.6 | 10.2 | 10.5 | 10.3 | 10.4 | 9.8 | 10.4 | 10.0 | 10.1 | 10.1 | 10.5 | 10.2 | 10.4 |
| MnO | 0.2 | 0.1 | 0.3 | 0.2 | 0.3 | 0.3 | 0.2 | 0.2 | 0.3 | 0.2 | 0.1 | 0.2 | 0.1 | 0.2 | 0.3 | 0.2 | 0.1 | 0.2 | 0.2 | 0.1 | 0.2 |
| MgO | 3.2 | 3.3 | 3.2 | 3.3 | 3.4 | 3.0 | 3.1 | 3.1 | 2.9 | 3.2 | 3.1 | 3.4 | 3.4 | 3.3 | 3.2 | 3.0 | 3.1 | 3.3 | 3.1 | 3.1 | 3.2 |
| CaO | 8.4 | 8.3 | 8.5 | 8.9 | 8.7 | 8.3 | 7.9 | 7.9 | 7.9 | 8.1 | 8.0 | 8.3 | 8.2 | 7.7 | 7.8 | 7.8 | 7.8 | 8.0 | 8.0 | 7.9 | 8.0 |
| $Na_2O$ | 4.9 | 5.2 | 5.3 | 4.7 | 5.1 | 5.3 | 6.0 | 6.1 | 5.6 | 5.8 | 5.4 | 5.6 | 5.8 | 6.0 | 5.7 | 5.4 | 5.4 | 5.4 | 5.2 | 5.4 | 5.5 |
| $K_2O$ | 2.9 | 2.8 | 2.9 | 2.7 | 2.7 | 3.0 | 3.0 | 2.9 | 2.9 | 3.0 | 2.8 | 3.0 | 3.0 | 2.8 | 3.0 | 2.9 | 2.9 | 2.9 | 2.9 | 2.9 | 2.9 |
| $P_2O_5$ | 1.7 | 1.2 | 1.4 | 1.5 | 1.5 | 1.7 | 1.6 | 1.5 | 1.6 | 1.8 | 1.6 | 1.7 | 1.7 | 1.8 | 1.6 | 1.8 | 1.7 | 1.5 | 1.7 | 1.7 | 1.5 |
| $SO_3$ | 0.26 | 0.33 | 0.15 | 0.12 | 0.26 | 0.17 | 0.23 | 0.26 | 0.25 | 0.26 | 0.26 | 0.25 | 0.1 | 0.3 | 0.17 | 0.11 | 0.21 | 0.2 | 0.22 | 0.14 | 0.14 |
| Cl | 0.11 | 0.11 | 0.09 | 0.1 | 0.05 | 0.05 | 0 | 0.11 | 0.05 | 0.1 | 0.05 | 0.1 | 0.08 | 0.11 | 0.12 | 0.11 | 0.09 | 0.06 | 0.08 | 0.05 | 0.08 |
| $Cr_2O_3$ | <0.11 | 0.05 | <0.03 | 0.09 | 0 | <0.03 | 0.1 | <0.05 | 0.08 | 0.01 | <0.01 | <0.06 | 0.11 | <0.01 | 0.01 | 0.05 | 0.05 | 0.19 | 0.09 | 0.04 | <0.03 |
| NiO | 0.03 | -0.04 | <0.05 | <0.09 | 0.02 | 0.02 | 0.08 | <0.2 | 0.21 | <0.01 | 0.08 | <0.19 | 0.07 | 0.17 | <0.03 | 0.23 | <0.01 | 0.02 | 0.08 | <0.09 | 0.02 |
| Total | 99.12 | 98.42 | 99.4 | 98.63 | 99.08 | 98.27 | 99.2 | 98.57 | 98.41 | 99.73 | 98.54 | 99.54 | 99.63 | 98.65 | 99.12 | 97.5 | 96.68 | 98.08 | 98.49 | 98.04 | 98.06 |
| | | | | | | | | | | | | | | | | | | | | | |
| Sample | PH3-2a | PH3-2b | PH3-3a | PH3-3b | PH3-3c | PH3-4a | PH3-4b | PH3-5a | PH3-5b | PH3-6a | PH3-6b | PH3-7a | PH3-7b | PH3-7c | PH4-1a | PH4-1b | PH4-1c | PH4-2a | PH4-2b | PH4-3a | PH4-3b |
| $SiO_2$ | 46.6 | 46.4 | 46.6 | 46.6 | 46.7 | 46.8 | 46.6 | 47.6 | 46.5 | 47.0 | 47.0 | 46.1 | 46.8 | 46.6 | 46.6 | 46.4 | 46.5 | 46.6 | 46.5 | 46.9 | 46.8 |
| $TiO_2$ | 2.8 | 2.9 | 2.6 | 2.8 | 2.8 | 2.7 | 2.7 | 2.7 | 2.8 | 2.6 | 2.5 | 2.6 | 2.9 | 2.9 | 2.7 | 2.7 | 2.7 | 2.9 | 2.9 | 2.8 | 2.7 |
| $Al_2O_3$ | 17.1 | 16.9 | 17.0 | 17.0 | 17.1 | 16.8 | 17.1 | 17.2 | 17.2 | 17.2 | 17.1 | 16.8 | 16.7 | 16.6 | 16.8 | 16.8 | 16.6 | 16.9 | 16.7 | 16.8 | 16.8 |
| FeO | 10.0 | 10.0 | 10.3 | 10.2 | 10.2 | 10.5 | 10.6 | 10.4 | 10.3 | 10.0 | 10.0 | 10.5 | 10.5 | 10.5 | 10.2 | 10.5 | 10.5 | 10.3 | 10.3 | 10.4 | 10.5 |
| MnO | 0.2 | 0.1 | 0.2 | 0.2 | 0.2 | 0.2 | 0.1 | 0.3 | 0.3 | 0.3 | 0.1 | 0.2 | 0.1 | 0.3 | 0.1 | 0.1 | 0.2 | 0.2 | 0.3 | 0.2 | 0.2 |
| MgO | 3.1 | 3.0 | 3.2 | 3.0 | 3.2 | 3.3 | 3.4 | 3.1 | 3.2 | 3.2 | 3.1 | 3.2 | 3.3 | 3.3 | 3.2 | 3.2 | 3.3 | 3.2 | 3.3 | 3.3 | 3.2 |
| CaO | 8.0 | 7.9 | 8.0 | 8.1 | 8.0 | 8.0 | 8.1 | 7.9 | 7.8 | 7.8 | 7.5 | 7.8 | 8.3 | 8.1 | 8.2 | 7.9 | 8.3 | 8.2 | 8.3 | 8.2 | 7.9 |
| $Na_2O$ | 6.1 | 5.8 | 5.6 | 5.3 | 5.3 | 5.4 | 5.4 | 5.4 | 5.9 | 5.5 | 5.6 | 4.1 | 5.5 | 5.5 | 5.6 | 5.8 | 5.6 | 5.1 | 5.1 | 5.4 | 5.5 |
| $K_2O$ | 2.8 | 2.8 | 2.9 | 2.9 | 2.9 | 2.8 | 2.9 | 2.9 | 3.0 | 2.9 | 2.9 | 2.7 | 2.8 | 2.8 | 2.9 | 2.8 | 2.8 | 2.9 | 2.8 | 2.9 | 2.9 |
| $P_2O_5$ | 1.7 | 1.5 | 1.7 | 1.7 | 1.6 | 1.8 | 1.6 | 1.7 | 1.7 | 1.6 | 1.6 | 1.5 | 1.5 | 1.5 | 1.7 | 1.5 | 1.6 | 1.6 | 1.6 | 1.6 | 1.5 |
| $SO_3$ | 0.1 | 0.2 | 0.3 | 0.2 | 0.2 | 0.3 | 0.2 | 0.3 | 0.2 | 0.2 | 0.1 | 0.2 | 0.1 | 0.3 | 0.2 | 0.1 | 0.1 | 0.1 | 0.2 | 0.3 | 0.2 |
| Cl | 0.1 | 0.1 | 0.1 | 0.1 | 0.1 | 0.1 | 0.1 | 0.1 | 0.1 | 0.1 | 0.1 | 0.1 | 0.1 | 0.1 | 0.1 | 0.1 | 0.1 | 0.1 | 0.1 | 0.1 | 0.1 |
| $Cr_2O_3$ | 0 | 0.08 | <0.02 | 0.03 | <0.05 | 0 | 0.03 | 0.04 | 0.17 | 0.06 | 0.1 | <0.08 | 0.13 | <0.02 | 0.15 | 0.04 | 0.05 | <0.07 | <0.13 | <0.08 | 0.16 |
| NiO | <0.01 | <0.27 | <0.1 | 0 | <0.01 | <0.02 | 0 | <0.12 | 0.21 | <0.19 | 0.04 | <0.03 | 0.07 | 0.02 | 0.18 | <0.08 | 0.01 | <0.05 | <0.05 | 0.02 | 0.09 |
| Total | 98.63 | 97.44 | 98.38 | 98.03 | 98.09 | 98.79 | 98.83 | 99.4 | 99.36 | 98.2 | 97.68 | 95.72 | 98.73 | 98.4 | 98.64 | 97.99 | 98.27 | 98.03 | 97.79 | 98.47 | 98.5 |

**Table C.3**. Glass compositions of 17 selected sideromelane clasts from North Head volcano. PH1-3-4 indicates the phreatomagmatic subunit where samples were collected. Samples come from varied stratigraphic positions within the units. The letters a, b, and c refer to the different spots analysed within the same clast.

## Appendix D.1 Motukorea stratigraphic logs, grain size distribution and juvenile/lithic content of selected samples.

### D.1.1 Motukorea stratigraphic logs

This part of the appendix first presents the total of logs corresponding to Motukorea volcano (Figs. D.1.2 to D.1.7). There are 3 extra logs included (SS1, SS2, and SS3). The logs showed in chapter 6 (S1, S2a, S2b, S3) are also included. See Table 6.2 in chapter 6 and Appendix D-2 for description of lithofacies included in logs and pictures.

Fig. D.1.1 shows an aerial photograph of Motukorea volcano. The exposed tephra ring deposits are clearly seen on the eastern-southern side of the island. The horizontal/vertical scale is approximate. Alongside the 4 sites described in chapter 6, other 3 sites are included (SS1, SS2, and SS3).

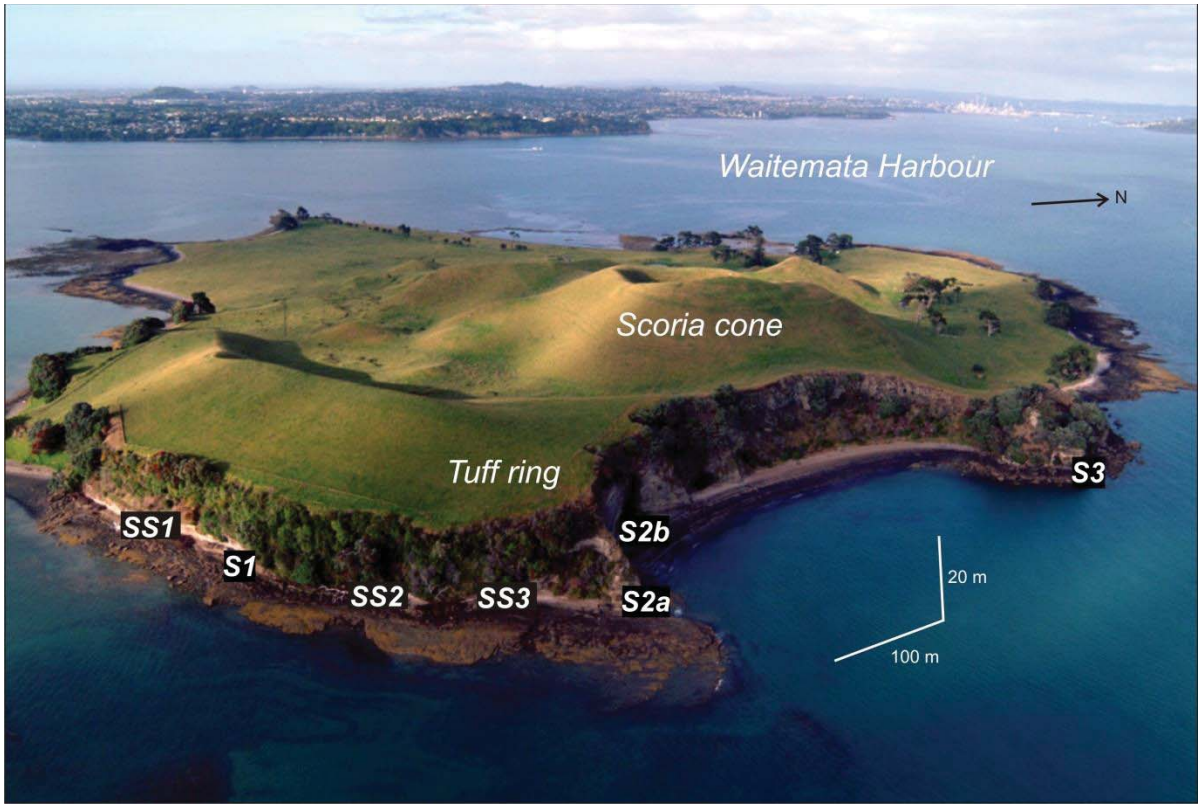


**Fig. D.1.1** Location of complete studied sites.

The stratigraphic logs are presented starting from SS1 to S3. Except for exposures at site S2b (whose exposure base is at the back beach level) all other exposures' bases intersect a wave-cut platform that marks approximately the highest tide sea level in the area. The boxes, at the left of logs, containing the grain size and juvenile content are not to scale and do not represent stratigraphic columns. See Table 6.2 in chapter 6 and ***Appendix D.2*** for description of lithofacies

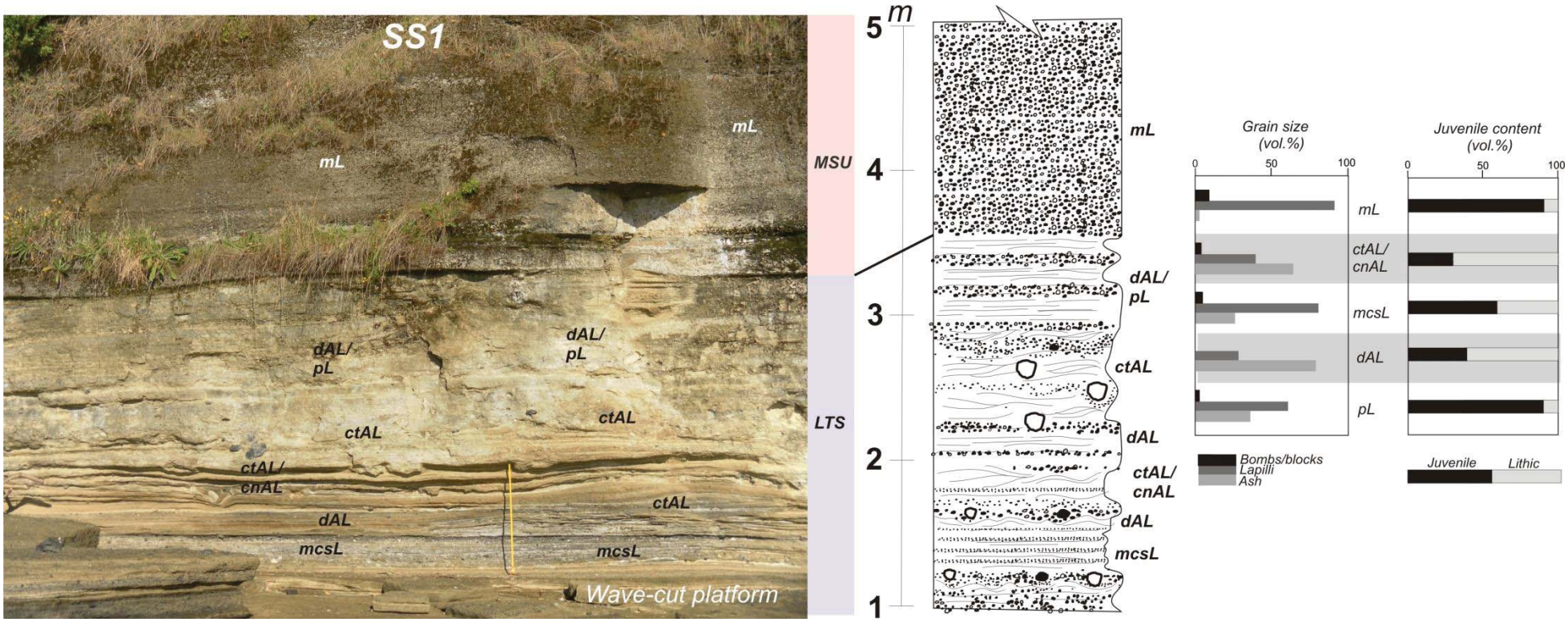


**Fig. D.1.2** Site SS1. Base of sequence intersects a wave-cut platform that marks approximately the highest tide sea level in the area. Thickness of log (in metres) corresponds to thickness of sequence in photograph.

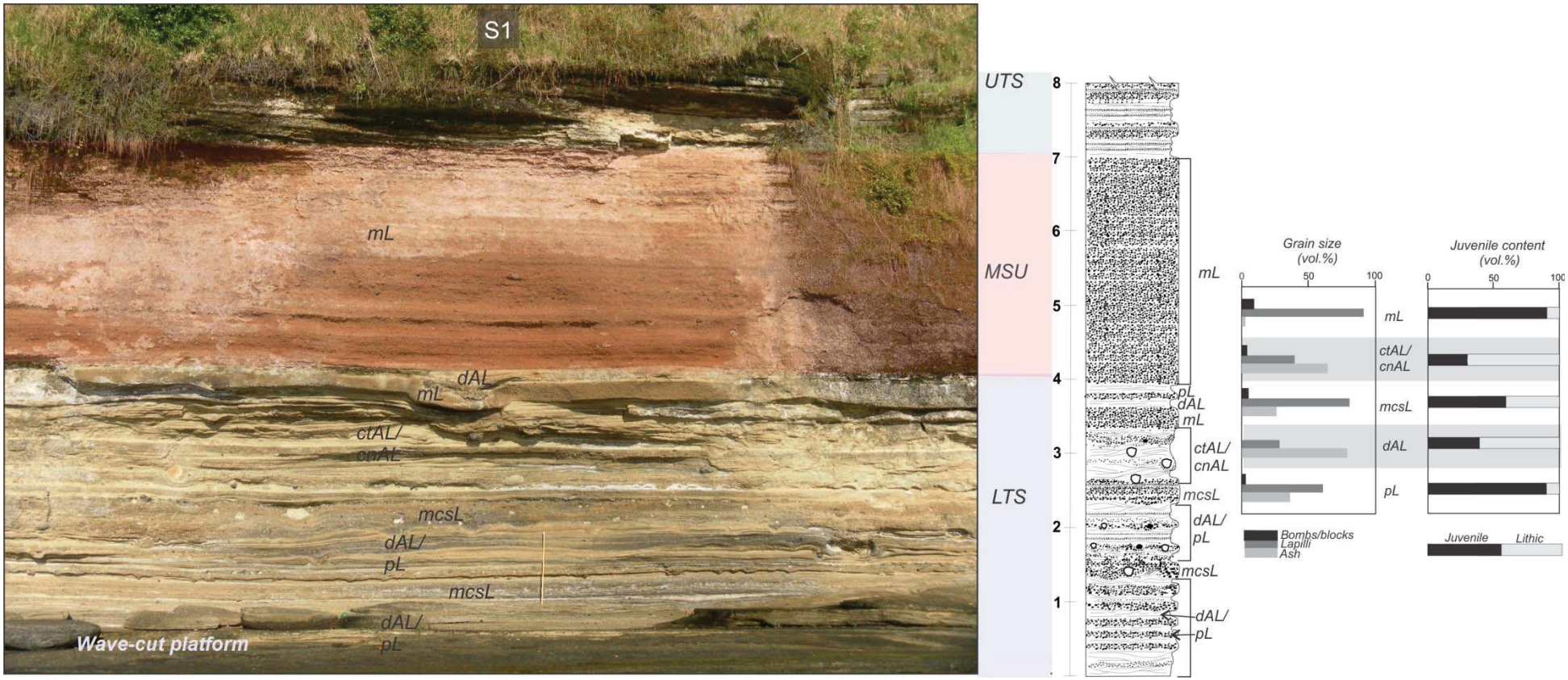


**Fig. D.1.3** Site S1. Base of sequence intersects a wave-cut platform that marks approximately the highest tide sea level in the area. Thickness of log (in metres) corresponds to thickness of sequence in photograph.

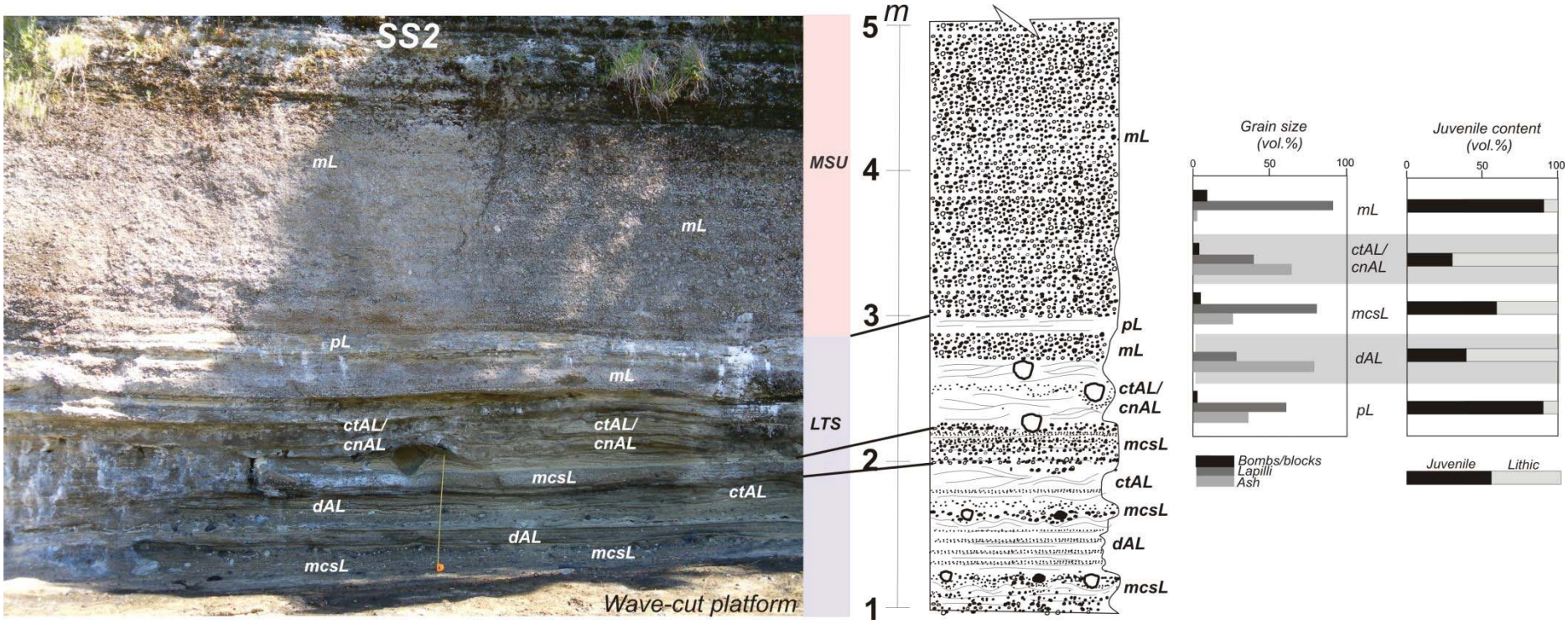


**Fig. D.1.4** Site SS2. Base of sequence intersects a wave-cut platform that marks approximately the highest tide sea level in the area. Thickness of log (in metres) corresponds to thickness of sequence in photograph.

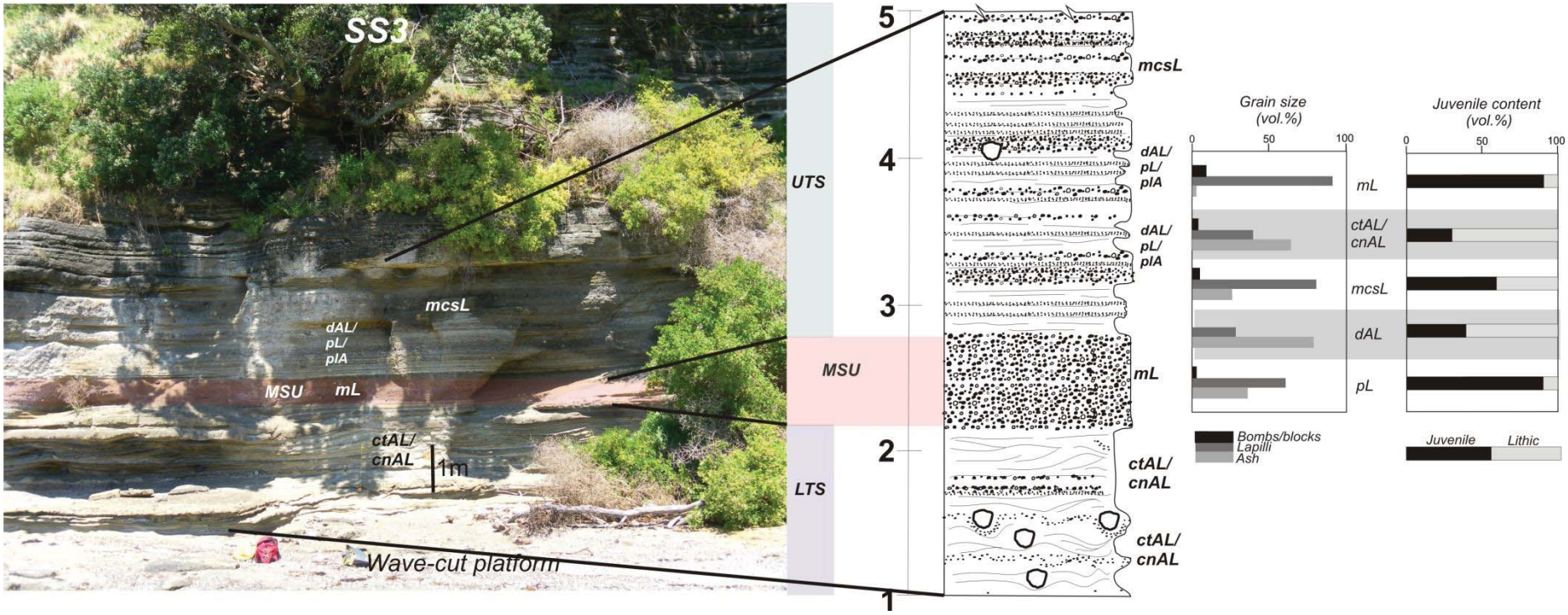


**Fig. D.1.5** Site SS3. Base of sequence intersects a wave-cut platform that marks approximately the highest tide sea level in the area. Thickness of log (in metres) does not correspond to thickness of sequence in photograph (see scale bar in photograph).

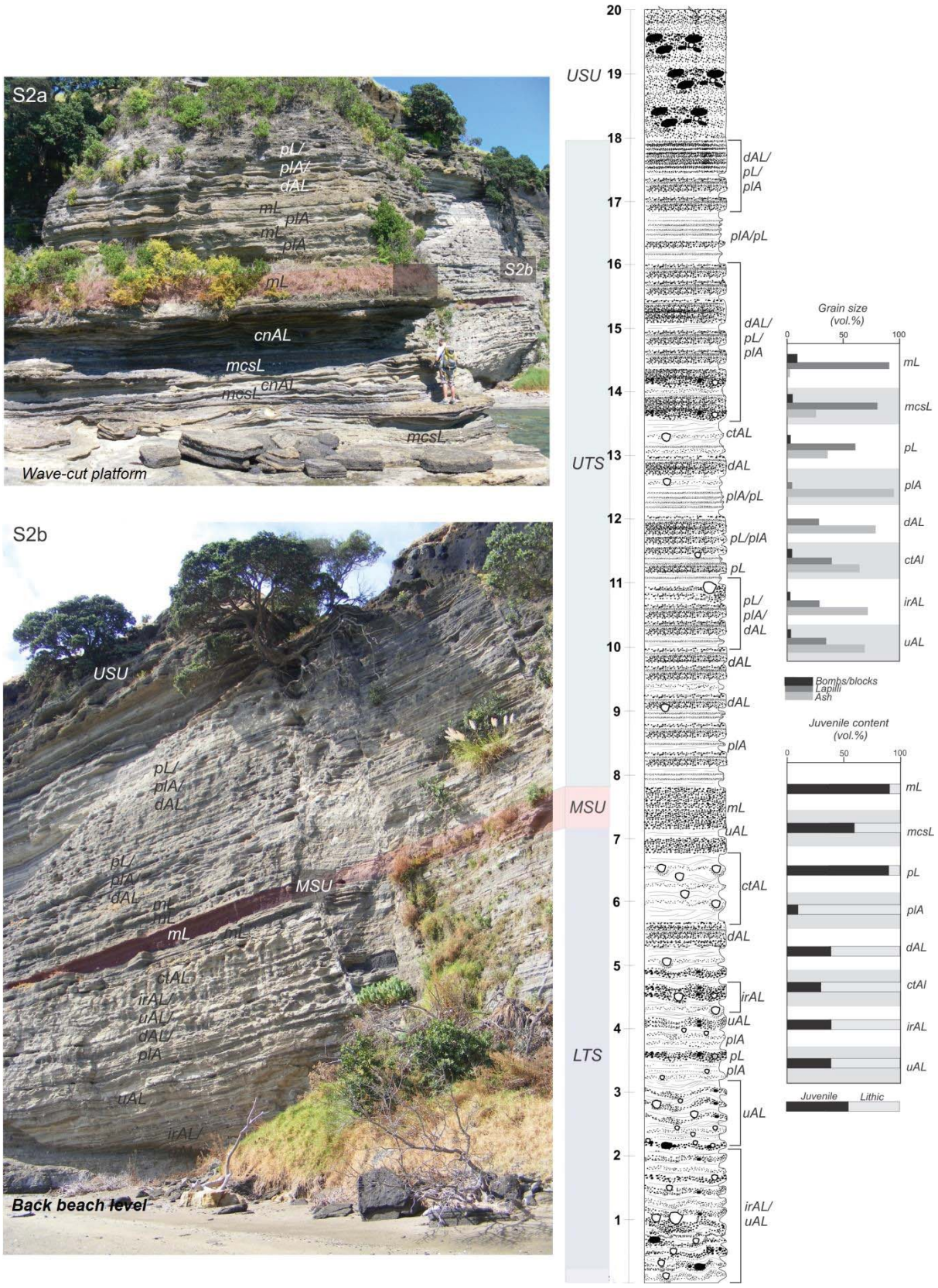


**Fig. D.1.6** Sites S2a and S2b. Base of sequence at S2a intersects a wave-cut platform that marks approximately the highest tide sea level in the area. Base of sequence at S2b intersects the back beach level. Thickness of log (in metres) corresponds to thickness of sequence in photograph S2b. Person in picture S2a is 1.8 m high.

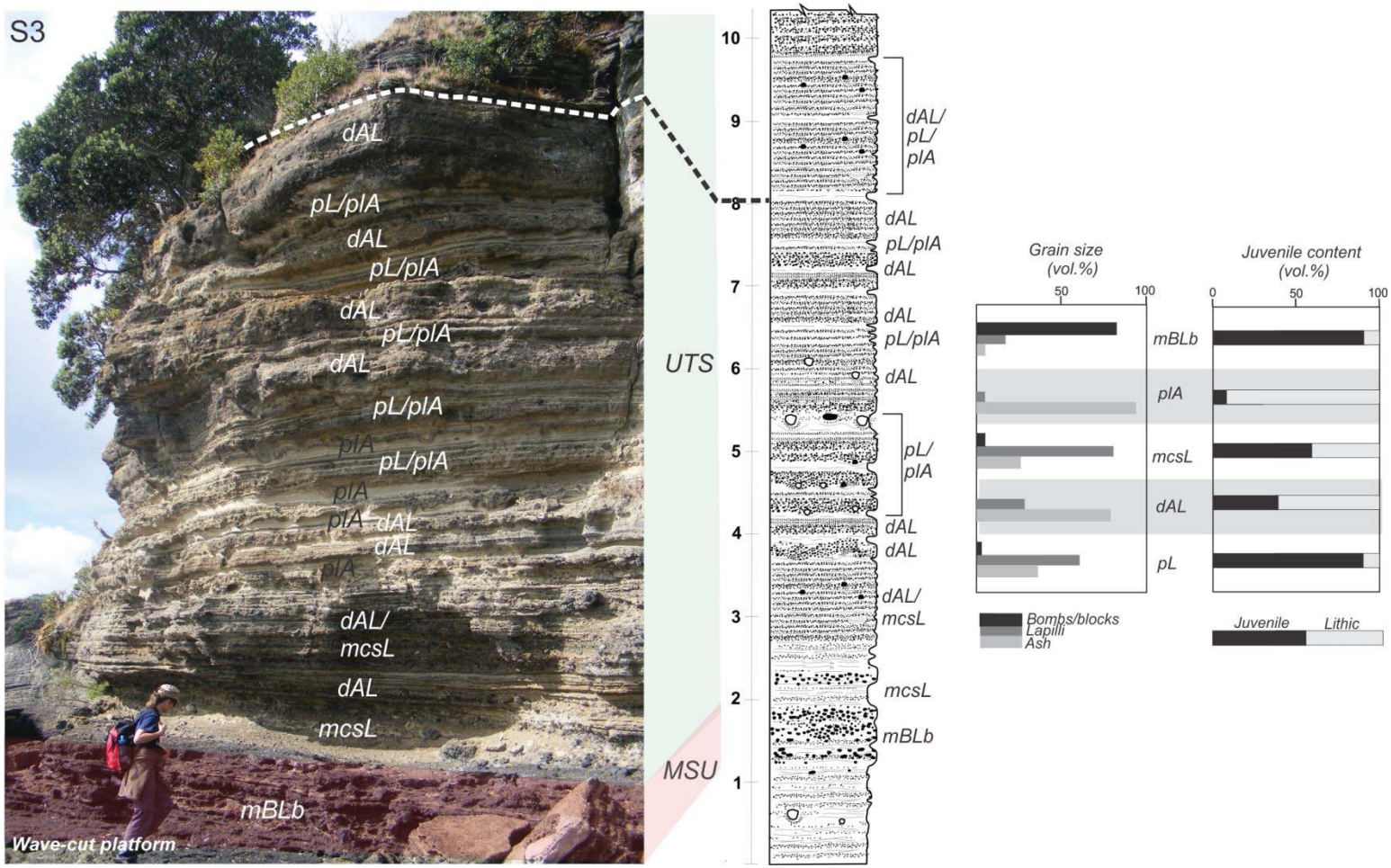


**Fig. D.1.7** Site S3. Base of sequence intersects a wave-cut platform that marks approximately the highest tide sea level in the area. Thickness of log (in metres) corresponds to thickness of sequence of photograph.

**D.1.2 Grain size distribution and juvenile/lithic content of Motukorea samples (chapter 6). These results are not presented in the chapter as explained in section 6.5.2 of chapter 6.**

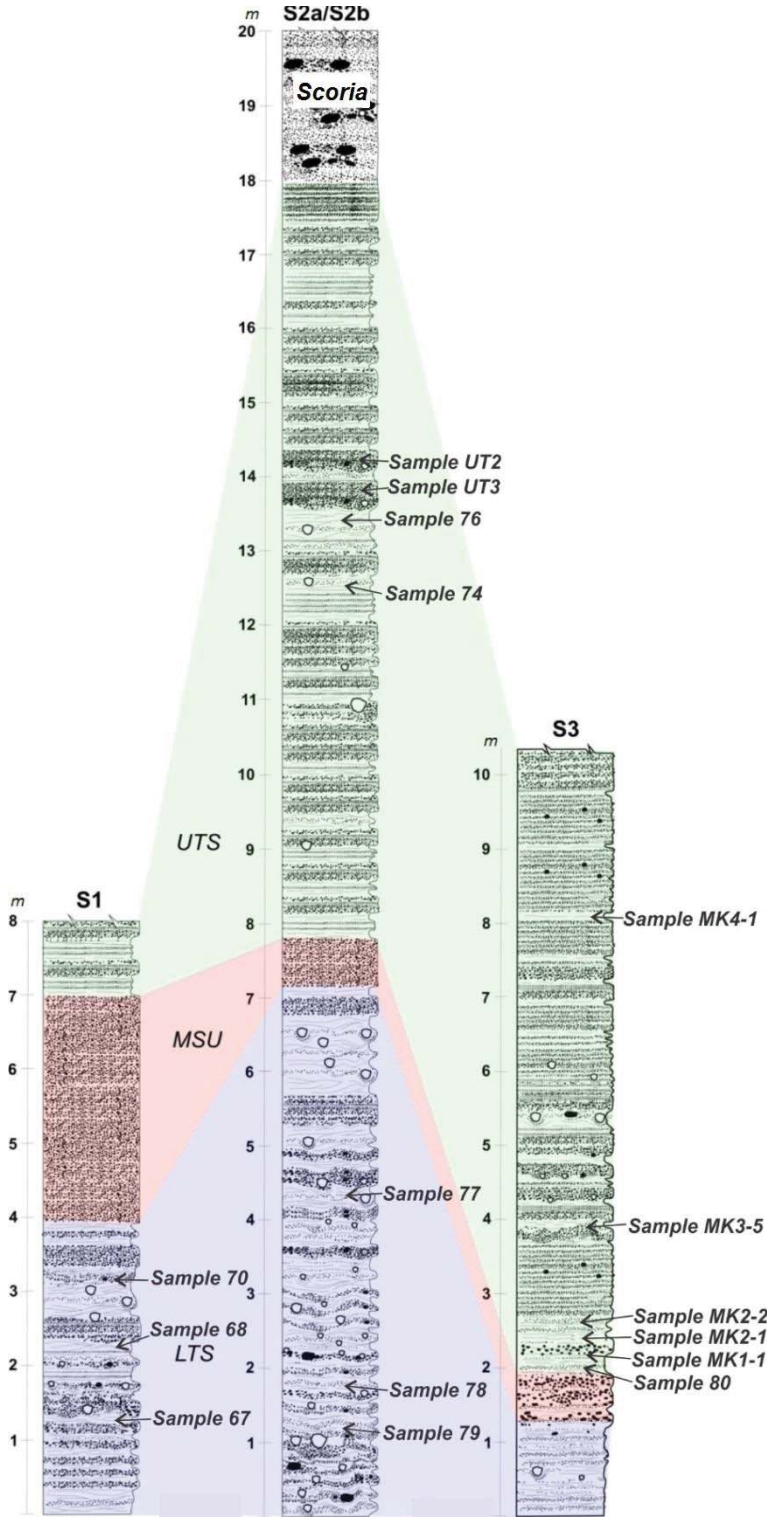


**Fig. D.1.8** Location of sampling sites within the Motukorea sequence (for location of sites see Fig. D.1.1). Scale of logs indicates thicknesses. See Figs. D.1.3, D.1.6, and D.1.7 for details of stratigraphic logs.

| Grain size | Phi | Samples / vol.% | | | | | | | | | | | | | | |
|---|---|---|---|---|---|---|---|---|---|---|---|---|---|---|---|---|
| | | 67 | 68 | 70 | 74 | 76 | 77 | 78 | 79 | 80 | MK2-1 | MK2-2 | MK3-5 | MK4-1 | UT2 | UT3 |
| | -3.5 | | | | | | | | | | | | | | 0.877095 | 1.635562 |
| | -3 | 1.680351 | | | 1.846038 | | | | | 2.450548 | | | 2.163253 | 2.382093 | 3.622034 | 4.481007 |
| | -2.5 | 6.938359 | | | 4.703001 | 0.734118 | 0.626478 | | | 7.682798 | 6.456548 | | 6.957144 | 5.369507 | 3.605974 | 8.006672 |
| | -2 | 12.24316 | 4.143556 | 5.515954 | 10.83762 | 3.626981 | 3.496772 | | | 13.05634 | 20.89963 | 2.583927 | 11.69995 | 10.61272 | 6.711633 | 11.3352 |
| | -1.5 | 14.5446 | 11.06036 | 11.54956 | 11.67902 | 3.612444 | 9.441923 | | 6.442411 | 13.42723 | 18.51285 | 11.59715 | 12.28738 | 11.90175 | 11.54801 | 14.94211 |
| Medium Lapilli | | 35.40647 | 15.20392 | 17.06551 | 29.06568 | 7.973543 | 13.56517 | | 6.442411 | 36.61692 | 45.86903 | 14.18108 | 33.10773 | 30.26608 | 26.36475 | 40.40055 |
| | -1 | 12.5452 | 15.04894 | 15.17312 | 11.57855 | 4.252072 | 11.04647 | 9.579277 | 9.104957 | 9.691805 | 12.8519 | 18.92167 | 10.67324 | 9.615468 | 14.65244 | 16.96977 |
| | -0.5 | 10.09061 | 14.26591 | 15.30041 | 10.25995 | 5.298735 | 9.154254 | 9.318498 | 11.73184 | 8.336277 | 8.904529 | 19.30824 | 9.562241 | 7.991116 | 16.71423 | 16.40761 |
| Fine Lapilli | | 22.63581 | 29.31485 | 30.47352 | 21.8385 | 9.550807 | 20.20073 | 18.89777 | 20.8368 | 18.02808 | 21.75643 | 38.22991 | 20.23548 | 17.60658 | 31.36666 | 33.37738 |
| | 0 | 7.031948 | 8.727569 | 9.869314 | 8.068567 | 3.692397 | 6.737838 | 8.918637 | 9.538809 | 5.797421 | 6.150551 | 11.29196 | 7.202329 | 6.157732 | 13.70616 | 10.44702 |
| | 0.5 | 5.087846 | 6.182708 | 7.5611 | 6.297878 | 2.122402 | 5.19082 | 9.179416 | 7.090218 | 5.024726 | 4.299266 | 7.548321 | 5.552434 | 5.713539 | 10.17184 | 6.633233 |
| | 1 | 4.500787 | 5.88907 | 6.491853 | 5.607183 | 2.318651 | 5.216391 | 9.753129 | 5.877808 | 4.759802 | 3.687271 | 6.429298 | 5.445165 | 5.730958 | 7.837033 | 4.061826 |
| | 1.5 | 3.488323 | 5 | 5.049219 | 4.621374 | 2.405873 | 4.660231 | 8.310153 | 4.802092 | 4.150477 | 2.922277 | 4.679552 | 4.663636 | 4.938379 | 3.449085 | 1.845694 |
| Coarse ash | | 20.1089 | 25.79935 | 28.97149 | 24.595 | 10.53932 | 21.80528 | 36.16134 | 27.30893 | 19.73243 | 17.05936 | 29.94914 | 22.86356 | 22.54061 | 35.16412 | 22.98777 |
| | 2 | 3.269846 | 4.575856 | 4.296829 | 3.270439 | 3.909734 | 4.519899 | 10.10127 | 5.187071 | 2.3944 | 2.895068 | 3.688566 | 3.40238 | 3.453129 | 2.21621 | 1.108066 |
| | 2.5 | 3.353401 | 4.475688 | 3.867511 | 3.958522 | 7.02782 | 5.386498 | 10.41234 | 7.5413 | 4.950615 | 3.542872 | 3.660186 | 4.390305 | 6.568666 | 1.559006 | 0.726796 |
| | 3 | 3.862736 | 5.223638 | 3.795115 | 5.133574 | 10.10057 | 7.168268 | 10.12466 | 10.98907 | 3.050467 | 4.224149 | 4.156225 | 4.202815 | 5.088131 | 1.066103 | 0.391018 |
| | 3.5 | 1.151946 | 1.574099 | 1.598235 | 2.027524 | 5.639729 | 2.57859 | 3.533977 | 4.218346 | 1.846406 | 1.324902 | 1.149457 | 1.439065 | 2.341211 | 0.744913 | 0.367189 |
| | 4 | 1.760338 | 2.372412 | 2.050871 | 2.353396 | 7.489317 | 4.273988 | 3.463384 | 4.738935 | 2.355548 | 1.349387 | 1.575557 | 1.837475 | 2.807541 | 0.459549 | 0.220963 |
| Medium ash | | 13.39827 | 18.22169 | 15.60856 | 16.74345 | 34.16717 | 23.92724 | 37.63564 | 32.67472 | 14.59744 | 13.33638 | 14.22999 | 15.27204 | 20.25868 | 6.045782 | 2.814033 |
| | 4.5 | 1.595406 | 2.081443 | 1.726726 | 1.869357 | 6.986461 | 4.349271 | 2.397724 | 3.465568 | 1.963338 | 0.869852 | 1.206204 | 1.525617 | 2.293734 | 0.447195 | 0.137561 |
| | 5 | 1.127925 | 1.446964 | 1.152886 | 1.241542 | 5.39716 | 3.359208 | 1.41267 | 2.135505 | 1.348822 | 0.433421 | 0.68652 | 1.031729 | 1.548471 | 0.611496 | 0.282703 |
| | 5.5 | 0.917809 | 1.192774 | 0.856912 | 0.936128 | 4.498303 | 2.639332 | 0.90749 | 1.557897 | 1.108219 | 0.23015 | 0.424565 | 0.831551 | 1.158509 | | |
| | 6 | 1.049231 | 1.414882 | 0.893822 | 0.934004 | 4.832383 | 2.623358 | 0.734576 | 1.498781 | 1.31333 | 0.156107 | 0.344016 | 0.988241 | 1.122514 | | |
| | 6.5 | 1.27237 | 1.781558 | 1.04714 | 0.996253 | 5.476616 | 2.754798 | 0.675559 | 1.514024 | 1.680749 | 0.122719 | 0.304932 | 1.292823 | 1.158456 | | |
| | 7 | 1.130466 | 1.616848 | 0.945432 | 0.82137 | 4.708907 | 2.226029 | 0.528331 | 1.193686 | 1.572761 | 0.085704 | 0.221225 | 1.235841 | 0.934957 | | |
| | 7.5 | 0.725679 | 1.044145 | 0.634095 | 0.509788 | 3.012751 | 1.353582 | 0.331801 | 0.723421 | 1.056758 | 0.049614 | 0.126351 | 0.841704 | 0.576237 | | |
| Fine ash (silt) | | 7.818885 | 10.57861 | 7.257012 | 7.308441 | 34.91258 | 19.30558 | 6.988151 | 12.08888 | 10.04398 | 1.947567 | 3.313812 | 7.747506 | 8.792879 | 1.058691 | 0.420264 |
| | 8 | 0.375843 | 0.533854 | 0.349888 | 0.26605 | 1.606472 | 0.695952 | 0.185123 | 0.379454 | 0.56624 | 0.026347 | 0.063598 | 0.451162 | 0.3043 | | |
| | 8.5 | 0.165449 | 0.22768 | 0.166379 | 0.121869 | 0.750356 | 0.316387 | 0.09442 | 0.179928 | 0.255265 | 0.00483 | 0.028985 | 0.200516 | 0.143766 | | |
| | 9 | 0.075796 | 0.100705 | 0.081202 | 0.057834 | 0.36568 | 0.152499 | 0.037557 | 0.088956 | 0.118321 | | 0.003537 | 0.090909 | 0.07199 | | |
| | 9.5 | 0.01477 | 0.019186 | 0.026436 | 0.003134 | 0.134253 | 0.031087 | | | 0.041333 | | | 0.03105 | 0.01506 | | |
| Fine ash (clay) | | 0.631857 | 0.881425 | 0.623905 | 0.448887 | 2.856761 | 1.195926 | 0.3171 | 0.648337 | 0.981158 | 0.031177 | 0.09612 | 0.773638 | 0.535116 | | |

**Table D.1** Volume percentage values for phi fractions of selected sieved-Motukorea samples. The fractions are grouped in grain size grades. For location of samples see Fig D.1.8 above . Samples UT2 and UT3 are loose lapilli that belong to beds related to fall out inter-bedded with subtle base surges (facies dAl and pL).

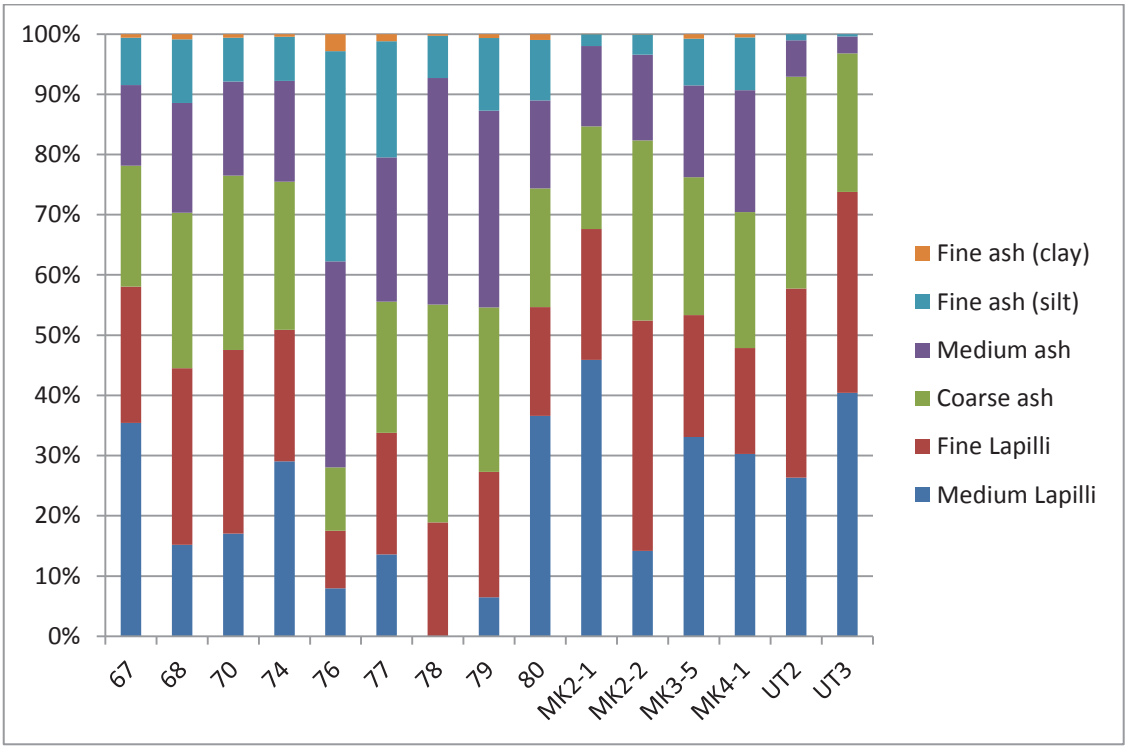


**Fig. D.1.9** Graph representing values for grain size grades of Table D.1. For location of samples see Fig. D.1.8.

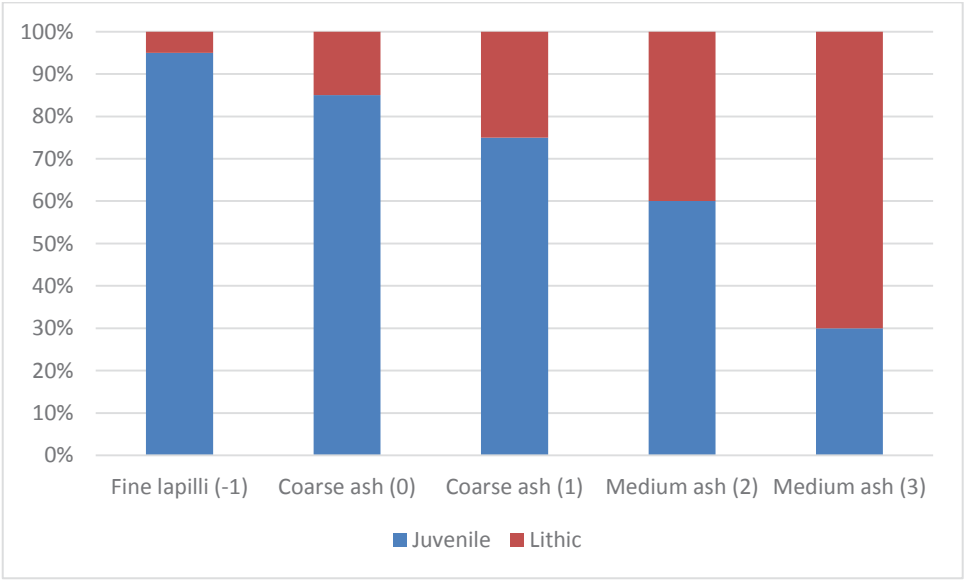


**Fig. D.1.10** Graph showing the volume percentage of juvenile and lithic pyroclasts within a specific grain size grade. The number in parenthesis are the phi fractions corresponding to the grain size grade. For the volume percentages of grain size grades in the entire deposit see Table 6.1 in the text.

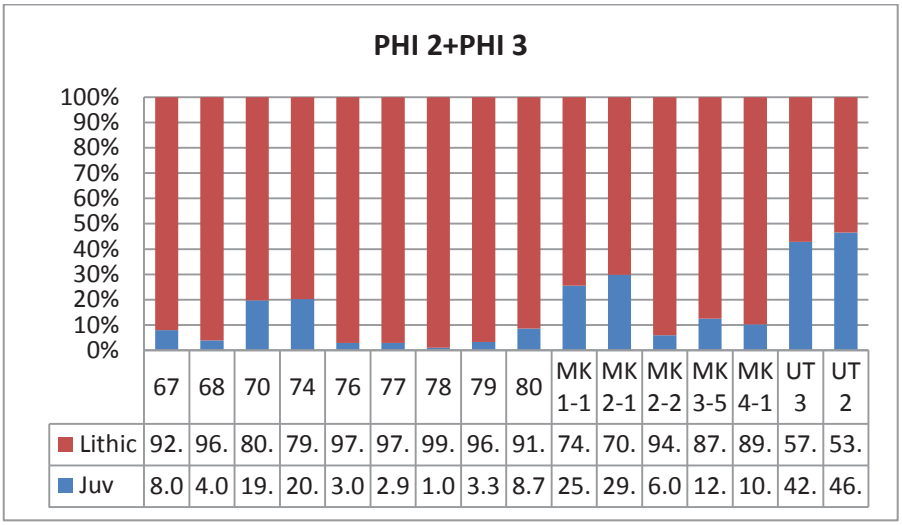


| | 67 | 68 | 70 | 74 | 76 | 77 | 78 | 79 | 80 | MK 1-1 | MK 2-1 | MK 2-2 | MK 3-5 | MK 4-1 | UT 3 | UT 2 |
|---|---|---|---|---|---|---|---|---|---|---|---|---|---|---|---|---|
| Lithic | 92. | 96. | 80. | 79. | 97. | 97. | 99. | 96. | 91. | 74. | 70. | 94. | 87. | 89. | 57. | 53. |
| Juv | 8.0 | 4.0 | 19. | 20. | 3.0 | 2.9 | 1.0 | 3.3 | 8.7 | 25. | 29. | 6.0 | 12. | 10. | 42. | 46. |

**Fig. D.1.11** Lithic and Juvenile volume percentage for 2 and 3 phi fractions. Counts of 500 grains were performed. For location of samples see Fig. D.1.8.The presence of lithic grade fragments is greatly reduced in fractions >2 phi.

## Appendix D.2 Lithofacies of Motukorea volcano

The sedimentary criteria to group and describe the lithofacies are provided in chapter 6. The referred figures for lithofacies are also displayed in chapter 6. The summarized information of these lithofacies is presented in Table 6.2 in chapter 6. The vol.% for grain size represents the approximate volume percentage of grain size within lithofacies

### *Clast-supported and juvenile-rich lithofacies*

**Massive bomb/lapilli breccia (mBLb)** (Fig. 6.7a). Up to 40 cm-thick. Grain size: Small bombs (up to 90 vol.%). Sedimentary characteristics: Proportion of juvenile to lithic: 9:1. Dominantly massive, poorly sorted, ungraded, consolidated beds. In some sections, fine the coarser juvenile fragments appear to be embedded in an incipient fine ash matrix. Few lithic of coarse size (small bomb to lapilli size).

Interpretation: Scarce of lithic fragments and coarse-juvenile-rich, poorly sorted beds suggest deposition by fall from magmatic activity. The degree of consolidation indicates that fragments were hot at the time of deposition.

**Massive lapilli tuff (mL)** (Fig. 6.7b). Thickness: From cm up to 3 m (very variable). Grain size: coarse and medium lapilli (70 to 90 vol.%), little ash. Proportion of juvenile to lithic: 9:1. Dominantly massive, moderately sorted, ungraded, moderately consolidated, laterally parallel, continuous beds with transitional boundaries. Palagonitization may be present in sections at lower altitude. Scarce lithic of lapilli size.

Interpretation: Ungraded, massive and moderately sorted layers of dominantly juvenile lapilli point to deposition by fall from magmatic activity. The degree of consolidation can be attributed to the deposition of fragments when still hot.However the presence of palagonitization in sections relatively located at lower levels (the more consolidated parts) could indicate post-deposition alteration.

### *Matrix supported dominantly, variable proportion of juvenile to lithic lithofacies*

**Massive to crudely stratified lapilli tuff (mcsL)** (Fig. 6.7c). Thickness: Tens of cm (<1 m). Grain size: medium lapilli to coarse ash (up to 90 vol.%) (considering only the juvenile-rich sections of the sequence); lithic: lapilli size (<10 vol.%) (in the total sequence), ash (up to 90 vol.%) (considering only the lithic-rich sections). Proportion of juvenile to lithic is variable, but approximately 6:4. Sedimentary characteristics: Ungraded to crudely stratified, poorly sorted, consolidated beds whose thickness may vary laterally and may show basal scour surfaces. Some juvenile/lithic block/lapilli are either embedded within the beds or form shallow impact structures. Scarce accretionary lapilli.

Interpretation: Poor sorting, relatively massive beds with coarse fragments embedded, and scour surfaces at their base imply dense, relatively erosive pyroclast density currents (high shear stresses at their basal boundary) with high sedimentation rates where turbulence and flow segregation was not relevant. Impact structures and accretionary lapilli indicate some water during deposition.

**Parallel bedded lapilli tuff (pL) in combination with parallel bedded lapilli/ash (plA) (Fig. 6.7d)**. **pL**: Thickness: <1 m. Grain size: medium lapilli to coarse ash (>40 vol.%). Proportion of juvenile to lithic 9:1. **plA**: Thickness: <1 m. Grain size: medium to fine ash (>90 vol.%). Proportion of juvenile to lithic 1:9. In combination these two lithofacies reach few meters in thickness. Sedimentary characteristics: Poorly consolidated, rhythmic sequences composed by the combination of juvenile-rich (lapilli/coarse ash) with lithic-rich (ash) layers with sharp, but gradational boundaries. Layers are continuous laterally and individually have varied thicknesses. Juvenile-rich layers are usually reversed graded and moderately sorted, whereas lithic strata are non-erosive,

non-graded and laminated (include cross-lamination). Scarce subtle plastic deformation by coarser juvenile/lithic clasts is present.

Interpretation: Reverse grading of juvenile-rich layers with moderate sorting are related to deposition from grain flows that originated from rapidly falling pyroclasts from a cloud related to magmatic activity. Laminated nature of lithic-rich layers and some presence of juvenile trains indicate low sedimentation rate from turbulent diluted base surges with tractional flow boundaries, but the lack of scour and truncation characteristics suggest flows with low shear stresses. Subtle plastic deformation attests to the presence of some water in the deposition process.

### *Matrix supported, lithic dominated lithofacies*

**Diffusely bedded ash/lapilli (dAL)** (Fig. 6.7e,b). Thickness: decimetres. Grain size: ash (lithic) (>60 vol.%); lapilli (juvenile) (<40 vol.%) (within the whole sequences). Proportion of juvenile to lithic: 4:6. Sedimentary characteristics: Diffusely stratified, poorly sorted, poorly consolidated ash beds with continuous trains of juvenile lapilli. The lapilli trains may show reverse grading and in some sections the trains thin upwards, as well as the grain size of the juvenile lapilli. The beds may be relatively plane parallel to slightly wavy and vary in thickness laterally. The bottom of these beds may define bed-load structures.

Interpretation: Crude beeding, diffuse stratification, and reverse grading of juveniles suggest tractional flow boundaries in turbulent base surges with relatively high rate of deposition. The lack of erosive boundaries suggests flows with low shear stresses at the basal boundaries.

Laminated ash (lA). Thickness: cm to dm. Grain size: ash (lithic) (>90 vol.%). Proportion of juvenile to lithic: 1:9. Sedimentary characteristics: Laminated, moderately sorted, poorly consolidated ash beds. They may contain subtle trains of juvenile, coarse ash. Cross lamination is present. Beds are laterally continuous and their thicknesses remain relatively constant, but may be deformed by impacts of coarse lithic/juvenile clasts. The bottom of these beds do not show erosive boundaries.

Interpretation: Overall well developed lamination points to low rates of sedimentation and high rate of deposition of dilute base surges. Cross lamination indicates transport in the turbulent regime, but the lack erosive boundaries suggest low shear stresses. Soft deformation suggests the presence of water during deposition.

**Cross-stratified ash/lapilli (ctAL)** (Fig. 6.7f). Thicknes: decimetres. Grain size: ash (lithic) (>60 %); lapilli (juvenile) (<40 vol.%). Proportion of juvenile to lithic: 3:7. Sedimentary characteristics: Consolidated dune bedforms with internal layers lying at low angles (<20°) on both sides. Height of dune bedforms is <0.5 m and their length within a range of 2 m. Dune bedforms are usually stoss-side truncated and aggraded. Some dune bedforms show lensoidal shapes on the lee-side section with accumulation of coarser fragments towards the bottom. Laterally, dune bedforms may show symmetrical or random distribution. The sequences are formed by a rhythmic alternation of lithic-rich (ash) with relatively juvenile-rich (fine lapilli) layers. The former may exhibit reverse grading. Dune bedforms may be plastically deformed by block/bomb/coarse lapilli size fragments (both of juvenile and lithic), and show basal erosive boundaries.

Interpretation: Cross-stratification indicates transport in the turbulent regime of dilute base surges with tractional flow boundaries. The presence of well-developed beds containing reversed graded, coarser juvenile fragments suggest that flow segregation and a basal flow characterized by traction mechanisms may have been relevant. Truncation and erosive basal boundaries point to flows with high shear stresses, whereas some soft deformation characteristics are related to the presence of water during deposition. The presence of normally graded, lensoidal structures indicates the deposition of coarser clasts at flow margins of granular flows.

**Convoluted, cross-bedded ash/lapilli tuff (cnAL)** (Fig. 6.7g). Thickness: 1-1.5 m. Grain size: ash (lithic) (>60 vol.%); lapilli (juvenile) <40 vol.%). Proportion of juvenile to lithic: 3:7. Sedimentary characteristics: This consolidated lithofacies share similar sedimentary characteristics as ***ctAL***, but dune bedforms show clearly more evidence of soft deformation: impact structures, bed-load structures, and high angle undulations. The impact structures are caused by block/bomb/coarse lapilli size fragments (both juvenile and lithic).

Interpretation: Cross-stratification indicates transport in the turbulent regime of dilute base surges with tractional flow boundaries. The presence of well-developed beds containing reversed graded, coarser juvenile fragments suggest that flow segregation and a basal flow characterized by traction mechanisms may have been relevant. Truncation and erosive basal boundaries point to flows with high shear stresses, whereas some soft deformation characteristics are related to the presence of water during deposition. The presence of normally graded, lensoidal structures indicates the deposition of coarser clasts at flow margins of granular flows. Pervasive soft deformation characteristics are related to the presence of relatively abundant water during deposition.

**Crudely stratified, irregularly bedded ash/lapilli (irAL)** (Fig. 6.7h). Thickness: ~1 m. Grain size: ash (lithic) (>60 vol.%); lapilli (juvenile) (<40 vol.%). Proportion of juvenile to lithic: 4:6. Sedimentary characteristics: Poorly consolidated, poorly sorted, rhythmic sequence formed by the combination of juvenile-rich (fine lapilli) and lithic (ash) layers. Individual layers subtly pinch and swell and are relatively continuous laterally. Juvenile-rich layers contain lithic lapilli, show reverse/normal grading, crude cross lamination, and may form faint lense-type structures. Also, they may exhibit subtle "ripple-type" undulations. Lithic layers may show cross lamination and subtle juvenile (fine lapilli)-rich layers. Coarse lapilli/block/bomb fragments do not usually form impact structures, but are embedded within the beds. In some parts these fragments show disorganized diffuse bedding or lenses. Contacts between layers are gradational.

Interpretation: Separation of upper finer material from reversed graded, lower, coarser material indicates flow segregation in flows characterized by a denser basal flow where tractional were dominant. Cross lamination suggests that the upper diluted part of the flow travelled in the turbulent regime at low rates of sedimentation. The virtual absence of erosive basal surfaces and the relatively plane parallel bedding point to low shear stress of relatively low energy flows.

**Undulating, cross-laminated ash/lapilli (uAL)** (Fig. 6.7i). Thickness: dm. Grain size: ash (lithic) (>60 vol.%); lapilli (juvenile) (<40 vol.%). Proportion of juvenile to lithic: 4:6. Sedimentary characteristics: This lithofacies shares most sedimentary characteristics with ***irAL***. The main difference is that ***uAL*** does not exhibit "ripple-type" structures and the lithic segments are thicker (up to 30 cm) than the juvenile layers (10-15 cm). In addition, the dune bedforms show symmetrical and rhythmic undulations. Height of "crests" is <40 cm and distance between crests is about 2 m. Block/bomb/coarse lapilli size fragments (both juvenile and lithic) form scarce subtle impact structures, otherwise they are embedded in the sequence without deforming beds. Contacts between layers are gradational.

Interpretation: Separation of upper finer material from reversed graded, lower, coarser material indicates flow segregation in flows characterized by a denser basal flow where tractional were dominant. Cross lamination suggests that the upper diluted part of the flow travelled in the turbulent regime at low rates of sedimentation. The virtual absence of erosive basal surfaces and the relatively plane parallel bedding point to low shear stress of relatively low energy flows. Thicker fine-ash beds and dune bedforms with symmetrical undulations suggest the presence of a thicker suspended load and more energetic flow in comparison to the base surges that formed ***irAL.***

## Appendix E.1 North Head stratigraphic logs, frequency histograms, grain size distribution and juvenile/lithic content of selected samples.

### E.1.1 North Head stratigraphic logs, frequency histograms

This appendix first presents the total of logs corresponding to North Head volcano (Figs. E1 to ). There are 2 extra logs included (PH1-B and PH3-B).The logs showed in chapter 7 (PH1, PH2, PH3, and PH4) are also included.

Fig. E.1. shows the plan view of North Head volcano. Alongside the 4 sites described in chapter 7, other 2 sites are included (PH1-B, PH3-B).

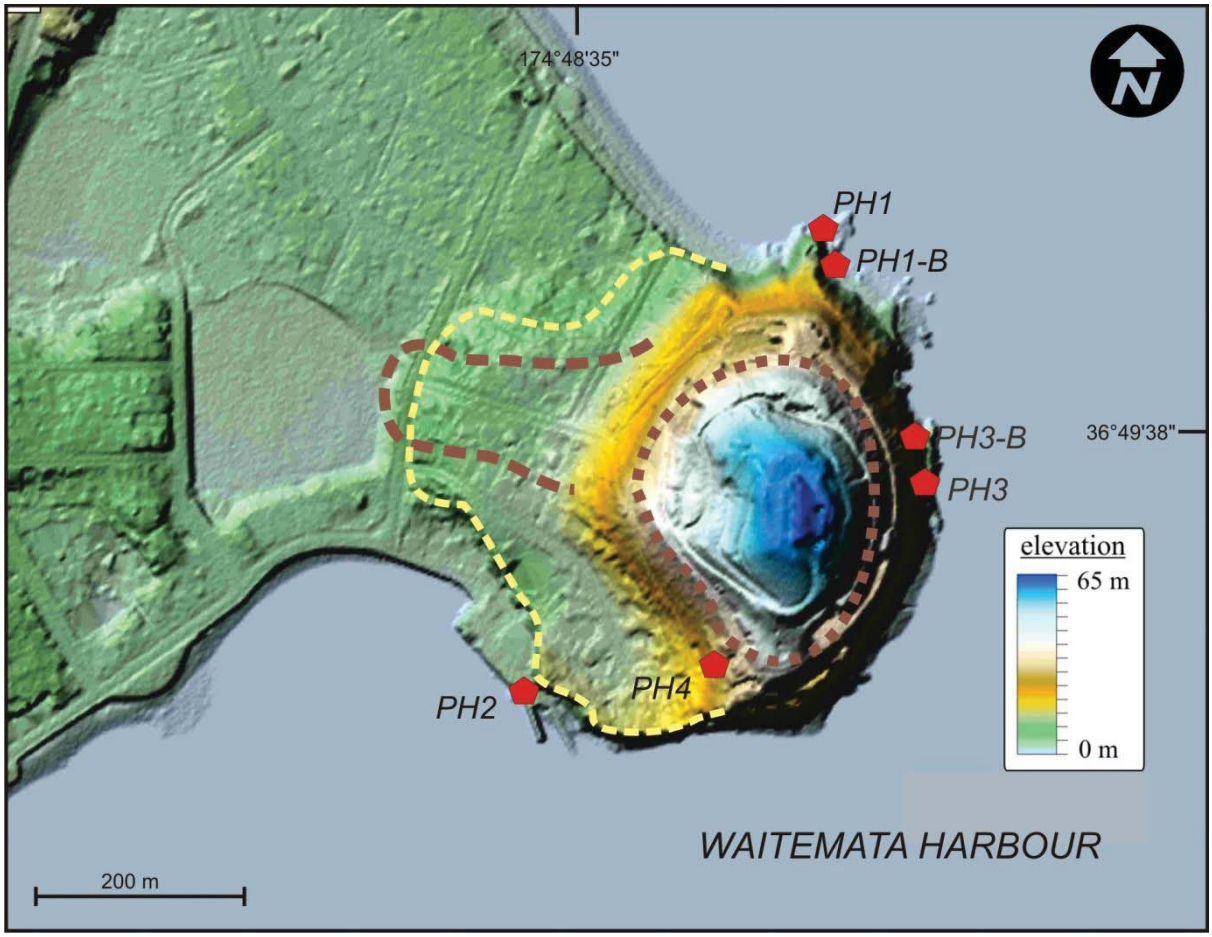


**Fig. E.1.** Location of sites

The stratigraphic logs are presented in the order showed in chapter 7 (from NH1 to NH4). All histograms show grain size distribution of the 11 sample numbers on Table E.1. Sample number is shown in histograms as *NH-"number".* Lithofacies of sequences are described in section 7.5.2 and Table 7.2 in chapter 7.

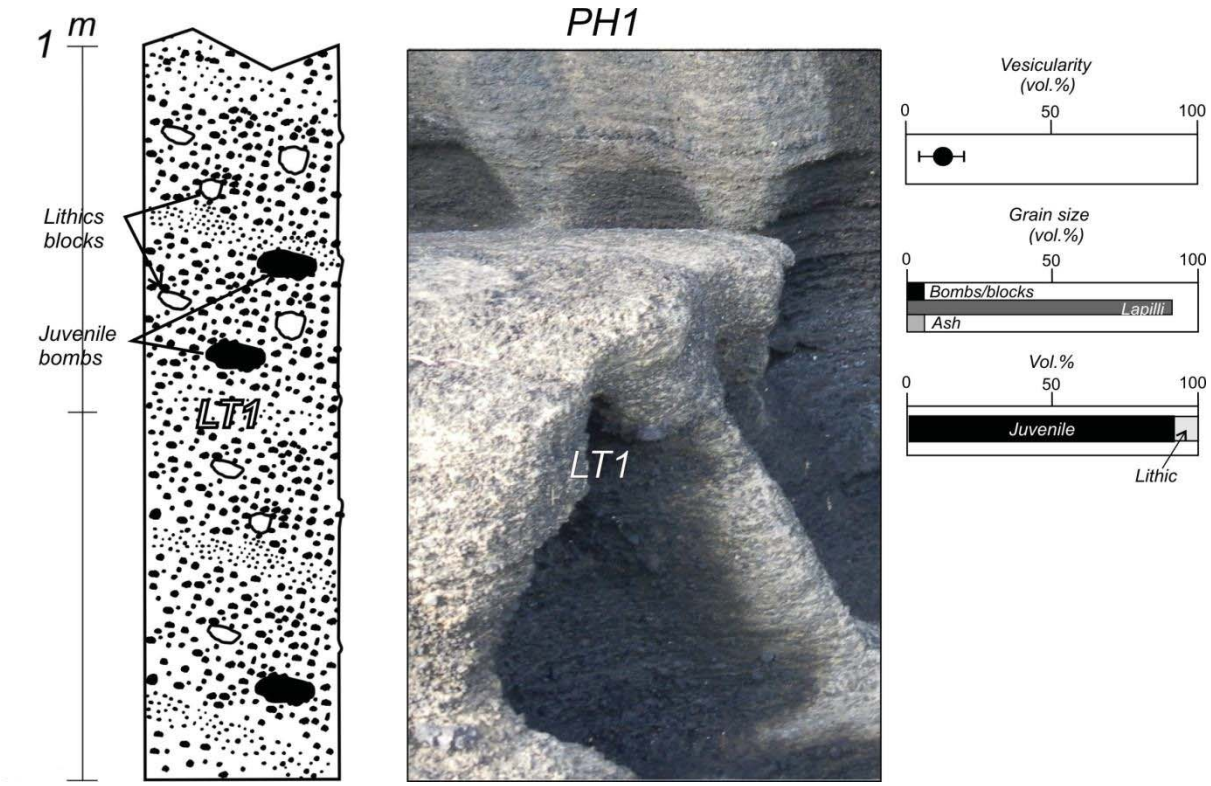


**Fig.E.2** Site PH1. The picture represents a segment of an approximately 4 metre-thick sequence. Base of exposed sequence is approximately at Chart Datum which is approximately Lowest Astronomical Tide (from data in nautical chart 5322, Land Information New Zealand). Part of the sequence lies beneath reduced Chart Datum.

Fig. E.3 exhibits a wider view of the sequence at site PH1.

**Fig. E.3** Bag is approximately 0.5 m-high. The whole sequence is constituted by lithofacies LT1.

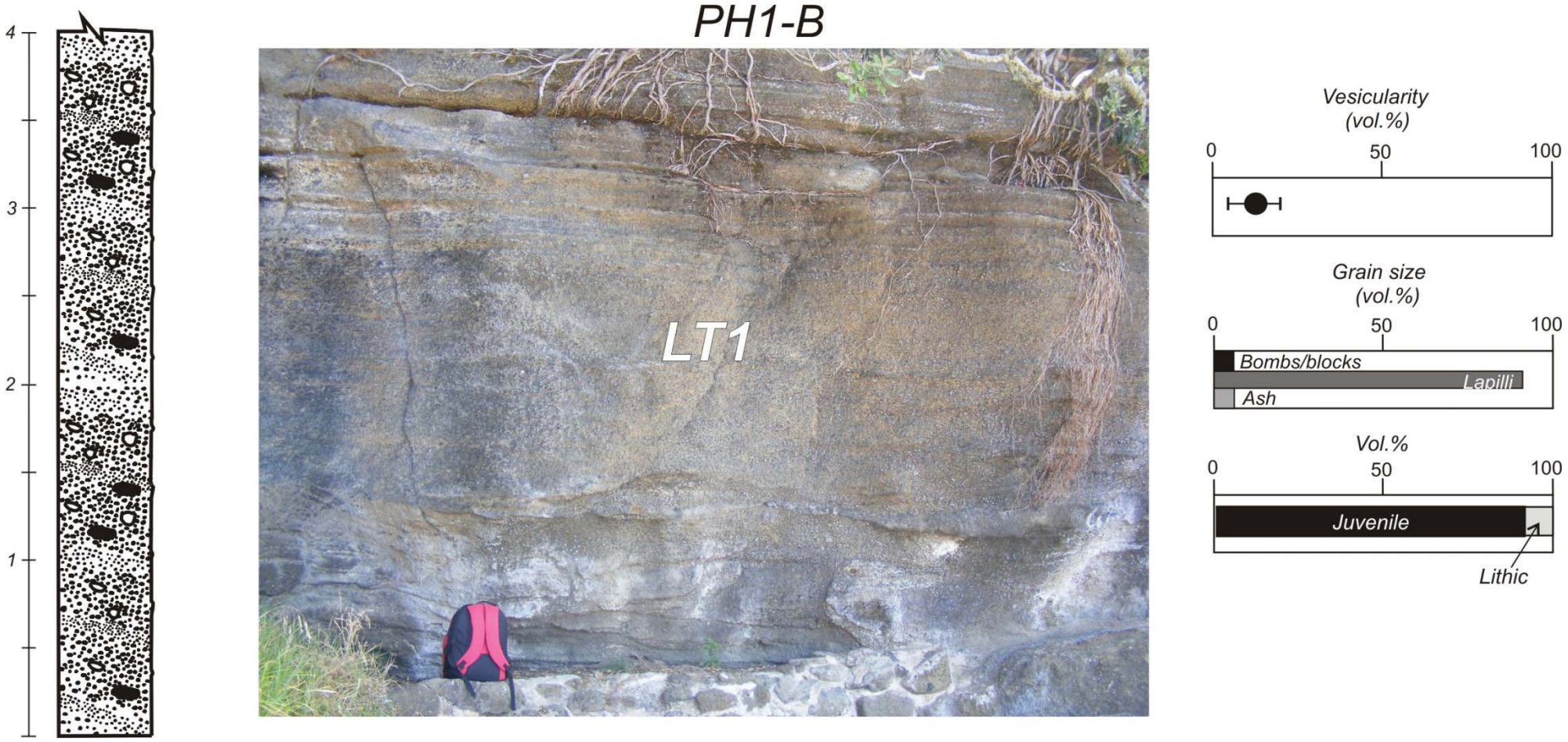


**Fig. E.4**. Site PH1-B. Base of exposed sequence is approximately at 2-3 m above Chart Datum which is approximately Lowest Astronomical Tide (from data in nautical chart 5322, Land Information New Zealand). Scale indicates thickness in metres.

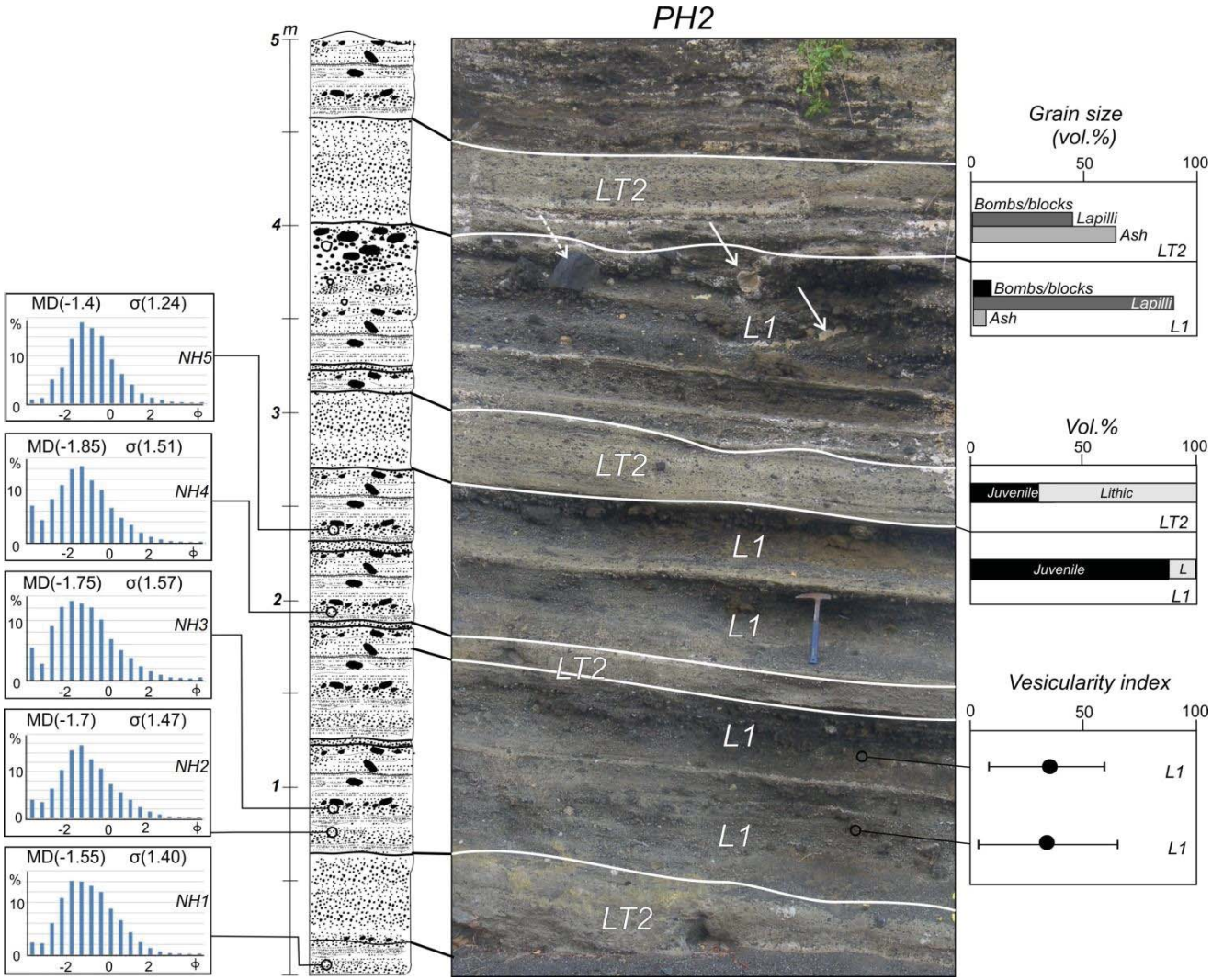


**Fig. E.5**. Site PH2. Base of exposed sequence is approximately at 3-4 m above Chart Datum which is approximately Lowest Astronomical Tide (from data in nautical chart 5322, Land Information New Zealand). Scale indicates thickness in metres.

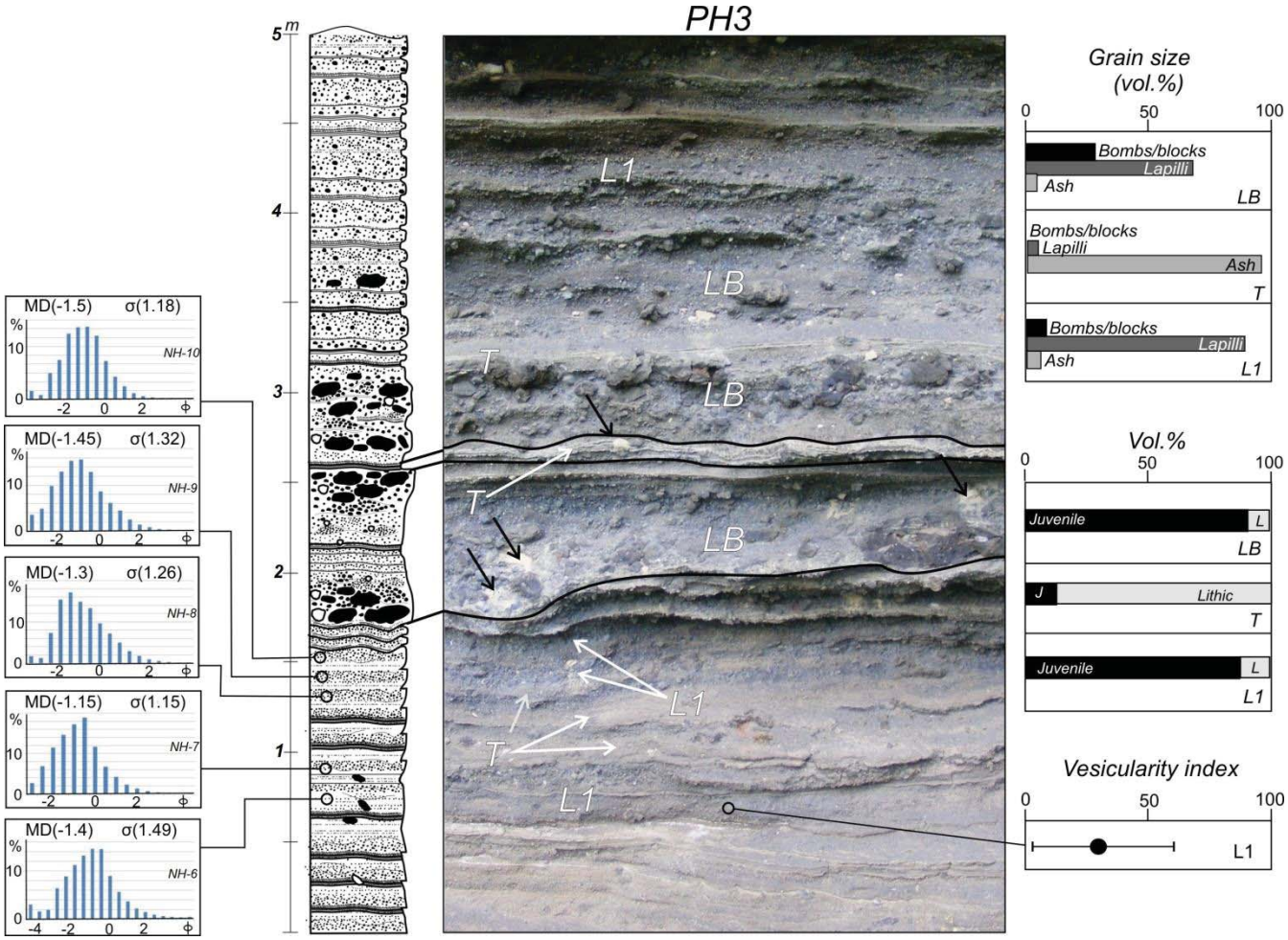


**Fig. E.6**. Site PH3. Base of exposed sequence is approximately at 7-8 m above Chart Datum which is approximately Lowest Astronomical Tide (from data in nautical chart 5322, Land Information New Zealand). Scale indicates thickness in metres.

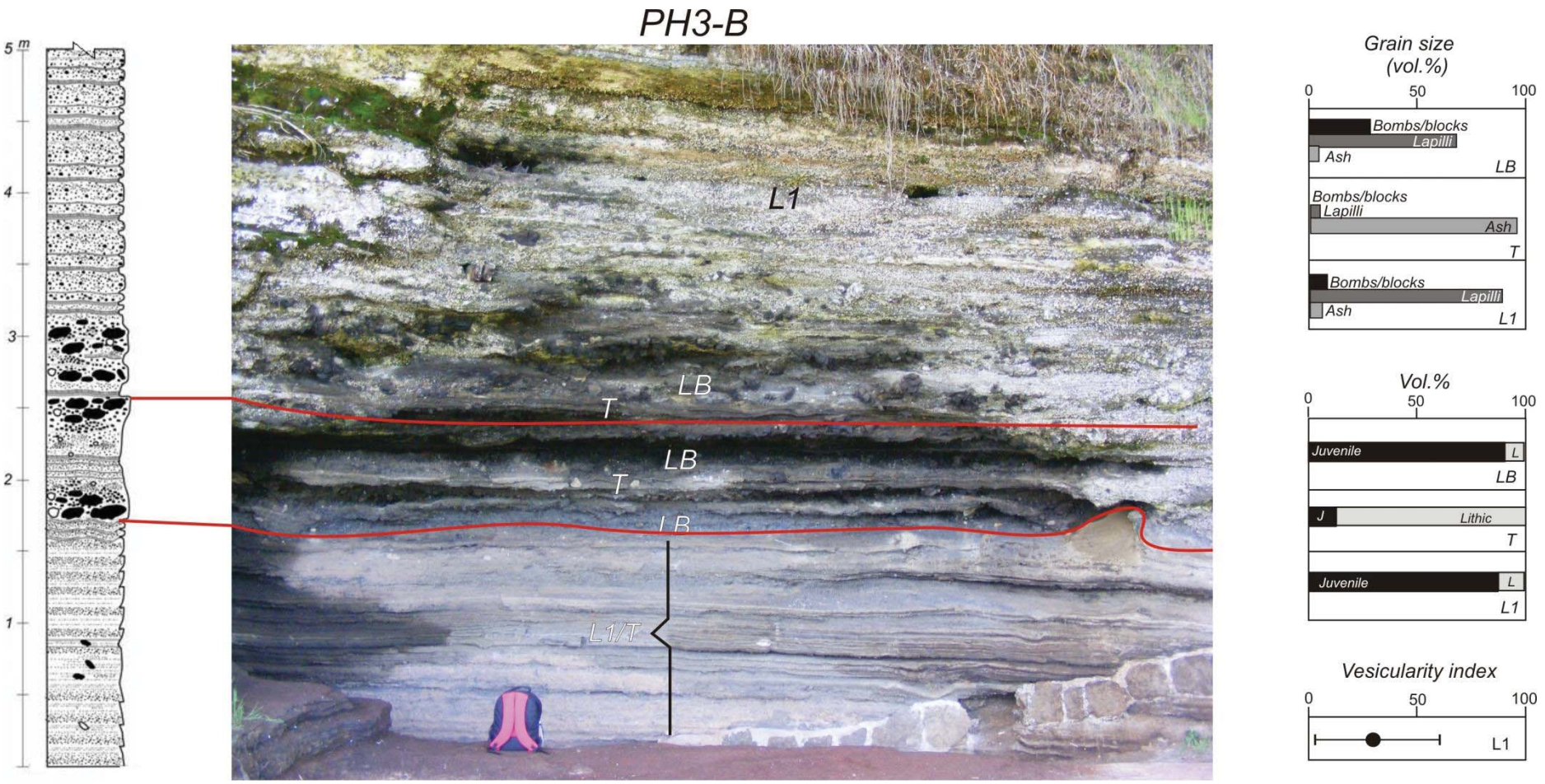


**Fig. E.7**. Site PH3-B. Base of exposed sequence is approximately at 5-6 m above Chart Datum which is approximately Lowest Astronomical Tide (from data in nautical chart 5322, Land Information New Zealand). Scale indicates thickness in metres.

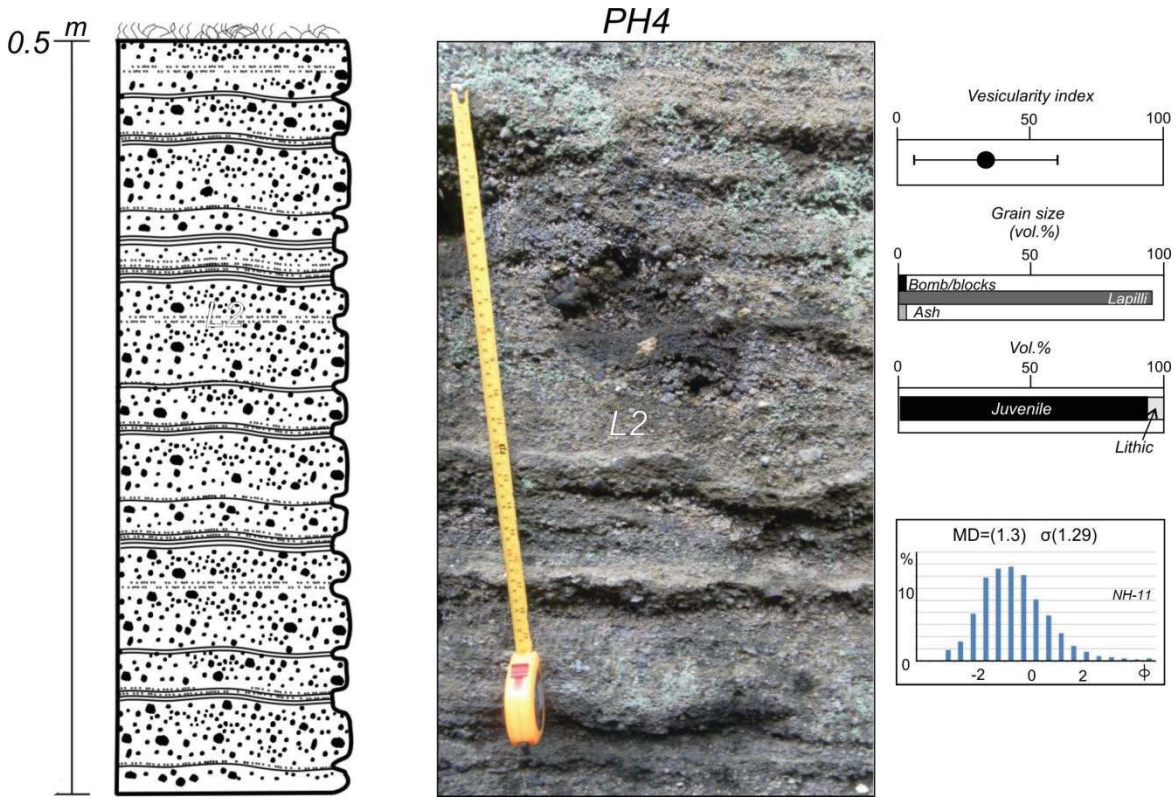


**Fig. E.8**. Site PH4. The picture represents a segment of an approximately 25 metre-thick sequence. Base of exposed sequence is approximately at 35-40 m above Chart Datum which is approximately Lowest Astronomical Tide.

## E.1.2 Grain size distribution and juvenile/lithic content of selected North Head samples.

Table E.1 contain volume percentage values for phi fractions of selected sieved North Head-samples. The fractions are grouped in grain size grades. For location of samples see histograms in logs..

| Grain size | Phi | Sample / vol.% | | | | | | | | | | |
|---|---|---|---|---|---|---|---|---|---|---|---|---|
| | | NH-1 | NH-2 | NH-3 | NH-4 | NH-5 | NH-6 | NH-7 | NH-8 | NH-9 | NH-10 | NH-11 |
| | -4.5 | 0.00 | 0.00 | 0.00 | 0.00 | 0.00 | 3.05 | 0.00 | 0.00 | 0.00 | 0.00 | 0.00 |
| | -4 | 2.38 | 3.97 | 5.47 | 7.04 | 0.79 | 1.55 | 0.00 | 0.00 | 0.00 | 1.91 | |
| Coarse lapilli | | 2.38 | 3.97 | 5.47 | 7.04 | 0.79 | 4.60 | 0.00 | 0.00 | 0.00 | 1.91 | 0.00 |
| | -3.5 | 2.24 | 3.44 | 2.80 | 4.29 | 1.18 | 1.89 | 0.00 | 1.71 | 3.52 | 0.99 | 1.79 |
| | -3 | 6.05 | 6.34 | 9.02 | 8.26 | 5.01 | 6.39 | 2.67 | 1.31 | 4.85 | 5.96 | 3.19 |
| | -2.5 | 10.84 | 10.32 | 12.22 | 10.89 | 7.48 | 8.84 | 6.88 | 7.36 | 9.87 | 8.94 | 7.80 |
| | -2 | 14.12 | 14.53 | 13.21 | 13.92 | 13.65 | 11.19 | 11.55 | 15.37 | 13.00 | 14.89 | 13.76 |
| | -1.5 | 13.98 | 15.64 | 12.75 | 14.47 | 17.06 | 13.22 | 14.69 | 17.14 | 15.35 | 16.33 | 15.26 |
| Medium lapilli | | 47.23 | 50.27 | 50.00 | 51.82 | 44.37 | 41.53 | 35.79 | 42.90 | 46.60 | 47.10 | 41.80 |
| | -1 | 13.15 | 12.60 | 12.10 | 11.80 | 15.89 | 14.57 | 17.29 | 14.87 | 15.64 | 16.45 | 15.55 |
| | -0.5 | 12.04 | 10.61 | 10.08 | 9.96 | 14.21 | 14.55 | 18.92 | 13.32 | 12.93 | 14.45 | 14.19 |
| Fine lapilli | | 25.19 | 23.21 | 22.17 | 21.76 | 30.10 | 29.12 | 36.21 | 28.19 | 28.57 | 30.90 | 29.74 |
| | 0 | 8.83 | 7.32 | 6.85 | 6.59 | 9.28 | 8.94 | 11.75 | 9.66 | 8.66 | 8.68 | 10.18 |
| | 0.5 | 6.64 | 5.57 | 5.05 | 4.73 | 6.25 | 5.66 | 6.74 | 7.20 | 6.14 | 5.16 | 7.48 |
| | 1 | 4.29 | 3.98 | 3.72 | 3.38 | 3.96 | 3.68 | 4.25 | 5.03 | 4.44 | 2.97 | 4.57 |
| | 1.5 | 2.42 | 2.40 | 2.38 | 1.91 | 2.14 | 2.21 | 2.31 | 2.94 | 2.48 | 1.41 | 2.46 |
| Coarse ash | | 22.18 | 19.26 | 18.00 | 16.60 | 21.63 | 20.49 | 25.04 | 24.83 | 21.72 | 18.22 | 24.69 |
| | 2 | 1.30 | 1.43 | 1.53 | 1.14 | 1.26 | 1.46 | 1.32 | 1.82 | 1.38 | 0.77 | 1.49 |
| | 2.5 | 0.69 | 0.80 | 0.97 | 0.69 | 0.72 | 0.96 | 0.72 | 0.97 | 0.79 | 0.46 | 0.74 |
| | 3 | 0.37 | 0.40 | 0.55 | 0.34 | 0.40 | 0.60 | 0.38 | 0.59 | 0.37 | 0.27 | 0.56 |
| | 3.5 | 0.23 | 0.28 | 0.44 | 0.22 | 0.25 | 0.44 | 0.25 | 0.34 | 0.26 | 0.18 | 0.38 |
| | 4 | 0.18 | 0.17 | 0.33 | 0.17 | 0.20 | 0.33 | 0.14 | 0.18 | 0.14 | 0.06 | 0.21 |
| Medium ash | | 2.77 | 3.07 | 3.83 | 2.55 | 2.83 | 3.79 | 2.81 | 3.89 | 2.95 | 1.74 | 3.37 |
| | <4.0 | 0.24 | 0.21 | 0.52 | 0.23 | 0.28 | 0.46 | 0.15 | 0.19 | 0.17 | 0.13 | 0.39 |
| Fine ash | | 0.24 | 0.21 | 0.52 | 0.23 | 0.28 | 0.46 | 0.15 | 0.19 | 0.17 | 0.13 | 0.39 |

**Table E.1**

The above data is presented as percentage of grain size grades in the following figure.

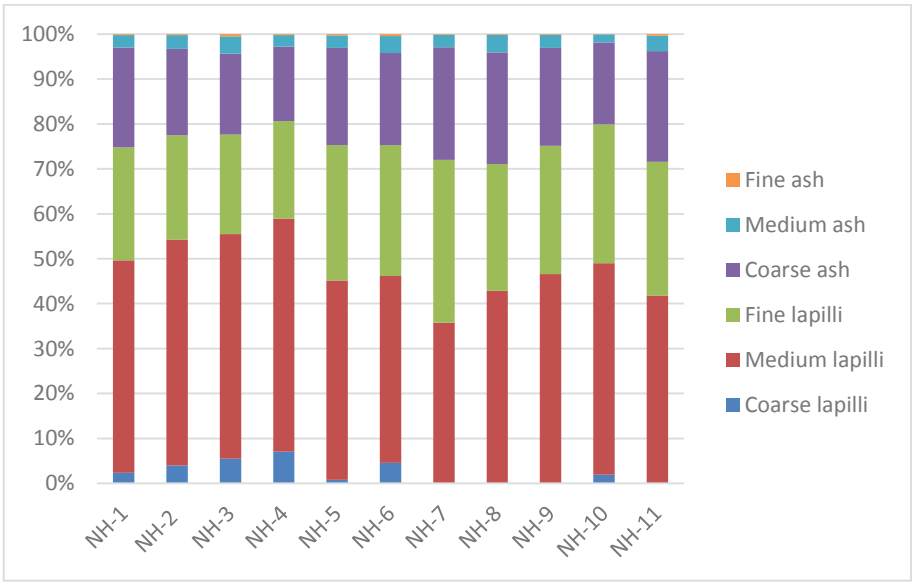


**Fig. E.9** Graph representing values for grain size grades of Table E.1. For location of samples see histograms in logs.

Counts of 500 grains were performed for the same samples.The presence of lithic grade fragments is greatly reduced in fractions >2 phi.

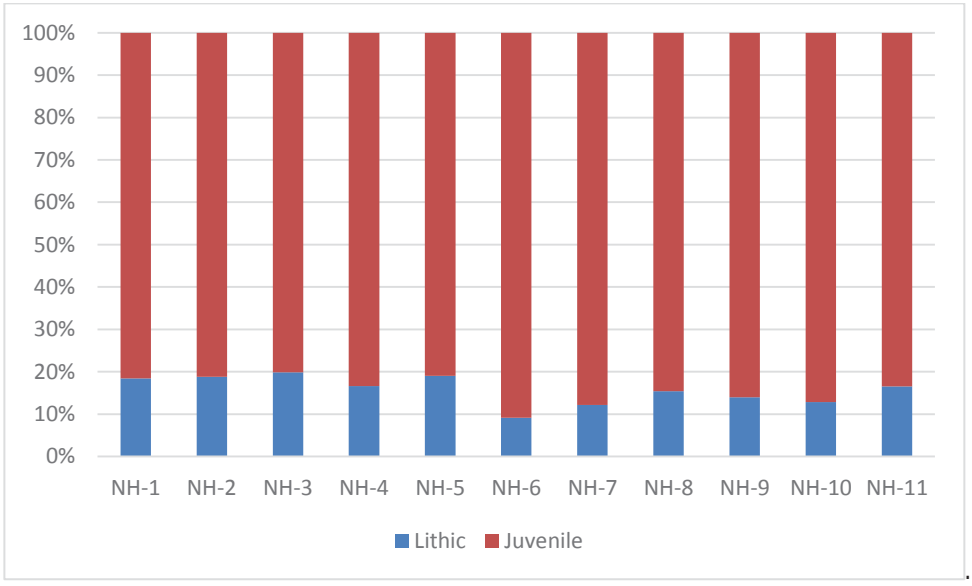


**Fig. E.10** Lithic and juvenile volume percentage for 2 and 3 phi fractions.